

https://dspace.org/

Synthesis, characterization and investigation of the mode of action in the anticancer activity of novel platinum complexes

Peega, Tebogo

2024

University of the Witwatersrand, Johannesburg

https://hdl.handle.net/10539/41819

Peega, Tebogo. (2024). Synthesis, characterization and investigation of the mode of action in the anticancer activity of novel platinum complexes [PhD thesis, University of the Witwatersrand, Johannesburg]. WireDSpace.

Downloaded from a DSpace repository. https://dspace.org/

Synthesis, characterization and investigation of the mode of action in the anticancer activity of novel platinum complexes

By

Tebogo Peega

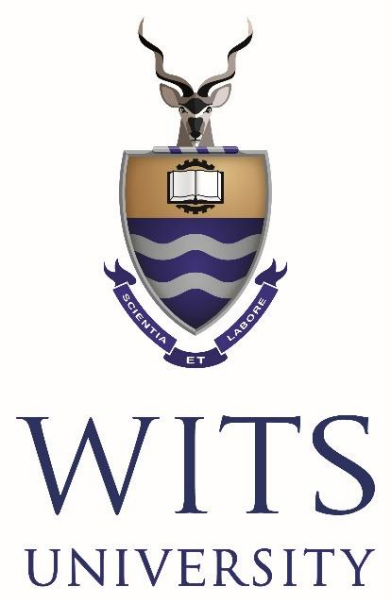
(835353)

A thesis submitted in fulfilment of the requirements for the degree of

Doctor of Philosophy in **Chemistry**

to the Faculty of Science, University of the Witwatersrand, Johannesburg,

South Africa



Supervised by: **Dr Izak. A. Kotzé**

Co-supervised by: **Dr Leonie Harmse**

May, 2024

Declaration

I, Tebogo Peega, declare that the research on this thesis is my own, unaided work. It does not contain any other persons' data unless expressly acknowledged as being sourced from them.

It does not contain any other persons' writing unless explicitly acknowledged as being sourced from other researchers.

It does not contain text, graphics, or tables copied and pasted from the Internet unless specifically acknowledged, and the source being detailed in the thesis and the references section(s)

It is being submitted for the degree of Doctor of Philosophy at the University of the Witwatersrand, Johannesburg.

It has not been submitted for any degree or examination at this or other universities.



_____

Tebogo Peega

Date: 24 May 2024

Supervisor certification

This is to certify that this research is a record of original work conducted by **Tebogo Peega** under my supervision in the School of Chemistry, at the University of the Witwatersrand in fulfilment of the requirements for the award of Doctor of Philosophy degree in Chemistry.



Dr Izak A. Kotzé

Date: 30 May 2024

Abstract

Cancer remains a global health concern, causing approximately 10 million deaths in 2020. Lung cancer, accounting for 18% of cancer-related deaths, and colorectal cancer, contributing 9.4%, are major contributors to this alarming statistic, emphasizing the urgent need for innovative and effective treatment options. Despite the success of platinum-based drugs such as cisplatin, carboplatin, and oxaliplatin, their limitations and severe adverse effects necessitate the exploration of alternative chemotherapeutic agents. This research project focused on synthesizing and characterizing square planar platinum(II) complexes bearing variations of two bidentate coordinating ligands; disubstituted acylthiourea and diimine ligands, each possessing unique physical and chemical properties.

A series of cationic [Pt(diimine)(L^n-κ*O,S*)]Cl complexes were successfully synthesized and characterized using nuclear magnetic resonance spectroscopy, infrared spectroscopy, mass spectrometry, and elemental analysis. The anticancer activity of these complexes was evaluated against two lung cancer cell lines, A549 and H1975, and a colorectal cancer cell line, HT-29. *In vitro* cytotoxicity studies included the determination of IC_{50} values of active complexes and assessing their cell death mechanisms through multiple biochemical marker assays. These included annexin-V binding, caspase-3/7 and caspase-8 activity, mitochondrial membrane potential (MMP), reactive oxygen species (ROS) and immunofluorescence for the expression of key proteins involved in the DNA damage response and oxidative stress response, such as p21 and haemoxygenase-1 (HO-1). A proteome array was employed to investigate the effects on apoptosis-associated proteins.

The results indicated that these platinum complexes were more cytotoxic than cisplatin with IC_{50} values ranging between 0.68 μM and 2.28 μM. Further investigation showed that the platinum complexes induced cell stress, chromatin condensation, nuclear fragmentation, increased phosphatidylserine (PS) on the outer cell membranes and activated caspase-3/7. Platinum complexes induced intrinsic apoptosis in cancer cells, as evidenced by the loss of mitochondrial membrane potential and the absence of caspase-8 activity. Elevated ROS levels, increased HO-1 expression and increased expression of p21 suggested oxidative

stress and DNA damage as the trigger source for intrinsic apoptotic cell death. The active complexes downregulated pro-survival proteins (IGFs) in lung cancer cells and anti-apoptotic proteins (survivin and HSP70) and upregulated pro-apoptotic proteins (p21, TRAIL R2), across the three cancer cell lines, indicating potential dual activation of apoptotic pathways. DNA binding studies indicated groove binding and intercalation as the mode of interaction with DNA. The findings highlight the potential of these platinum complexes as promising candidates for further development as cancer therapeutics.

Keywords: Cancer, synthesis, characterization, disubstituted acylthiourea, diimine, platinum(II) complexes, bidentate coordination, apoptosis, oxidative stress, groove binding, intercalation

Dedication

I dedicate this thesis to my parents, Elizabeth and Joseph Peega for their outpouring love, support and prayers throughout my life and this academic journey. My beloved son, sister and beautiful niece. My late grandmother, for her everlasting faith in me. Her encouragement will live with me forever.

All of my help comes from the Lord!

Be joyful in hope, patient in affliction, faithful in prayer.

Romans 12:12

Acknowledgments

To the most high God, Jehovah, thank you for the gift of life!

I would like to extend my utmost gratitude to my supervisor, Dr Izak Kotzé; thank you for believing in me from the beginning and entrusting me with a project of this magnitude. Your unwavering confidence and encouragement have been instrumental, I wouldn't have undertaken this PhD journey without your support.

I extend my heartfelt thanks to my co-supervisor, Dr Leonie Harmse, thank you for your consistent support and patience throughout this project. Your guidance has been invaluable. I deeply appreciate your love for research and teaching, and I am forever grateful for your contribution to the successful completion of this research work.

I would like to acknowledge the following people for their role and contribution towards the completion of my research project:

- Dr Edmore Kangara, for guiding me with synthesis in the chemistry lab.
- Dr Eric Morifi, Mr Thapelo Mbhele and Ms Refiloe for Mass Spectrometry training and their help with data processing.
- Dr Cathryn Slabber, Mr Mark Blow and Dr Sheldon Sookai from Wits Bioinorganic lab, for your assistance in obtaining data for DNA binding studies. I also appreciate your accessibility and willingness to help me access the lab at any given time.
- My family for supporting me throughout my studies and encouraging me to pursue my dreams despite the challenges. You are the best! Mosetsana wa lona o ithutile! Fa tsotlhe di apare tshiamo.
- My loving partner, Katlego Mkhize, thank you for keeping me sane and supporting me throughout the journey.
- My friends, Boitumelo, Kebuile, Masego, Dineo, Lebogang, Iris, Nonzuzo and Thokozile, thank you for consistently checking in and cheering me on.
- Special thanks to the Wits Inorganic Coordination Chemistry Group and the Pharmacology Cancer Group for making the lab a safe space to conduct research, learn, share knowledge, vent, and simply have fun. In you, I have a family!
- A big thank you to the following funding bodies that enabled me to complete my studies: The National Research Foundation (NRF), the McGill Bequest

to Wits Pharmacology Department and the University of the Witwatersrand for the Postgraduate Merit Award.

Research Outputs

Publications

- T. Peega, R. N. Magwaza, L. Harmse and I. A. Kotzé. Synthesis and evaluation of the anticancer activity of [Pt(diimine)(*N*,*N*-dibutyl-*N*'-acylthiourea)]$^{+}$ complexes. *Dalton Transactions*, 2021, **50**, 34, 11742-11762. DOI: 10.1039/d1dt01385h.

- E. F. Kangara, T. Peega, L. Harmse, J. L. van Wyk , D. C. Levendis and I. A. Kotzé. Conformational analysis and potential anticancer activity of [Pt(phen)(L^1-κ:S)$_2$] studied by single crystal X-ray diffraction and variable temperature ^{1}H and ^{195}Pt NMR spectroscopy. *New Journal of Chemistry*, 2019, **43**, 3665–3672. DOI: 10.1039/c8nj06010j.

Conference Proceedings

- Poster presentation, Investigating the mechanism of action of novel platinum complexes on lung and colorectal cancer cell lines, South African Society for Basic and Clinical Pharmacology (SASBCP) 55th Annual Conference, (North-West University, South Africa), October 2022.

- Poster presentation, Evaluation of the anticancer activity and mechanism of cell death of novel platinum(II) complexes, European Association for Cancer Research (EACR), (Seville, Spain), June 2022.

- Oral presentation, Synthesis and characterization of novel platinum(II) complexes and their potential as chemotherapeutic agents, Wits University, Faculty of Health Science Research Day, (Johannesburg, South Africa), October 2020.

- Poster presentation, Synthesis and evaluation of novel platinum(II) complexes for anticancer activity, SASBCP 53rd Annual Conference, University of Pretoria, (Pretoria, South Africa), October 2019.

- Poster presentation, Synthesis and evaluation of novel platinum(II) complexes for anticancer activity. Wits University, Faculty of Health Sciences Research Day, (Johannesburg, South Africa), September 2019.

Table of Contents

Declaration……..……..ii

Supervisor certification……...iii

Abstract ……..iv

Dedication……...vi

Acknowledgements……vii

Research outputs……..…ix

Table of contents…….x

List of figures and schemes…..……..xv

List of tables……..xix

Abbreviations, acronyms, and symbols……....xxi

Chapter 1: Introduction and Literature review 1

1.1 Cancer 1

1.2 Cancer statistics 2

1.2.1 Cancer incidence in Africa 5

1.3 Cancer treatment 5

1.4 Current platinum drugs in cancer chemotherapy 6

1.4.1 Platinum(II)-diimine complexes 9

1.4.2 Platinum(II)-acylthiourea complexes 11

1.5 Drug-DNA interactions 14

1.5.1 Covalent binding 14

1.5.2 Non-covalent binding 15

1.6 Cell death mechanisms and cancer 17

1.6.1 Apoptosis 18

1.6.2 Paraptosis 22

1.6.3 Autophagy 22

1.6.4 Necrosis 23

1.7 Research proposal 24

1.7.1 Problem statement 24
1.7.2 Aim 25
1.7.3 Objectives 25
1.8 Cancer cell models for *in vitro* studies 26
1.9 Thesis outline 27
Chapter 2: Synthesis and characterization of ligands and [Pt(diimine)(L^n-κ*O*,*S*)]$^+$ complexes 28
2.1 Introduction 28
2.2 Experimental 32
2.2.1 Materials and measurements for chemical synthesis 32
2.2.2 Characterization techniques 32
2.2.3 Synthesis of *N*,*N*-di(alkyl)-*N*'-acylthiourea ligands (HL^n) 33
2.2.4 Synthesis of the metal precursor $PtCl_2$(diimine) 36
2.2.5 Synthesis of [Pt(diimine)(L^n-κ*O*,*S*)]Cl complexes 37
2.3 Results and Discussion 41
2.3.1 Synthesis of *N*,*N*-di(alkyl)-*N*'-acylthiourea ligands 41
2.3.2 Characterization of *N*,*N*-di(alkyl)-*N*'-acylthiourea ligand 43
2.3.3 Synthesis and characterization of the platinum precursor $PtCl_2$(diimine) 48
2.3.4 Synthesis of [Pt(diimine)(L^n-κ*O*,*S*)]Cl complexes 50
2.3.5 Characterization of [Pt(dmp)(L^1-κ*O*,*S*)]Cl complexes using ^{1}H, ^{13}C and 2D NMR Spectroscopy and Mass Spectrometry 52
Chapter 3: Cytotoxic effects of platinum complexes on lung and colorectal cancer cells and their mechanism of cell death 59
3.1 Introduction 59
3.2 Experimental 60
3.2.1 Cell culture 60
3.2.2 Preparation of reagents 62
3.2.3 The MTT cell viability assay 62
3.2.4 Cell morphology 63
3.2.5 Detection of apoptosis by annexin-V/propidium iodide staining 65
3.2.6 Determination of caspase-3/7 activity 66

3.2.7 Determination of caspase-8 activity 67
3.2.8 Evaluation of the mitochondrial membrane potential by MitoProbe™ JC-1 68
3.2.9 Evaluation of Reactive Oxygen Species 69
3.2.10 Immunofluorescence 70
3.2.10.2 Evaluation of p21 expression 71
3.3 Results 72
3.3.1 Cytotoxic effects of [Pt(diimine)(L^n-κ*O*,*S*)]Cl complexes and free diimine ligands on H1975, A549 and HT-29 cells 72
3.3.2 IC_{50} values of platinum complexes and cisplatin on H1975, A549 and HT-29 cells 75
3.3.3 Study concentrations: platinum complexes and positive controls 76
3.3.4 Effects of platinum complexes and cisplatin on cancer cell morphology 77
3.3.5 Determination of phosphatidylserine exposure by Annexin-V binding 83
3.3.6 Activation of caspase-3/7 in H1975, A549 and HT-29 cells 86
3.3.7 Evaluation of caspase-8 activity 94
3.3.8 Measurement of the mitochondrial membrane potential ($\Delta\Psi_M$) 96
3.3.9 Measurement of Reactive Oxygen Species (ROS) in cancer cells 101
3.3.10 Haemoxygenase-1 (HMOX1/HO-1/HSP32) expression in cancer cells 103
3.3.11 The effect of platinum complexes on p21 expression in cancer cell 110
3.4 Discussion 112
3.4.1 Platinum complexes are cytotoxic to H1975, A549 and HT-29 cancer cells 112
3.4.2 Platinum complexes caused the externalization of PS and increase annexin-V binding indicating the induction of apoptosis 113
3.4.3 Platinum complexes increase caspase-3/7 activity in H1975, A549 and HT-29 cells 114
3.4.4 The effect of platinum complexes on caspase-8 activity 116
3.4.5 Markers of apoptosis 116
3.4.6 Platinum complexes cause a loss of MMP in H1975, A549 and HT-29 cells 117
3.4.7 Platinum complexes induce oxidative stress 118

3.4.8 Platinum complexes increased the expression of HO-1 120
3.4.9 Platinum complexes increased the expression of p21 122
3.5 In summary 123
Chapter 4: Evaluation of the effect of platinum complexes on the expression of apoptosis-associated proteins in cancer cells 125
4.1 Introduction 125
4.1.1 An overview of important apoptosis-associated proteins and their role in apoptosis 126
4.1.2 The Bcl-2 family of proteins 126
4.1.3 Death receptor proteins 127
4.1.4 Tumour suppressor protein p53 128
4.1.5 Cell cycle protein p21Cip1/Waf1/CDKN1A 129
4.1.6 Heat shock proteins 130
4.1.7 Inhibitors of apoptosis (IAPs) 131
4.1.8 Smac/DIABLO and HTRA2/Omi 132
4.1.9 Insulin-like Growth Factors (IGFs) and IGF-Binding Proteins (IGFBPs) 132
4.2 Experimental 133
4.2.1 Human apoptotic proteome array 134
4.2.2 Treatment of cells 135
4.2.3 Lysate preparation 136
4.2.4 Protein quantification (Bradford assay) 137
4.2.5 Preparation of membrane arrays (HT-29) 137
4.2.6 Preparation of membrane arrays (H1975 and A549) 140
4.3 Results 142
4.3.1 Apoptosis-associated proteins in HT-29 cells 142
4.3.2 Apoptosis-associated proteins in A549 cells 148
4.3.3 Apoptosis-associated proteins in H1975 cells 155
4.4 Discussion 160
4.4.1 Bad, Bax, Bcl-2 and cytochrome c 163
4.4.2 Caspase-3 and cleaved caspase-3 164
4.4.3 Platinum complexes increased the expression of TRAIL R2 165
4.4.4 Platinum complexes decreased the expression of HSPs 166

4.4.5 Platinum complexes decreased the expression of IAPs 167
4.4.6 Smac/DIABLO and HTRA2/Omi 168
4.4.7 The expression of cell cycle proteins; p21, p27 and p53 169
4.4.8 Other important apoptosis-associated proteins in HT-29 cells 171
4.4.9 Other important apoptosis-associated proteins in A549 and H1975 cells. 173
4.5 In summary 176
Chapter 5: DNA binding studies with active platinum complexes 177
5.1 Introduction 177
5.2 Experimental 178
5.2.1 Chemicals and solvents 178
5.2.2 Electrophoretic Mobility Shift Assay 178
5.2.3 DNA thermal degradation 179
5.2.4 Circular dichroism 181
5.2.5 Electronic absorption titration spectroscopy 183
5.3 Results and Discussion 185
5.3.1 Electrophoretic Mobility Shift Assay 185
5.3.2 DNA thermal degradation 188
5.3.3 Circular dichroism 190
5.3.4 Electronic absorption titration spectroscopy 192
5.4 In summary 195
Chapter 6: Summary and Conclusion 197
6.1 Synthesis and characterization of platinum complex; [Pt(diimine)(*N*,*N*-dialky-*N'*-acylthiourea)]Cl 197
6.2 Platinum complexes are cytotoxic to lung and colorectal cancer cells 198
6.3 Platinum complexes induce intrinsic apoptosis in HT-29 and H1975 and A549 cells 199
6.4 The effect of active platinum complexes on the expression of apoptosis-associated proteins in HT-29, A549 and H1975 cells 200
6.5 DNA Binding Studies 201
6.6 Conclusion 201
6.7 Future work 202
References 204

Appendix A: Chapter 2 226
Appendix B: Chapter 3 236
Appendix C: Chapter 5 250

List of Figures and Schemes

Chapter 1

***Figure 1.1**: Six hallmarks of cancer described as biological capabilities acquired during the multistep development of human tumours*……1

***Figure 1.2**: The global estimates of new cancer cases and cancer deaths reported by the World Health Organization in 2020*……4

***Figure 1.3**: Chemical structures of six clinically approved platinum(II)-drugs currently used in cancer chemotherapy*……8

***Figure 1.4**: Biologically active platinum(II)-diimine complexes with potential anti-cancer activity reported in literature*……11

***Figure 1.5:** The molecular structure of thiourea derived acylthiourea ligands distinguished by the presence of an acyl group (blue) in the 1-amine (position - 1)*……12

***Figure 1.6:** Illustration of possible non-covalent DNA binding modes 1) major groove binding 2) minor groove binding, 3) electrostatic interactions and 4) Intercalation*……16

***Figure 1.8**: A diagram showing the components of the extrinsic apoptotic signaling pathway (Type I) and intrinsic apoptotic signaling pathway (Type II).*……21

***Scheme 1.1:** Classification of cell death mechanism categorized into programmed cell death which include apoptosis, autophagy and paraptosis; as well as non-programmed cell death, necrosis*……18

Chapter 2

***Figure 2.1**: Structural variations of the diimine ligands showing unsubstituted and substituted diimines. A) 1,10-phenanthroline (phen) B) 5,6-dimethyl-1,10-phenanthroline (dmp) C) dipyrido [3.2-f:2',3'-h] quinoxaline (dpq)*.....30

***Figure 2.2**: Chemical structures of a series of nine [Pt(diimine)(L^n-κO,S)]Cl complexes previously synthesized and evaluated for anticancer activity in H1975 lung cancer cell line*.....31

***Figure 2.3**: Chemical structure of synthesised N,N-di(alkyl)-N'-acylthiourea ligands showing the R^1 and R^2 substituents, where R^1 represents the acyl/aryl substituents and R_2 represents the alkyl substituents*.....43

***Figure 2.4**: ^{1}H-NMR spectrum of N,N-di(butyl)-N'-benzoylthiourea (HL^1) in chloroform-d at 25 ℃*.....44

***Figure 2.5**: ^{1}H-^{1}H COSY (2D NMR) spectrum of **HL^1** in chloroform-d at 25 ℃*.....44

***Figure 2.6**: ^{13}C NMR spectrum of N,N-dibutyl-N'-benzoylthiourea ligand in methanol-d_4 at 25 ℃*.....46

***Figure 2.7**: The high resolution mass spectrum of N,N-dibutyl-N'-benzoylthiourea (**HL^1**) prepared in HPLC grade methanol showing the abundant peak observed at 293.16 m/z (L+H) while the expected peak (292.16 m/z), confriming the pure structure of the prepared ligand*.....47

***Figure 2.8**: ^{1}H-NMR spectrum of $PtCl_2$(phen) in DMSO at 25 ℃ showing C_2 symmetry*.....49

***Figure 2.9**: ^{1}H-NMR spectrum of $PtCl_2$(dmp) in DMSO at 25 ℃. The spectrum is cut between 5.20 -7.50 ppm to show all peaks and expanded in the aromatic region*.....49

***Figure 2.10**: Stacked 1D ^{1}H NMR spectrum of the N,N-dibutyl-N'-benzoylthiourea ligand (**HL^1**) and [Pt(dmp)(L^1-κO,S)]$^+$ complex in $CDCl_3$ at 25 ℃ with all assignments*.....52

***Figure 2.11**: ^{1}H-^{1}H COSY NMR spectrum of [Pt(dmp)(L^1-κO,S)]Cl in methanol-d_4 at 25 ℃ showing the expanded aromatic region*.....54

***Figure 2.12**: ^{13}C-NMR spectrum of [Pt(dmp)(L^1-κO,S)]Cl complex in methanol-d_4 at 25 ℃*.....55

***Figure 2.13**: FT-IR spectrum of [Pt(dmp)(L^1-κO,S)]Cl stacked alongside the free **HL^1** ligand*.....56

***Figure 2.14**: The high resolution mass spectrum of [Pt(dmp)(L^1-κO,S)]Cl prepared in HPLC grade methanol showing the major peak of the complex and the isotopologue pattern of the Pt, the most abundant being ^{195}Pt 694.211 m/z*.....58

***Scheme 2.1**: General depiction of an anionic bidentate and neutral monodentate coordination mode of N,N-di(alkyl)-N'-acylthiourea ligand (O,S) to a metal (M) following deprotonation by a base*……..29

***Scheme 2.2**: Synthetic procedure for the preparation of N,N-di(alkyl)-N'-acylthiourea ligand*……..41

***Scheme 2.3:** Preparation of $PtCl_2$(diimine) in deionised water where drops of HCl were added to prevent aquation of potassium tetra-chloroplatinate upon dissolution*……48

***Scheme 2.4**: Reaction scheme showing the preparation of [Pt(dmp)(L^n-κO,S)]Cl complexes from HL^n and platinum precursor in excess sodium acetate*……..51

Chapter 3

***Figure 3.1**: The effect of the platinum complexes (A) and free diimine ligands (B) on the viability of H1975, A549 and HT-29 cells at 5 µM concentration*……...73

***Figure 3.2**: Photomicrographs of H1975 lung cancer cells showing changes in cell morphology after 18 hour treatment with 3 µM of active [Pt(dmp)(L^n-κO,S)]Cl complexes and 15 µM cisplatin*……78

***Figure 3.3**: Photomicrographs of A549 lung cancer cells, showing changes in cell morphology after treatment with 5 µM of active [Pt(dmp)(L^n-κO,S)]Cl complexes and 25 µM cisplatin for 18 hours*……80

***Figure 3.4**: Photomicrographs of HT-29 cells showing changes in cell morphology following an 18 hour treatment with 3 µM [Pt(dmp)(L^n-κO,S)]Cl complexes and 15 µM cisplatin*……82

***Figure 3.5**: The percentage of H1975, A549 and HT-29 cells with active caspase-3/7 following treatment with the platinum complexes and cisplatin*……...87

***Figure 3.6**: Representative photomicrographs of H1975 cells showing caspase-3/7 activity*……..89

***Figure 3.7**: Representative photomicrographs of A549 cells showing caspase-3/7 activity*……91

***Figure 3.8**: Representative photomicrographs of HT-29 cells showing caspase-3/7 activity*……93

***Figure 3.9**: Photomicrographs of H1975, A549, and HT-29 cells showing the absence of caspase-8 activity after an 18-hour treatment with platinum complexes and cisplatin*……..*95*

***Figure 3.10**: Effects of platinum complexes, cisplatin and staurosporine on mitochondrial membrane potential in H1975 cells*……97

***Figure 3.11**: Effects of platinum complexes, cisplatin and staurosporine on mitochondrial membrane potential in A549 cells*……99

***Figure 3.12**: Effects of platinum complexes, cisplatin and staurosporine on mitochondrial membrane potential in HT-29 cells*……100

***Figure 3.13**: Effects of platinum complexes and cisplatin on the expression level of HO-1 in H1975 cells*……*105*

***Figure 3.14**: Effects of platinum complexes and cisplatin on the expression level of HO-1 in A549 cells*……107

***Figure 3.15:** Effects of platinum complexes and cisplatin on the expression level of HO-1 in HT-29 cells*……109

Chapter 4

***Figure 4.1**: Coordinates of 35 human apoptosis target proteins, reference spot (positive control) and PBS (negative control) spotted in duplicates on each of the four-nitrocellulose membrane array from R&D system*……138

***Figure 4.2**: Chemiluminescent signals of the apoptosis array membranes (R&D Systems) showing the effect of the platinum complexes and cisplatin in HT-29 cells*……142

***Figure 4.3**: Chemiluminescent signals of the apoptosis array membranes (RayBiotech) showing the effect of the platinum complexes and cisplatin in A549 cells*……148

***Figure 4.4**: Chemiluminescent signals of the apoptosis array membranes (RayBiotech) showing the effect of the platinum complexes and cisplatin in in H1975 cell*……155

***Scheme 4.1**: Summary of the principle and general procedure of the proteome array*..135

Chapter 5

***Figure 5.1**: EMSA gel showing the effects of the interaction of Ethidium Bromide (EB) and Hoechst-33258 (HS) with pUC57 plasmid DNA*……185

***Figure 5.2**: EMSA gel of pUC57 plasmid DNA in the presence of increasing concentrations of a) [Pt(dmp)(L^1-κO,S)]Cl and b) [Pt(dmp)(L^3-κO,S)]Cl (0.05 -50 μM)*……187

***Figure 5.3**: Melting temperature of ctDNA (*100 μM) *in the absence and presence* 2.5 μM *[Pt(dmp)(L^1-κO,S)]Cl and [Pt(dmp)(L^3-κO,S)]Cl* respectively……189

***Figure 5.4**: CD spectrum of ctDNA (100 μM) and the effect of the platinum complexes on the spectrum*……191

***Figure 5.5**: Electronic absorption spectrum of [Pt(dmp)(L^1-κO,S)]Cl complex in the absence and presence of increasing concentrations of ctDNA*……193

***Figure 5.6**: Representative plot of [DNA] versus [DNA]/(εa − εf) for the titration of the [Pt(dmp)(L^1-κO,S)]Cl complex with ctDNA*……194

List of Tables

Chapter 2

***Table 2.1**: FT-IR wavenumber (cm^{-1}) values assigned to each functional group in HL^1 and [Pt(dmp)(L^1-κO,S)]Cl from the spectrum respectively*……57

Chapter 3

***Table 3.1:** The IC_{50} values* of three active *[Pt(dmp)(L^n-κO,S)]Cl* complexes and cisplatin *against H1975, A549 and HT-29 cancer cell lines after 48 hours*……75

***Table 3.2:** The concentration of [Pt(dmp)(L^n-κO,S)]Cl complexes, cisplatin, staurosporine and tertiary-butylhydroperoxide used to study biochemical changes in H1975, A549 and HT-29 cancer cell lines*……76

***Table 3.3:** Percentage of cells showing annexin-V binding and PI uptake in H1975 cells, A549 cells and HT-29 cells*……84

***Table 3.4:** A summary of the percentage of cells showing the elevated ROS levels in H1975, A549 and HT-29 cells after a 4 hour treatment with [Pt(dmp)(L^n-κO,S)]Cl complexes, cisplatin and tertiary-butylhydroperoxide*……101

***Table 3.5:** The percentage of cells showing the expression of nuclear p21 following an 18 hour treatment with platinum complexes and cisplatin*……110

Chapter 4

***Table 4.1:** List of reagents and preparation method followed using the Proteome Profiler™ Human Apoptosis Array Kit (ARY009, R&D Systems) for HT-29 cell lines and the RayBio® C-Series Human Apoptosis Antibody Array C1 kit for lung cancer cell lines A549 and H1975 respectively*……136

***Table 4.2**: The proteome array map (R&D Systems) for HT-29 cells*……139

***Table 4.3**: **T**he proteome array map (RayBiotech) for A549 and H1975 cells*……140

Table 4.4: *Baseline expression level of apoptotic protein (pixel density) in HT-29, H1975 and A549 cells*……141

Table 4.5*: The expression level of apoptotic proteins and the percentage change in HT-29 cells after an 18 hour treatment with concentration equivalent to* IC_{80} *values of [Pt(dmp)(*L^1*-κO,S)]Cl, [Pt(dmp)(*L^3*-κO,S)]Cl and cisplatin*……143

Table 4.6*: The expression level of apoptotic proteins in A549 cells and the percentage change caused by treatment with concentration equivalent* IC_{80} *values of [Pt(dmp)(*L^1*-κO,S)]Cl, [Pt(dmp)(*L^3*-κO,S)]Cl and cisplatin for 18 hours*……..149

Table 4.7*: The expression level of apoptotic proteins in H1975 cells and the percentage change caused by treatment with concentration equivalent* IC_{80} *values of [Pt(dmp)(*L^1*-κO,S)]Cl, [Pt(dmp)(*L^3*-κO,S)]Cl and cisplatin for 18 hours*……..156

Table 4.8: *A summary and comparison of the percentage change in expression of commonly evaluated apoptotic-regulatory proteins calculated in HT-29, A549 and H1975 cell lines respectively*……161

Table 4.9: *The expression level of HO-1 in HT-29 cells*……172

Chapter 5

Table 5.1: *Melting temperature of ctDNA* (100 μM) *in the absence and presence* 2.5 μM *[Pt(dmp)(*L^1*-κO,S)]Cl and [Pt(dmp)(*L^3*-κO,S)]Cl respectively*……189

Abbreviations, acronyms and symbols

A549	Lung cancer cell line
AO	Acridine Orange
APAF-1	Apoptotic protease-activating factor 1
ATP	Adenosine triphosphate
AV	Annexin-V
BSA	Bovine Serum Albumin
CDK	Cyclin dependent kinase
COSY	Correlated spectroscopy
ctDNA	calf thymus DNA
DIABLO	Direct IAP binding protein with low PI
DMEM	Dulbecco's Modified Eagle's Medium
dmp	5,6-dimethyl-1,10-phenanthroline
DMSO	Dimethyl sulfoxide
DNA	Deoxyribonucleic acid
dpq	dipyrido [3.2-f:2',3'-h] quinoxaline
EtBr	Ethidium bromide
FADD	Fas-associated death domain
FBS	Fetal bovine serum
FDA	Food and Drug Administration
FT-IR	Fourier Transform Infra-Red
H1975	Lung cancer cell line
HMBC	Heteronuclear Multiple Bond Correlation
HO	Hoechst-33342
HO-1	Haemoxygenase-1
HRMS	High resolution mass spectrometry

HRP	Horse radish peroxidase
HSP	Heat shock proteins
HSQC	Heteronuclear single quantum correlation
HT-29	Colorectal cancer cell line
HTRA2	Heat temperature requirement protein
IAP	Inhibitors of apoptosis
IARC	International Agency of Research on Cancer
IC_{50}	Half maximal inhibitory concentration
JC-1	5,5',6,6'-tetrachloro-1,1',3,3'tetraethylbenzimidazoylcarbocyanine iodide
MOMP	Mitochondrial outer membrane permeabilization
MTT	3-(4-5-dimethylthioazol-2-yl)-2,5-diphenyl tetrazolium bromide
NMR	Nuclear magnetic resonance spectroscopy
p21	Cyclin dependent kinase inhibitor
p53	Tumour suppressor protein 53
PBS	Phosphate buffer saline
PC	Phase contrast
phen	1.10-phenanthroline
PI	Propidium Iodide
PS	Phosphatidylserine
ROS	Reactive oxygen species
rpm	Rotations per minute
RPMI	Rosewell park memorial institute
SD	Standard deviation
Smac	Second mitochondria-derived activator of caspase
TA	Tris acetate

TBS	Tris buffer saline
T_m	melting temperature
TNF	Tumour necrosis factor
TRAIL	TNF-related apoptosis-inducing ligand
WHO	World health organization
XIAP	X-linked inhibitor of apoptosis
$\Delta\psi m$	Mitochondrial membrane potential
κ	Kappa
m/z	mass to charge ratio
mL	millilitre
µl	microliter
µM	micromolar
mmol	milimolar
ppm	parts per million

Chapter 1: Introduction and Literature review

1.1 Cancer

Cancer refers to a diverse group of potentially life-threatening diseases characterized by an uncontrollable growth of abnormal cells. These cells invade neighbouring tissues and metastasize, spreading to distant organs within the body (Sarkar *et al.*, 2013; Fares *et al.*, 2020). The transformation of normal cells to cancer cells involves a complex multistep process that is triggered by changes in the genetic material; DNA mutations, which accumulate through the process of cell division. A collection of six well-recognized biological characteristics, referred to as cancer hallmarks, play a role in the initiation and progression of cancer (*Figure 1.1*) (Hanahan and Weinberg, 2000).

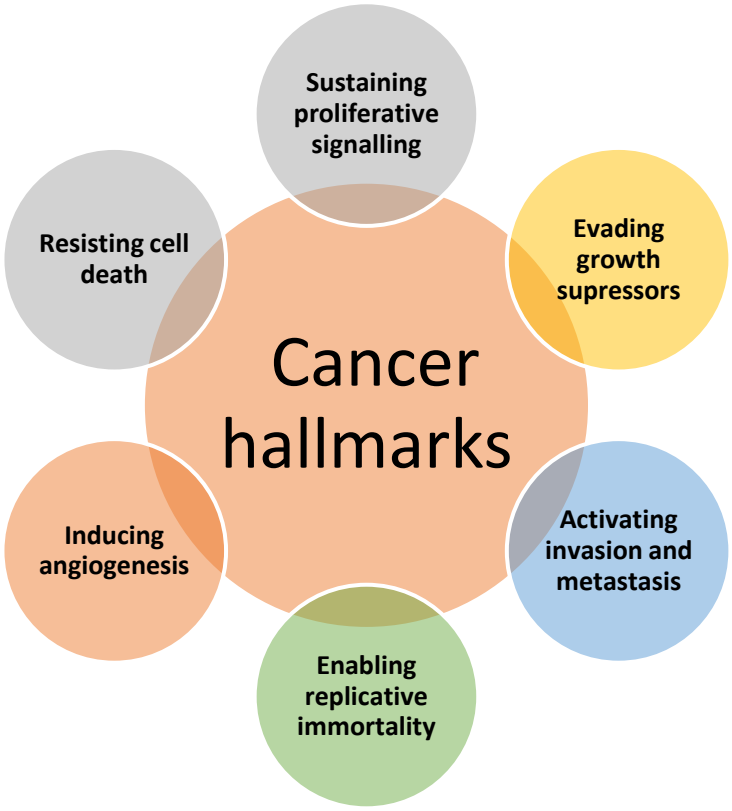


Figure 1.1*: Six hallmarks of cancer described as biological capabilities acquired during the multistep development of human tumours* (Hanahan and Weinberg, 2000, 2011).

Cancer cells are known to thrive by;

i) sustaining proliferative signalling (cells receive and send signals that promote their own growth and division despite the absence of external signals),
ii) evading growth suppressors, (acquire mutations that enable them to bypass growth-inhibiting mechanisms),
iii) activating invasion and metastasis (invade and spread within the body forming secondary tumours)
iv) enabling replicative immortality (unlike normal cells which have a limited number of divisions due to the shortening of telomeres, cancer cells maintain telomeres and can replicate indefinitely),
v) inducing angiogenesis (grow new blood vessels that supply oxygen and nutrients to developing tumours)
vi) and resisting cell death (cancer cells evade programmed cell death such as apoptosis which allows cell growth despite DNA mutations that would otherwise be repaired) (Hanahan and Weinberg, 2000, 2011).

It is important to note that not all cancers exhibit all these hallmarks to the same extent.

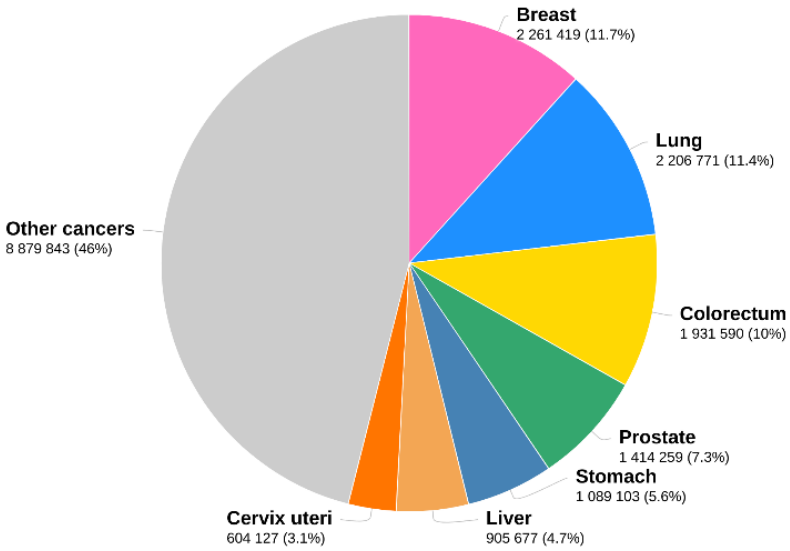
1.2 Cancer statistics

According to the GLOBOCAN database compiled by the International Agency of Research on Cancer (IARC), an estimate of 19.3 million new cancer cases and 10 million cancer deaths were reported worldwide in 2020 (Ferlay *et al.*, 2021; Sung *et al.*, 2021). Presently, cancer is the second major cause of death before the ages of 70 years worldwide. This is true not only on a global scale but also in countries with a high Human Development Index (HDI). Based on these estimates, the global cancer burden is projected to rise by 47%, reaching 28.4 million new cases by 2040 (Sung *et al.*, 2021).

Lung cancer is the leading cause of cancer-related deaths and the second most common cancer diagnosed in both men and women worldwide (incidence: 11.4%, mortality: 18%) *(Figure 1.2*) (Sung *et al.*, 2021). The high mortality rate attributed to poor prognosis and development of resistance in lung cancer patients, drives the search for new anticancer agents.

Colorectal cancer, which includes cancers of the colon and rectum, is the second major cause of cancer-related deaths and the third most common cancer diagnosed in both men and women (incidence: 10%, mortality: 9.4%) (*Figure 1.2*) (Sung *et al.*, 2021). Colorectal cancer is characterized by asymptomatic early stages, resulting in delayed diagnoses, which in turn reduce treatment options and survival rates (WHO, 2023).

A.



B.

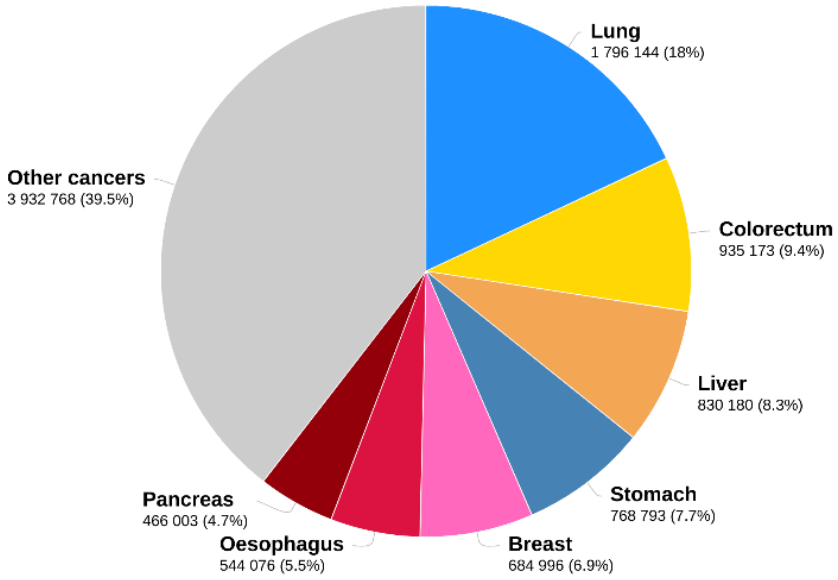


Figure 1.2: The global estimates of A) new cancer cases and B) cancer deaths reported by the World Health Organization in 2020 for both men and women at all ages (WHO, 2021). *The data shows lung and colorectal cancer as the top two most fatal types of cancer worldwide. Note: Data excludes non-melanoma skin cancers.*

1.2.1 Cancer incidence in Africa

Africa accounted for 5.7% of new cancer cases and 7.2% of cancer-related deaths. These values are significantly lower in comparison to Asia (incidence: 49.3%; mortality: 58.3%), Europe (22.8%; 19.6%), and Americas (20.9%; 14.2%), attributed to differences in population, geographical environmental factors, lifestyle and genetics (Sung *et al.*, 2021).

In South Africa, cancer is ranked the 4th primary cause of human death. Among the top five diagnosed cancers were breast (Incidence:14.3%), prostate (12.2%), cervical (9.9%), lung (8.3%) and colorectal cancers (6.8%) in that order (NCR, 2020). Despite this, lung cancer remains the primary cause of cancer-related deaths, similar to the global impact.

It is important to note that due to the underreporting of certain cancer-related deaths in registries, these estimates may not accurately reflect the extent of cancer impact in South Africa. This is primarily caused by limited access to healthcare and treatment options in specific areas of South Africa. This poses a significant public health challenge, leading to an underestimated assessment of the actual cancer burden concerning both incidence and mortality rates (Mbeje, Ginindza and Jafta, 2021).

Since there exists over 200 different types of cancer, early diagnosis is often challenging, resulting in high global rates of both cancer incidence and mortality. Therefore, current research efforts are directed towards developing biologically more potent and less harmful cancer treatments.

1.3 Cancer treatment

Traditional cancer treatment involves chemotherapy, radiotherapy and surgery, while recent advances include stem cell therapy, targeted therapy, ablation therapy, nanoparticles, and chemodynamic therapy (Debela *et al.*, 2021). Despite the integration of new approaches, conventional methods are still used in combination to achieve partial or complete remission in diagnosed patients. Treatment selection

depends on factors such as tumour type, size, location, stage of spread, and overall patient well-being.

Some large tumours may require size reduction before surgical removal, involving radiotherapy and/or chemotherapy. Radiotherapy uses high-energy radiation to destroy cancer cells, while chemotherapy administers clinically approved drugs to kill cancer cells, reduce tumour size and prevent recurrence (Baskar *et al.*, 2012; Liu *et al.*, 2021). Despite successes, therapeutic failures, especially in late-stage diagnosis, highlight the need for innovative and advanced treatment approaches alongside traditional methods.

1.4 Current platinum drugs in cancer chemotherapy

Metal-based compounds have gained significant attention in medicinal chemistry after the accidental discovery of cisplatin ($[Pt(NH_2)_2Cl_2$/cis-diaminedichloroplatinum(II) by Barnet Rosenberg in the 1960s. The anti-proliferative properties of cisplatin were initially discovered against *Escherichia-coli* bacteria in 1965 and later, it was developed as a cancer chemotherapeutic drug (Rosenberg, Van Camp and Krigas, 1965; Rosenberg, 1978). This metallodrug was the first of its kind to be approved by the Food and Drug Administration (FDA) in 1978 and has been successfully used to treat testicular cancer for which it has a 90% cure rate (Rosenberg, 1978). Cisplatin has also been used in a wide range of other cancers such as ovarian, head and neck, bladder, lung cancer; lymphomas, myelomas (cancer of immune system) and melanomas (skin-related cancers) (Rosenberg, 1978; Wheate *et al.*, 2010; Dasari and Tchounwou, 2014; Brown, Kumar and Tchounwou, 2019).

The success of cisplatin in cancer treatment is based on its mechanism of action with the DNA molecule where the electrophilic platinum centre of cisplatin and nucleophilic nitrogen (N-7) of purine residues, usually guanine, form an irreversible covalent bond, thereby producing DNA adducts. Platinum-DNA adducts prevent DNA unwinding, halting the replication and transcription processes which trigger the DNA damage response and ultimately induce cell death. Cisplatin and

analogues (i.e carboplatin, oxaliplatin) are classified as alkylating agents despite not transferring alkyl groups to the DNA. They modify the DNA through covalent (irreversible) binding. Although cisplatin has been effective in treating cancers, it has dose-limiting toxicities such as nephrotoxicity, neurotoxicity, and ototoxicity. Moreover, the lack of selectivity, low bioavailability, and drug resistance have reduced its efficacy.

Second and third-generation analogues of cisplatin such as carboplatin, oxaliplatin, nedaplatin, lobaplatin, and heptaplatin have been developed to address these limitations and each have unique advantages over the parent drug (*Figure 1.3*). The structural difference between cisplatin and carboplatin is the replacement of chloride leaving groups with cyclobutanedicarboxylate ligand, which significantly reduced toxicity without compromising the anti-tumour potency (Dasari and Tchounwou, 2014). Oxaliplatin replaced both chlorines and amines with oxalate and 1,2-diaminocyclohexane (chiral 1R,2R-dach) ligands. The oxalate ligand, which acts as a leaving group, was found to play a major role in reducing the reactivity of the drug and improving its safety profile over cisplatin (Tyagi, Gahlot and Kakkar, 2008). The dach ligand was reported to increase passive uptake of the drug due to the increased lipophilicity (Ali, McCrudden and McCarthy, 2017; Lucaciu *et al.*, 2022). As result, oxaliplatin has been used in combination with other drugs such as 5-fluorouracil (5-FU) and folinic acid to treat metastatic colorectal cancer in patients with low tolerance for cisplatin (Jonker *et al.*, 2006).

Nedaplatin features cis-ammine and a non-leaving group ligand (glycolate) which increases its water solubility and reduces nephrotoxicity. It has mainly been used in combination therapy to manage urological tumours (Pedrosa *et al.*, 2018). Lobaplatin showed greater stability and lower toxicity compared to cisplatin and carboplatin. It demonstrated less gastrointestinal, auricular, liver and renal toxicity and displayed efficacy across various preclinical tumor models, overcoming resistance observed with cisplatin and carboplatin in some instances (McKeage, 2001; Wang *et al.*, 2015; Cheng *et al.*, 2019)

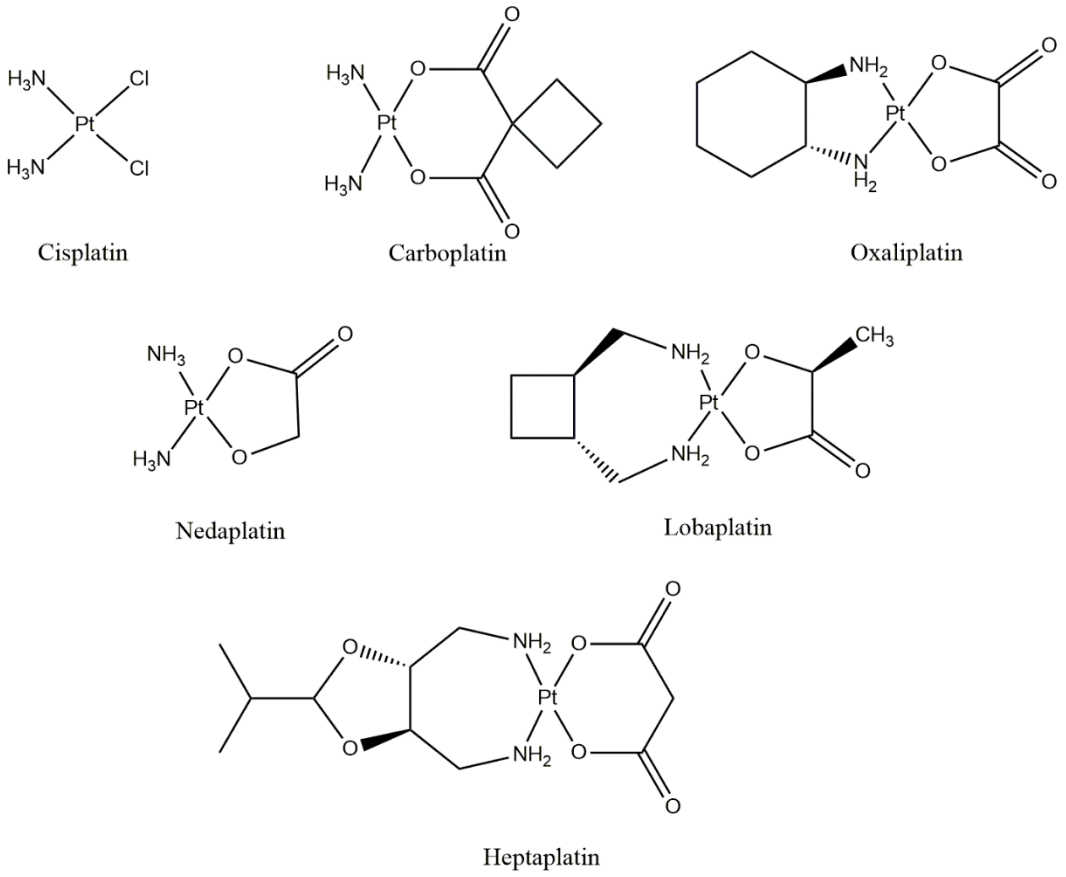


Figure 1.3: Chemical structures of six clinically approved platinum(II)-drugs currently used in cancer chemotherapy*. (Worldwide approved; cisplatin, carboplatin, oxaliplatin; Japan: nedaplatin; China approved: lobaplatin; Korea approved: heptaplatin).*

Heptaplatin is another third-generation platinum derivative that has been approved for use in Asia (Johnstone, Pil and Lippard, 2015). Currently, only cisplatin, carboplatin, and oxaliplatin are FDA-approved for clinical use worldwide while nedaplatin, lobaplatin, and heptaplatin have been approved in parts of Asia; including Japan, China and Korea respectively (Johnstone, Suntharalingam and Lippard, 2016; Ali, McCrudden and McCarthy, 2017).

Despite the progress made in developing second and third-generation platinum complexes, resistance to these agents remains a significant challenge in cancer treatment. This may be due to their mechanism of action, as each of these platinum complexes interact with DNA via a similar hydrolysis-mediated mechanism as

cisplatin. As a result, researchers are investigating new approaches to developing platinum complexes with structures that differ significantly from the typical cisplatin paradigm, favouring a non-covalent/reversible mechanism of action with DNA.

1.4.1 Platinum(II)-diimine complexes

Metallodrug research attempts to develop square planar platinum complexes that interact with DNA through a non-covalent mechanism, in contrast to the covalent binding seen with cisplatin and its analogues. This exploration involves the inclusion of diverse ligands, with a focus on diimine ligands in this study.

Diimine ligands are organic compounds possessing two imine groups (R_1R_2-C=N-$R_3)_2$ that coordinate to transition metals in a bidentate fashion via nitrogen donor atoms. Metal complexes coordinated by diimine ligands have been investigated as catalysts for various organic transformations, used as building blocks for the synthesis of functional materials such as luminescent polymers and shown as potential anticancer agents due to their ability to interact with the DNA molecule and induce cell death (Hissler *et al.*, 2000).

Common aromatic diimine ligands such as the 1,10-phenanthrolines (phen), 2,2-bipyridine (bp), and dipyridophenanzine (dppz) have been used in ruthenium, copper and platinum complexes that showed potential anti-cancer activities *in vitro* and *in vivo* due to their DNA intercalating properties (Strekas *et al.*, 1995; Di Pietro *et al.*, 2021). These ligands can also be functionalized with other groups to modulate the electronic properties and reactivity of the complex.

Previous studies have reported that platinum(II) complexes coordinated by 1,10-phenanthroline (phen) or a range of methylated-phenanthroline and ancillary ligands such as ethylenediamine (en) or chiral 1,2-diaminocyclohexane (R,R-dach or S,S-dach) have potential activity against the L1210 murine leukaemia cancer cell line (Wheate *et al.*, 2007a). The 50% inhibitory concentration (IC_{50}) values of active complexes; $[Pt(phen)(1S,2S\text{-dach})platinum]^{2+}$ (0.13 μM), $[(5,6\text{-dimethyl-phen})(1S,2S\text{-dach})platinum]^{2+}$ (0.00092 μM) and $[(5\text{-methyl-phen})(1S,2S\text{-dach})platinum]^{2+}$ (0.033 μM) displayed a higher cytotoxicity than cisplatin (1.0 μM) with the lead complex [(5,6-dimethyl-1,10-phenanthroline)(1S,2S-

dach)platinum]$^{2+}$ being a 100-fold more cytotoxic than cisplatin (Wheate *et al.*, 2007).

Brodie *et al* investigated platinum complexes bearing 1,10-phenanthroline (phen) and five variations of the methyl-substituted phenanthrolines (4-Methyl-phen, 5-methyl-phen, 4,7-dimethyl-phen, 5,6-dimethyl-phen and 3,4,7,8-tetramethyl-phen) against 1,2-ethylenediamine as the ancillary ligand. The platinum complexes with methylated derivatives were more cytotoxic than the complex containing unsubstituted phen since IC_{50} values were found to be 2.8 ± 0.8 μM and 1.5 ± 0.3 μM for [Pt(5-Me-phen)(en)]$^{2+}$ and [Pt(5,6-phen)(en)]$^{2+}$ respectively, whereas the complex, [Pt(phen)(en)]$^{2+}$ had an IC_{50} value of 9.7 ± 0.3 μM. Other methylated phen variations were less active, with IC_{50} values greater than 50 μM (Brodie, Collins and Aldrich-Wright, 2004).

The established structure-activity relationship indicated that the presence of methyl substituents on position 5 and 5,6 of 1,10-phenanthroline played a major role in the biological activity of the square planar platinum(II) complexes (*Figure 1.4*). The ancillary ligand 1S,2S-diaminocyclohexane (S,S-dach) was shown to improve efficacy of platinum complexes compared to R,R-enantiomer which was presumed to be unexpected since oxaliplatin possesses the R,R-dach instead and has high activity (Fisher *et al.*, 2007; Kemp *et al.*, 2007). In contrast, platinum complexes containing the achiral ethylenediamine (en) ligands had the least cytotoxic potential (Brodie, Collins and Aldrich-Wright, 2004; Wheate *et al.*, 2007b).

Another recent study on platinum(II) complexes coordinated to a chiral diamine, 1S,2S-dach or 1R,2R-dach and 1,10-phenanthroline or 3,4,7,8-tetramethyl-1,10-phenanthroline has been investigated in the renal proximal tubule cell line (HK-2) and ovarian cancer cell line (A2780). All platinum(II) complexes exhibited lower cytotoxicity in HK-2 cells (IC_{50} 1.7-25 μM) than in ovarian cancer cells (A2780) or cisplatin-resistant cells A2780cisR (IC_{50} 0.2-2.1 μM) (Ng *et al.*, 2018).

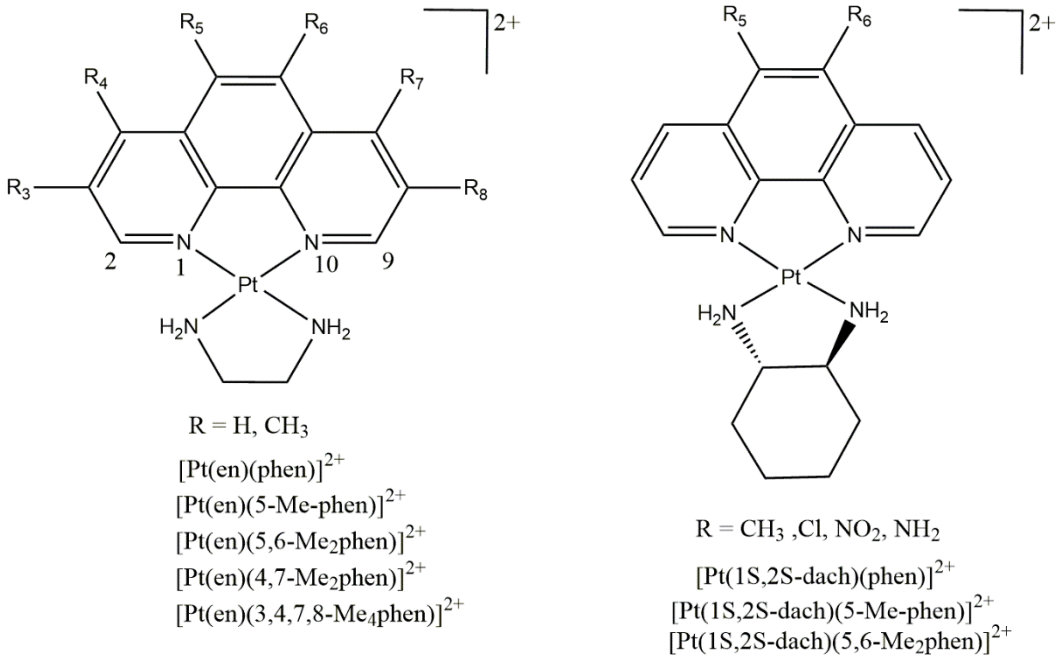


Figure 1.4**: **Biologically active platinum(II)-diimine complexes with potential anticancer activity reported in literature (Brodie, Collins and Aldrich-Wright, 2004; Wheate *et al.*, 2007b). *Phen represent 1,10-phenathroline and ancillary ligands en, 1S,2S-dach and 1S,2S-dacp represents ethylenediamine, 1,2-diaminocyclohexane and 1,2-diaminocyclopentane respectively. The methyl substituted phen are indicated by the position of methyl groups.*

1.4.2 Platinum(II)-acylthiourea complexes

Acyl/aroyl-thiourea ligands with the general formula (R_1-C(O)-$NH_{(1)}$-C(S)$_{(2)}$ -$NR_2R_{3(3)}$) are organosulfur compounds derived from thiourea (>$N_{(1)}$-C(S)$_{(2)}$-$N_{(3)}$<) with applications in the field of organic synthesis, coordination chemistry, material sciences and medicinal chemistry (Saeed, Flörke and Erben, 2014; Saeed *et al.*, 2019). Thioureas possess two amine groups and have a C_2 symmetry about the thiocarbonyl (C=S) group. Acy/aroyl thiourea ligands contain an acyl or aryl (R-C(O)-) on the amine group in position one, replacing one of the two amine protons (1-acyl-3-(unsubstituted) (*Figure 1.5*). The acyl or aroyl is distinguished by the R substituent being either an alkyl or aromatic group. The mono substituted and disubstituted version of these ligands (1-acyl-3-(monosubstituted)thiourea or 1-acyl-3,3-disubstituted)thiourea) contain a substituent (R) on the amine in position 3, replacing one or both proton (Saeed, Flörke and Erben, 2014).

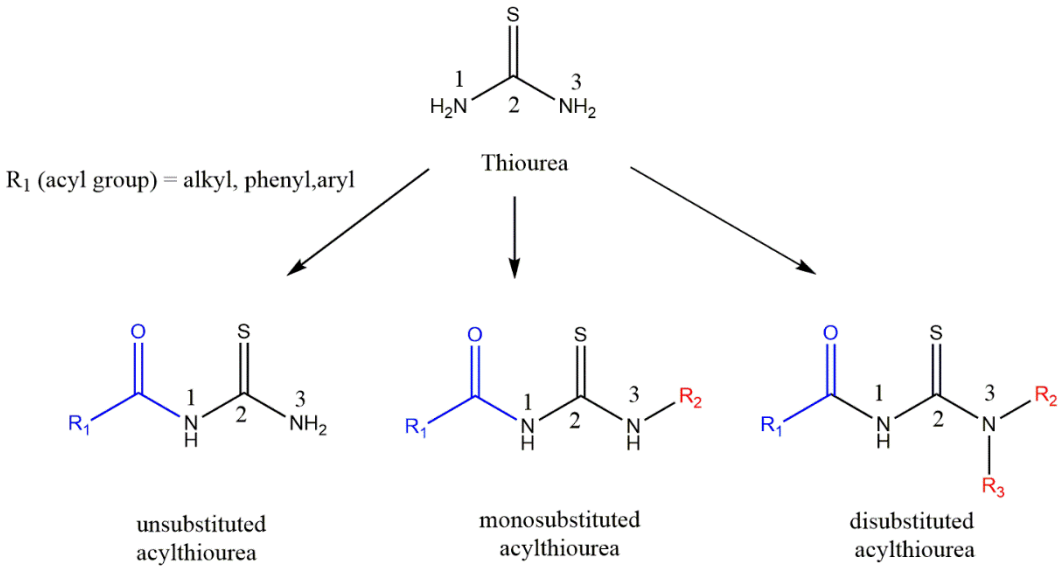


Figure 1.5: The molecular structure of thiourea derived acylthiourea ligands distinguished by the presence of an acyl group (blue) in the 1-amine (position -1). *The monosubstituted and disubstituted (N-monoalkyl-N'-acylthiourea and N,N-dialkyl-N'-acylthiourea) forms are indicated by the presence of R_2 or/and R_3 substituents in 3-amine (position-3).*

Acylthiourea ligands have gained attention in research due to their versatile coordination modes, which makes them useful in coordination chemistry and easy preparation. Their coordination behaviour changes depending on the metal they react with. Typically, these ligands coordinate to Pt(II) and Pd(II) in a bidentate manner via sulfur and oxygen atoms (*S,O*). They also tend to coordinate to Ru(II), Rh(III), and Ir(III) through the sulfur donor atom (Lapasam and Kollipara, 2020).

Metal complexes bearing acylthiourea ligands have been shown to have improved biological activity compared to the ligands on their own (Saeed *et al.*, 2019; Mitrea and Cîrcu, 2021). For example, a recent study found that ruthenium(II)-diphosphine complexes containing acylthiourea ligand were effective against lung (A549) and breast (MDA-MB-231) cancer cell lines (Grawe *et al.*, 2022). All the complexes showed cytotoxicity against the cancer cell lines, with IC_{50} values in the micromolar range (0.07–0.70 μM). One of the complexes was 160 times more cytotoxic than

cisplatin against A549 cells, indicating improved activity towards the lung cancer cell line. (Grawe *et al.*, 2022).

The incorporation of acylthiourea ligands to transition metals have been previously shown to possess, antimicrobial, antimalarial and antitumor properties (Egan *et al.*, 2004; Wu *et al.*, 2005; Kangara *et al.*, 2019).

Plutin *et al* found that a class [Pt(II)-(dppf)(disubstitutedacylthiourea]PF_6 complexes where dppf represents 1,1-bis(diphenylphosphine)ferrocene, have anti-*Myocobacterium tuberculosis* activity against the H37Rv strain. The complexes were found to be 10-fold to 20-fold more active than their respective free ligands. A minimum inhibitory concentrations (MIC) of 4.74 ± 0.06 μmol/mL for the most active complex Pt(dppf)(*N*,*N*-diethyl-*N*'-furoylthiourea)]PF_6 was reported (Plutín *et al.*, 2016). Egan *et al* investigated the antimalarial activity of platinum(II) complexes of 2,2'-bipyridyl (bp), 1,10-phenanthroline (phen) and benzoylthiourea with different alkyl substituents. Among the eight complexes tested, four demonstrated antimalarial activity *in vitro*, with [Pt(*N*,*N*-di-(2-hydroxyethyl)-*N*'-benzoylthiourea)(4,4'-di-tert-butyl-2,2'-bipyridyl)]Cl showing the highest level of activity (Egan *et al.*, 2004). Furthermore, Wu *et al* found that the intercalative DNA binding properties of water soluble platinum(II)-acylthiourea-diimine complexes containing bp and phen against a hydrophilic (*N*,*N*-di-(2-hydroxyethyl)-*N*'-benzoylthiourea ligand were comparable to those of ethidium bromide with the phenanthroline moiety showing a higher binding affinity than the 2,2-bipryrine (Wu *et al.*, 2005).

A recent study conducted by Kangara *et al*. from our research group, indicated that neutral platinum(II)-complexes of the type [Pt(phen)(L-κS_2)], coordinated by 1,10-phenathroline and disubstituted acylthiourea in a monodentate fashion (S) have potential anticancer activity. The IC_{50} values of 2.39 ± 0.33 μM and 6.43 ± 0.94 μM were reported for [Pt(phen)(*N*,*N*-dibutyl-*N'*-1-napthoylthiourea)] and [Pt(phen)(*N*,*N*-diethyl-*N'*-1-napthoylthiourea)] respectively, against the A549 lung cancer cells (Kangara *et al.*, 2019).

1.5 Drug-DNA interactions

Many FDA-approved anticancer agents primarily target DNA as their key pharmacological site (Gibson, 2002; Weber, 2015). Therefore, the interaction between small molecules and nucleic acids has been intensely studied since it is important to understand their mechanism of action. Cancer drugs like doxorubicin bind to DNA and distort the DNA backbone, preventing the binding of proteins responsible for DNA replication and gene transcription (Sirajuddin, Ali and Badshah, 2013; Aleksić and Kapetanović, 2014). This disrupts the normal functioning of cells and leads to the inhibition of cell replication, causing cell cycle arrest.

1.5.1 Covalent binding

Anticancer drugs like cisplatin exert their effects by binding covalently to the DNA, forming adducts and permanently altering the natural structure of DNA. Covalent binding is considered irreversible, causing complete inhibition of DNA function and induce cell death (Rehman *et al.*, 2015). The advantage of covalent binding of small molecules to DNA is the high binding strength. This causes distortion of the DNA sugar-phosphate backbone, preventing proteins such as DNA/or RNA polymerase to bind, which affects both transcription and replication processes (Sirajuddin, Ali and Badshah, 2013).

Cisplatin is a prodrug that is activated through aquation upon entering the cell. The chlorine atoms are displaced with water molecules, resulting in an electrophilic product that reacts with DNA. Cisplatin thus undergoes a nucleophilic attack by the nitrogen-7 of guanines, forming covalent cross links between DNA strands (inter-strand-crosslinks) and within the same DNA strand (intra-strand crosslinks) (Dasari and Tchounwou, 2014).

1.5.2 Non-covalent binding

The non-covalent binding mode of DNA refers to the process by which molecules interact with DNA without forming a permanent covalent bond (reversible). This binding mode relies on electrostatic forces, hydrogen bonding, van der Waals forces and hydrophobic interactions. Non-covalent binding is considered less toxic and is typically preferred over covalent adduct formation (Sirajuddin, Ali and Badshah, 2013; Puyo, Montaudon and Pourquier, 2014). The non-covalent binding modes of small molecules are classified into three groups:

i. Intercalation
ii. Groove binding (major, minor)
iii. Electrostatic interactions

1.5.2.1 Intercalation

Intercalating agents are typically aromatic planar or nearly planar molecules with a size and shape that allows them to fit between the base pairs of DNA. They bind to the DNA by stacking between the base pairs perpendicular to the DNA backbone and cause distortion and unwinding of the duplex by breaking the hydrogen bonds between the bases. DNA-intercalating complex is mainly stabilized by π-π stacking interactions between the DNA base pairs. The other molecular forces that maintain the stability of a DNA-intercalating complex are van der Waals, hydrogen bonding and hydrophobic interactions (Sirajuddin, Ali and Badshah, 2013). Examples of intercalating agents include doxorubicin, which is a chemotherapy drug used to treat a variety of cancers (i.e breast and lung cancer), and ethidium bromide, a fluorescent dye. Metal-based drugs that have been shown to intercalate to the DNA include ruthenium-based complexes (NAMI-A and KP1019) and copper based complexes e.g Triapine which bind to the DNA and inhibits the activity of ribonucleotide reductase, an important enzyme for DNA synthesis (Ishiguro *et al.*, 2014; Alessio and Messori, 2019). Other ruthenium complexes with aromatic diimine ligands have been reported to have intercalative binding properties (i.e $[Ru(phen)Cl_2]$. Chiral octahedral complexes made with zinc, iridium, iron, cobalt, osmium, rhodium, and ruthenium, as well as tetrahedral complexes like

$[Co(phen)2]^{2+}$ and $[Cu(phen)_2]^{2+}$ have also been shown to have intercalative binding properties (García-Ramos *et al.*, 2017).

1.5.2.2 Groove binding

The double helix contains major and minor grooves formed by the twisting of the two DNA strands. Major groove binding occurs where the backbone strands are far apart, with a width of 11.6 Å and depth of 8.5 Å, while minor groove binding occurs where they are close together with a smaller depth of 8.2 Å (Neidle, 2001). The major groove has multiple strong binding sites and is easily accessible for bulky molecules, whereas the minor groove has fewer binding sites and is smaller but often unoccupied, making it available for attack by small drug molecules. Many drugs tend to bind to the minor groove as their primary binding site (i.e distamycin, netropsin, and Hoechst-33258).

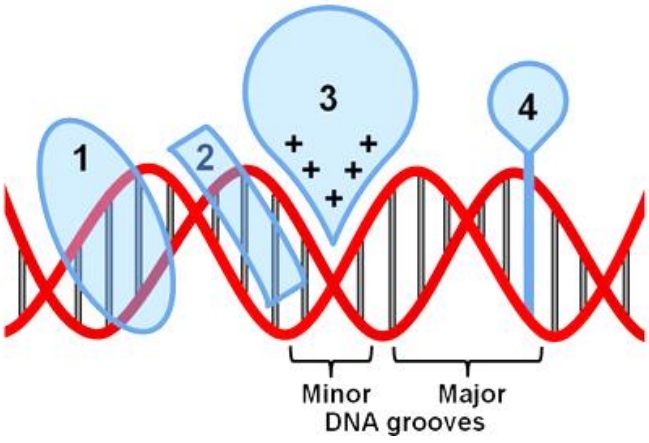


Figure 1.6: *Illustration of possible non-covalent DNA binding modes 1) major groove binding 2) minor groove binding, 3) electrostatic interactions and 4) Intercalation* (Almaqwashi *et al.*, 2016)

1.5.2.3 Electrostatic interactions

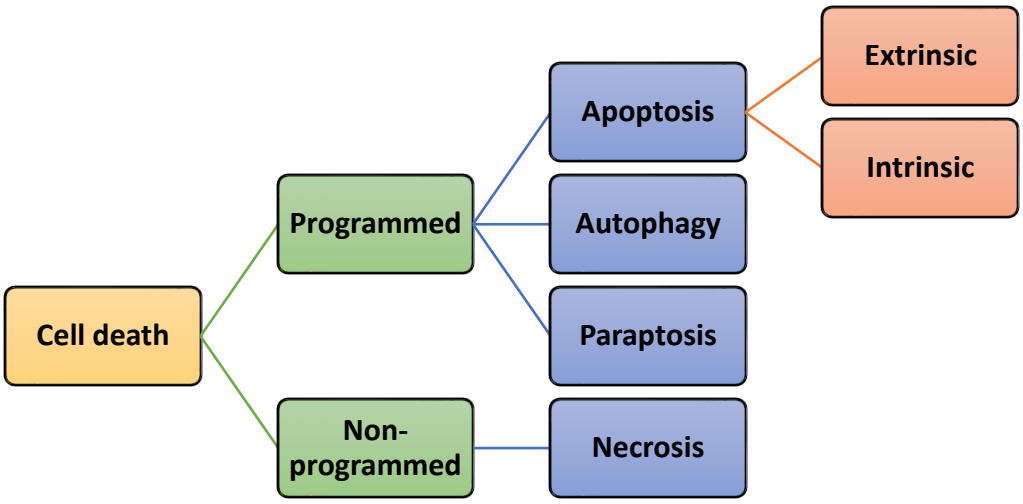
Electrostatic interactions occur between the small cationic molecules and negatively charged phosphate backbone of DNA. This mode of binding is usually referred to as external binding. In most cases, the luminescence of cationic metal

complexes upon binding to the DNA is highly dependent on ionic strength (Sirajuddin, Ali and Badshah, 2013).

Most small molecules of biological importance are known to interact with DNA through non-covalent interactions. Several studies have reported that more than one binding mode of interaction for a small molecule is likely to occur. Thus, mixed binding modes may be related to their mechanism of action and therapeutic efficiency (Sirajuddin, Ali and Badshah, 2013).

1.6 Cell death mechanisms and cancer

Cell death is a naturally occurring event that eliminates damaged, infected, or abnormal cells to maintain cellular homeostasis (Tower, 2015). However, the balance between cell survival and cell death is not maintained in cancer as cancer cells accumulate by evading cell death (Elmore, 2007; Kerr, 1994). The success of most anticancer drugs is based on their ability to induce cell death in highly proliferative tumour cells via regulated pathways such as apoptosis (Fontana *et al*, 2020). Highly regulated forms of cell death involve a series of molecular events that stimulate a controlled death referred to as programmed cell death (pcd) whereas the unregulated forms of cell death are referred to a non-programmed cell death (non-pcd) or accidental cell death leading to inflammation and diseases. The types of pcd known to date include apoptosis, autophagy and paraptosis while non-pcd mainly includes necrosis (Kroemer *et al.*, 2009). It is important to identify cell death pathways induced by potential anticancer chemotherapeutic agents to understand their possible mode of action.



Scheme 1.1: *Classification of cell death mechanism categorized into programmed cell death which include apoptosis, autophagy and paraptosis; as well as non-programmed cell death, necrosis.*

1.6.1 Apoptosis

Apoptosis is a highly regulated cell death mechanism which is key in the regulation of tissue homeostasis, necessary to maintain multicellular organisms. Cells undergoing apoptotic cell death typically exhibit a characteristic morphology that includes cell membrane blebbing, cell shrinkage, chromatin condensation, cell detachment from surface, externalization of phosphatidylserine, nuclear fragmentation and the formation apoptotic bodies (Kerr, Wyllie and Currie, 1972; Brauchle *et al.*, 2014).

Apoptosis is initiated either via the i) intrinsic (mitochondria-mediated) pathway or ii) extrinsic (extracellularly activated) pathway. The intrinsic apoptotic signaling pathway occurs in response to internal cell stress, such as DNA damage and involves non-receptor mediated stimuli that produce intracellular signals which directly act on targets within the cell and mitochondrial initiated events (Fulda and Debatin, 2006). On the other hand, the extrinsic signaling pathway occurs in response to external cellular damage and initiates apoptosis through transmembrane

receptor mediated interactions. This involves death receptors that are members of the tumour necrosis factor (TNF) superfamily. Both pathways result in the activation of pro-apoptotic proteins called the caspases (Wang and El-Deiry, 2003; Elmore, 2007; Carneiro and El-Deiry, 2020).

1.6.1.1 Caspases activation and apoptosis

Caspases are proteolytic enzymes synthesized in their inactive forms (procaspases) and are activated upon a response to apoptotic stimuli. Caspases become activated when they are cleaved on peptide bonds adjacent to aspartic residues or glutamate residues (Seaman *et al.*, 2016). Mammalian caspases are subdivided into three groups which are initiator caspases (caspase-2, -8, -9 and -10), executioner/effector caspases (caspase-3, -6 and -7) and inflammatory caspases (caspase-1, -4, -5, -11 and -12). Initiator caspases function to initiate the apoptosis signal pathway whereas the executioner caspases carry out the proteolysis of several proteins found in the cytoplasm and nucleus resulting in apoptotic cell death (Fulda and Debatin, 2006). The proteolysis of cytoskeletal proteins such as actin or fodrin result in a loss of cell shape, and this is a morphological feature of apoptotic cells. Inflammatory caspases do not function in apoptosis; they are involved in inflammatory cytokine signalling and other types of inflammatory cell death such as pyroptosis (Wang and Lenardo, 2000).

1.6.1.2 Extrinsic apoptotic pathway

The extrinsic signalling pathway of apoptosis is initiated outside the cell when death receptors located on the plasma membrane bind specific ligands such at tumour necrosis factor ligands (e.g TNF), Fas ligand (FasL) or TRAIL ligands ***(****Figure 1.7****)*** (Wang and El-Deiry, 2003; Elmore, 2007).

The binding of the death ligands causes the death domain (DD) in the receptors to aggregate and recruit respective adaptor proteins, Fas-associated death domain (FADD) or tumour necrosis factor receptor-associated death domain (TRADD) to form a death inducing signalling complex (DISC). The DISC transmits death signal

to the internal part of the cell by activating the initiator pro-caspase-8 into active caspase-8. Caspase-8 ultimately activates effector caspases such as caspase-3, -6 and -7 which cleave important structural and DNA proteins, causing apoptosis.

The dysregulation of this pathway has been implicated by anti-apoptotic proteins such as the cellular-Flice-like inhibitor (c-FLIP) and inhibitors of apoptosis (IAPs) (*Figure 1.7*). The c-FLIP protein inhibits apoptosis by interfering with the formation of DISC, which blocks the activation of procaspase-8 to active caspase-8 (Bagnoli, Canevari and Mezzanzanica, 2010). IAPs block pro-apoptotic protein caspase-8, and are in turn inhibited by the binding of Smac/DIABLO, which is a pro-apoptotic protein released into the cytosol from the mitochondria upon apoptosis induction (Roberts *et al.*, 2001).

1.6.1.3 Intrinsic apoptotic pathway

The intrinsic (mitochondria-mediated) apoptotic pathway is triggered by internal cellular stressors such as radiation, hypoxia, DNA damage and oxidative stress. This pathway is regulated by pro-apoptotic and anti-apoptotic Bcl-2 family of proteins; (Bad, Bax, Bak, Bcl-xS, Bid) and (Bcl-2, Bcl-x, Bcl-w, Bcl-xL) respectively (Bouillet and Strasser, 2002; Tzifi *et al.*, 2012). The cellular stress leads to an increase in mitochondrial membrane permeability, which causes the release of pro-apoptotic, cytochrome c from the the mitochondria into the cytosol. Cytochrome c then binds to the protein called apoptotic protease-activating factor-1 (APAF-1), along with procaspase-9 to form the apoptosome complex, which activates caspase-9 and subsequently, executioner caspases (caspase-3/7), ultimately resulting in cell death (*Figure 1.7*) (Elmore, 2007).

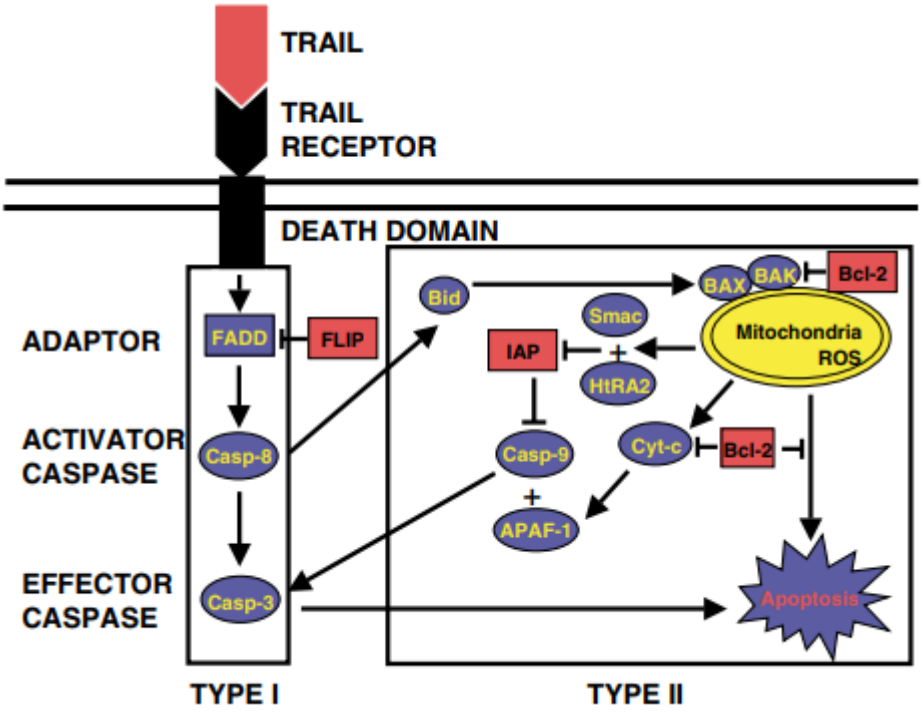


***Figure 1.7**: **A diagram showing the components of the extrinsic apoptotic signaling pathway (Type I) and intrinsic apoptotic signaling pathway (Type II).** Type I is initiated by the binding of TRAIL-Ligand on the TRAIL receptor located on the plasma membranes. The death domain recruits adaptor proteins (FADD) forming a death inducing signal complex (DISC) which activates caspase-8. Active caspase-8 cleaves effector procaspase-3 to form active caspase-3, which subsequently induces apoptosis. Intrinsic apoptotic signalling pathway (Type II) is mediated by the formation of mitochondrial outer membrane pores (MOMP) that release cytochrome c and other apoptotic proteins (Smac/DIABLO and HTRA2/Omi) to promote caspase-9 activation by binding to APAF-1. A link between the extrinsic and intrinsic apoptotic signalling pathway occurs via the activation of Bid by caspase-8 cleavage. Activated Bid (tBid) is then translocated to the mitochondria and activates Bax/Bak through oligomerization to form MOMP. Bcl-2 inhibits Bax/Bak activation and IAPs block procaspase-9 activation. Smac/DIABLO and HTRA2/Omi promote apoptosis by binding IAPs. Active caspase-9 or caspase-8 ultimately cleaves procaspase-3 and activate it to caspase-3, leading to apoptosis. Figure reproduced from the original text* (Wang and El-Deiry, 2003).

1.6.2 Paraptosis

Paraptosis is a type of programmed cell death (non-apoptotic) previously described as type III cell death until the term paraptosis was first introduced by Sabina Sperandio in 2000, which implies parallel to apoptosis (Sperandio, de Belle and Bredesen, 2000). Paraptosis causes morphological changes that are distinct from apoptosis and necrosis. These features primarily include cytoplasmic vacuole formation, enlargement of the mitochondria and endoplasmic reticulum as well as late mitochondrial swelling. Typical apoptotic features such as membrane blebbing, chromatin condensation, nuclei fragmentation are not observed in this type of cell death. Although the mechanism of paraptosis is not clearly understood, it is known to be independent of caspase activation (Sperandio, de Belle and Bredesen, 2000). Paraptotic cell death has attracted attention in the field of cancer research as it is a preferred method of inducing cell death in cancers that are resistant to apoptosis.

1.6.3 Autophagy

Autophagy is a type of programmed cell death originally described as a survival mechanism where cells degrade and recycle their own components to maintain cellular homeostasis (Denton and Kumar, 2019). The process of autophagy involves delivering cytoplasmic components to lysosomes which contain hydrolytic enzymes that break down the cell contents (Jung, Jeong and Yu, 2020). This process occurs in a stepwise manner, beginning with the formation of autophagosomes, which are double membrane sacs that contain cytoplasmic materials of damaged organelles and/or proteins (Schwartz, 2021). These autophagosomes then fuse with lysosomes, thereby causing the degradation of materials contained within the cell, which helps the cell survive by recycling their breakdown products for use as an energy source in anabolic pathways (Jung, Jeong and Yu, 2020). This process is triggered by environmental stresses such as starvation, lack of growth factors or infections by pathogens.

The autophagic related cell death can be categorized into three types i) autophagy-associated cell death, which occurs when autophagy is induced alongside apoptosis or other forms of cell death; ii) autophagy-mediated cell death, where the autophagy

pathway triggers apoptosis or other cell death pathways; and iii) autophagy-dependent cell death, which happens independently of apoptosis or necrosis (Denton and Kumar, 2019).

1.6.4 Necrosis

Necrosis is an uncontrolled form of cell death that occurs when a cell is subjected to severe stress such as hypoxia (low oxygen level) or toxin exposure. Cells undergoing necrotic cell death are morphologically characterized by the enlargement of cellular organelles such as the endoplasmic reticulum and mitochondria, disruption of the cell membrane and an uncontrolled release of cellular contents into the extracellular space, which causes inflammation and damage to surrounding tissues (Hajibabaie, Abedpoor and Mohamadynejad, 2023; Khalid and Azimpouran, 2023).

When the contents of the cells are released, they can overwhelm the body's detoxification systems, potentially resulting in conditions such as acute gout attacks, cognitive dysfunction and the tumour lysis syndrome. Necrosis is accompanied by the release of proteolytic enzymes, which are stored in lysosomes and capable of digesting cellular components (Jung, Jeong and Yu, 2020; Hajibabaie, Abedpoor and Mohamadynejad, 2023). Chemotherapeutic agents that cause cell death by necrosis are usually not preferred since it increases morbidity in cancer patients while programmed cell death such as apoptosis are preferred (Renehan, 2001) .

Recent studies have highlighted secondary necrosis as a regulated form of cell death that occurs after the completion of apoptotic cell death, especially when cells remain uncleared by phagocytes. The precise mechanism underlying this process is still unknown (Rogers *et al.*, 2017).

1.7 Research proposal

1.7.1 Problem statement

Cancer poses significant challenges in detection, treatment and survival as it is responsible for one in six deaths worldwide (Debela *et al.*, 2021). The poor efficacy of current cancer treatments and the expense of targeted treatments with monoclonal antibodies warrants a search for alternative platinum complexes as chemotherapeutic agents.

Rationale: This research project intends to address the pressing need for alternative cancer chemotherapeutic agents by focusing on the synthesis, characterization and anticancer evaluation of square planar platinum(II) complexes, bearing two bidentate coordinating ligands; being variations of *N*,*N*-dialkyl-*N*'-acylthiourea ancillary ligands and functional diimine ligands. This study was inspired by previous work conducted in our laboratory where the potential anticancer activity of this class of chelate platinum(II) complexes; [Pt(diimine)(*N*,*N*-dibutyl-*N*'-acylthiourea)]$^{+}$ was investigated against H1975 lung cancer cells (Magwaza, 2017). The proposed platinum(II) complexes differ from conventional cisplatin, since they possess distinct ligands (planar aromatic diimines and lipophilic acylthioureas) that could potentially yield non-covalent DNA interaction, a more preferred and safer mode of DNA interaction as opposed to covalent binding by alkylating agents.

Evaluation of these platinum complexes as cancer chemotherapeutic agents will involve comprehensive *in vitro* studies on lung and colorectal cancer cells. These include assessing cell viability and apoptosis induction upon exposure to different complex concentrations. Insights into their interactions with cellular components such as the DNA molecule and effect on cell death pathways compared to established platinum drugs can guide future investigations.

Overall, this project intends to elucidate the mechanisms of action of promising platinum complexes and identify potential target molecules for future investigations. Ultimately contributing to the advancement of cancer treatment options to improve patient survival outcomes.

1.7.2 Aim

The aim of this study was to synthesize and characterize [Pt(diimine)(*N*,*N*-dialky-*N*'-acylthiourea)]$^{+}$ complexes where the disubstituted acylthiourea ligands coordinate in a bidentate fashion to the platinum centre through the sulfur and oxygen donor atoms (*O*,*S*). Secondly, the aim was to investigate the anticancer activity of the platinum complexes against lung and colorectal cancer cell lines and determine their binding mode to the DNA target molecule.

1.7.3 Objectives

- Synthesize and characterize:
  - variations of *N*,*N*-dialky-*N*'-acylthiourea ligands (HL^n),
  - platinum diimine precursors; $PtCl_2$(1,10-phenanthroline) and $PtCl_2$(5,6-dimethyl-1,10-phenanthroline),
  - platinum complexes; [Pt(phen)(L^n-κ*O*,*S*)]Cl and [Pt(dmp)(L^n-κ*O*,*S*)]Cl respectively.
- Evaluate the efficacy of nine [Pt(diimine)(L^n-κ*O*,*S*)]$^{+}$ against lung (H1975, A549) and colorectal (HT-29) cancer cell lines using a cell viability (MTT) assay and identify active complexes from the series.
- Determine the IC_{50} values of active platinum complexes.
- Evaluate the effects of active platinum complexes on cancer cell morphology to exclude those that induce changes consistent with necrosis.
- Determine if platinum complexes induce apoptosis by evaluating their effects on apoptotic markers such as annexin-V binding and activation of caspase-3/7.
- Identify which apoptotic pathway is activated; i.e. intrinsic or extrinsic pathway by measuring caspase-8 activity and mitochondrial membrane potential.
- Determine the effect of platinum complexes on the induction of oxidative stress by detecting reactive oxygen species.

- Evaluate the effect of the most active platinum complexes on the protein expression level of apoptosis associated proteins using a proteome array.

- Evaluate the effect of platinum complexes on the expression level of the proteins; p21 (DNA damage response protein) and haemoxyganase-1 (oxidative stress response protein) using immunofluorescence assay.

- Investigate the DNA-binding mode of the two most active platinum complexes.

1.8 Cancer cell models for *in vitro* studies

Cancer cell lines are derived from patients diagnosed with the disease and serve as useful *in vitro* models for understanding cancer biology and developing new chemotherapeutic agents. Since lung cancer is ranked the major cause of cancer related deaths, closely followed by colorectal cancer in both men and women worldwide, it is therefore important to initially use cell models of these types of cancers to investigate the effect of new compounds of interest in this study.

1.8.1.1 H1975 and A549 lung cancer cell lines

The H1975 is a human lung cancer cell line with adenocarcinoma epithelial morphology. The cell line was isolated from the lungs of a non-smoking female patient in 1988 diagnosed with non-small cell lung cancer (ATCC) and has a double mutation in epidermal growth factor receptor (EGFR).

The A549 is a human lung adenocarcinoma cell line with epithelial morphology (squamous). The cell line was derived from a 58-year-old Caucasian male in 1972 from the pulmonary. The cell line has mutation in EGFR and KRAS gene.

Both these non-small lung cancer cell lines are adherent and grow as monolayers when cultured *in vitro*.

1.8.1.2 HT-29 colorectal cancer line

The HT-29 is an adherent human colorectal adenocarcinoma cell line with epithelial morphology. The cell line is derived from a primary tumour of a 44-yearold Caucasian female in 1964 (ATCC).

1.9 Thesis outline

Chapter 1 provides literature review on cancer development, current treatment regimens and challenges within chemotherapy, including the limitations of clinically approved platinum-based drugs.

Chapter 2 details the synthetic methods used and the characterization of the ligands and complexes.

Chapter 3 investigates the cytotoxic effects of platinum complexes and the mechanism of cell death against H1975, A549 and HT-29 cells.

In ***Chapter 4,*** the effect of active platinum complexes; [Pt(dmp)(L^1-κ*O*,*S*)]Cl and [Pt(dmp)(L^3-κ*O*,*S*)]Cl on the expression of apoptotic regulatory proteins is examined using human apoptotic-proteome arrays.

Chapter 5 investigates the interaction of two active platinum complexes; [Pt(dmp)(L^1-κ*O*,*S*)]Cl and [Pt(dmp)(L^3-κ*O*,*S*)]Cl with the DNA target molecule.

Chapter 6 provides an overview of the research findings from each of the previous chapters, concluding with suggestions for future research directions.

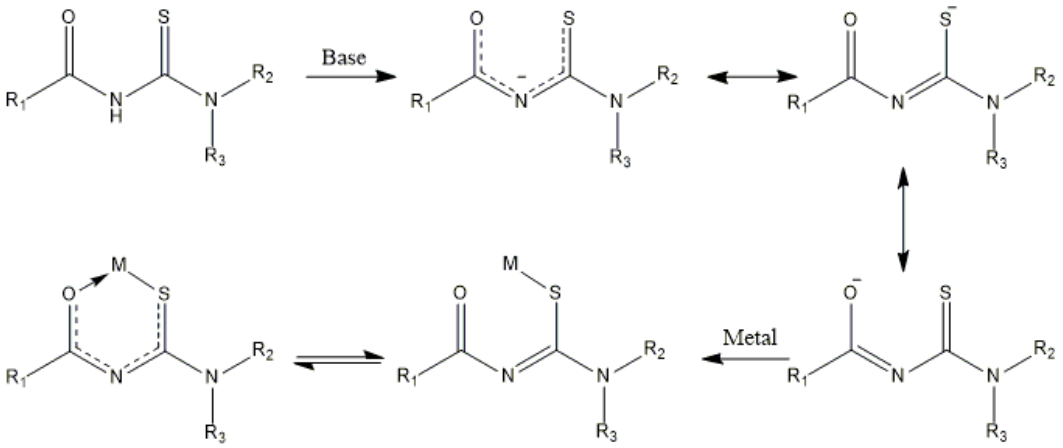
*Chapter 2: Synthesis and characterization of ligands and [Pt(diimine)(L^n-κ*O,S*)]$^+$ complexes*

2.1 Introduction

The synthesis and characterization of disubstituted acylthiourea ligands; *N,N*-di(alkyl)-*N'*-acylthiourea, herein presented as **HL^n** and square planar platinum(II) complexes bearing the mixed bidentate ligands; [Pt(phen)(L^n-κ*O,S*)]$^+$ and [Pt(dmp)(L^n-κ*O,S*)]$^+$ is detailed in this chapter. The diimine platinum precursors; $PtCl_2$(phen) and $PtCl_2$(dmp) were synthesized and characterized prior to the preparation of platinum complexes of interest, where phen and dmp represents 1,10-phenanthroline and 5,6-dimethyl-1,10-phenanthroline.

Disubstituted acylthiourea ligands (R_1-C(O)-NH-C(S)-N'-R_2R_3) are important organic compounds that are well known for their various applications and versatility in coordination mode (Saeed, Flörke and Erben, 2014; Zahra *et al.*, 2022). The presence of three donor atoms, sulfur (S), oxygen (O) and nitrogen (N) in *N,N*-di(alkyl)-*N*'-acylthioureas enables the ligands to coordinate to metals in several possible coordination modes forming charged or neutral complexes. These include a neutral or anionic monodentate coordination mode, where coordination takes place via the sulfur donor atom (*S*), monobasic/anionic bidentate which takes place via both oxygen and sulfur (*O,S*) and neutral bidentate coordination occurring via nitrogen and sulfur (*N,S*) (Cunha *et al.*, 2020; Lapasam and Kollipara, 2020).

In this study, the anionic bidentate chelation of acylthiourea ligands to the platinum center (*O,S*) was of interest (*Scheme 2.1*). This type of coordination is known to yield metal-ligand complexes with strong binding affinity since they are more thermodynamically stable than the monodentate metal complex (*S*) as explained by the chelate effect.



***Scheme 2.1**: General depiction of anionic bidentate (O,S) and monodentate (S) coordination mode of N,N-di(alkyl)-N'-acylthiourea ligand to a metal (M) following deprotonation by a base.*

The synthesis of the preferred class of platinum complexes [Pt(diimine)(L^n-κ*O,S*)]$^+$ was achieved by adding the acylthiourea ligand (1 eq) dropwise to a dilute suspension of the metal precursor (1 eq) in the presence of an excess weak base (2 eq). This allowed for *in situ* deprotonation during reflux, which made the nitrogen in the acylthiourea ligand more nucleophilic. The anion resonance around the O, N, and S donor atoms led to a bidentate coordination (*Scheme 2.1*).

Aromatic diimine ligands containing two imine groups (C=N) were incorporated in this study due to their well-known chemical properties and various biological activities. Previous research has demonstrated that metal complexes with diimine ligands, such as 1,10-phenanthroline, interact with DNA through non-covalent binding modes, resulting in a range of biological activities, including anti-proliferative properties (Pages *et al.*, 2014, 2018). These activities are thought to be due to the ligand's planar hydrophobic structure and their ability to stack with DNA base pairs through π-π interactions. Therefore, metal complexes containing aromatic diimine ligands are of interest for biological applications.

Koch and colleagues were the first to develop and investigate the antimicrobial activity of [Pt(phen)(L^n-κ*O,S*)]$^+$ complexes as well as their antimalarial activity (Koch, 2001; Egan *et al.*, 2004). Furthermore, the potential anticancer activity of

this class of platinum complexes, bearing variations of *N*,*N*-di(butyl)-*N*'-acylthiourea ligand and diimine ligands was previously studied in our research group by Magwaza, R.N (Magwaza, 2017). These variations included the unsubstituted 1,10-phenanthroline (phen), 5,6-dimethyl-1,10-phenanthroline (dmp) and dipyrido [3,2-f:2',3'-h] quinoxaline (dpq) as depicted in *Figure 2.1*.

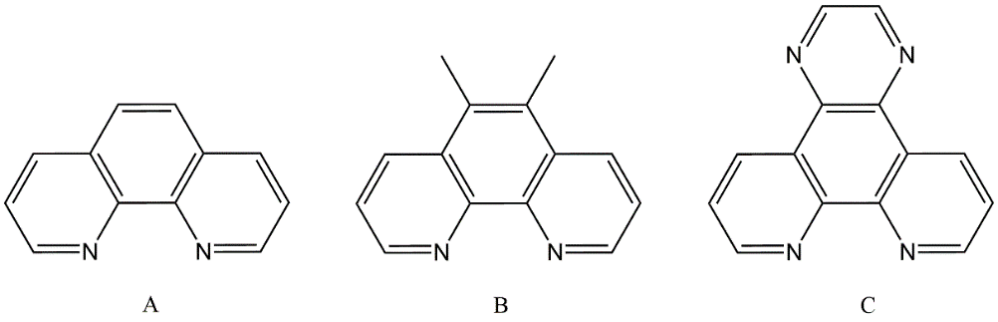


***Figure 2.1**: **Structural variations of the diimine ligands showing unsubstituted and substituted diimines**. A) 1,10-phenanthroline (phen) B) 5,6-dimethyl-1,10-phenanthroline (dmp) C) dipyrido [3.2-f:2',3'-h] quinoxaline (dpq).*

A series of nine square planar platinum complexes; [Pt(diimine)(*N*,*N*-di(alkyl)-*N*'-acylthiourea)]Cl were synthesized and evaluated for anticancer activity against the H1975 lung cancer cell line at concentrations of 50 µM and 5 µM for 48 hours (*Figure 2.2*). The structure-activity relationship (SAR) showed that the diimine ligands played a significant role in the anti-cancer activity of platinum complexes. The most active complexes were those bearing the dmp variation, followed by phen complexes, while dpq complexes were the least active from the series.

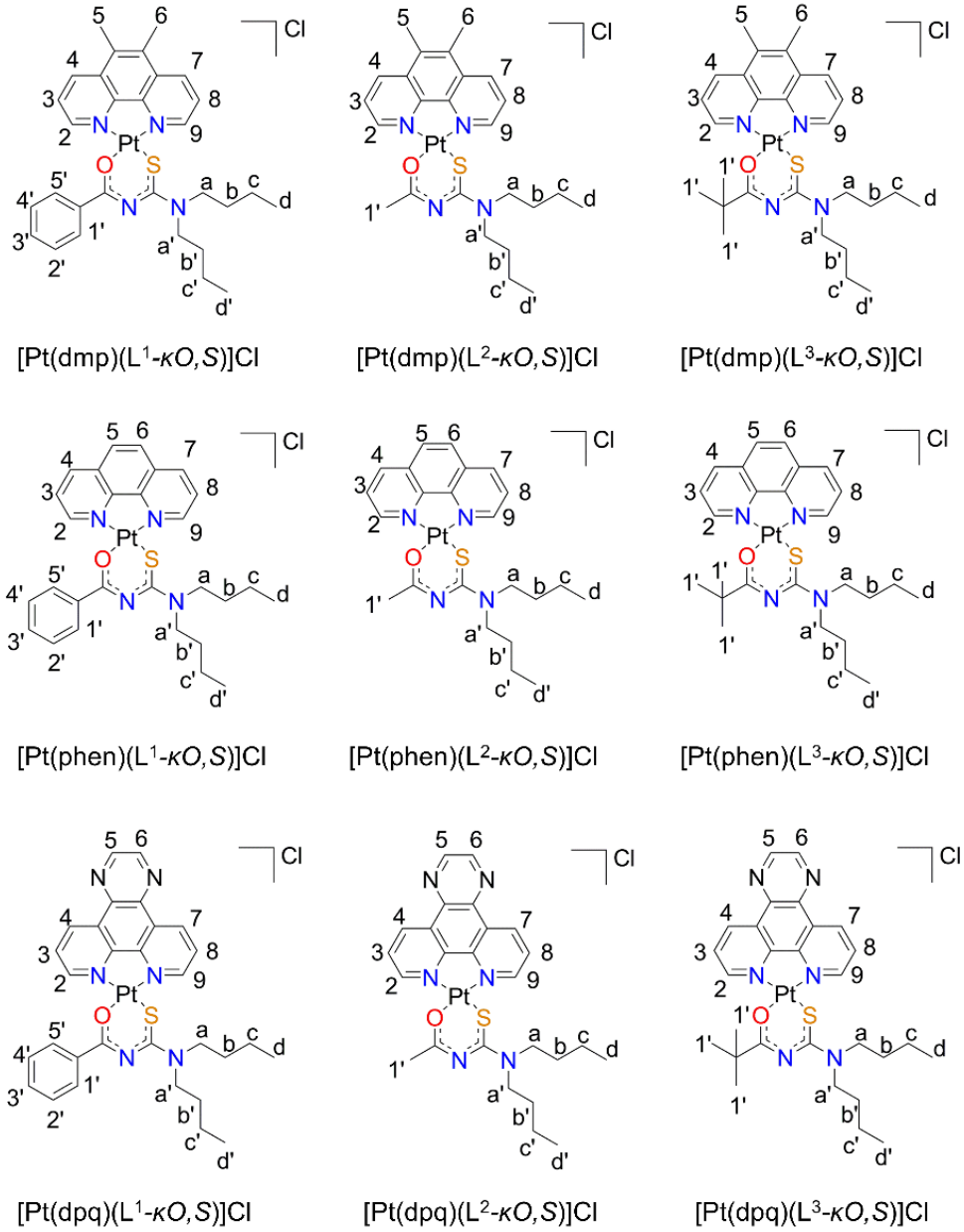


***Figure 2.2**: Chemical structures of a series of nine [Pt(diimine)(L^n-κO,S)]Cl complexes previously synthesized and evaluated for anticancer activity in H1975 lung cancer cell line*(Peega *et al.*, 2021) *(Magwaza., 2017, MSc;* Peega *et al.*, 2021*).*

According to Magwaza's report on the potential anticancer activity of this class of platinum complexes against the H1975 lung cancer cell line, the complex [Pt(dmp)(*N*,*N*-di(butyl)-*N*'-benzoylthiourea)]Cl was the most active, causing a 100% cell growth inhibition at 5 µM while [Pt(dpq)(*N*,*N*-di(butyl)-*N'*-benzoylthiourea)]Cl was found to be the least active. Based on these results, it was

important to further investigate the effectiveness of these platinum complexes and develop a second generation, given their promising anticancer properties.

Therefore, in this study, a series of first and second generation of [Pt(diimine)(L^n-κ*O,S*)]Cl complexes were synthesized. The second generation mainly included variations on the R^1 (acyl) and R^2 (alkyl) substituents of disubstituted acylthiourea ligands while maintaining the dmp and phen variations of the diimine.

The search for highly potent anticancer drugs remains relevant due to the limitations of currently approved treatments. The synthesized ligands and complexes were characterized using 1D and 2D NMR spectroscopy (^{1}H & ^{13}C), Fourier transform infra-red spectroscopy (FT-IR), High resolution mass spectrometry (HRMS), and/or Elemental analysis to confirm their molecular structure and purity.

2.2 Experimental

2.2.1 Materials and measurements for chemical synthesis

All reagents were purchased from Sigma Aldrich and used without further purification. The solvents were dried and distilled according to standard procedures.

2.2.2 Characterization techniques

2.2.2.1 Nuclear Magnetic Resonance (NMR) Spectroscopy

The ^{1}H and ^{13}C NMR spectra were recorded with Bruker Avance 300MHz, Avance 400MHz and/or Avance III 500MHz. All NMR spectra were recorded in an appropriate deuterated NMR solvents such as chloroform-*d*, dimethylsulfoxide-d_6 or methanol-d_4 ($CDCl_3$-*d*, DMSO-d_6 or CD_3OD-d_4) with chemical shifts reported in ppm, refenced to the internal standard, TMS. NMR samples were prepared by weighing approximately 5 mg of sample and dissolving them in ≤0.7 mL of an appropriate NMR solvent.

2.2.2.2 Fourier-transform infra-red (FT-IR) Spectroscopy

The infrared (FT-IR) spectra were recorded on a Bruker Tensor 27 spectrometer at a frequency range of 4000-500 cm^{-1}. All analyzed samples were dry powder or crystals.

2.2.2.3 High Resolution Mass Spectrometry (HRMS)

Mass spectrometry was performed on a Bruker Compact Q-tof high resolution mass spectrometer. Samples were prepared in HPLC grade methanol or acetonitrile at concentration of 5-10 µg.mL^{-1}.

2.2.3 Synthesis of *N,N*-di(alkyl)-*N*'-acylthiourea ligands (HL^n)

Potassium thiocyanate (KSCN) (15 mmol, 1.5 g) was dissolved in 40 mL of anhydrous acetone, followed by the addition of 1 molar equivalent of an appropriate acyl chloride (e.g naphthoyl chloride) (15 mmol, 2.26 mL). The reaction mixture was set to reflux for 30-60 minutes under inert gas (N_2) until a white precipitate was formed, indicating the presence of the isothiocyanate intermediate, and thereafter cooled to room temperature. This was then followed by a dropwise addition of an appropriate amine ligand (e.g dibutylamine) (15 mmol, 2.53 mL) for approximately 10 minutes. The reaction was set to reflux for a further two hours. The crude product was cooled to room temperature and then filtered to remove the insoluble white solid (KCl). Thereafter, a small volume of deionized water ≤10 mL was carefully added to precipitate the ligand product out of solution, where the resulting ligand product (white solid) was collected by filtration and recrystallized in acetone: water, methanol or ethanol to yield a pure crystalline ligand. All ligands were characterized by proton and carbon NMR spectroscopy, infrared spectroscopy, mass spectrometry and/or elemental analysis as reported below:

***N,N*-di(butyl)-*N*'-benzoylthiourea (HL^1):** Yield: 88%; mp: 92.5-93.0 ˚C. FT-IR (ATR): ν(cm^{-1}) = 3166 (N-H), 2959-2871 (C-H) 1685 (C=O), 1372 (C=S). ^{1}H NMR (300 MHz, $CDCl_3$) δ 8.21 (s, 1H, NH), 7.87 – 7.79 (m, 2H, H$^{1'+5'}$), 7.63 – 7.54 (m, 1H, H$^{3'}$), 7.53 – 7.44 (m, 2H, H$^{2'+4'}$), 3.98 (t, *J* = 7.6 Hz, 2H, H^a), 3.54 (t, J = 7.4 Hz, 2H, H$^{a'}$), 1.80 (p, *J* = 7.7 Hz, 2H, H^b), 1.66 (p, *J* = 7.8 Hz, 2H, H$^{b'}$), 1.45 (h, *J* = 7.4 Hz ,2H, H^c), 1.29 (h, *J* = 7.3 Hz, 2H, H$^{c'}$), 0.94 (dt, *J* = 23.1, 7.3 Hz, 6H, H^d, H$^{d'}$) ppm.^{13}C NMR (300 MHz, DMSO-*d*$_6$) δ = 180.9 (C=S), 163.8 (C=O), 132.9 (C^6), 132.2 (C$^{3'}$), 128.40 (C$^{1'+5'}$), 127.9 (C$^{2'+4'}$), 52.4 (C^a), 51.6 (C$^{a'}$), 29.7 (C^b), 27.8 (C$^{b'}$), 19.5 (C^c), 19.4 (C$^{c'}$), 13.8 (C^d), 13.5 (C$^{d'}$) ppm. ESI-MS (m/z): calculated 292.16 [L], observed. 293.16 [L+H]. Elemental analysis calculated (%) for HL^1

$C_{16}H_{24}N_2OS$: C 65.71 H 8.27 N 9.58 S 10.96, observed: C 65.72 H 8.19 N 9.61 S 10.73.

***N,N*-di(butyl)-*N'*-acetylthiourea (HL^2):** Yield: 84%; mp: 56.3 – 58.0 °C. FT-IR (ATR): ν(cm^{-1}) = 3166 (N-H), 1661 (C=O), 1416 (C=S). ^{1}H NMR (300 MHz, $CDCl_3$) δ 8.03 (s, 1H, NH), 3.89 (s, 2H, H^a), 3.46 (s, 2H, $H^{a'}$), 2.13 (s, 3H, H^1),1.83 - 1.51 (m, 4H, H^b, $H^{b'}$), 1.34 (s, 4H, H^c, $H^{c'}$), 0.93 (t, *J* = 7.2 Hz, 6H, H^d, $H^{d'}$) ppm.^{13}C NMR (300 MHz, DMSO-d_6) δ = 180.3 (C=S), 166.8 (C=O), 132.9 (C^6), 51.8 (C^a), 51.6 ($C^{a'}$), 29.5 (C^b), 27.9 ($C^{b'}$), 22.9 (C^1), 19.5 (C^c), 19.4 ($C^{c'}$), 13.7 (C^d), 13.5 ($C^{d'}$) ppm. ESI-MS (m/z): calculated 230.15 [L], observed. 231.15 [L+H]. Elemental analysis calculated (%) for $C_{11}H_{22}N_2OS$: C 57.35 H 9.63 N 12.16 S 13.92, observed: C 56.61 H 9.36 N 12.25 S 13.59.

***N,N*-di(butyl)-*N'*-pivaloylthiourea (HL^3):** Yield: 96%; mp: 85.4 – 85.9 °C. FT-IR (ATR): ν(cm^{-1}) = 3302 (N-H), 1654 (C=O), 1368 (C=S). ^{1}H NMR (400 MHz, $CDCl_3$) δ 7.63 (s, 1H, NH), 3.91 (t, J = 7.7 Hz, 2H, H^a), 3.40 (t, *J* = 7.6 Hz, 2H, $H^{a'}$), 1.79 – 1.66 (m(p), 2H, H^b), 1.67 – 1.50 (m(p), 2H, $H^{b'}$), 1.45 – 1.34 (m (h), 2H, H^c), 1.25 (s, 11H, $H^{c'}$, H^1), 0.93 (dt, *J* = 14.5, 7.3 Hz, 6H, H^d, $H^{d'}$). ^{13}C NMR (300 MHz, DMSO-d_6) δ(ppm) = 181.5 (C=S), 174.7 (C=O), 132.9 (C^6), 52.5 (C^a), 51.6 ($C^{a'}$), 29.8 (C^b), 27.8 ($C^{b'}$), 26.5 (C^1), 19.4 ($C^{c+c'}$), 13.7 (C^d), 13.5 ($C^{d'}$) ppm. ESI-MS (m/z): calculated. 272.19 [L], observed. 273.19 [L+H]. Elemental analysis calculated (%) for $C_{14}H_{28}N_2OS$: C 61.72 H 10.36 N 8.78, observed: C 61.73 H 10.72 N 10.28.

***N,N*-di(butyl)-*N'*-1-naphthoylthiourea (HL^4):** Yield: 62%; mp: 95.4 – 97.1 °C. FT-IR(ATR): ν(cm^{-1}) = 3174 (N-H), 2870-2954 (C-H), 1678 (C=O), 1419 (C=S). ^{1}H NMR (400 MHz, $CDCl_3$) δ 8.46 (d, *J* = 8.4 Hz, 1H, $H^{8'}$), 8.17 (s, 1H, NH), 8.01 (d, *J* = 8.2 Hz, 1H, $H^{3'}$), 7.90 (d, *J* = 8.0 Hz, 1H, $H^{1'}$), 7.76 (d, *J* = 7.1 Hz, 1H, H^5), 7.59 (dt, *J* = 19.2, 7.1 Hz, 2H, $H^{6'}$, $H^{7'}$), 7.50 (t, *J* = 7.7 Hz, 1H, $H^{2'}$), 4.01 (t, *J* = 7.7 Hz, 2H, H^a), 3.69 (t, *J* = 7.5 Hz, 2H, $H^{a'}$), 1.84 (p, *J* = 7.8 Hz, 2H, H^b), 1.74 (h, *J* =7.1Hz, 2H, $H^{b'}$), 1.47 (h, *J* = 7.6 Hz, 2H, H^c), 1.36 (h, *J* = 7.5 Hz, 2H, $H^{c'}$), 0.98 (dt, *J* = 19.5, 7.4 Hz, 6H, H^d, $H^{d'}$) ppm. ^{13}C NMR (400 MHz, $CDCl_3$) δ 179.73 (C=S), 165.57 (C=O), 134.33 ($C^{10'}$), 132.91 ($C^{3'}$), 132.16 ($C^{4'}$), 129.02 ($C^{1'}$), 128.29 ($C^{5'}$), 127.26 ($C^{2'}$), 126.71 ($C^{6'}$), 125.61 ($C^{8'}$), 124.98 ($C^{7'}$), 53.85 ($C^{a+a'}$),

30.72 (C^{b}), 29.01 ($C^{b'}$), 20.67 (C^{c}), 20.59 ($C^{c'}$), 14.35 (C^{d}), 14.25 ($C^{d'}$) ppm. ESI-MS (m/z): calculated. 342.18 [L], observed. 343.18 [L+H].

***N,N*-di(ethyl)-*N'*-benzoylthiourea (HL^{5}):** Yield: 84%; mp: 95.8 – 96.5 ℃. FT-IR(ATR): ν(cm^{-1}) = 3198 (N-H), 2865-3031(C-H), 1678 (C=O), 1418/1380 (C=S). ^{1}H NMR (400 MHz, DMSO-d_6) δ 10.54 (s, 1H, NH), 7.97 – 7.85 (m, 2H, $H^{1+5'}$), 7.64 – 7.56 (m, 1H, $H^{3'}$), 7.50 (dd, J = 8.2, 6.9 Hz, 2H, $H^{2+4'}$), 3.94 (q, J = 7.0 Hz, 2H, H^{a}), 3.51 (q, J = 7.2 Hz, 2H, $H^{a'}$), 1.21 (dt, J = 24.6, 7.1 Hz, 1H, H^{b}, $H^{b'}$) ppm. ^{13}C NMR (400 MHz, DMSO-d_6) δ 180.53 (C=S), 164.12 (C=O), 133.04 (C^{6}), 132.31 ($C^{3'}$), 128.51 ($C^{2'+4'}$), 128.10 ($C^{1'+5'}$), 47.29 (C^{a}), 46.56 ($C^{a'}$), 13.39 ($C^{b'}$), 11.17 (C^{b}) ppm. ESI-MS (m/z): calculated. 236.10 [L], observed. 237.10 [L+H].

***N,N*-di(ethyl)-*N'*-pivaloylthiourea (HL^{6}):** Yield: 78%; mp: 90.5 – 91.0 ℃. FT-IR(ATR): ν(cm^{-1}) = 3215 (N-H), 2971-2869 (C-H), 1645 (C=O), 1420/1356 (C=S). ^{1}H NMR (400 MHz, $CDCl_3$) δ 7.63 (s, 1H, NH), 3.97 (s, 2H, H^{a}), 3.48 (s, 2H, $H^{a'}$), 1.25 (s, 15H, H^{b}, $H^{b'}$, H^{1}) ppm. ^{1}H NMR (400 MHz, DMSO-d_6) δ 9.54 (s, 1H, NH), 3.88 (q, J = 7.0 Hz, 2H, H^{a}), 3.42 (s, 2H, $H^{a'}$), 1.14 (s, 15H, H^{b}, H^{b}, H^{1}) ppm. ESI-MS (m/z): calculated. 216.13 [L], observed. 217.13 [L+H].

***N,N*-di(ethyl)-*N'*-1-naphthoylthiourea (HL^{7}):** Yield: 89%; mp: 151.6 – 152.2 ℃. FT-IR(ATR): ν(cm^{-1}) = 3177 (N-H), 2874-2977 (C-H), 1679 (C=O), 1427/1378 (C=S). ^{1}H NMR (400 MHz, DMSO-d_6) δ 10.78 (s, 1H, NH), 8.30 – 8.22 (m, 1H, $H^{8'}$), 8.08 (d, J = 8.1 Hz, 1H, $H^{3'}$), 8.04 – 7.97 (m, 1H, $H^{1'}$), 7.69 (dd, J = 7.1, 1.3 Hz, 1H, $H^{5'}$), 7.65 – 7.53 (m, 3H, $H^{2'+6'+7'}$), 3.96 (q, J = 7.1 Hz, 2H, H^{a}), 3.68 (q, J = 7.1 Hz, 2H, $H^{a'}$), 1.26 (t, J = 7.1 Hz, 6H, H^{b}, $H^{b'}$) ppm. ^{13}C NMR (400 MHz, DMSO-d_6) δ 180.66 (C=S), 166.83 (C=O), 133.84 (C^{10}), 133.30 ($C^{4'}$), 131.47 ($C^{3'}$), 130.49 ($C^{9'}$), 129.05 ($C^{1'}$), 127.80 ($C^{5'}$), 127.07($C^{2'}$), 126.81 ($C^{6'}$), 125.68 ($C^{8'}$), 125.56 ($C^{7'}$), 47.89 (C^{a}), 47.22 ($C^{a'}$), 14.13(C^{b}), 11.85 ($C^{b'}$) ppm. ESI-MS (m/z): calculated. 286.11 [L], observed. 287.12 [L+H].

***N,N*-di(phenyl)-*N'*-benzoylthiourea (HL^{8}):** Yield: 76%; mp: 121.6 – 122.9 ℃ FT-IR(ATR): ν(cm^{-1}) = 3202 (N-H), 3128-2952 (C-H), 1690 (C=O), 1487/1353 (C=S). ^{1}H NMR (400 MHz, $CDCl_3$) δ 8.56 (s, 1H, NH), 7.63 – 7.56 (m, 2H, $H^{1'+5'}$), 7.56 – 7.42 (m, 3H, $H^{2'+4}$, $H^{3'}$), 7.36 (d, J = 4.3 Hz, 8H, H^{a+e}, H^{b+d}, $H^{a'+e'}$, $H^{b'+d'}$),

7.24 (d, J = 4.7 Hz, 2H, $H^{c+c'}$) ppm. ESI-MS (m/z): calculated. 332.10 [L], observed. 333.10 [L+H].

***N*,*N*-di(phenyl)-*N*'-pivaloylthiourea (HL^9):** Yield: 91%; mp: 107.3 – 109.6 ℃. FT-IR(ATR): ν(cm^{-1}) = 3365 (N-H), 3044-2954 (C-H), 1705 (C=O), 1360 (C=S). ^{1}H NMR (400 MHz, $CDCl_3$) δ 8.08 (s, 1H, NH), 7.40 – 7.17 (m, 10H, H^{a+e}, H^{b+d}, H^c, $H^{a'+e}$, $H^{b'+d'}$, $H^{c'}$), 0.96 (s, 9H, H^1) ppm. ESI-MS (m/z): calculated 312.13 [L], observed. 313.14 [L+H].

2.2.4 Synthesis of the metal precursor $PtCl_2$(diimine)

Platinum(II) precursors were synthesized by firstly dissolving potassium tetrachloroplatinate/K_2PtCl_4 (0.9636 mmol, 400.0 mg) in 40 mL deionized water. This was followed by the addition of six drops of HCl to prevent aquation of K_2PtCl_4. Thereafter, an equivalent mole (1 eq) of the appropriate diimine ligand, (e.g 5,6-dimethyl-1,10-phenanthroline) (0.9636 mmol, 200.7 mg) was added. The reaction mixture was set to reflux for three hours until a yellow precipitate was obtained. The crude precursor product was transferred into a 50 mL centrifuge tube and washed with three aliquots of 30 mL deionized water and acetonitrile via a centrifuge system at 3000 rpm per five minutes. This was to remove any trace amounts of the unreacted starting materials; K_2PtCl_4 which solubilized in water and phenanthroline ligands which dissolves in acetonitrile respectively. Furthermore, the obtained platinum precursor product was then dried under vacuum and characterized using proton NMR spectroscopy, infrared spectroscopy, and elemental analysis. The characterization techniques were limited due to their poor solubility in a range of polar aprotic or non-polar solvents. The results obtained are reported below:

[$PtCl_2$(1,10-phenanthroline)]: Yield: 86%; FT-IR (ATR): ν(cm^{-1}) = 3057 (C-H_{arom}), 1627 (C=N_{arom}), 1208 (C-C_{arom}). ^{1}H NMR (500 MHz, DMSO-d_6) δ 9.70 (dd, J = 5.6, 1.3 Hz, 2H, H^2, H^9), 9.04 (dd, J = 8.4, 1.2 Hz, 2H, H^4, H^7), 8.29 (s, 2H, H^5, H^6), 8.17 (dd, J = 8.2, 5.3 Hz, 2H, H^3, H^8) ppm. Elemental analysis (%) calculated for $C_{12}H_8Cl_2N_2Pt$: C 32.30 H 1.81 N 6.28; observed: C 32.16 H 1.72 N 6.27.

[$PtCl_2$(5,6-dimethy-1,10-phenanthroline)]: Yield: 82%; FT-IR (ATR): ν(cm^{-1}) = 3077 (C-H_{arom}), 1616 (C=N_{arom}), 1222 (C-C_{arom}). ^{1}H NMR (500 MHz, DMSO-d_6) δ 9.13 (dd, *J* = 4.3, 1.6 Hz, 2H, H^2, H^9), 8.64 (dd, *J* = 8.4, 1.6 Hz, 2H, H^4, H^7), 7.64 (dd, *J* = 8.4, 4.3 Hz, 2H, H^3, H^8), 2.72 (s, 6H, H^5, H^6) ppm. Elemental analysis (%) calculated for $C_{14}H_{12}Cl_2N_2Pt$: C 35.46 H 2.55 N 5.91; observed: C 35.12 H 2.05 N 5.88.

2.2.5 Synthesis of [Pt(diimine)(L^n-κ*O,S*)]Cl complexes

Platinum complexes of *N,N*-di(alkyl)-*N*'-acylthiourea and diimine were synthesized using a modified method described by Koch *et al*. In a 250 mL three necked round bottom flask, a suspension of the appropriate diimine platinum precursor; e.g $PtCl_2$(dmp) (15 mmol) was prepared in 60 mL acetonitrile, to this, an excess of sodium acetate (2 eq, 30 mmol) was added. This was followed by a separate dissolution of an appropriate *N,N*-di(alkyl)-*N*'-acylthiourea ligand (15 mmol) in ~10 mL acetonitrile and a dropwise addition into the dilute suspension under reflux for 8 -24 hours, until a clear yellow-orange solution was obtained. The solution was then filtered to remove unreacted sodium acetate and/or sodium chloride. Thereafter, the solvent was removed using a rotary evaporator and the crude product was dissolved in 10 mL dichloromethane to further remove trace amounts of the unwanted salts by filtration. This was followed by a complete evaporation of the solvent and concentrating the dry complex with 5 mL acetonitrile. To this concentrate, 20 mL of diethyl ether was slowly added to allow selective precipitation of the complex and this was kept in the freezer overnight. The product was washed with 5 mL aliquots (x3) of diethyl ether via a centrifuge system to remove any remains of unreacted ligand or trace amounts of monodentate complex as this was seen with (HL^1 and HL^4) benzoyl and naphthoyl variations. In the case of these HL^1 and HL^4 variations, a suspension of the precursor and sodium acetate was mixed in 1:20 water: acetonitrile, a 5% binary water: acetonitrile system (3 mL: 57 mL) was heated under reflux followed by a dropwise addition of the ligand. The system was used to improve the solubility of the precursor in acetonitrile and drive the reaction to completion. The crude product was selectively precipitated, with diethyl ether:acetonitrile or hexane:dichloromethane mixture.

The complex filtrate was re-suspended several times to get a clean product. The complexes were dried for 5-10 hours under vacuum and characterized.

***[Pt(dmp)(L^1-κO,S)]Cl*:** Yield: 86%; FT-IR(ATR): ν(cm^{-1}) = 1397 (C-O), 1216 (C-S). ^{1}H NMR (400 MHz, CD_3OD-*d*$_4$) δ 8.81 (d, *J* = 8.5 Hz, 1H, H^2), 8.71 (d, *J* = 8.5 Hz, 1H, H^9), 8.53 (d, *J* = 5.0 Hz, 1H, H^4), 8.39 (d, *J* = 5.4 Hz, 1H, H^7), 8.06 (t, *J* = 7.0 Hz, 1H, H^3), 7.80 – 7.60 (m, 4H, H$^{1'}$, H$^{3'}$, H$^{5'}$, H^8), 7.49 (t, *J* = 7.6 Hz, 2H, H$^{2'}$, H$^{4'}$), 3.76 – 3.54 (m, 4H, H$^{a'+a}$), 2.49 (d, *J* = 11.2 Hz, 6H, H^{5+6}), 1.83 (d, *J* = 8.6 Hz, 2H, H^b), 1.65 (q, *J* = 7.9 Hz, 2H, H$^{b'}$), 1.56 (q, *J* = 7.4 Hz, 1H, H^c), 1.46 (q, *J* = 7.4 Hz, 1H, H$^{c'}$), 1.14 (t, *J* = 7.4 Hz, 3H, H^d), 1.04 (t, *J* = 7.4 Hz, 3H, H$^{d'}$) ppm. ^{13}C NMR (400 MHz, CD_3OD-*d*$_4$) δ 168.99 (C=O), 165.07 (C=S), 147.77 (C^2), 147.49 (C^{1a}), 144.75 (C^{2a}), 144.06 (C^9), 137.97 (C^4), 137.75 (C^7), 135.18 (C$^{1'+5'}$), 133.92 (C$^{3'}$), 133.64 (C$^{2'+4'}$), 132.12 (C^{3a}), 131.90 (C^{4a}), 129.93 (C^5), 129.50 (C^6), 126.92 (C^3), 126.44 (C^8), 54.30 (C^a), 52.97 (C$^{a'}$), 30.76 (C^b), 29.89 (C$^{b'}$), 20.93 (C^{5+6} ,CH_3), 15.00 (C^c), 14.92 (C$^{c'}$), 13.90 (C^d), 13.85 (C$^{d'}$) ppm. ESI-MS (m/z): expected. 694.21 [M]$^+$, observed 694.21 [M]$^+$.

***[Pt(dmp)(L^2-κO,S)]Cl*:** Yield: 73%; FT-IR(ATR): ν(cm^{-1}) = 1422 (C-O), 1208 (C-S). ^{1}H NMR (400 MHz, CD_3OD-*d*$_4$) δ 8.99 (dd, *J* = 15.3, 8.3 Hz, 2H, H^2, H^9), 8.94 – 8.83 (m, 1H, H^4) 8.68 – 8.55 (m, 1H, H^7), 8.18 – 8.08 (m, 1H, H^3), 7.97 – 7.82 (m, 1H, H^8), 3.97 – 3.75 (m , 4H, H^a, H$^{a'}$), 2.32 (s, 2H, H^5, H^6), 1.99 – 1.84 (m, 2H, H^b), 1.82 – 1.67 (m , 2H, H$^{b'}$), 1.65 – 1.52 (m, 2H, H^c), 1.53 – 1.39 (m, 2H, H$^{c'}$), 1.14 (t, *J* = 7.3 Hz, 3H, H^d), 1.06 (t, *J* = 7.2 Hz, 1H, 3H, H$^{d'}$) ppm. ^{13}C NMR (400 MHz, CD_3OD-*d*$_4$) δ 177.14 (C=O), 165.90 (C=S), 148.38 (C^2), 148.02 (C^{1a}), 144.56 (C^9), 138.35 (C^4), 137.84 (C^7), 134.12 (C^5), 133.87 (C^6), 132.60 (C^{3a}), 132.22 (C^{4a}), 126.78 (C^{3+8}), 53.98 (C^a), 52.39 (C$^{a'}$), 30.78 (C^b), 30.06 (C$^{b'}$), 26.87 (C^1), 21.10 (C^c), 20.93 (C$^{c'}$), 15.28 (C^5, CH_3), 15.23 (C^{6,} CH_3), 14.07 (C^d), 13.96 (C$^{d'}$) ppm. ESI-MS (m/z*)*: calculated. 632.20 [M]$^+$, observed. 632.20 [M]$^+$.

***[Pt(dmp)(L^3-κO,S)]Cl*:** Yield: 71%; FT-IR(ATR): ν(cm^{-1}) = 1359 (C-O), 1221 (C-S). ^{1}H-NMR (400 MHz, $CDCl_3$) δ 9.22 – 9.07 (m, 3H, H^2, H^4, H^7), 8.89 (d, *J* = 5.3 Hz, 1H, H^9), 8.43 (td, *J* = 9.8, 8.6, 5.1 Hz, 2H, H^3, H^8), 3.84 (t, *J* = 8.0 Hz, 2H, H^a), 3.78 – 3.66 (m, 2H, H$^{a'}$), 2.24 – 2.13 (m, 6H, H^{5+6}) 1.88 (p, *J* = 7.9 Hz, 2H, H^b), 1.69 (s, 2H, H^b), 1.62 – 1.45 (m, 2H, H^c), 1.41 – 1.36 (m, 11H, H$^{c'}$,H^1), 1.08 (t, *J* =

7.3 Hz, 3H, H^{d}), 0.98 (t, *J* = 7.3 Hz, 3H, $H^{d'}$) ppm. ESI-MS (m/z*)*: calculated. 674.25 $[M]^+$, observed. 674.25 $[M]^+$.

[Pt(dmp)(L⁴-κO,S)]Cl: Yield: 92%; FT-IR(ATR): *ν*(cm^{-1}) = 1382 (C-O), 1222 (C-S) ^{1}H-NMR (400 MHz, $CDCl_3$) δ 9.20 (d, *J* = 8.4 Hz, 1H, H^2), 9.05 (d, *J* = 8.4 Hz, 1H, H^9), 8.95 (d, *J* = 5.2 Hz, 1H), 8.46 (d, *J* = 8.6 Hz, 2H), 8.06 (d, *J* = 8.2 Hz, 1H), 7.99 (dd, *J* = 11.2, 7.7 Hz, 2H), 7.57 (dt, *J* = 7.8, 3.9 Hz, 2H), 7.51 (t, *J* = 7.6 Hz, 1H), 3.91 (t, *J* = 7.9 Hz, 2H, H^{a}), 3.86 – 3.73 (m, 2H, $H^{a'}$), 2.87 (s, 3H, H^5), 2.84 (s, 3H, H^6), 1.92 (p, *J* = 7.9 Hz, 2H, H^{b}), 1.74 (p, *J* = 7.6 Hz, 2H, $H^{b'}$), 1.58 (h, *J* = 7.4 Hz, 2H, H^{c}), 1.35 (h, *J* = 7.3 Hz, 2H, $H^{c'}$), 1.10 (t, *J* = 7.3 Hz, 3H, H^{d}), 0.92 (t, *J* = 7.4 Hz, 3H, $H^{d'}$). ESI-MS (m/z): calculated $[M]^+$ 744.23, observed 744.23.

[Pt(dmp)(L⁵-κO,S)]Cl: Yield: 67%; FT-IR(ATR): *ν*(cm^{-1}) = 1396 (C-O), 1205 (C-S). ^{1}H NMR (400 MHz, DMSO-d_6) δ 8.84 (d, *J* = 8.4 Hz, 1H,), 8.74 (d, *J* = 8.5 Hz, 1H), 8.44 (s, 1H), 8.33 (d, *J* = 5.2 Hz, 1H), 8.07 (s, 1H), 7.83 (s, 1H), 7.71 (dt, *J* = 22.0, 7.5 Hz, 4H), 7.49 (t, *J* = 7.6 Hz, 2H), 7.25 (s, 1H), 3.69 (dd, *J* = 20.2, 7.4 Hz, 4H, $H^{a+a'}$), 2.42 (d, *J* = 13.3 Hz, 6H, H^{5+6}), 1.35 (t, *J* = 7.2 Hz, 3H, H^{b}), 1.20 (t, *J* = 7.0 Hz, 3H, $H^{b'}$). ESI-MS (m/z): calculated 638.16 $[M]^+$, observed 638.16 $[M]^+$.

[Pt(dmp)(L⁶-κO,S)]Cl: Yield: 85%; FT-IR(ATR): *ν*(cm^{-1}) = 1418 (C-O), 1245(C-S) . ^{1}H NMR (400 MHz, DMSO-d_6) δ 9.05 (d, *J* = 8.6 Hz, 1H), 8.95 (s, 1H), 8.87 (t, *J* = 7.2 Hz, 1H), 8.62 (s, 1H), 8.25 (s, 1H), 8. 00 – 7.77 (m, 1H), 3.92 (d, *J* = 7.3 Hz, 2H, H^{a}), 3.81 (q, *J* = 7.0 Hz, 2H, $H^{a'}$), 2.80 – 2.61 (m, 2H, H^{6+5}), 1.40 (t, *J* = 7.1 Hz, 1H, H^{b}), 1.34 (s, 9H, H^1), 1.27 (t, *J* = 7.1 Hz, 3H, $H^{b'}$). ESI-MS (m/z*)*: calculated. 618.19 $[M]^+$, observed. 618.18 $[M]^+$.

[Pt(dmp)(L⁷-κO,S)]Cl: Yield: 72%; FT-IR(ATR): *ν*(cm^{-1}) = 1391 (C-O), 1215 (C-S). ^{1}H NMR (400 MHz, DMSO-d_6) δ 8.84 (d, *J* = 8.4 Hz, 1H), 8.74 (d, *J* = 8.5 Hz, 0H), 8.44 (s, 0H), 8.33 (d, *J* = 5.2 Hz, 0H), 8.07 (s, 0H), 7.71 (dt, *J* = 22.0, 7.5 Hz, 1H), 7.49 (t, *J* = 7.6 Hz, 1H,), 3.69 (dd, *J* = 20.2, 7.4 Hz, 2H, H^{a}), 2.42 (d, *J* = 13.3 Hz, 2H, $H^{a'}$), 1.35 (t, *J* = 7.2 Hz, 3H, H^{b}), 1.20 (t, *J* = 7.0 Hz, 3H, $H^{b'}$). ESI-MS (m/z*)*: calculated. 688.17 $[M]^+$, observed. 688.17 $[M]^+$.

***[Pt(phen)(L¹-κO,S)]Cl*:** Yield 71%; FT-IR(ATR): *ν*(cm^{-1}) = 1203 (C-S), 1368 (C-O) . ^{1}H NMR (400 MHz, $CDCl_3$) δ (ppm) 9.08 (d, *J* = 5.2 Hz, 1H, H^2), 8.98 (dd, *J*

= 17.8, 8.1 Hz, 2H, H^4, H^7), 8.64 (d, *J* = 5.4 Hz, 1H, H^9), 8.34 (t, *J* = 6.7 Hz, 1H, H^6), 8.14 – 8.00 (m, 5H, H^5, H^3, H^8, $H^{1'}$, $H^{5'}$), 7.62 (d, *J* = 7.3 Hz, 1H, $H^{3'}$), 7.53 (t, *J* = 7.5 Hz, 2H, $H^{2'}$, $H^{4'}$), 3.74 (q, *J* = 9.2 Hz, 4H, H^a, $H^{a'}$), 1.81 (p, *J* = 7.6 Hz, 2H, H^b), 1.69 (p, *J* = 7.7 Hz, 1H, $H^{b'}$), 1.52 (q, *J* = 7.5 Hz, 1H, H^c), 1.41 (q, *J* = 7.4 Hz, 1H, $H^{c'}$), 1.07 (t, *J* = 7.3 Hz, 1H, H^d), 0.98 (t, *J* = 7.4 Hz, 1H, $H^{d'}$). ESI-MS (m/z): calculated. 666.2 $[M]^+$. observed. 667.2 $[M+H]^+$.

***[Pt(phen)(L²-κO,S)]Cl*:** Yield: 88%. FT-IR(ATR): *ν*(cm^{-1}) = 1259 (C-S), 1369 (C-O) cm^{-1}. ^1H NMR (300MHz, $CDCl_3$) δ (ppm) 9.07 (d, *J* = 2.7 Hz, 1H; H^2), 8.95 (d, *J* = 5.4 Hz, 1H; H^9), 8.90 (d, *J* = 8.3 Hz, 1H; H^4), 8.82 (d, *J* = 7.6 Hz, 1H: H^7), 8.32 – 8.17 (m, 3H; H^3,H^5,H^6), 7.99 (dd, 8.2, 5.4 Hz, 1H; H^8), 3.84 – 3.67 (m, 2H; H^a, $H^{a'}$), 2.28 (s, 3H; H^1), 2.04 – 1.77 (m, 2H; H^b), 1.72 (p, *J* = 7.8 Hz, 2H; $H^{b'}$), 1.55, (q, *J* = 7.4 Hz, 2H; H^c), 1.44 (q, *J* = 7.4 Hz, 2H; $H^{c'}$), 1.11 (t, *J* = 7.3 Hz, 3H; H^d), 1.03 (t, *J* = 7.3 Hz, 3H; $H^{d'}$). ESI-MS (m/z): calculated. 604.2 $[M]^+$, observed. 605.3 $[M+H]^+$.

***[Pt(phen)(L³-κO,S)]Cl*:** Yield: 78%. FT-IR(ATR): *ν*(cm^{-1}) = 1431 (C-O), 1220 (C-S) cm^{-1}. ^1H NMR (300 MHz, CD_3Cl) δ (ppm) 9.26 – 9.15 (m, 3H, H^2, H^7,H^9), 8.88 (d, *J* = 5.3 Hz, 1H, H^4), 8.39 (s, 2H, H^5, H^6), 8.31 – 8.21 (m, 1H, H^8), 8.17 (dd, *J* = 8.2, 5.4 Hz, 1H, H^3), 3.88 – 3.77 (m, 2H, H^a), 3.78 – 3.69 (m, 2H, $H^{a'}$), 1.94 – 1.80 (m, 2H, H^b), 1.76 – 1.61 (m, 2H, $H^{b'}$), 1.54 (h, *J* = 7.4 Hz, 2H, H^c), 1.46 – 1.31 (m, 11H, H^1, $H^{c'}$), 1.07 (t, *J* = 7.3 Hz, 3H, H^d), 0.98 (t, *J* = 7.3 Hz, 3H, $H^{d'}$). ESI-MS (m/z): calculated. 646.2 $[M]^+$, observed. 647.2 $[M+H]^+$.

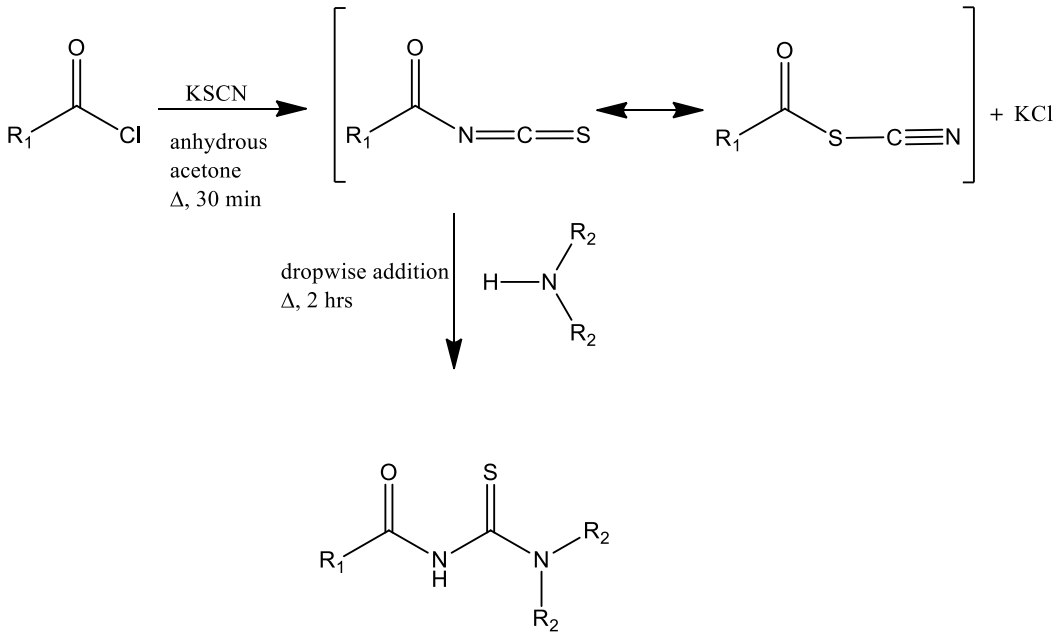
[Pt(phen)(L⁴-κO,S)]Cl: Yield: 83%. FT-IR(ATR): *ν*(cm^{-1}) = 1502 (C-O), 1379 (C-S). ^1H NMR (300 MHz, $CDCl_3$) δ 9.40 (d, *J* = 8.1 Hz, 1H, H^2), 9.17 (d, *J* = 8.2 Hz, 1H, H^9), 9.05 (d, *J* = 5.2 Hz, 1H), 9.02 (d, *J* = 5.5 Hz, 1H), 8.57 – 8.39 (m, 3H), 8.30 (dd, *J* = 8.3, 5.5 Hz, 1H), 8.09 (d, *J* = 7.5 Hz, 1H), 8.07 – 7.94 (m, 3H), 7.65 – 7.48 (m, 3H, $H^{2'+6'+7'}$), 3.94 (t, 2H, H^a), 3.84 (t, 2H, $H^{a'}$), 1.96 (p, *J* = 15.5, 6.8 Hz, 2H, H^b), 1.78 (p, *J* = 7.6 Hz, 2H, $H^{b'}$), 1.61 (h, *J* = 7.2 Hz, 2H, H^c), 1.39 (h, *J* = 7.3 Hz, 2H, $H^{c'}$), 1.13 (t, *J* = 7.3 Hz, 3H, H^d), 0.95 (t, *J* = 7.3 Hz, 3H, $H^{d'}$).^{13}C NMR (500 MHz, DMSO-*d_6*): (C=O) 172.05, (C=S) 165.00, 149.63, 148.12, 145.59, 141.38, 140.86, 134.49, 134.08, 132.20, 131.37, 131.14, 130.27, 129.29, 128.72, 128.51, 127.57, 126.86, 126.72, 125.68, 53.19 (C^d), 51.69 ($C^{d'}$) , 29.97 (C^c), 29.14

($C^{c'}$), 20.19 (C^{b}), 20.02 ($C^{b'}$),14.23 (C^{a}), 13.99 ($C^{a'}$) ppm. ESI-MS (m/z): calculated. 716.20 $[M]^+$, observed. 716.15 $[M]^+$.

2.3 Results and Discussion

2.3.1 Synthesis of *N,N*-di(alkyl)-*N'*-acylthiourea ligands

N,N-di(alkyl)-*N'*-acylthiourea ligands were synthesized following a one-pot synthesis method reported by Douglass and Dain (Douglass and Dains, 1934). The method involved dissolving potassium thiocyanate in anhydrous acetone, followed by the addition of an appropriate acyl chloride in a 1:1 molar ration. The reaction was refluxed under inert conditions as shown in *Scheme 2.2*.

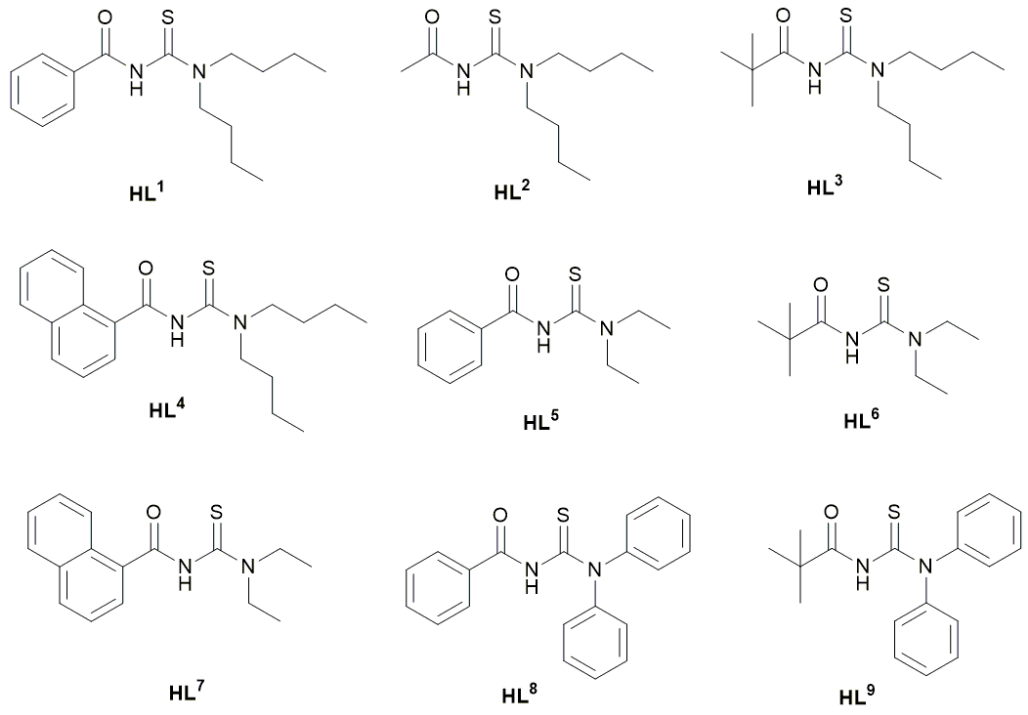


***Scheme 2.2**: Synthetic procedure for the preparation of N,N-di(alkyl)-N'-acylthiourea ligand.*

The reaction mixture was set to reflux until a white precipitate was formed, indicative of an isothiocyanate intermediate, and was thereafter cooled to room temperature. This was followed by a dropwise addition of an appropriate amine ligand (e.g dibutylamine), allowed to reflux for two hours to reach completion (*Scheme 2.2*). The crude product was cooled to room temperature and filtered to

remove the insoluble white solid (KCl). Thereafter, a small volume of deionized water ≤10 mL was carefully added to precipitate the ligand product from solution. The resulting ligand product (white solid) was collected by filtration and recrystallized in acetone: water, methanol, or ethanol to yield a pure crystalline ligand.

N,*N*-di(alkyl)-*N*'-acylthiourea ligands were prepared with variations made on the acyl/aryl (R^1) and alkyl (R^2) substituents (***Figure 2.3)***. The R^1 acyl substituents included aromatic rings such as benzoyl and naphthoyl groups (HL^1, HL^4, HL^5, HL^7, HL^8) as well as the alkyl groups; pivaloyl/tertiary butyl (HL^3, HL^6, HL^9) and acetyl (HL^2). The R^2 alkyl substituents included the butyl chains (HL^{1-4}), ethyl chains (HL^{5-7}) and phenyl rings (HL^8 and HL^9).



HL[1]: *N,N*-dibutyl-*N'*-benzoylthiourea
HL[2]: *N,N*-dibutyl-*N'*-acetylthiourea
HL[3]: *N,N*-dibutyl-*N'*-pivaoylthiourea
HL[4]: *N,N*-dibutyl-*N'*-napthoylthiourea
HL[5]: *N,N*-diethyl-*N'*-benzoylthiourea
HL[6]:*N,N*-diethyl-*N'*-pivaloylthiourea
HL[7] : *N,N*-diphenyl-*N'*-benzoylthiourea
HL[8]: *N,N*-diphenyl-*N'*-pivaloylthiourea

Figure 2.3*: Chemical structures of the N,N-di(alkyl)-N'-acylthiourea ligands synthesised showing the R^1 and R^2 substituents, where R^1 represents the acyl/aryl substituents and R_2 represents the alkyl substituents.*

2.3.2 Characterization of *N*,*N*-di(alkyl)-*N*'-acylthiourea ligand

The ligand *N*,*N*-di(butyl)-*N*'-benzoylthiourea **(HL^1)** was used to illustrate the characterization techniques applied to confirm the structure and purity of the synthesized acylthiourea ligands. The ^{1}H-NMR spectrum of **HL^1** shows 11 signals integrating for a total of 24 protons with a broad singlet at 8.21 ppm, integrating for one proton ***(****Figure 2.4)*. This signal was assigned to the amidic proton (N-H) as it is the most deshielded proton in the molecule.

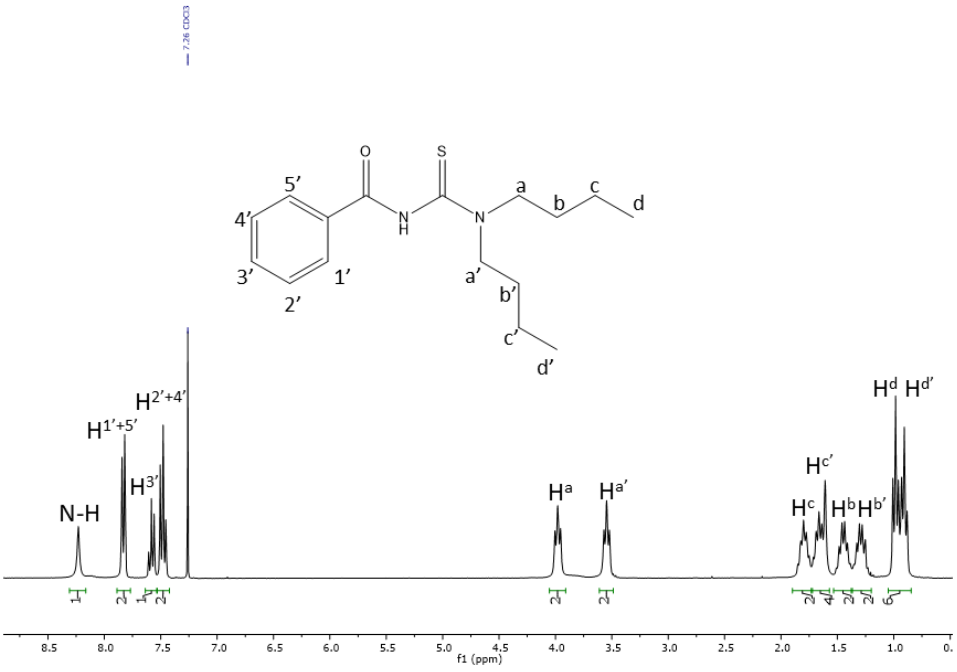


Figure 2.4*: ^{1}H-NMR spectrum of N,N-di(butyl)-N'-benzoylthiourea (HL^1) in chloroform-d at 25 ℃.*

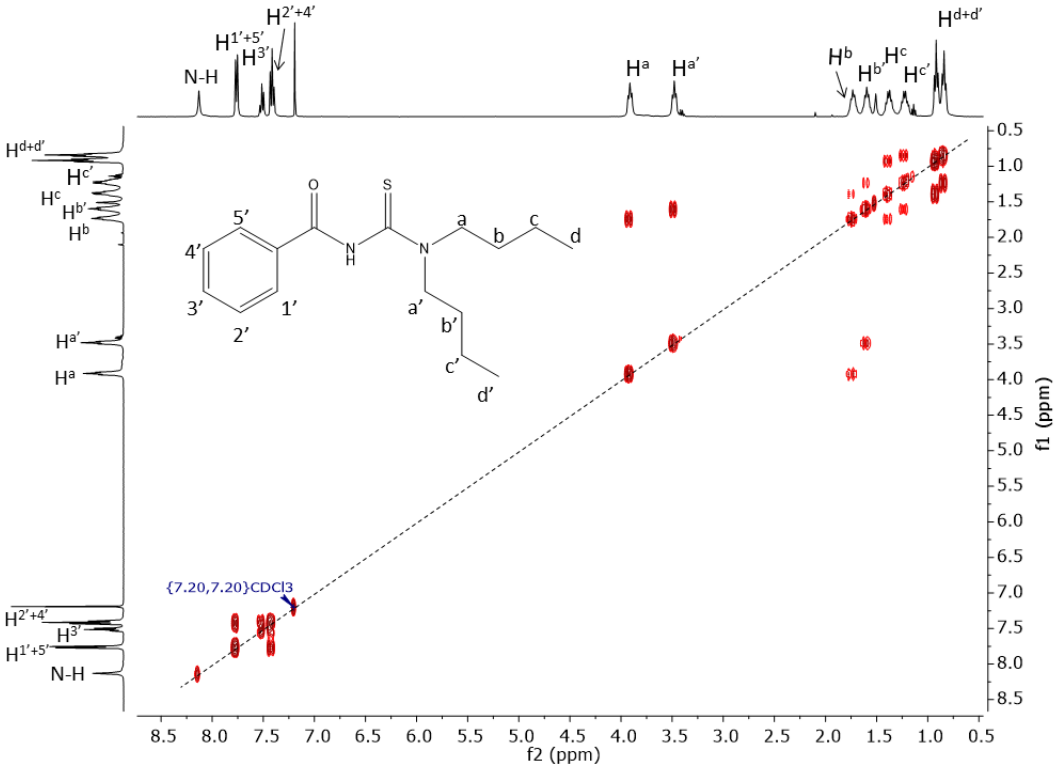


***Figure 2.5**: ^{1}H-^{1}H COSY (2D NMR) spectrum of **HL^{1}** in chloroform-d at 25 ℃.*

The proton signals in the aliphatic region integrates for a total of 18 protons accounted to the butyl chains (R^2) while the aromatic region integrates for five protons on the benzoyl group (R_1). The aromatic protons were unambiguously assigned with the use of 2D NMR, particularly a proton-proton correlation (COSY) spectrum (*Figure 2.5)*. The most de-shielded aromatic protons (2H) shown by a multiplet (dd) at a range of 7.87 - 7.79 ppm were assigned to $H^{1'+5}$ as they are closest to the electron withdrawing group (C=O), which strongly cause a deshielding effect of the aromatic proton. The most shielded aromatic protons at 7.53 - 7.44 ppm were assigned to $H^{2'+4'}$ since the signal also integrates for two protons and showed coupling to neighbouring protons, $H^{1'+5}$ and $H^{3'}$. Therefore, the multiplet at 7.63 - 7.54 ppm was assigned to $H^{3'}$ as it integrates for one proton and showed strong coupling to adjacent protons, $H^{2'+4}$.

The most deshielded aliphatic protons H^{a} and $H^{a'}$ were assigned to 3.98 ppm and 3.54 ppm signals respectively. The chemical shifts of each of these proton signals is distinct, and this can be explained by the difference in their chemical environment

due to a restricted rotation of the alkyl chains about the C-N bond. The nature of this C-N bond is reported to have a partial double bond character due to a tautomeric effect between the thio-carbonyl (C=S) and amidic group (C-N), making the bond stronger, thus restricting rotation of each butyl chain. This then leads to each alkyl chain with a different chemical environment and the signal appearing as distinct on the spectrum. This effect is reduced further down the butyl chain as seen by the overlapping of signals in the up-field region of the spectra (*Figure 2.4*).
The protons H^{b} and $H^{b'}$ were assigned to a pentet/quintet (4 neighbouring protons) at 1.80 ppm and 1.66 ppm respectively. The H^{c} and $H^{c'}$ protons were assigned to a heptet peaks (five neighbouring protons) at 1.45 ppm and 1.29 ppm respectively. Lastly, the two triplet signals overlapping at 0.94 ppm were assigned to H^{d} and $H^{d'}$ protons since they integrated for six protons.

The ^{13}C NMR spectrum (*Figure 2.6**)** showed deshielded carbon signals at 166.92 ppm and 182.35 ppm which were assigned to the carbonyl carbon (C=O) and thiocarbonyl carbon (C=S) respectively following literature reports. The aromatic and aliphatic carbons were successfully assigned with an aid of DEPT-135 to distinguish between the $-CH_2$ and $-CH_3$ carbons; 2D NMR (HSQC-Heteronuclear single quantum coherence spectroscopy) to identify the single carbon-proton bond correlation and Heteronuclear multiple bond correlation (HMBC) to detect carbon-proton bond correlation that is separated by two, three or four bonds. The quaternary carbon of the benzoyl group directly bonded to the carbonyl carbon in **HL^{1}** C^{6}; was assigned to the peak at 134.53 ppm following the use of HSQC spectrum that showed no single carbon-proton correlation, thereby confirming the absence of a proton on this carbon.

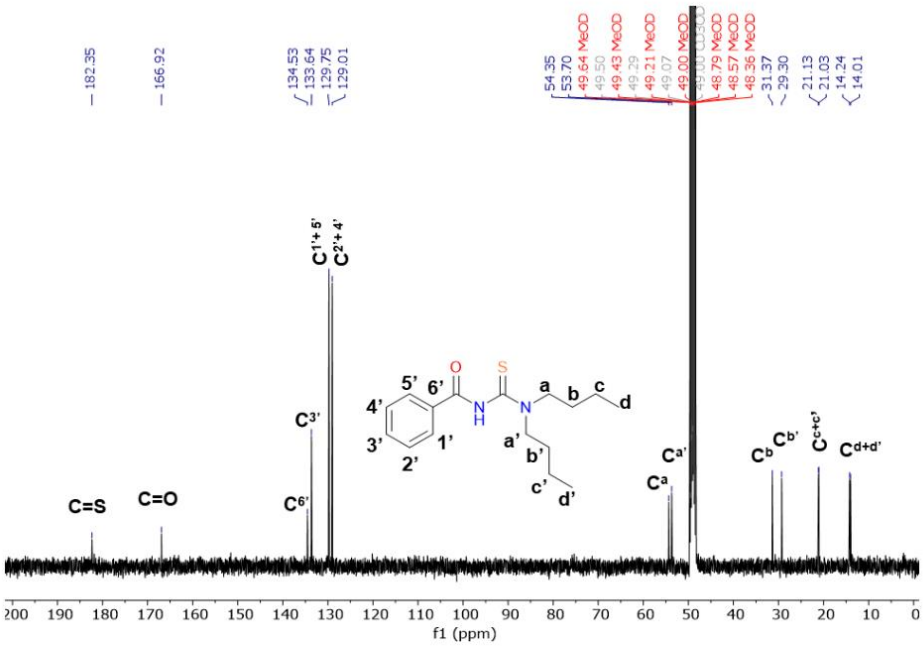
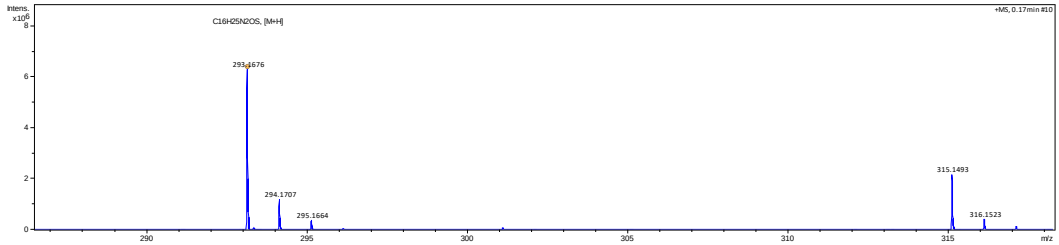


***Figure 2.6**: ^{13}C NMR spectrum of N,N-dibutyl-N'-benzoylthiourea ligand in methanol-d_4 at 25 °C.*

The structure of *N*,*N*-di(alkyl)-*N*'-acylthiourea ligands were further characterized using infra-red spectroscopy (IR). The presence of four functional groups; a secondary amine group *v*(N-H), an aliphatic and/or aromatic *v*(C-H), the carbonyl *v*(C=O) and thiocabonyl *v*(C=S) groups were observed and assigned for each acylthiourea ligand . The IR spectrum of HL^1 showed a broad absorption band at 3159 cm^{-1} which was assigned to the secondary amine *v*(N-H), followed by the aromatic *v*(C-H) 3062 , aliphatic *v*(C-H) ranging at 2871 – 2959 cm^{-1}, a sharp and intense band at 1685 cm^{-1} stretching frequency was assigned to the carbonyl *v*(C=O) and strong sharp peak at 1372 cm^{-1} assigned to the *v*(C=S).



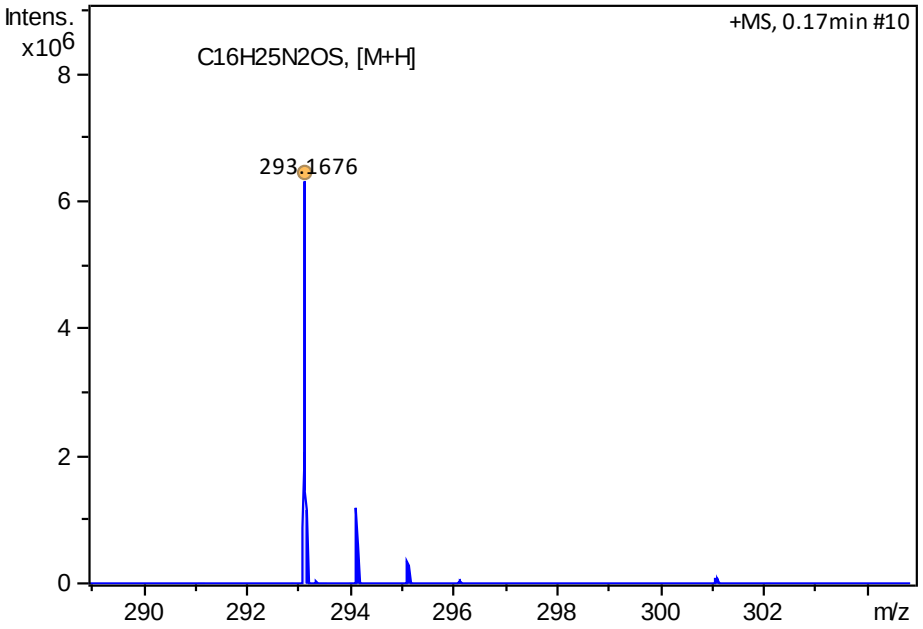
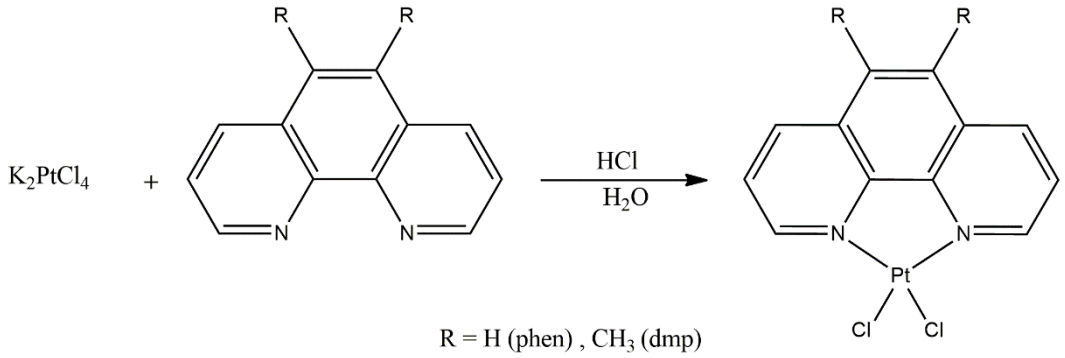


***Figure 2.7**: The high resolution mass spectrum of N,N-dibutyl-N'-benzoylthiourea (**HL^1**) prepared in HPLC grade methanol showing the abundant peak observed at 293.16 m/z (L+H) while the expected peak (292.16 m/z), confriming the pure structure of the prepared ligand.*

High resolution mass spectrometry further confirmed the structure and purity of the ligands by showing a clean MS spectrum with the abundant peak for HL^1 observed at 293.16 [L^1+H] mass to charge ration (m/z) corresponding to the calculated/predicted peak of 292.16 m/z [L^1] (*Figure 2.7)*.

2.3.3 Synthesis and characterization of the platinum precursor $PtCl_2$(diimine)

The metal precursors $PtCl_2$(phen) and $PtCl_2$(dmp) were synthesized following a modified method described by Morgan and Bustall on the synthesis of 2:2′-Dipyridyl platinum salts (Morgan and Burstall, 1934). The precursor was synthesized using potassium tetrachloroplatinate (K_2PtCl_4) salt as the source of platinum(II), dissolved in deionized water to form a deep red-brown solution (Scheme 2.3). Six drops of HCl were added to this solution to prevent aquation of K_2PtCl_4.



Scheme 2.3: *Preparation of $PtCl_2$(diimine) by reflux in deionised water where drops of HCl were added to prevent aquation of potassium tetra-chloroplatinate upon dissolution.*

An equivalent mole of the appropriate diimine ligand, 1,10-phenanthroline (phen) or 5.6-dimethyl-1,10-phenanthroline (dmp) was added to the solution. The reaction mixture was then refluxed for approximately three hours, until a bright yellow precipitate was observed. The formed product was transferred into a centrifuge tube and washed with deionized water followed by acetonitrile via centrifuge system. This was to remove any trace amounts of the unreacted starting materials. The platinum precursor was then dried under vacuum and characterized.

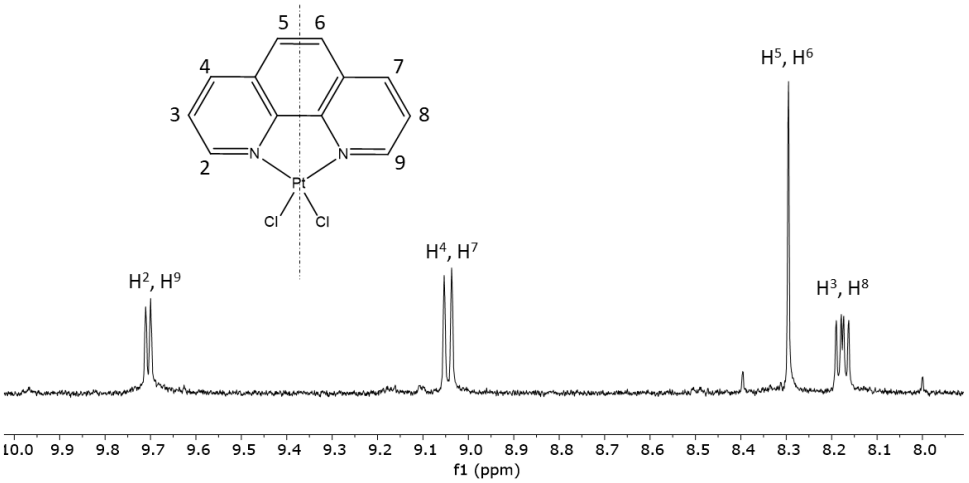


***Figure 2.8**: [1]H-NMR spectrum of $PtCl_2$(phen) in DMSO-d_6 at 25 ℃ showing C_2 symmetry.*

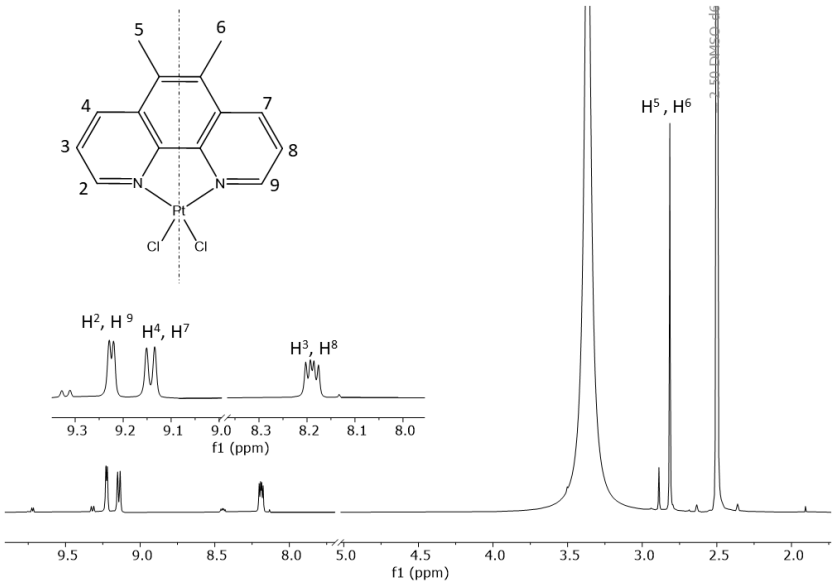


***Figure 2.9**: [1]H-NMR spectrum of $PtCl_2$(dmp) in DMSO-d_6 at 25 ℃. The spectrum is cut between 5.20 -7.50 ppm to show all peaks and expanded in the aromatic region.*

The ^{1}H NMR spectra of metal precursors $PtCl_2$(phen) and $PtCl_2$(dmp) with assigned aromatic protons were reported (*Figure 2.8 and Figure 2.9)*. Both platinum precursors have C_2 symmetry, as a result, *Figure 2.8* shows a proton NMR spectrum with four equivalent aromatic proton signals accounting for eight protons while *Figure 2.9* shows three aromatic proton signals and one methyl proton signal (6H)

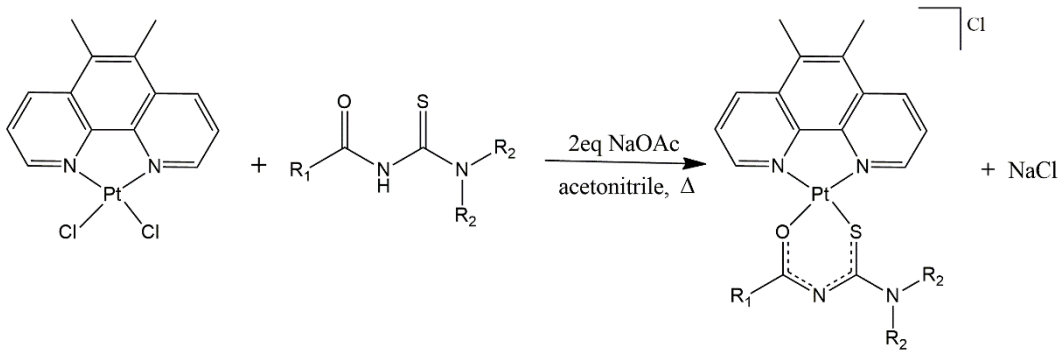
on the aliphatic region. The most deshielded proton signal on $PtCl_2$(phen) spectrum at 9.70 ppm was assigned to H^2 and H^9 protons as they are bonded to electron withdrawing nitrogen atoms. The signal at 8.29 ppm was assigned to H^5 and H^6 protons since they do not couple to any other protons in the complex and this signal appears as a singlet on the spectrum (*Figure 2.8*). The most shielded proton signal at 8.17 ppm was assigned to H^3 and H^8 as these protons couple to two adjacent protons that are in close proximity, hence a large coupling constant (J = 8.2, 5.3 Hz) is observed with a doublet of doublet that resembles a triplet. The other doublet of doublet at 9.04 ppm was assigned to H^4 and H^7 protons. The minor peaks observed in the aliphatic region were accounted for as trace amount of water, acetone and acetonitrile solvent used during the washing step. The peaks observed in the aromatic region were presumed to be due to the presence of trace amount of unreacted phenanthroline ligand.

The infra-red spectrum of platinum precursors $PtCl_2$(phen) and $PtCl_2$(dmp) showed expected aromatic C-H bands at ν(C-H) stretching frequencies of 3057 cm^{-1} and 3077 cm^{-1} respectively. The aromatic imine group ν(C=N) was assigned to the absorption bands with stretching frequencies of 1627 cm^{-1} and 1616 cm^{-1} corresponding to the expected range in literature (expected as per Sigma-Aldrich IR table).

2.3.4 Synthesis of [Pt(diimine)(L^n-κ*O,S*)]Cl complexes

Platinum complexes [Pt(diimine)(L^n-κ*O,S*)]Cl were synthesized following a modified method described by Koch (Koch, 2001).The method involved adding the acylthiourea ligand dropwise into a dilute suspension of an appropriate metal precursor $PtCl_2$(dmp) and excess weak base (2 eq) in acetonitrile (Scheme 2.4). The dilute suspension was stirred and refluxed while an appropriate *N*,*N*-di(alkyl)-*N*'-acylthiourea ligand (1 eq), also dissolved in acetonitrile; was slowly added dropwise into a suspension of the precursor and base. The mixture was refluxed for 24 hours to allow a substitution of two chloro ligands on $PtCl_2$(dmp) by one chelating *N*,*N*-di(alkyl)-*N*'-acylthiourea, coordinating to the platinum centre via

sulfur and oxygen atoms following deprotonation by a base. The reaction was refluxed until a clear yellow or orange/brown solution was obtained.



***Scheme 2.4**: Reaction scheme showing the preparation of [Pt(dmp)(L^n-κO,S)]Cl complexes from HL^n and platinum precursor in excess sodium acetate.*

The reaction was worked up by dissolving the complex in dichloromethane and filtering the solution through cotton or celite to remove insoluble salts (NaOAc and/or NaCl). The solvent was evaporated under vacuum and the product concentrated in a small volume of acetonitrile followed by selective precipitation with diethyl ether or hexane.

The synthesis of complexes bearing *N*,*N*-di(alkyl)-*N*'-arylthiourea ligand, where R^1 is an aromatic variation such as *N*,*N*-di(alkyl)-*N*'-benzoylthiourea (**HL^1**, **HL^5** and **HL^8**) or *N*,*N*-di(alkyl)-*N*'-1-napthoylthiourea (**HL^4** and **HL^7**) was conducted in 5% binary water:acetonitrile system (1:20). This was done to favour a formation of bidentate coordination of acylthiourea ligand to form the cationic [Pt(diimine)(L^n-κ*O*,*S*)]$^+$Cl$^-$ complex as the major product over a monodentate coordination, forming a neutral [Pt(diimine)(L^n-κ*O*,*S*)$_2$] complex. The system was used to improve the solubility of the precursor in acetonitrile and drive the reaction to completion. The crude product was selectively precipitated, and the complex filtrate was re-suspended several times to obtain a clean product. Complexes were dried under vacuum and characterized using ^{1}H and ^{13}C NMR spectroscopy, infrared spectroscopy, and high resolution mass spectrometry.

2.3.5 Characterization of [Pt(dmp)(L^1-κ*O*,*S*)]Cl complexes using ^{1}H, ^{13}C and 2D NMR Spectroscopy and Mass Spectrometry

The ^{1}H NMR spectrum of the complex [Pt(dmp)(L^1-κ*O*,*S*)]Cl prepared in chloroform-*d* and stacked alongside the respective free ligand **HL^1**, confirmed the structure of the chelate complex *(Figure 2.10)*. A successful complexation was firstly indicated by the disappearance of the broad N-H signal on the complex spectrum due to deprotonation of the **HL^1** ligand Additionally, the appearance of aromatic peaks from the dmp ligand and a downfield shift of benzoyl proton peaks ($H^{1'+5'}$) including the butyl chain peaks (H^a, $H^{a'}$; H^d, $H^{d'}$) also confirmed a successful coordination of **HL^1** ligand to the platinum precursor $PtCl_2$(dmp).

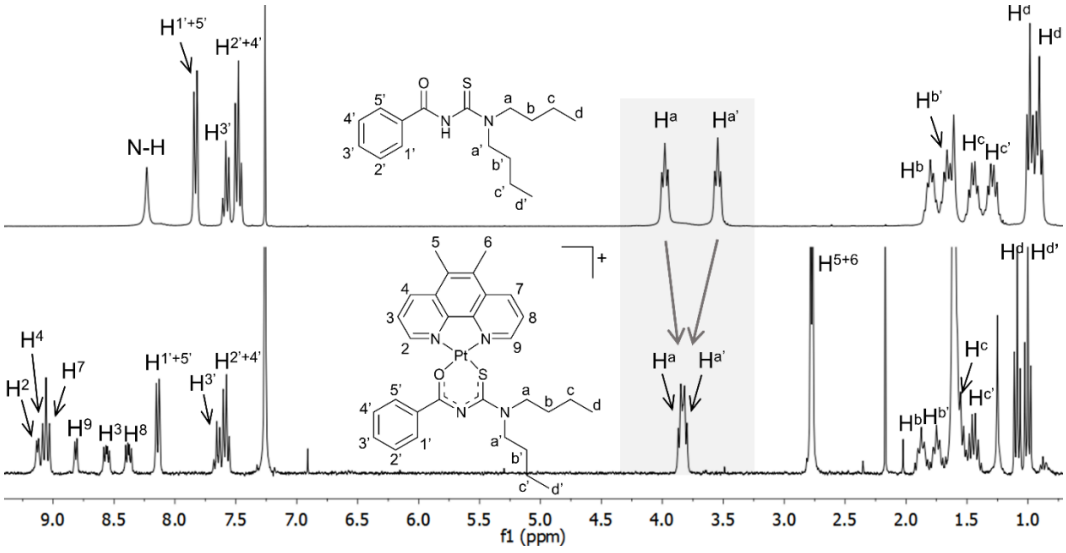


***Figure 2.10**: Stacked 1D ^{1}H NMR spectrum of the N,N-dibutyl-N'-benzoylthiourea ligand (**HL^1**) and [Pt(dmp)(L^1-κO,S)]$^+$ complex in $CDCl_3$ at 25 ℃ with all assignments.*

The aliphatic proton peaks between 1.04 ppm – 3.67 ppm appear much sharper/ more resolved upon complexation; this is indicative of a more restricted rotation about the thio-amidic bond compared to the free ligand. The H^a and $H^{a'}$ proton signals overlap at 3.83 ppm relative to the distinct signals of the free ligand at 3.98 ppm and 3.54 ppm as annotated (*Figure 2.10)*. The observed overlap in peaks is attributed to the proximity of individual proton signals, rather than a coalescence

resulting from rapid exchange. This shared characteristic is evident in the ^{1}H NMR spectra presented in Appendix A for the complexes in the series (Figure A1-A3). The H^{d} and $H^{d'}$ proton signal slightly shifted downfield and also showed less overlapping upon complexation due to the restricted free rotation about the amidic bond.

The 2D NMR of [Pt(dmp)(L^{1}-κ*O,S*)]Cl complex was obtained by running the sample in methanol-d_4 (*Figure 2.11)*. The signals in the aromatic region appear to be slightly different relative to the observed spectrum in chloroform-*d* and were assigned accordingly. The proton spectrum was assigned following an assumption that N^{1} is the nitrogen trans to sulfur and H^{2} is the most deshielded proton following the NOE results reported by Kotzé (Kotzé, 2009).

The aliphatic region shows assignment of proton in the butyl chains whereas the aromatic region accounts for the proton on the benzoyl group and the phenanthroline ring. Protons on the butyl chain were assigned similar to the **HL^{1}** ligand, with the most deshielded proton signal at 3.67 ppm assigned to $H^{a'}$ and H^{a} since they overlap and intergrate for 4 protons. The second most deshielded protons of the butyl chains at 1.83 & 1.65 ppm were assigned to $H^{b'}$& H^{b} while the signals at 1.56 & 1.46 ppm were assigned to $H^{c'}$ & H^{c} respectively. Lastly, the most shielded proton signal was assigned to the methyl groups H^{d}'and H^{d} at 1.14 and 1.04 ppm appearing as a triplet.

In the aromatic region, the most shielded signal appearing at 7.49 ppm, intergrating for two protons was assigned to two equivalent benzoyl protons $H^{2'}$and $H^{4'}$ as they couple to other benzoyl protons at 7.73 ppm (7.63 -7.81 ppm). The multiplet at 7.63 - 7.81 ppm showed overlapping signals that intergrated for four aromatic protons and was assigned to $H^{3'}$, $H^{1'}$and $H^{5'}$ of the benzoyl group as well as H^{8} of the phenanthroline group.

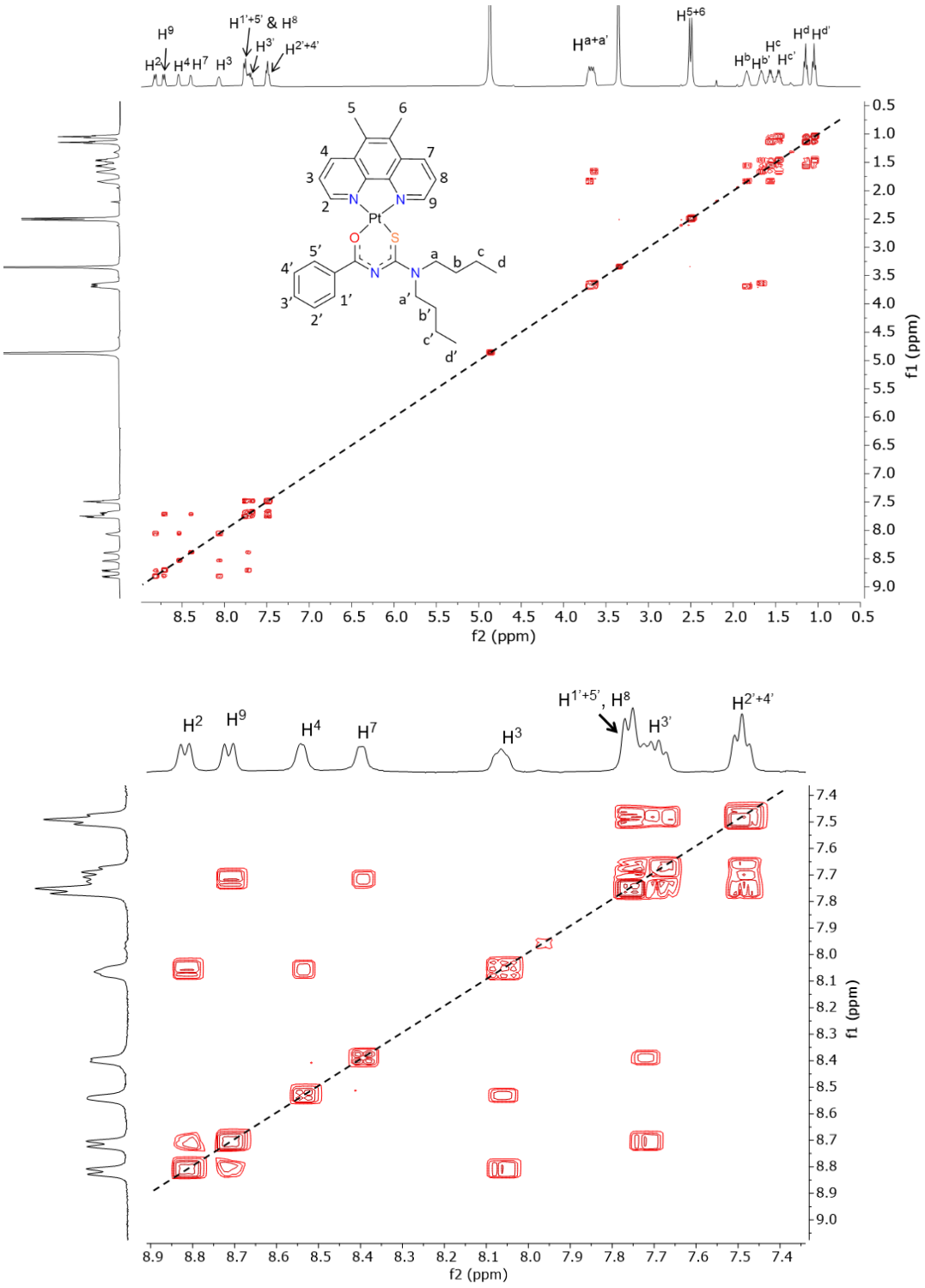


***Figure 2.11**: ^{1}H-^{1}H COSY NMR spectrum of [Pt(dmp)(L^{1}-κO,S)]Cl in methanol-d_4 at 25 ℃ showing the expanded aromatic region.*

The H^8 proton appeared to couple to two phenanthroline protons at 8.39 ppm and 8.71 ppm which were assigned to H^7 and H^9 respectively. Again, this proton (H^9) only appears to couple to H^8 while H^8 couples to both H^9 and H^7, confirming the spacial arrangement of these protons on the phenanthroline ligand. Similar to H^8, the proton signal at 8.06 ppm appeared to be coupling to two other protons at 8.81 ppm and 8.53 ppm and was therefore assigned to H^3. The most deshielded proton on the spectrum at 8.81 ppm was assigned to H^2 since it also coupled to a relatively more shielded proton signal at 8.06 ppm (H^3). As a result, the signal at 8.53 ppm was assigned to H^4 as it showed coupling to H^3 at 8.07 ppm. The methyl substituents at positions 5 and 6 are indistingushable and were assigned to the aliphatic signal at 2.50 ppm which intergrated for six protons.

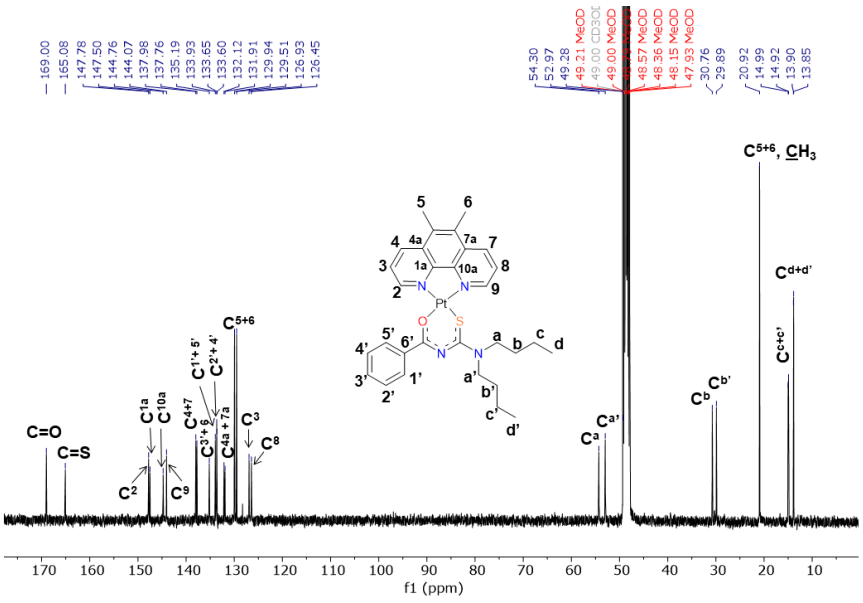


***Figure 2.12**: ^{13}C-NMR spectrum of [Pt(dmp)(L^1-κ*O,S*)]Cl complex in methanol-d_4 at 25 ℃.*

The ^{13}carbon NMR spectrum of [Pt(dmp)(L^1-κ*O,S*)]Cl *(Figure 2.12)* was assigned using 2D nmr spectroscopy (HSQC, HMBC and DEPT-135 spectra). The double bond character of the carbonyl and thio-carbonyl functional group was signficantly reduced due to deprotonation and coordination via the sulfur and oxygen atoms. This resulted in a partial double bond character of C=O and C=S facilitated by the

presence of a delocalised anion. A change in the chemical shift of C=O and C=S signals was closely observed upon complexation. The carbon spectrum of [Pt(dmp)(L^1-κ*O*,*S*)]Cl complex showed signals at 168.99 ppm (C-O) and 165.07 ppm (C-S) respectively while these signals were observed at 166 ppm (C=O) and 182 ppm (C=S) in the free ligand **HL^1**. This implies that the thiocarbonyl bond (C=S) is weaker than the carbonyl group (C=O) upon coordination to platinum; whereas the opposite is true in the respective free ligand. The aliphatic and aromatic carbons were assigned in the range 13.85 - 54.30 ppm and 126.44 -147.77 ppm respectively by the use of 2D NMR and DEPT-153 (*Figure 2.12*).

The infrared spectrum (IR) obtained for [Pt(dmp)(L^1-κ*O*,*S*)]Cl complex (*Figure 2.13; Table 2.1*) confirmed a loss of N-H depicted by the disapperance of the broad secondary amine absorption band at 3166 cm^{-1} upon complexation of **HL^1** ligand.

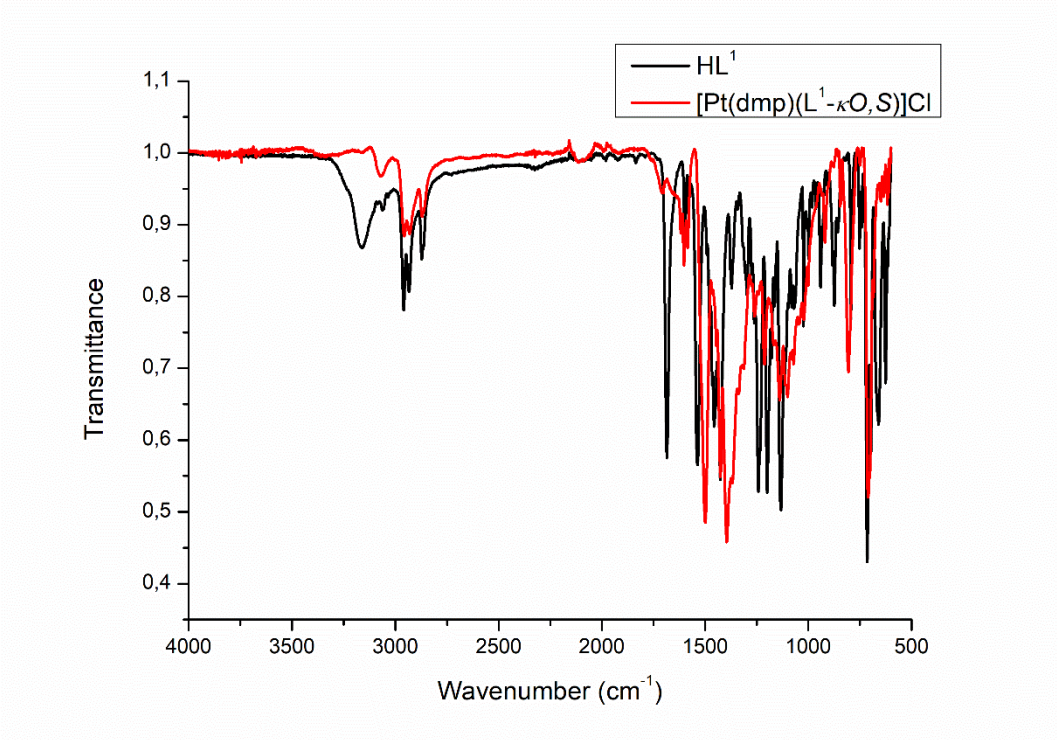


***Figure 2.13**: FT-IR spectrum of [Pt(dmp)(L^1-κO,S)]Cl stacked alongside the free **HL^1** ligand.*

***Table 2.1**: FT-IR wavenumber (cm^{-1}) values assigned to each functional group in HL^1 and [Pt(dmp)(L^1-κO,S)]Cl from the spectrum respectively.*

IR (cm^{-1})	HL^1	[Pt(dmp)(L^1-κ*O,S*)]Cl
N-H	3166	-
C-$H_{aromatic}$	3062	3063
C-H_{alkyl}	2959-2871	2959-2871
C=O	1685	1397 (C-O)
C=S	1372	1216 (C-S)

The sharp/strong stretching bands of *v*(C=O) and *v*(C=S) observed at range of 1685-1661 cm^{-1} and 1461-1368 cm^{-1} in the free ligands were not observed in the complexes. The change in bond order upon complexation (partial double bond) resulted in a shift of these sharp bands to lower stretching frequencies ranging between 1422- 1359 cm^{-1} and 1304 -1203 cm^{-1} for *v*(C-O) and *v*(C-S) respectively.

The assignment of *v*(C=S) bands was rather challenging as there are many sharp peaks within the expected range (fingerprint region), however, the C=S bond in free ligands and complex were assigned based on the reported data in literature for **HL^1** and [Pt(dmp)(L^1-κ*O,S*)]Cl respectively (Magwaza, 2017).

A high resolution electron spray mass spectrometry (ESI^+) was used to further characterize and confirm the purity of synthesized ligands and cationic platinum complexes. The experimentally obtained mass spetrum of [Pt(dmp)(L^1-κ*O,S*)]$^+$ prepared in HPLC grade methanol (*Figure 2.14*) confirmed the identity of the cationic complex by showing an abundant peak with a mass to charge ratio of 694.21 *m/z*. This abundant peak and isotopologue pattern are in 100% agreement with the predicted spectrum of the complex, showing a parent peak of 694.21 *m/z.* The most abundant Pt isotope is ^{195}Pt (33.8%) responsible for the identified parent peak. The spectra also showed the absence of impurities thereby confiming the purity of the complex.

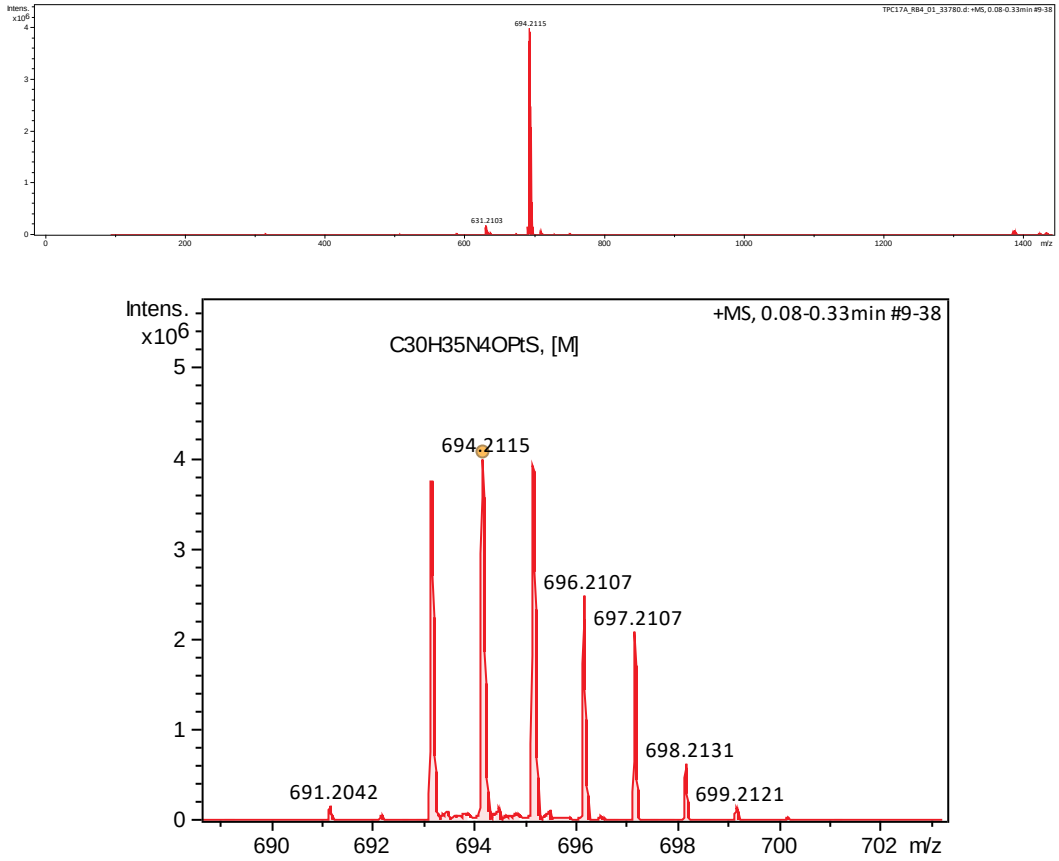


***Figure 2.14**: The high resolution mass spectrum of [Pt(dmp)(L[1]-κO,S)]Cl prepared in HPLC grade methanol showing the major peak of the complex and the isotopologue pattern of the Pt, the most abundant being [195]Pt 694.211 m/z.*

Chapter 3: Cytotoxic effects of platinum complexes on lung and colorectal cancer cells and their mechanism of cell death

3.1 Introduction

Cytotoxicity, whether induced by chemical substances or pathogens, refers to their ability to kill or damage cells. Cell death can be described as an irreversible deterioration of vital cellular functions. These include the loss of ATP production and a disruption of the redox balance, leading to the loss of cellular integrity, either through permanent permeabilization of the plasma membrane or fragmentation of cell organelles (Galluzzi *et al.*, 2018). Various biochemical and morphological changes in cells have been used to differentiate between cell death mechanisms. These mechanisms include both regulated pathways, such as apoptosis, and unregulated or accidental pathways, such as necrosis, previously described in chapter 1 (Kroemer *et al.*, 2009; Galluzzi *et al.*, 2018).

The success of most anti-cancer drugs is based on their ability to cause cell death of highly proliferative tumour cells. Chemotherapeutic agents that induce cell death by regulated pathways are preferred and considered safer than those that induce necrotic cell death (Elmore, 2007).

Understanding the cytotoxic effects of investigational compounds is important for assessing both their safety and potency. Essential tools for this assessment include cell cytotoxicity and proliferation assays, which measure the effect of test compounds on cell proliferation through metabolic activity and viability (Adan, Kiraz and Baran, 2016). Additional assays, such as those examining biochemical factors such as caspase activity, contribute to identifying cell death pathways (Kari *et al.*, 2022).

In this chapter, the cytotoxic effects of nine platinum complexes, synthesized and characterized as described in chapter 2, were evaluated against two human lung epithelial cancer cell lines (H1975 & A549) and a colorectal cancer cell line (HT-

29). The complexes have the general formula, [Pt(diimine)(L^n-κ*O*,*S*)]Cl, where diimine ligands represents; 1,10-phenanthrolines (phen), 5,6-dimethyl-1,10-phenanthroline (dmp), and dypirido[3,2-f:2',3'-h]quinoxaline (dpq); whilst the disubstituted acylthiourea ligands presented as HL^1, HL^2 and HL^3 refer to *N*,*N*-dibutyl-*N*'-benzoylthiourea, *N*,*N*-dibutyl-*N*'-acetylthiourea and *N*,*N*-dibutyl-*N*'-pivaloylthiourea respectively. The antiproliferative activity of free diimines ligands was also investigated considering their recognized bioactivity resulting from interactions with DNA. (Brodie, Collins and Aldrich-Wright, 2004; Novoa-Ramírez *et al.*, 2023; Todorov and Kostova, 2023).

3.2 Experimental

3.2.1 Cell culture

The A549 and HT-29 cells used in this study were purchased from the Fox Chase Cancer Institute (Philadelphia, Pennsylvania, USA). H1975 cells were purchased from Cellonex (Johannesburg, South Africa). The cell lines were authenticated by short tandem repeat (STR) analysis conducted by Inqaba Biotechnical Industries, Pretoria, South Africa. An ethics waiver; W-CBP-180420-06 granted by the Human Research Ethics Committee in the Faculty of Health Sciences at the University of the Witwatersrand was obtained to permit the usage of these cancer cell lines for this study (*Appendix B*).

3.2.1.1 Maintenance and sub-culturing

Cells were cultured in 25 cm^2 or 75 cm^2 cell culture flasks (Sigma-Aldrich/Merk, Johannesburg, South Africa) and maintained at 37℃ in a humified 5% CO_2 atmosphere incubator. The A549 cells were maintained in a 1:1 mixture of Dulbecco's Modified Eagle Medium (DMEM) and Ham F-12 media (Thermo Fisher Scientific, Johannesburg, South Africa) while HT-29 and H1975 cells were maintained with Roswell Park Memorial Institute (RPMI) media (Sigma-Aldrich/Thermo Fisher Scientific, Johannesburg, South Africa) respectively. Culture media was supplemented with 10% (v/v) heat-inactivated fetal bovine serum (FBS) (Thermo Fisher Scientific, Johannesburg, South Africa), 1% (v/v) L-glutamine (Merk, Johannesburg, South Africa) and 1% (v/v) sodium pyruvate

(Merk, Johannesburg, South Africa). The cell media was replaced every second day.

Upon reaching 70% - 80% confluence, cells were sub-cultured by removing 70% of cells using Trypsin ethylenediamine tetraacetate (Trypsin-EDTA) (Sigma-Aldrich, South Africa) and replacing it with fresh culture media. Cells were observed daily using the Olympus CKX41 (Tokyo, Japan) inverted phase contrast microscope to monitor growth and check for microbial contamination.

3.2.1.2 Cryopreservation of cells

Cells were harvested by centrifugation and resuspended in freezing media made up of 1:1 mixture of DMEM and Ham-F12 media (H1975 and A549) or RPMI media (HT-29) and supplemented with 20% fetal bovine serum 5% (v/v) cell culture grade DMSO (Thermo Fisher Scientific/Sigma-Aldrich, Johannesburg, South Africa). The cell suspension was aliquoted in 2 mL cryopreservation vials placed in a Corning® CoolCell® freezing container (Thermo Fisher Scientific, South Africa) at -70 ℃ for controlled freezing over 3-4 days. After freezing, the vials were stored in a -70 ℃ freezer or transferred to liquid nitrogen.

3.2.1.3 Trypan blue assay

Trypan blue exclusion assay was used to determine the percentage of viable cells in a cell suspension before experimental usage. Trypan blue powder (Sigma-Aldrich, Johannesburg, South Africa) was dissolved in 1X PBS to a final concentration of 0.2% (w/v). The solution was filtered through a 0.22 µm membrane and subsequently stored in a light-shielded container at room temperature. The exclusion assay was performed as follows; 20 µL of a 0.2% trypan blue solution was carefully pipetted into 20 µL of the cell suspension. Subsequently, a 1:1 mixture consisting of 20 µL of this trypan blue-cell suspension mixture was added into a hemocytometer, where a cell count was conducted in each quadrant and then averaged. To calculate the cell concentration per milliliter, the resulting average cell count was multiplied by the dilution factor (×2) and further multiplied by 10^4. It's important to note that only cells with a viability exceeding 95% were utilized for subsequent experiments.

3.2.2 Preparation of reagents

3.2.2.1 Test compounds

Stock solutions of each [Pt(diimine)(L^n-κ*O*,*S*)]Cl complex were prepared as 10 mM concentration in cell culture grade dimethyl sulfoxide: ethanol mixture [25:75] (Sigma-Aldrich, Johannesburg, South Africa). Fresh dilutions were prepared from the stock before each experiment. The pure platinum(II) complexes were synthesized and characterized as reported in chapter 2. The positive control cisplatin (Sigma-Aldrich/Merk, Johannesburg, South Africa) was prepared on the day of use in 1X PBS. Staurosporine and tertiary-butyl hydroperoxide (BIOCOM Africa, Pretoria, South Africa, Abcam) were also freshly prepared and diluted with cell media on the day of the experiment.

3.2.2.2 Phosphate Buffer Saline

Phosphate buffered saline (PBS) solution was used to wash cells in culture flasks and to remove residual media that would inhibit the trypsinization process. The PBS solution consisted of 1.37 mM NaCl, 27 mM KCl, 100 mM Na_2HPO_4 and 18 mM KH_2PO_4 (Merck/Sigma-Aldrich, Johannesburg, South Africa) (pH 7.2-7.4). The solution was then autoclaved and stored at 4˚C but warmed to room temperature before usage.

3.2.2.3 MTT solution

The MTT powder (3-(4,5-dimethylthiazol-2-yl)-2,5-diphenyltetrazolium bromide) (Merck, South Africa) was dissolved in PBS at a concentration of 5 mg/mL (250 mg in 50 mL PBS), sterile filtered and stored in the dark at 4˚C.

3.2.3 The MTT cell viability assay

Principle for the assay

An MTT assay is a rapid colorimetric assay that measures cell viability and cell growth inhibition. This assay is based on the conversion (reduction) of the MTT dye (3-(4,5-dimethylthiazol-2-yl)-2,5-diphenyl tetrazolium bromide) into purple formazan crystals ((E,Z)-5-(4,5-dimethylthiazol-2-yl)-1,3-diphenyl formazan) in healthy cells through mitochondrial enzyme activity (*Figure 3.1*) (Mosmann, 1983;

van Meerloo, Kaspers and Cloos, 2011). Formazan crystals are then solubilized by a non-polar solvent (i.e DMSO) yielding a purple solution. The intensity of the purple solution, measured at 540 nm with spectrophotometry is proportional to the number of viable cells with healthy mitochondrial enzyme activity and thus can be quantified (Kamiloglu *et al.*, 2020).

Cells were seeded at a density of 10 000 cells per well in 100 microliters in a 96 well plate and allowed to adhere overnight. On the next day, cells were treated with a range of concentrations prepared at 2X the final concentration in culture media and 100 uL of each was added to each well. Each concentration was carried out in quadruplicate. Cytotoxicity screening involved testing complexes at 50 µM and 5 µM concentrations for 46 hours. IC_{50} values for active complexes were determined within a concentration range of 0.05 - 100 µM over the same time period. Following treatment, 40 µL of 5 mg/mL MTT solution was added into each well and incubated for two hours. The 96 well plates were then centrifuged using Heraeus Megafuge 40 centrifuge at 1000 rpm for 5 minutes. The cell media containing the MTT solution was aspirated from each well. Following this step, 200 µL of DMSO was added to each well to dissolve formazan crystals. The 96-well plate was then shaken at 1000 rpm for 5 minutes, and the absorbance was measured using a microplate Labsystems iEMS Reader at wavelengths of 540 nm and a reference wavelength of 690 nm. The blank wells contained only cell culture media. The experiment was repeated a minimum of three times. The formula for calculating percentage cell viability is shown below where 'Abs' represents the absorbance measured at 540 nm, subtracted by the reference absorbance at 690 nm:

$$Cell\ viability\ (\%) = \frac{Abs_{treated\ cells} - Abs_{blank}}{Abs_{untreated\ control\ cells} - Abs_{blank}} \times 100$$

3.2.4 Cell morphology

Changes in cancer cell morphology were evaluated using phase contrast microscopy and fluorescent dyes; (Hoechst-33342 (HO), Acridine orange (AO) and propidium iodide (PI). HO highlighted nuclear status, with apoptotic cells showing increased blue fluorescence (due chromatin condensation) or fragmented nuclei

(Bucevičius, Lukinavičius and Gerasimaitė, 2018). PI is a nucleic acid binding dye (intercalator) used as a cell viability marker since it only permeates dead/dying cells with disrupted plasma membrane but does not permeate healthy cells with intact membranes. PI non-uptake indicated intact cell membranes, while a red-stained nucleus identified necrotic cell death, enabling PI use for necrosis identification (Crowley *et al.*, 2016). Apoptosis markers included membrane blebbing, chromatin condensation, and nuclear fragmentation (De Vitto, Valencia and Radosevich, 2018). Necrosis was identified by round, swollen cells with compromised membranes but intact nuclei (Atale *et al.*, 2014).

Cells were seeded on sterile coverslips in a six-well culture plate at a density 200 000 cells per coverslip in 2 mL of culture media and allowed to adhere on the surface overnight. Cells were then treated with the appropriate concentration of each test complex, [Pt(dmp)(L^1-κ*O*,*S*)]Cl, [Pt(dmp)(L^2-κ*O*,*S*)]Cl, [Pt(dmp)(L^3-κ*O*,*S*)]Cl and cisplatin for 18 hours. Following treatment, the culture media was carefully removed, and cells were gently rinsed with 2 mL of 1X PBS. Following this, cells were incubated with 500 µL of the dye mixture in each well for 20 minutes in the dark at room temperature. The dye mixture consisted of Hoechst 33342 (5 µg/mL) (Sigma-Aldrich, Johannesburg, South Africa), Acridine Orange (10 µg/mL) and Propidium Iodide (10 µg/mL) (Thermo Fisher Scientific, Johannesburg, South Africa) in 10 mL of 1X PBS. Thereafter, coverslips were mounted faced down on microscope slides and cells were viewed with an Olympus BX41 epifluorescent microscope (Olympus, Tokyo, Japan), using the Olympus filter cube sets U-MWU2 (Excitation: 365/10, Emission:420 nm long pass) for HO, U-MWIG2 (Excitation: 535/30, Emission:580 nm long pass) for PI and U-MNIB3 (Excitation:480/20, Emission:510/50) for AO. Images were captured with Olympus DP72 digital camera at 400X magnification, constant exposure time and ISO settings. Images were analysed using the Olympus CellSens Software Program (Olympus, Tokyo, Japan). The images included in each figure were selected from a single experiment and are representative of at least three independent experiments. Images were optimized for brightness and contrast using identical settings.

3.2.5 Detection of apoptosis by annexin-V/propidium iodide staining

The externalization of phosphatidylserine (PS) on cell plasma membrane is an early event in apoptosis and can be assessed by the binding annexin-V (AV), a calcium (Ca^{2+}) dependent phospholipid-binding protein, that has a high affinity for PS (Fadok *et al.*, 1992; Vermes *et al.*, 1995). Necrosis is associated with the loss of membrane integrity, which was assessed using propidium iodide (PI). PI cellular uptake is used as a marker for necrosis/secondary necrosis and/or late apoptosis. Healthy non-apoptotic cells do not bind annexin-V (-) nor permeate PI (-), while early apoptotic cells with externalized PS bind annexin-V (+) without permeating PI (-), late apoptotic or secondary necrotic cells loose membrane integrity and are thus identified by binding annexin-V (+) and permeating PI (+), whereas necrotic cells permeate PI (+) without binding annexin-V (-). Annexin-V is conjugated to a fluorochrome (i.e Alexa fluor 488 or fluorescein isothiocyanate/FITC) for luminescence detection of cells undergoing apoptosis. Alexa Fluor 488 and FITC both results in bright green fluorescence that can be observed under a fluorescence microscope.

Cells were seeded on coverslips in a six-well plate and treated as previously described in cell morphology. The negative control was incubated with 2 mL of complete cell media. This was followed by a gentle removal of the cell media and pipetting of floating cells into 2 mL microcentrifuge tubes. Adherent cells on coverslips were gently rinsed with 2 mL of 1X PBS (pH 7.4) while floating cells were harvested by centrifuging at 1000 rpm for 5 minutes at room temperature. A working solution mixture was prepared by diluting the stock solutions of annexin-V and propidium iodide in annexin-V binding buffer (ABB) following the appropriate protocols. Cells were then incubated with 150 µL of the working solution for 20 minutes in the dark at room temperature. Coverslips with adhered cells were then mounted faced down on microscope slides whilst 30 µL of the harvested stained cell suspension was transferred to a microscope slide and covered with sterile coverslip. Cells were viewed with Olympus BX41 epifluorescence microscope using a U-MNIB3 filter cube (Excitation:480/20, Emission:510/50) to detect the green fluorescence by Alexa Fluor 488 or FITC and a U-MWIG2

(Excitation: 535/30, Emission:580 nm long pass) for PI. Images were captured and analysed as previously described (section 3.2.4).

3.2.6 Determination of caspase-3/7 activity

Executioner caspase-3 and caspase-7 both carry out apoptotic cell death when activated. The induction of caspase-3/7 activity by platinum complexes in cancer cells was detected using the CellEvent™ Caspase-3/7 Green Detection Reagent (Cat. No 14040133, Thermo Fisher Scientific, Johannesburg, South Africa). The reagent is a substrate for active caspase-3/7 and consists of a four amino acid peptide chain; Asp-Glut-Val-Asp (DEVD) conjugated to a nucleic acid binding dye. The DEVD peptide chain prevents the dye from binding to the nucleic acid, making the reagent non-fluorescent. Apoptotic cells with active caspase-3 or caspase-7 allow the cleavage of the DEVD peptide on aspartate residues (D); enabling the dye to bind to DNA and produce bright green nuclear fluorescence in a cell with an absorption/emission maximum of ~502/530 nm. The detection of the green nuclear stains fluorogenic response in cells is therefore regarded as a direct indicator of caspase-3/7 activity in the cell.

Cells were seeded on coverslips in a six-well plate previously described. Cells were treated with platinum complexes and cisplatin for 24 hours. The CellEvent™ Caspase-3/7 Green Detection Reagent was prepared by diluting the stock solution/reagent (2.0 mM, 100 µL in DMSO) in 1X PBS solution enriched with 5% FBS to a final concentration of 5 µM. The media was carefully removed from each well and cells were gently rinsed with 2 mL of 1X PBS. Following this, cells were incubated with 150 µL of the prepared reagent in each well for 30 minutes at 37 °C while kept in a humid container to prevent drying. Cells were then gently rinsed with 1 mL of 1X PBS solution and coverslips were mounted faced down on the microscope slides. Cells were viewed with Olympus BX41 epifluorescence microscope using phase contrast and the U-MNIB3 filter (Excitation:480/20, Emission:510/50). Images were captured and analysed as previously described in (section 3.2.4). At least three independent fields were used to determine the percentage cells with caspase-3/7 activity for each experiment.

3.2.7 Determination of caspase-8 activity

The initiator caspase-8 is known to be activated early on in cells undergoing apoptosis via the extrinsic pathway. The induction of caspase-8 activity by platinum complexes in cancer cells was detected using Abcam Caspase-8 Red Staining Reagent kit (BIOCOM Africa PTY LTD, Pretoria, South Africa, ab273416). The reagent consists of a cell permeant fluoromethyl ketone (FMK) derived peptide, IETD-FMK which is a known caspase-8 inhibitor. The caspase-8 inhibitor is conjugated to a red fluorescent dye, sulforhodamine (SR), with an absorption/emission maxima of 565/586 nm causing a red fluorogenic response when bound to active caspase-8. When introduced into the cell, the Red/SR-IETD-FMK reagent permeates and forms an irreversible bond with active caspase-8 in apoptotic cells, resulting in a red cytosolic stain. The red staining observed under the fluorescence microscope serves as a direct measure of the quantity of active caspase-8 present within the cell.

Cells were grown on sterile coverslips in a six-well plate as previously described in cell morphology and treated with platinum complexes and cisplatin for 18 hours. The caspase-8 red detection reagent was prepared by adding 3 µL of Red-IETD-FMK reagent into 900 µL of wash buffer. The cell culture media was removed from each well and cells were gently rinsed with 2 mL of 1X PBS (pH 7.4) solution. Subsequently, cells were incubated in the dark with 150 µl of caspase-8 red staining reagent for 1 hour, at 37 ℃ in a 5% CO_2 atmosphere in a humidified incubator. Following this, cells were gently rinsed with 1X PBS solution to prevent a high background signal. Each coverslip was then mounted on a microscope slide faced down and cells were viewed on the Olympus BX41 epifluorescence microscope using the U-MWIG2 filter (Excitation: 535/30, Emission:580 nm long pass). Images were captured using the Olympus DP72 digital camera and analysed with Olympus CellSens software programme as previously described (section 3.2.4).

3.2.8 Evaluation of the mitochondrial membrane potential by MitoProbe™ JC-1

Changes in the mitochondrial membrane potential (MMP/$\Delta\psi_m$) following exposure to test compounds were evaluated using a lipophilic mitochondria-specific cationic dye; 5,5,6'-tetrachloro-1,1',3,3'-tetraethylbenzimidazoylcarbocyanine iodide (JC-1). Healthy cells with intact mitochondrial membranes have a high $\Delta\psi_m$, driven by the negatively charged inner mitochondria and accumulate JC-1 dye, forming red-orange J aggregates (excitation/emission: ~585/590 nm). The loss of mitochondrial membrane potential, referred to as depolarization, is associated with unhealthy cells or apoptosis (due to mitochondrial membrane leaking) and can be detected by the presence of J monomers, causing cells to appear green since JC-1 dye (excitation/emission: 485/530 nm). Therefore, healthy non-apoptotic cells with high MMP were identified by the red-orange/yellow fluorescence, while unhealthy apoptotic cells with low MMP were identified by the green fluorescence.

Cells were seeded on sterile coverslips in a six-well plate at a density of 250 000 cells per well in 2 mL media and allowed to adhere to the coverslip surface. Cells were thereafter treated with platinum complexes as well as the two positive controls cisplatin and staurosporine for 18 hours. The untreated control cells were incubated with 2 mL media. The JC-1 dye working solution (5 µg/mL) was prepared by diluting 3 µl of the stock solution (5 mg/mL) into 3 mL of warm (37 ℃) cell culture media. The reagent was mixed gently by pipetting up and down and precipitates (aggregates) of the dye were removed by centrifuging at 3500 rpm for 10 minutes followed by sterile filtration with 0.22 µm membrane. Cells were then incubated with 500 µL of the prepared JC-1 dye for 30 minutes in the dark at 37 ℃, 5% CO_2 atmosphere. The JC-1 dye was then gently removed and cells were rinsed with 2 mL of 1X PBS. Coverslips were mounted faced down on microscope slides and viewed with Olympus BX41 epifluorescence microscope using filter cubes U-MNIB3 (Excitation:480/20, Emission:510/50) for detecting J-monomers and U-MWIG2 filter (Excitation: 535/30, Emission:580 nm long pass) for J-aggregates. Images were captured using the Olympus DP72 digital camera and thereafter overlayed using Olympus CellSens software program.

3.2.9 Evaluation of Reactive Oxygen Species

Reactive oxygen species (ROS) are highly reactive oxygen-containing molecules generated as natural byproducts during typical aerobic cell metabolism. The levels of ROS are regulated by antioxidant defence systems, comprising both enzymatic and nonenzymatic antioxidants. An imbalance between ROS production and the capacity of antioxidant systems to effectively neutralize these reactive molecules leads to oxidative stress. Excessive ROS levels cause damage to DNA, proteins and lipids, thereby compromising cellular health and inducing cell death. One method to detect cellular ROS levels is by employing fluorogenic probes (Katerji, Filippova and Duerksen-Hughes, 2019).

The induction of oxidative stress by active platinum complexes in cancer cells was measured using CellROX™ Deep Red Reagent (C10422, Invitrogen, Thermo Fisher Scientific). The deep red dye is non-fluorescent in its reduced state and fluoresces red upon oxidation by reactive oxygen species in a cell (ex/em maxima: 644/665 nm). The red fluorescent dye was therefore used as a direct measure of reactive oxygen species in cancer cells and detected using fluorescence microscopy.

Cells were grown on sterile coverslips in a 12-well plate at a density of 50 000 cells per well in 1 mL media. Cells were allowed to adhere on coverslip surface overnight. The CellROX™ Deep Red Reagent working solution was prepared by diluting the reagent (50 µL, 2.5 mM in DMSO) with cell culture media to a final concentration of 2.5 µM. This was achieved by adding 12 µL into 12 mL cell culture media (1 mL per well). The prepared working solution mixture was then aliquoted to 1 mL micro-centrifuge/Eppendorf tubes, followed by the addition of an appropriate volume of each test compound, to make up the desired final concentration. Cells were then treated with the test compound-reagent media mixture and incubated for 4 hours in a humified incubator at 37 ℃ in a 5% CO_2 atmosphere. The untreated negative control cells were incubated with 1 mL of the reagent-media mixture. Tertiary-butyl hydroperoxide (tBHP) was used as a positive control for this experiment. The cell media was removed and cells were gently rinsed with 1 mL of 1X PBS and viewed using Olympus BX41 epifluorescence microscope using the U-MWIG2 filter (Excitation: 535/30, Emission:580 nm long pass). Images were captured and analysed as previously described (section 3.2.4).

3.2.10 Immunofluorescence

Immunofluorescence is an important technique for visualizing and detecting proteins or antigens in cells or tissues. It employs fluorescently labelled antibodies that bind to the specific target molecules of interest. Immunofluorescence can therefore be used to examine how specific proteins are distributed and localized within cells or tissues when observed through a fluorescence microscope (Im *et al.*, 2019). The expression of two important proteins of interest; p21 and haemoxygenase-1 (HMOX1/HO-1/HSP32) were evaluated following an 18-hour exposure to platinum complexes and cisplatin.

3.2.10.1 Evaluating Haemoxygenase-1 expression

Haemoxygenase-1 (HO-1) is an antioxidant enzyme and cytoprotective protein that is upregulated in response to oxidative stress (Chiang, Chen and Chang, 2021). The expression of HO-1 in cancer cells was evaluated by an immunofluorescence assay, using a rabbit HO-1 polyclonal antibody as the primary antibody. Detection was facilitated by a goat anti-rabbit polyclonal antibody labelled with Alexa Fluor 488, emitting green fluorescence under an epifluorescence microscope. An increase in the intensity of green fluorescence indicated increased HO-1 expression in the cell.

Cells were grown on sterile coverslips in a six-well plate at a density of 250 000 cells per/well and treated with the platinum complexes and cisplatin for 18 hours. A control well to detect non-specific binding of the secondary antibody was included. Cells were gently rinsed with 1X PBS and fixed with 3% formaldehyde in PBS for 20 minutes. Thereafter, cells were permeabilized with 0.25% molecular grade Triton-X100 (Sigma Aldrich/Merck, Johannesburg, South Africa) and blocked for one hour with 0.5% bovine serum albumin (Sigma Aldrich/Merck, Johannesburg, South Africa). Cells were incubated overnight with a 1:200 dilution of HO-1 primary antibody (Thermo Fisher Scientific, Invitrogen, Johannesburg, South Africa). Following washing with 1X PBS the cells were incubated for 1 hour with an Alexa-fluor 488 conjugated anti-rabbit secondary antibody (Thermo Fisher,

Johannesburg, South Africa). After removal of the antibody, cells were incubated for 20 minutes with HO and then mounted faced down on a microscope slide using Fluoromount (Sigma Aldrich/Merck, Johannesburg, South Africa). Slides were left to dry before viewing the cells with an Olympus BX41 epifluorescent microscope. The filter cubes U-MNIB3 (Excitation:480/20, Emission:510/50) and the UMWU2 (Excitation: 365/10, Emission:420 nm long pass) were used to detect HMOX-1and the Hoechst-33342 signals, respectively. Images were captured with the Olympus DP72 digital camera and processed using the Olympus CellSens software program.

3.2.10.2 Evaluation of p21 expression

DNA damage triggers the cellular signalling pathway known as the DNA damage response. P21, a cyclin-dependent kinase inhibitor, is a key player in this response. It is upregulated in response to DNA damage, serving the dual purpose of facilitating DNA repair and initiating cell cycle arrest (Cmielová and Rezáčová, 2011). The expression of p21 in cells exposed to test compounds was evaluated by immunofluorescence assay.

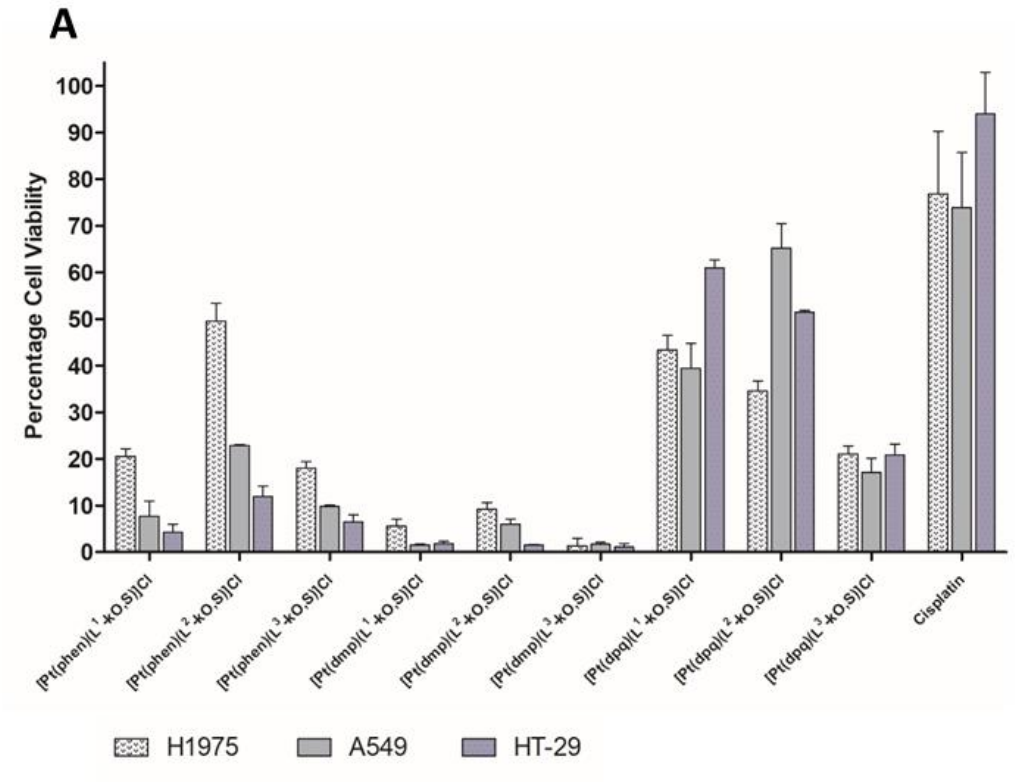
Cells were grown on sterile coverslips in a six-well plate and prepared as previously described 3.2.11. The coverslips were incubated overnight with a 1:200 dilution of p21 primary antibody (Invitrogen, Thermo Fisher Scientific, South Africa). Following washing with PBS, cells were incubated for 1 hour with an Alexa-fluor 488 conjugated anti-mouse secondary antibody (Thermo Fisher Scientific, Johannesburg, South Africa). After removal of the antibody, cells were incubated for 20 minutes with HO and then mounted on a microscope slide using Fluoromount (Sigma-Aldrich/Merck, Johannesburg, South Africa). Slides were left to dry before viewing the cells with an Olympus BX41 epifluorescent microscope. The U-MNIB3 (Excitation:480/20, Emission:510/50) and the UMWU2 (Excitation: 365/10, Emission:420 nm long pass) filter cubes were used to detect the p21 and the HO signals, respectively. Images were captured with the Olympus DP72 digital camera and processed using the Olympus CellSens software program. Atleast three independent fields were used to detect the percentage of p21 in cancer cells.

3.3 Results

3.3.1 Cytotoxic effects of [Pt(diimine)(L^n-κ*O,S*)]Cl complexes and free diimine ligands on H1975, A549 and HT-29 cells

The effect of nine platinum(II) complexes; [Pt(diimine)(L^n-κ*O,S*)]Cl and free diimine ligands (1,10-phenanthroline (phen), 5,6-dimethyl-1,10-phenanthroline (dmp) and dipyrido[3,2-f:2',3'-h]quinoxaline (dpq) on cell viability was evaluated against human lung (H1975, A549) and colorectal (HT-29) cancer cell lines. Platinum complexes and diimine ligands were tested at both high (50 µM) and low (5 µM) concentrations for 48 hours to assess their activity against cancer cells. (*Figure 3.1; Appendix B, Table B1*). Cisplatin was used as the positive control, while untreated cells incubated with fresh culture media served as the untreated negative control. It is important to note that the ability of test complexes to significantly inhibit cell survival at concentrations below 5 µM indicates their potential to effectively hinder cancer growth at clinically relevant concentrations.

[Pt(diimine)(L^n-κ*O,S*)]Cl were cytotoxic at 50 µM, inhibiting cell growth by 92% to 99.4% across the three cancer cell lines. A qualitative structure-activity relationship was evident at a lower concentration of 5 µM, with noticeable variations in the activity of platinum complexes among the three cancer cell lines (*Figure 3.1*).



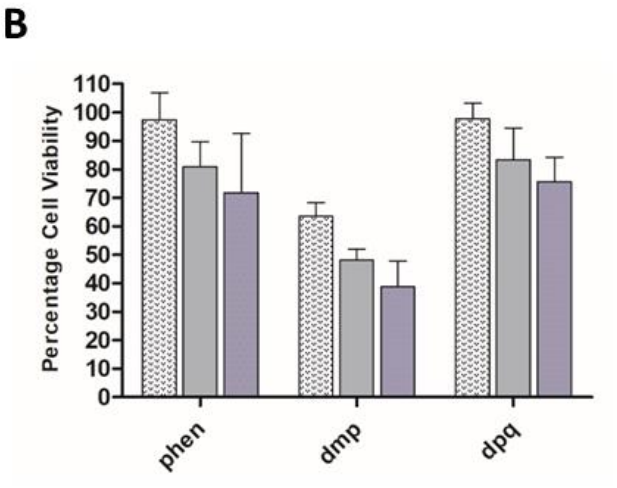


Figure 3.1 The effect of the platinum complexes (A) and free diimine ligands (B) on the viability of H1975, A549 and HT-29 cells at 5 µM concentration. ***(****A) Cells were treated with 5 µM of [Pt(diimine)(L^n-κO,S)]Cl complexes and the positive control cisplatin for 48 hours showing the superior decrease in the cell viability of the 5,6-dimethyl-1,10-phenanthroline (dmp) complexes. (B) shows the effect of the ligand on the viability of cells when treated with 5 µM concentration of 1,10-phenanthroline (phen), 5,6-dimethyl-1,10-phenanthroline (dmp) and dipyrido[3,2-f:2',3'-h]quinoxaline (dpq) for 48 hours.*

At this 5 μM concentration, promising active complexes were identified and selected for determination of their IC_{50} values using the MTT assay. The three complexes bearing 5,6-dimethyl-1,10-phenathroline (dmp); [Pt(dmp)(L^1-κ*O,S*)]Cl, [Pt(dmp)(L^2-κ*O,S*)]Cl, and [Pt(dmp)(L^3-κ*O,S*)]Cl, were found to be the most cytotoxic in all three cancer cell lines compared to other complexes with varying activity across the cell lines. The observed percentage cell viability ranged between (1.4 - 9.2%) in H1975, (1.5 - 6.0%) in A549 and (1.1 - 1.8%) in HT-29. Based on these results, it was apparent that HT-29 cells were the most sensitive cell line to platinum complexes containing the dmp ligand. The most potent complex from the series was [Pt(dmp)(L^3-κ*O,S*)]Cl since it showed the highest cytotoxicity across the three cancer cell lines (*Figure 3.1A*). The least active platinum complexes were those containing with the dipyrido[3,2-d:2′,3′-f] quinoxaline (dpq) variation, whereas the 1,10-phenanthroline (phen) complexes exhibited some variation in activity across the three cell lines since [Pt(phen)(L^1-κ*O,S*)]Cl showed a relatively lower activity compared to [Pt(dpq)(L^1-κ*O,S*)] in H1975 cells.

The effect of free diimine ligands at 5 μM indicated that platinum complexes had superior activity compared to the free diimine ligands (*Figure 3.1B*). In the case of phen, dmp and dpq ligands, the percentage cell viability ranged between 63.6% - 97.7% in H1975, 48.1% - 83.4% in A549, and 38.7% - 75.7% in HT-29 cells. Among these, dmp ligands caused the lowest percentage cell viability, while dpq showed the highest cell viability in each cell line (*Figure 3.1B*; *Appendix B, Table B1*), similar to the observed trend with platinum complexes.

The cytotoxicity of these complexes was primarily attributed to the presence of the diimine ligand since variations in the R^1 substituents on acylthiourea ligands did not exhibit a significant effect, as their activity varied between different cell lines. This was confirmed by initially testing the anticancer activity of free acylthiourea ligands against H1975 at 50 μM. The results showed a high percentage of cell survival ranging between 70.4% and 94.4% (*Appendix B; Table B2*), indicative of low activity.

3.3.2 IC_{50} values of platinum complexes and cisplatin on H1975, A549 and HT-29 cells

The IC_{50} values of the three most cytotoxic platinum complexes; Pt(dmp)(L^1-κ*O,S*)]Cl, [Pt(dmp)(L^2-κ*O,S*)]Cl and [Pt(dmp)(L^3-κ*O,S*)]Cl, as well as the positive control cisplatin, were determined using a concentration range of 0.05 - 100 μM after 48-hour treatment (*Table 3.1*)**.** The values were calculated using data obtained from at least three independent experiments and each data point was obtained in quadruplicate. Graph Pad Prism version 5.1 software was used to generate sigmoidal dose-response curves and calculate the IC_{50} values using non-linear regression analysis. Representative dose-response curves are plots are shown in *Appendix B*, *Figure B1*.

Table 3.1: The IC_{50} values* of three active *[Pt(dmp)(L^n-κO,S)]Cl* complexes and cisplatin *against H1975, A549 and HT-29 cancer cell lines after 48 hours.

Platinum complexes	**Cell line IC_{50} (μM)**		
	H1975	**A549**	**HT-29**
[Pt(dmp)(L^1-κ*O,S*)]Cl	1.6 ± 0.3	1.0 ± 0.34	0.95 ± 0.06
[Pt(dmp)(L^2-κ*O,S*)]Cl	2.1 ± 0.18	2.3 ± 0.69	0.73 ± 0.10
[Pt(dmp)(L^3-κ*O,S*)]Cl	1.4 ± 0.06	1.4 ± 0.81	0.68 ± 0.06
Cisplatin	19.4 ± 1.4	14.6 ± 1.9	12.5 ± 0.59

Note: All IC_{50} data are expressed as mean ± SD

The IC_{50} values of [Pt(dmp)(L^1-κ*O,S*)]Cl, [Pt(dmp)(L^2-κ*O,S*)]Cl, and [Pt(dmp)(L^3-κ*O,S*)]Cl were in the low micromolar range across the three cancer cell lines. In H1975, IC_{50} values ranged between 1.4 - 2.1 μM, while in A549 cells, they ranged between 1.0 - 2.3 μM. HT-29 cells were the most sensitive with IC_{50} values ranging between 0.68 μM and 0.95 μM. Compared to cisplatin, the three test complexes

showed superior activity (*Table 3.1*) In comparison to A549 and HT-29 cells, platinum complexes exhibited lower activity in H1975 cells.

These findings confirmed that platinum complexes are effective inhibitors of the three cancer cell lines tested with IC_{50} values in the low micromolar range.

3.3.3 Study concentrations: platinum complexes and positive controls

H1975, A549 and HT-29 cells were treated with active [Pt(dmp)(L^n-κ*O,S*)]Cl complexes and cisplatin at concentrations optimized to each cell line for 18 hours. These concentrations were selected based on observed changes in cancer cell morphology upon microscopic evaluation within 18 hours of exposure period. For each experiment conducted in chapter 3, the following concentrations were employed unless stated otherwise (*Table 3.2*). Staurosporine served as the positive control for assessing mitochondrial membrane potential, whereas tertiary-butyl-hydroperoxide (tBHP) was used as a positive control for evaluating reactive oxygen species.

Table 3.2: The concentration of [Pt(dmp)(L^n-κO,S)]Cl complexes, cisplatin, staurosporine and tertiary-butylhydroperoxide used to study biochemical changes in H1975, A549 and HT-29 cancer cell lines.

Platinum complexes (µM)	**Cell line**		
	H1975	**A549**	**HT-29**
[Pt(dmp)(L^1-κ*O,S*)]Cl	3	5	3
[Pt(dmp)(L^2-κ*O,S*)]Cl	3	5	3
[Pt(dmp)(L^3-κ*O,S*)]Cl	3	5	3
Cisplatin	15	25	15
Staurosporine (nM)	200	200	200
tBHP	20	20	20

3.3.4 Effects of platinum complexes and cisplatin on cancer cell morphology

Representative phase contrast (PC) and Hoechst (HO) images showing the effects of platinum complexes and cisplatin on cancer cell morphology after an 18-hour treatment are shown in *Figure 3.2, Figure 3.3* and *Figure 3.4* for H1975, A549 and HT-29 cells respectively. Supplementary images showing propidium iodide and acridine orange staining are included the Appendix B as *Figure B2* and *Figure B3.*

3.3.4.1 Effects of platinum complexes and cisplatin on H1975 cell morphology

The control cells showed a typical normal morphology of intact H1975 cells and uniformly stained nuclei (*Figure 3.2, panels a-c*). Phase contrast images showed changes in cell shape, the presence of cytoplasmic vacuoles and fibrils. Cells treated with [Pt(dmp)(L^1-κ*O,S*)]Cl, [Pt(dmp)(L^2-κ*O,S*)]Cl and [Pt(dmp)(L^3-κ*O,S*)]Cl appeared to be rounded up while some remained attached to the growth surface (*Figure 3.2, panels d, g, h*). Hoechst stain indicates the presence of apoptotic nuclei and all three platinum complexes caused nuclei fragmentation shown by HO images (*Figure 3.2, panels e, h and k*). Staining with acridine orange showed green stained nuclei and cytoplasm, indicative of intact cell plasma membrane (*Appendix B, Figure B2)* while the lack of bright red nuclei staining in propidium iodide images indicated the absence of necrosis (*Appendix B, Figure B3*).

Cells treated with cisplatin retained the characteristic H1975 morphology, with a few cells showing an increased nuclear intensity of HO, suggesting early apoptotic cells with condensed chromatin (*Figure 3.2, panels n and o*)

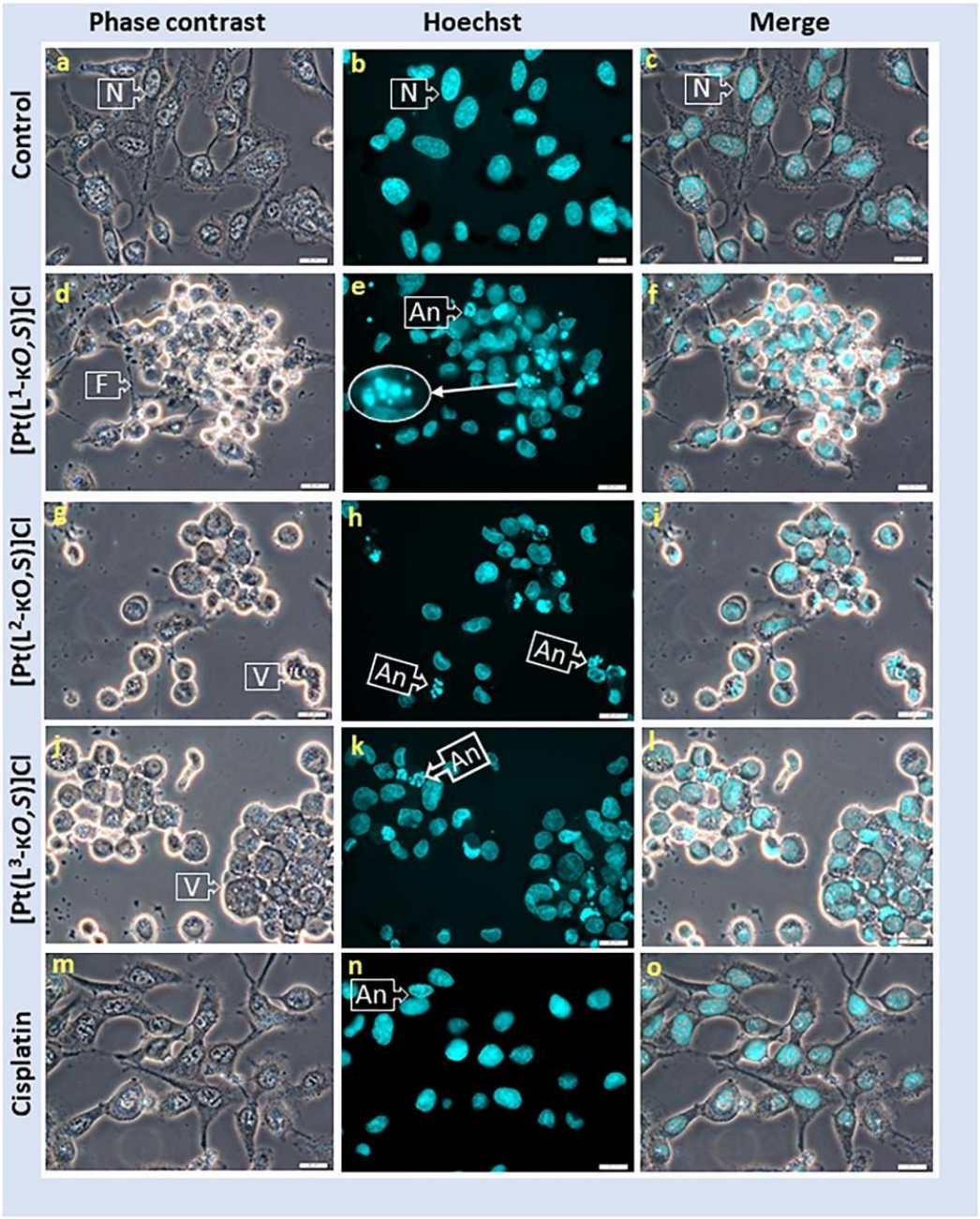


Figure 3.2: Photomicrographs of H1975 lung cancer cells showing changes in cell morphology after 18 hour treatment with 3 µM of active [Pt(dmp)(L^n-κO,S)]Cl complexes and 15 µM cisplatin. *Cells were stained with HO and observed with an Olympus BX41 epifluorescence microscope at a 400X magnification, scalebar: 20 µm. Images were captured with an Olympus Dp72 camera and processed using the Olympus CellSens software package. Panel e, insert shows a fragmented nucleus. Legend: N=nucleus; An=apoptotic nucleus; F=fibril; V=vacuoles, An insert in panel e shows an apoptotic nuclei*

3.3.4.2 Effects of platinum complexes and cisplatin on A549 cell morphology

The untreated control cells showed a typical normal morphology of A549 cells with large round-shaped nuclei stained uniformly blue by HO (*Figure 3.3, panels a-c*). Phase contrast images showed that the platinum complexes; [Pt(dmp)(L^1-κ*O,S*)]Cl and [Pt(dmp)(L^2-κ*O,S*)]Cl caused the formation of large cytoplasmic vacuoles indicative of cell stress (*Figure 3.3, panels d and g)* while all three complexes, including [Pt(dmp)(L^3-κ*O,S*)]Cl caused cell shrinking and with a rounded up morphology. Cells with numerous vacuoles did not show any propidium iodide staining of the nucleus which indicated that their plasma membranes were intact despite the extensive vacuole formation (*Appendix B, Figure B2, panel f*). All three platinum complexes caused nuclear fragmentation, indicative of apoptosis (*Figure 3.3, panel e, h, k).* [Pt(dmp)(L^3-κ*O,S*)]Cl caused the highest percentage of cells with apoptotic nuclei compared to both [Pt(dmp)(L^1-κ*O,S*)]Cl and [Pt(dmp)(L^2-κ*O,S*)]Cl. [Pt(dmp)(L^3-κ*O,S*)] showed nuclei at various stages of apoptosis and numerous cells with irregular shaped nuclei (*Figure 3.3, panel j-l*). Late-stage apoptotic nuclei were identified by the fragmented nuclei (insert panel k) while early-stage apoptotic nuclei (chromatin condensation) increased the intensity of HO stain. The lack of bright PI staining indicated that the complex platinum did not induce necrosis in A549 cells (*Appendix B, Figure B3, panel h*). Minimal necrosis was observed in cells treated with [Pt(dmp)(L^1-κ*O,S*)]Cl, indicated by the bright PI stain of intact round-shaped nuclei, indicative of damaged cell membranes without fragmentation of the nuclei (*Appendix B, Figure B3, panel f).*

Cisplatin, even at a concentration 5 times higher (25 μM) than the platinum complexes, did not significantly alter the morphology of A549 cells. This suggests that cisplatin is a less potent inducer of apoptosis compared to the dmp platinum complexes.

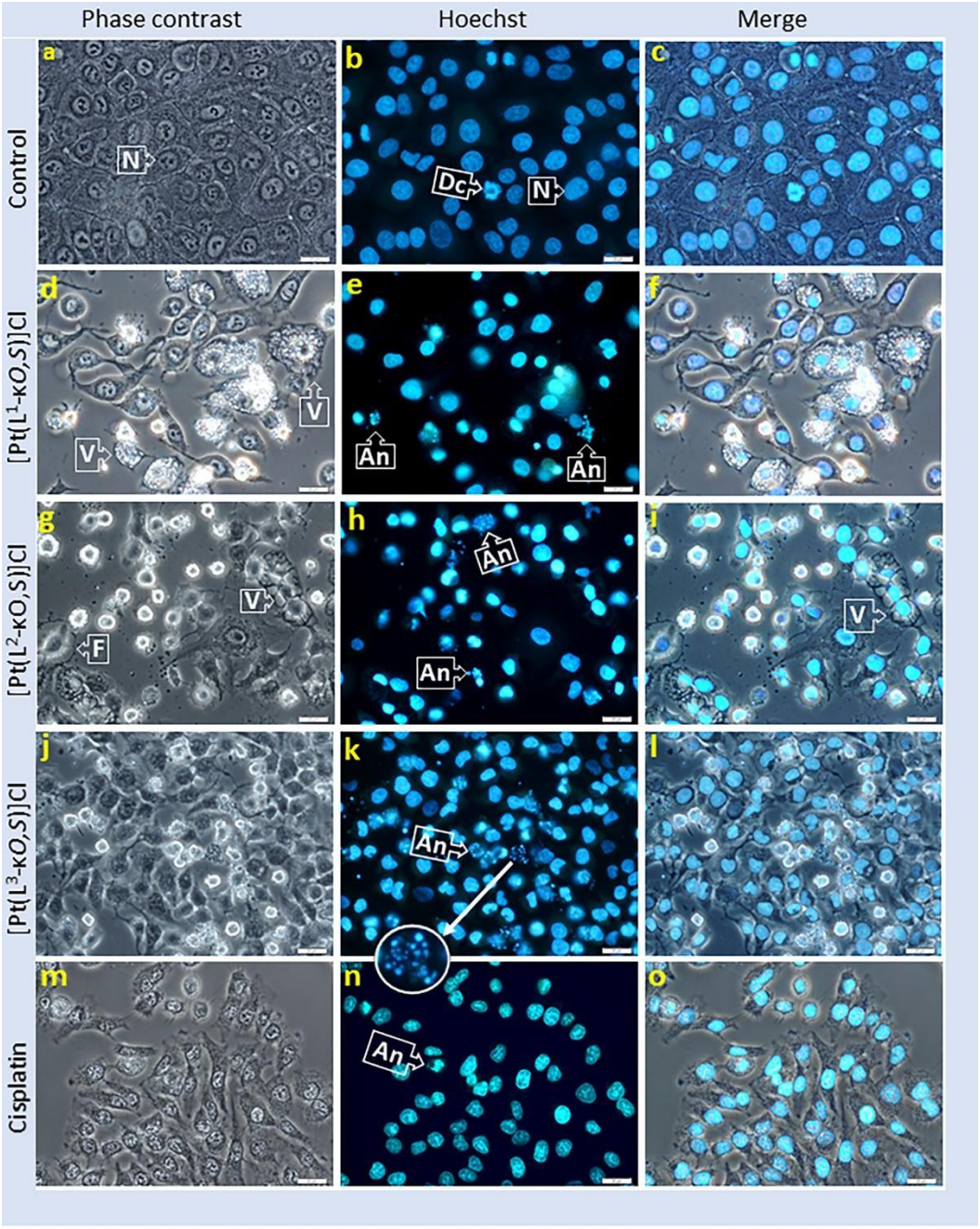


Figure 3.3: Photomicrographs of A549 cells showing changes in cell morphology following an 18 hour treatment with 5 µM [Pt(dmp)(L^n-κO,S)]Cl complexes and 25 µM cisplatin. *Cells were stained with HO and viewed with an Olympus BX41 epifluorescence microscope at a 400× magnification, scalebar: 20 µm. Images were captured with an Olympus DP72 camera and processed using the Olympus CellSens software package. Legend: N=nucleus; An=apoptotic nucleus; F=fibril; V=vacuoles. An insert panel k shows fragmented nuclei.*

3.3.4.3 Effects of platinum complexes and cisplatin on HT-29 cell morphology

The untreated control cells showed the normal morphology of HT-29 cells with cuboidal cell and round shaped nuclei, stained uniformly blue by HO (*Figure 3.4, panel a-c*).

The phase contrast image of cells treated with [Pt(dmp)(L^1-κ*O,S*)]Cl appeared to have a combination of rounded up cells as well as elongated cells that remained attached to growth surface (*Figure 3.4, panel d and f*). The nuclei deviated from their typical round shape and a few apoptotic nuclei were present (*Figure 3.4, panels e and f*). Cells treated with [Pt(dmp)(L^2-κ*O,S*)]Cl caused similar changes to the cell morphology which included cell elongation and formation of fibrils (*Figure 3.4, panels g*-i). The complex [Pt(dmp)(L^2-κ*O,S*)]Cl also induced the formation of apoptotic as seen in panel h. Cells treated with [Pt(dmp)(L^3-κ*O,S*)]Cl were tightly packed with numerous cells showing apoptotic nuclei *(Figure 3.4, panels j-l*). In addition, AO and PI staining of [Pt(dmp)(L^3-κ*O,S*)]Cl treated cells showed red-orange dots in the cytoplasm of most cells, which could be attributed to the presence of acidic granules, presumably indicative of autophagy (*Appendix B, Figure B2 and Figure B3, panel l*).

Cisplatin treated cells, had an elongated appearance and no cytoplasmic vacuoles were observed (*Figure 3.4, panels m-o*). A few cells were rounded up and showed increased HO intensity, indicative of early apoptosis. Cisplatin did not show any advantage over the newly tested platinum complexes; instead, it was less active than the respective platinum complexes at the time of evaluation. No evidence of necrosis was observed in HT-29 cells *(Appendix B, Figure B3, panel i-l*).

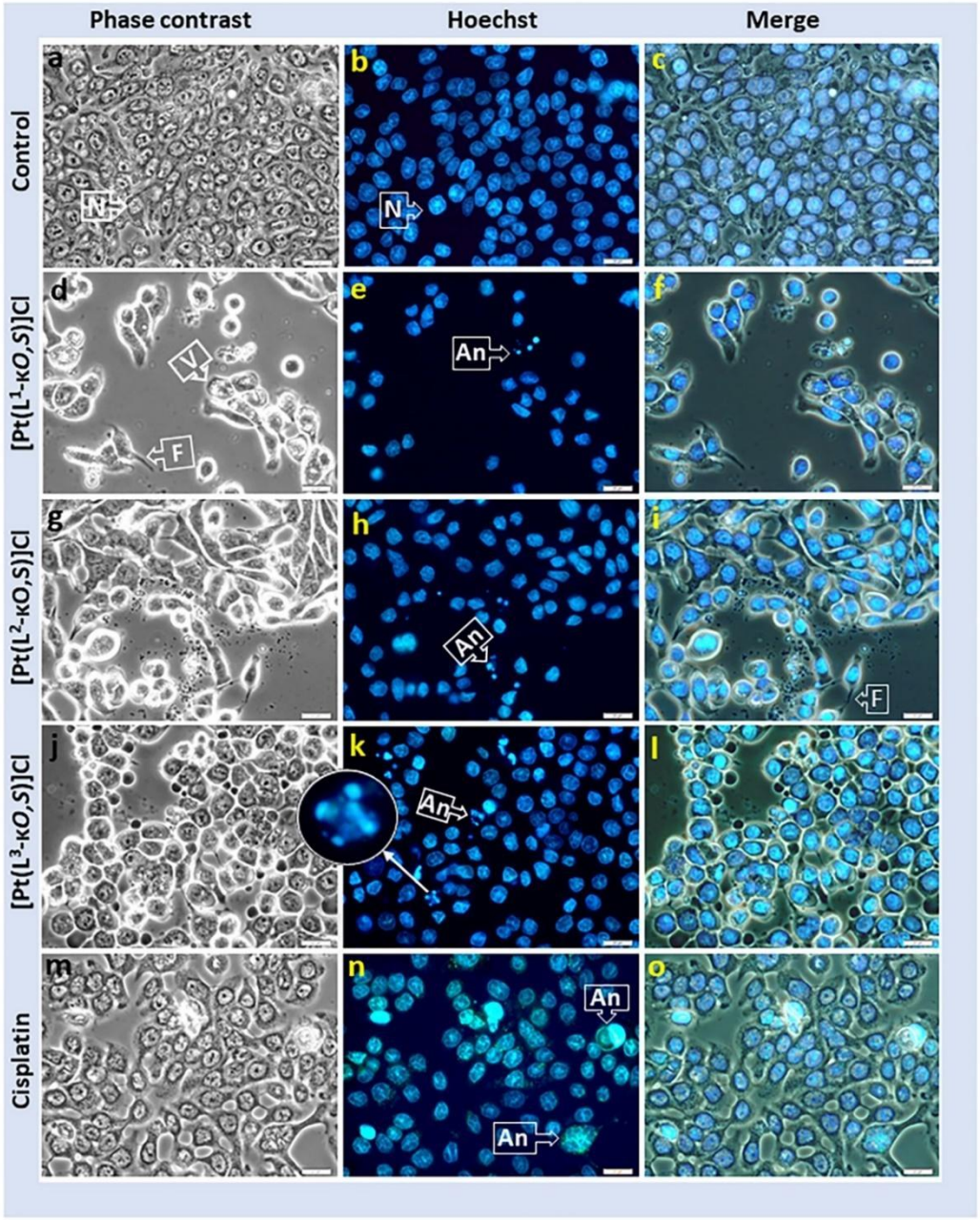


Figure 3.4: Photomicrographs of HT-29 cells showing changes in cell morphology following an 18 hour treatment with 3 µM [Pt(dmp)(L^n-κO,S)]Cl complexes and 15 µM cisplatin. *Cells were stained with HO and viewed with an Olympus BX41 epifluorescence microscope at a 400× magnification, scalebar: 20 µm. Images were captured with an Olympus DP72 camera and processed using the Olympus CellSens software package. Legend: N=nucleus; An=apoptotic nucleus; F=fibril; V=vacuoles. An insert panel k shows an apoptotic cell with fragmented nuclei.*

All three platinum complexes induced nuclear changes consistent with apoptosis and triggered the formation of cytoplasmic vacuoles, albeit to a lesser extent in HT-29 cells compared to H1975 and A549 cells. In contrast to cisplatin, platinum complexes synthesized in this work showed greater efficacy in inducing morphological changes indicative of apoptotic cell death and cellular stress. Therefore, the next step was to evaluate the effects of the platinum complexes and cisplatin on the expression of PS on the cell membranes, a biochemical marker of apoptosis.

3.3.5 Determination of phosphatidylserine exposure by Annexin-V binding

The translocation of phosphatidylserine (PS) to the outer plasma membrane is an early indicator for apoptosis and was detected using annexin-V(AV) probe with fluorescence microscopy. PI was included in the reaction mixture to differentiate between healthy non-apoptotic cells (viable), early apoptotic, late apoptotic and necrotic cells. Healthy non-apoptotic cells are AV and PI negative (-), early apoptotic cells are AV positive (+) and PI negative (-), late apoptotic cells are both AV (+) and PI (+) positive, and necrotic cells are AV negative (-) and PI positive (+).Cells were treated with platinum complexes; [Pt(dmp)(L^1-κ*O,S*)]Cl, [Pt(dmp)(L^2-κ*O,S*)]Cl, [Pt(dmp)(L^3-κ*O,S*)]Cl and cisplatin for 18 hours and thereafter stained with annexin-V and propidium iodide.

Results are presented as the percentage of cells with AV and PI staining in *Table 3.3*. Corresponding photomicrographs and bar graphs for each cell line can be found in *Appendix B,* specifically in *Figure B4* for H1975, *Figure B5* for A549 and *Figure B6* for HT-29.

Table 3.3: Percentage of cells showing annexin-V binding and PI uptake in H1975 cells, A549 cells and HT-29 cells. *H1975 and HT-29 cells were treated with 3 μM [Pt(dmp)(L^1-κO,S)]Cl, [Pt(dmp)(L^2-κO,S)]Cl, [Pt(dmp)(L^3-κO,S)]Cl, and 15 μM cisplatin for 18 hours. A549 cells were exposed to 5 μM of [Pt(dmp)(L^1-κO,S)]Cl, [Pt(dmp)(L^2-κO,S)]Cl, [Pt(dmp)(L^3-κO,S)]Cl and 25 μM cisplatin for 18 hours.*

H1975 cells				
Cell type	**Viable cells (%)**	**Early apoptotic cells (%)**	**Late apoptotic cells (%)**	**Necrotic cells (%)**
AV/PI staining	**AV(-)/PI(-)**	**AV(+)/ PI(-)**	**AV(+)/PI(+)**	**AV(-)/PI(+)**
Control	100	0	0	0
[Pt(dmp)(L^1κ*O,S*)]Cl	80.4	0	13.7	5.9
[Pt(dmp)(L^2κ*O,S*)]Cl	90.6	0	9.4	0
[Pt(dmp)(L^3κ*O,S*)]Cl	77.3	0	22.7	0
Cisplatin	70	30	0	0
A549 cells				
Control	100	0	0	0
[Pt(dmp)(L^1κ*O,S*)]Cl	73.5	26.5	0	0
[Pt(dmp)(L^2κ*O,S*)]Cl	93.3	6.7	0	0
[Pt(dmp)(L^3κ*O,S*)]Cl	73.7	26.3	0	0
Cisplatin	87.5	12.5	0	0
HT-29 cells				
Control	100	0	0	0
[Pt(dmp)(L^1κ*O,S*)]Cl	87.3	11.1	0	1.6
[Pt(dmp)(L^2κ*O,S*)]Cl	50	44.1	5.9	0
[Pt(dmp)(L^3κ*O,S*)]Cl	77.2	22.8	0	0
Cisplatin	95	0	5	0

In H1975 cells, annexin-V (AV) binding to PS was evaluated after an 18 hour treatment with 3 μM [Pt(dmp)(L^1-κ*O,S*)]Cl, [Pt(dmp)(L^2-κ*O,S*)]Cl, [Pt(dmp)(L^3-κ*O,S*)]Cl, and 15 μM cisplatin (*Table 3.3*).

The untreated control cells did not show any positive staining of AV binding or propidium iodide uptake, confirming 100% of healthy non-apoptotic cells (*Table 3.3*). Platinum complexes caused low levels of PS exposure in H1975 cells at this exposure period, with not more than 22.7% of cells being positive for both AV and PI, indicating late apoptosis/necrosis in all complexes. Since necrosis was not observed in cell morphology experiments, this PI uptake may be attributed to secondary necrosis, a form of programmed cell death triggered by apoptotic stimuli (Strzyz, 2017). Amongst the three complexes, [Pt(dmp)(L^3-κ*O,S*)]Cl caused the highest PS exposure while [Pt(dmp)(L^2-κ*O,S*)]Cl caused the lowest exposure. Minimal secondary necrosis was observed only in cells treated with [Pt(dmp)(L^1-κ*O,S*)]Cl. Cisplatin caused a 30% increase of AV binding with no PI uptake, indicative of early apoptosis (*Table 3.3*).

A549 cells were treated with 5 µM [Pt(dmp)(L^1-κ*O,S*)]Cl, [Pt(dmp)(L^2-κ*O,S*)]Cl, [Pt(dmp)(L^3-κ*O,S*)]Cl and 25 µM cisplatin for 18 hours and evaluated for AV binding (*Table 3.3*). Control cells showed no staining of both AV and PI, confirming 100% cell viability of A549 cells (*Table 3.3)*. No uptake of PI dye was observed in A549 cells, indicating that the cells maintained intact plasma membranes, thus confirming the absence of late apoptotic and/or necrotic cells following the 18-hour treatment period. Cells treated with the three active platinum complexes only showed AV binding, indicated by the green fluorescence, indicative of the induction early apoptosis (*Table 3.3*, *Figure B4*) [Pt(dmp)(L^1-κ*O,S*)]Cl (26.5%) and [Pt(dmp)(L^3-κ*O,S*)]Cl (26.3%) increased AV binding similarly compared to Pt(dmp)(L^2-κ*O,S*)]Cl (6.7%) (*Table 3.2*). [Pt(dmp)(L^2-κ*O,S*)]Cl caused the least amount of AV binding (6.7%), thus the lowest exposure of PS, with no PI uptake. Cisplatin did not cause any significant binding of AV since only 12.5% of cells were positive for AV, indicative of early apoptosis (*Table 3.3).* Necrosis was not observed in A549 treated cells.

HT-29 cells were evaluated for AV binding after treatment with 3 µM [Pt(dmp)(L^1-κ*O,S*)]Cl, [Pt(dmp)(L^2-κ*O,S*)]Cl, [Pt(dmp)(L^3-κ*O,S*)]Cl and 15 µM cisplatin for 18 hours (*Table 3.3*)

The untreated control cells showed no staining of both AV and PI, confirming that all cells were viable after an 18-hour incubation with cell media (*Table 3.3*). Cisplatin-treated cells showed positive AV binding and PI staining in 5% of cells, indicative of late apoptosis. Compared to cisplatin, platinum complexes increased the binding of AV, indicating PS exposure in HT-29 cells. The complex [Pt(dmp)(L^2-κ*O,S*)]Cl was the most potent inducer of apoptosis showing the highest increase in AV binding (50%) and a lower percentage of cells positive for PI uptake (5.9%) (*Table 3.3)*. This was followed by [Pt(dmp)(L^3-κ*O,S*)]Cl (22.8%) and [Pt(dmp)(L^1-κ*O,S*)]Cl (11.1%). These results indicated that the three complexes were able to induce apoptosis, with most cells in the early apoptotic stage. This aligns with observations from cell morphology studies, where most cells showed intact nuclei, indicative of the absence of nuclei fragmentation usually observed in late-stage apoptosis.

Among the three cancer cell lines, A549 cells showed the highest levels of early apoptosis followed by HT-29 cells, while H1975 cells displayed characteristics of late apoptosis. The complex [Pt(dmp)(L^3-κ*O,S*)]Cl proved to be the most effective inducer of PS exposure in H1975 cells, whereas [Pt(dmp)(L^2-κ*O,S*)]Cl demonstrated superior effectiveness in HT-29 cells. Both [Pt(dmp)(L^1-κ*O,S*)]Cl and [Pt(dmp)(L^3-κ*O,S*)]Cl showed similar effect in A549 cells. Cisplatin showed varying effects, demonstrating reduced efficacy in H1975 and HT-29 compared to platinum complexes synthesized in this work. To further confirm that these platinum complexes induce apoptotic cell death, the activation of caspase-3/7 was evaluated.

3.3.6 Activation of caspase-3/7 in H1975, A549 and HT-29 cells

Caspase-3 and caspase-7 are executioner caspases that are directly cleaved by active initiator caspases-8 or caspase-9, marking the late stage of apoptosis. Their activation is considered a late apoptotic event, that results in cytoskeletal changes

and DNA fragmentation, causing morphological changes characteristic of apoptotic cell death (Elmore, 2007; McIlwain, Berger and Mak, 2013; Eskandari and Eaves, 2022). Caspase-3/7 active cells were quantified by calculating the percentage of cells displaying a bright green fluorescence against the total number of cells in the field of view, this was obtained from at least three independent fields. These results from three independent experiments are shown in *Figure 3.5 to Figure 3.8.*

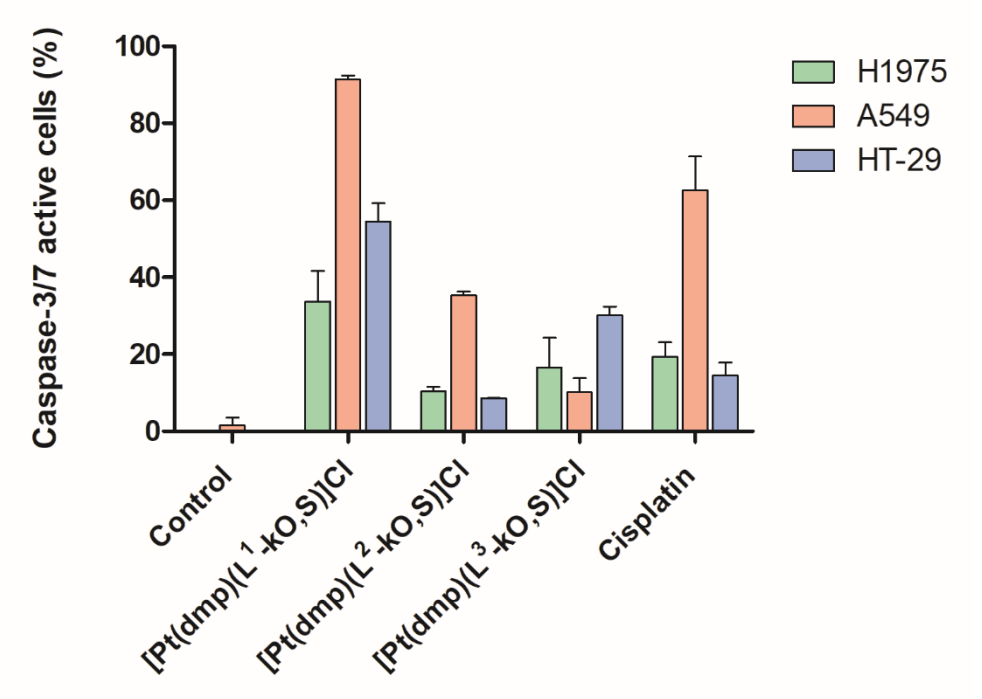


Figure 3.5: The percentage of H1975, A549 and HT-29 cells with active caspase-3/7 following treatment with the platinum complexes and cisplatin*. H1975 and HT-29 cells were treated with 3 µM of [Pt(dmp)(L¹-κO,S)]Cl, [Pt(dmp)(L²-κO,S)]Cl, [Pt(dmp)(L³-κO,S)]Cl and 15 µM cisplatin, and A549 cells were treated with 5 µM of [Pt(dmp)(L¹-κO,S)]Cl [Pt(dmp)(L¹-κO,S)]Cl, [Pt(dmp)(L²-κO,S)]Cl, [Pt(dmp)(L³-κO,S)]Cl and 25 µM cisplatin for 24 hours. Each bar represents the mean ± SD of values obtained from three independent experiments.*

The H1975 untreated control cells showed no caspase-3/7 activity, indicated by the absence of the green fluorescence (Figure 3.5; *Figure 3.6, panels a and b*). All three active platinum complexes were able to activate caspase-3/7, with complex [Pt(dmp)(L^1-κ*O*,*S*)]Cl being the most active, showing 33.7 ± 8.0% of cells with

green fluorescence (*Figure 3.6, panels c and d*). Cells treated with [Pt(dmp)(L^3-κ*O,S*)]Cl showed caspase-3/7 activity in 16.5 ± 7.8% of cells (Figure 3.6, *panels e and f*), while those treated with [Pt(dmp)(L^2-κ*O,S*)]Cl had 10.3 ± 1.17% cells with caspase-3/7 activity (Figure 3.6, *panels g and h*). Cisplatin-treated cells had 19.3 ± 3.8% with caspase-3/7 activity (Figure 3.7, *panels i and j*). [Pt(dmp)(L^1-κ*O,S*)]Cl was at this single time point superior to cisplatin which in turn was better than [Pt(dmp)(L^2-κ*O,S*)]Cl and [Pt(dmp)(L^3-κ*O,S*)]Cl in inducing caspase-3/7 activity.

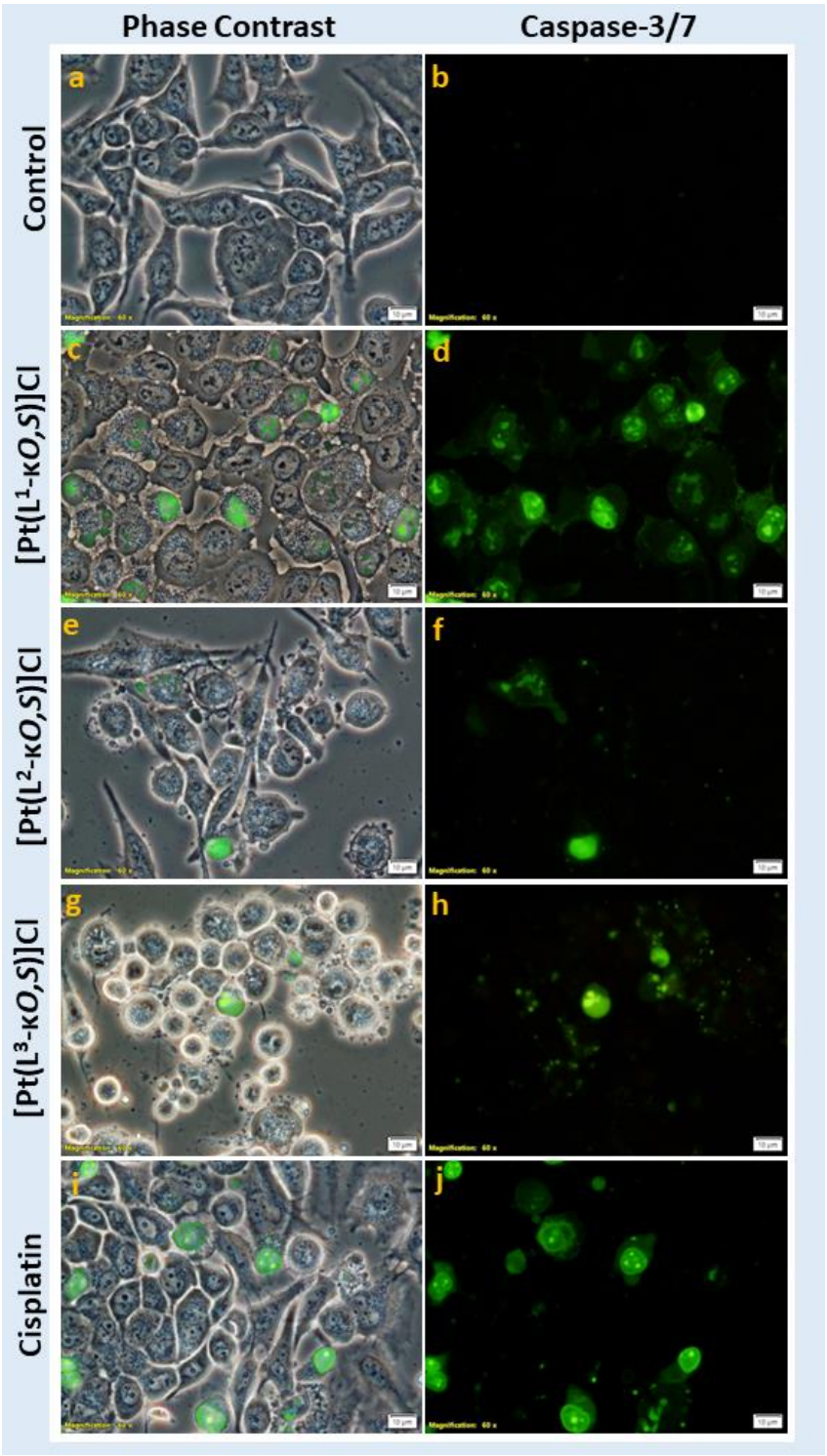


***Figure 3.6**: **Representative photomicrographs of H1975 cells showing caspase-3/7 activity.** Green fluorescence indicates cells with active caspase -3/7. H1975 cells were treated with 3 µM of [Pt(dmp)(L^1-κO,S)]Cl, [Pt(dmp)(L^2-κO,S)]Cl, [Pt(dmp)(L^3-κO,S)]Cl complexes and 15 µM cisplatin for 24 hours. Images were captured with the Olympus DP72 digital camera. Magnification: 400X, Scale bar: 20 µm*

Compared to untreated controls, platinum complexes increased caspase-3/7 activity in A549 cells (*Figure 3.5; Figure 3.7*). Similar to H1975 cells, [Pt(dmp)(L^1-κ*O,S*)]Cl proved to be the most effective caspase-3/7 inducer in A549 cells, with 91.4 ± 1.0% of cells showing positive green fluorescence (*Figure 3.7, panels c and d*). This was followed by [Pt(dmp)(L^3-κ*O,S*)]Cl with 35.3 ± 1.0% increase (*Figure 3.7, panels g and h*) and lastly, [Pt(dmp)(L^2-κ*O,S*)]Cl with 10.1 ± 3.7% of cells showing caspase-3/7 activation (*Figure 3.7, panels e and f*).

Although cisplatin increased caspase-3/7 activity in 62.6 ± 8.8% of cells (*Figure 3.7; panels i and j*), the intensity of the green fluorescence appeared to be lower than that observed in cells treated with [Pt(dmp)(L^1-κ*O,S*)]Cl, [Pt(dmp)(L^2-κ*O,S*)]Cl and [Pt(dmp)(L^3-κ*O,S*)]Cl. Despite this observation, [Pt(dmp)(L^1-κ*O,S*)]Cl showed superior activation of caspase-3/7 relative to cisplatin in A549 cells (*Figure 3.5*) .

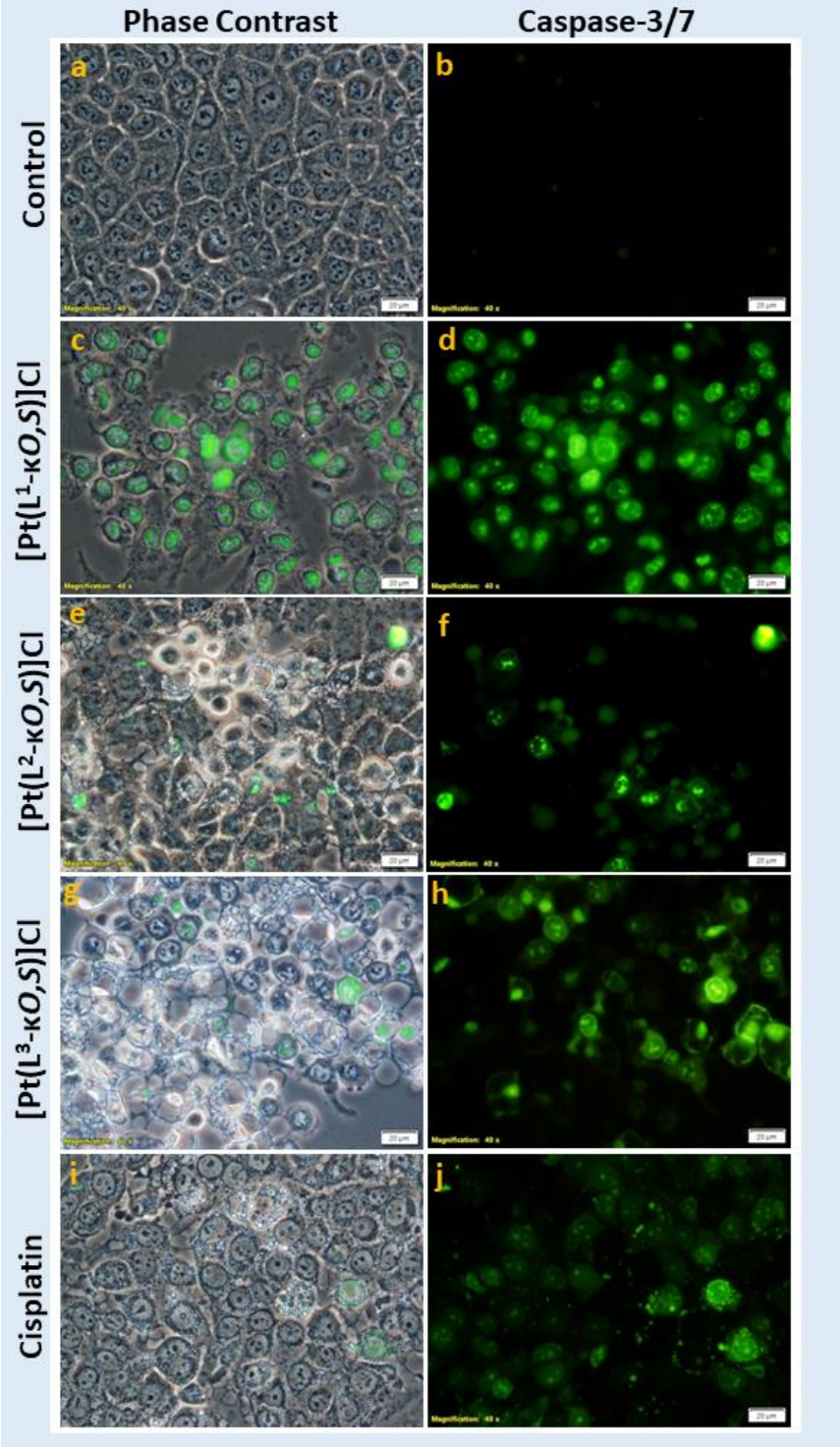


Figure 3.7: Representative photomicrographs of A549 cells showing caspase-3/7 activity. *Green fluorescence indicates cells with active caspase -3/7. A549 cells were treated with 5 µM of [Pt(dmp)(L^1-κO,S)]Cl, [Pt(dmp)(L^2-κO,S)]Cl, [Pt(dmp)(L^3-κO,S)]Cl complexes and 25 µM cisplatin for 24 hours. Images were captured with the Olympus DP72 digital camera. Magnification: 400X, Scale bar: 20 µm.*

HT-29 control cells displayed no fluorogenic response, confirming the absence of caspase-3/7 activation in untreated HT-29 cells (*Figure 3.5; Figure 3.8, panels a and b*). The complex [Pt(dmp)(L^1-κ*O,S*)]Cl, significantly increased caspase-3/7 activity in 54.5 ± 4.7% of cells, confirming the induction of apoptosis while cells treated with [Pt(dmp)(L^2-κ*O,S*)]Cl showed the least caspase-3/7 activation in HT-29 cells (8.5 ± 0.05%) (*Figure 3.8, panels e and f*). The complex [Pt(dmp)(L^3-κ*O,S*)]Cl (*Figure 3.8, panels g and h*) increased caspase-3/7 activity in 30.1 ± 2.2% of cells while cisplatin-induced caspase-3/7 activity in 14.5 ± 3.4% of HT-29 cells. The two complexes [Pt(dmp)(L^1-κ*O,S*)]Cl and [Pt(dmp)(L^3-κ*O,S*)]Cl showed superior activity compared to cisplatin in this cell line.

Platinum complexes, including cisplatin, were confirmed to activate effector caspase-3/7, demonstrating their capacity to induce apoptosis in cancer cells. Subsequently, the study aimed to determine whether the complexes triggered the intrinsic or extrinsic apoptotic signalling pathway. Caspase-8 activation was assessed to investigate the activation of the extrinsic apoptosis pathway (Ovadje *et al.*, 2011; Kominami *et al.*, 2012).

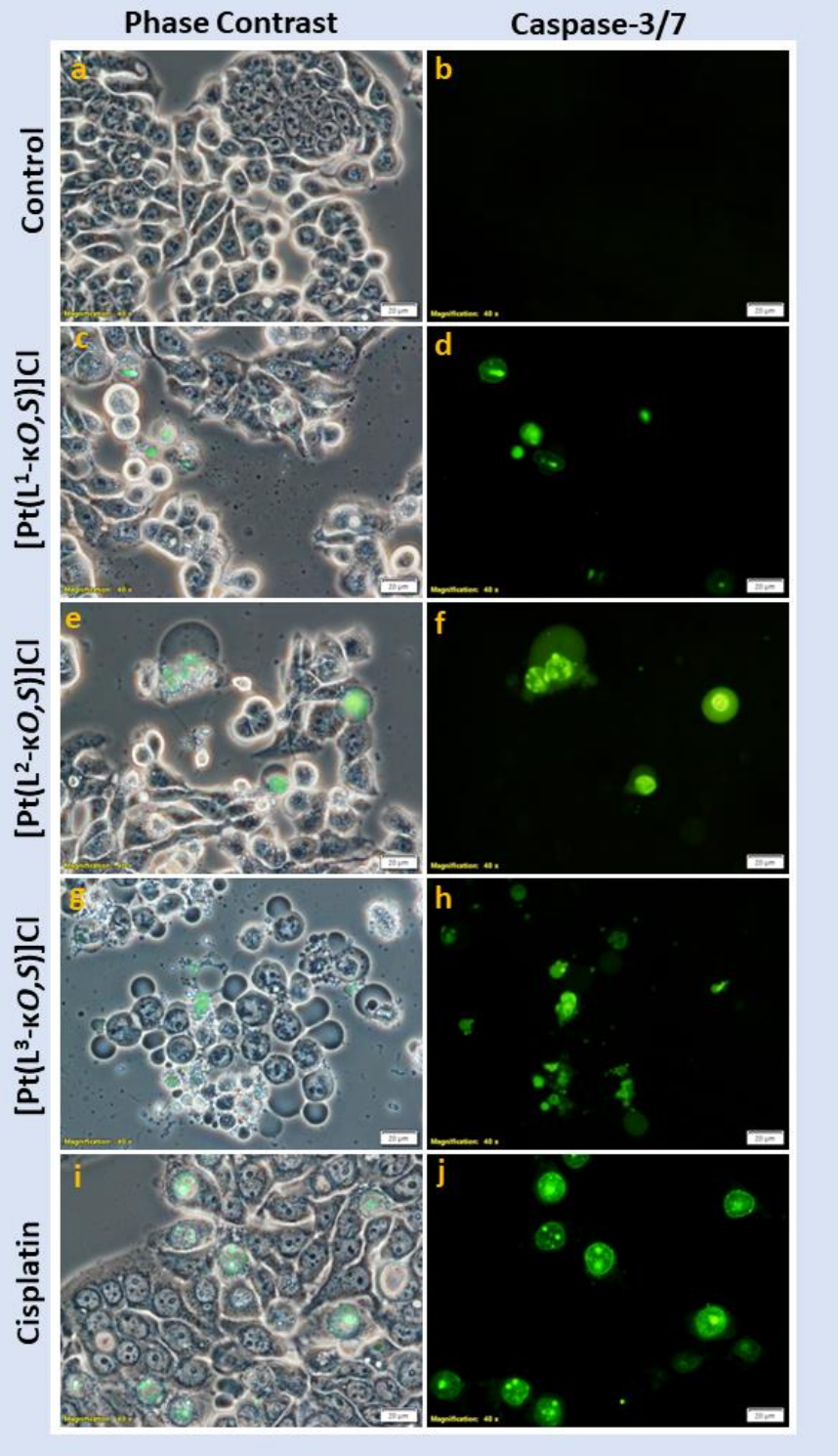


Figure 3.8: Photomicrographs of HT-29 cells showing caspase-3/7 activity*. Green fluorescence indicates cells with active caspase -3/7.HT-29 cells were treated with 3 µM of [Pt(dmp)(L^1-κO,S)]Cl, [Pt(dmp)(L^2-κO,S)]Cl, [Pt(dmp)(L^3-κO,S)]Cl complexes and 15 µM cisplatin for 24 hours. Images were captured with the Olympus DP72 digital camera. Magnification: 400X, Scale bar: 20 µm.*

3.3.7 Evaluation of caspase-8 activity

Caspase-8 is primarily activated through the extrinsic apoptotic pathway, which is initiated by death signals from outside the cell. The activation of initiator caspase-8 is considered an early apoptotic event, taking place before the activation of executioner caspases (caspase-3 or -7) (Mandal *et al.*, 2020). The effect of platinum complexes and cisplatin on caspase-8 activity in H1975, A549, and HT-29 cells was investigated using the Caspase-8 Red staining kit (Abcam) after subjecting cells to an 18-hour treatment. The purpose of this investigation was to determine whether platinum complexes induce apoptosis through the extrinsic pathway. In this assay, an increase in the red fluorescence serves as an indicator of caspase-8 activation. The results obtained are presented in *Figure 3.9.*

3.3.7.1 Caspase-8 activity in H1975, A549 and HT-29 cells

The absence of the red fluorescence in untreated control cells of H1975 (*Figure 3.9, panels a and b*), A549 (*panels a' and b'*) and HT-29 cells (*panels a'' and b''*) indicates that caspase-8 was not activated. Caspase-8 activity was not observed in H1975 cells treated with [Pt(dmp)(L^1-κ*O,S*)]Cl (*panel c*) and only minimal activation was observed in cells treated with [Pt(dmp)(L^2-κ*O,S*)]Cl (*panel f*) and [Pt(dmp)(L^3-κ*O,S*)]Cl (*panel h*). This minimal activation was indicated by the less intense red fluorescence detected in a small percentage of cells, which was considered insignificant (*panels f and h*). Cisplatin did not show any caspase-8 activation in H1975 cells (*panels j*).

In A549 cells, all three platinum complexes; [Pt(dmp)(L^1-κ*O,S*)]Cl (*Figure 3.9, panels c' and d'*), [Pt(dmp)(L^2-κ*O,S*)]Cl (*panel e' and f'*), [Pt(dmp)(L^3-κ*O,S*)]Cl (*panel c' and d'*) and cisplatin (*panels i' and j'*) showed a lack of caspase-8 activation, indicated by a very small percentage (negligible) of cells showing the red fluorescence in the cytoplasm. Phase contrast images showed that all three platinum complexes caused an extensive formation of cytoplasmic vacuoles in A549, indicative of cell stress (*panels a', c', e', g'*). Caspase-8 appeared to be activated in cells that showed a changed morphology, specifically in cells that

appeared to have rounded up and detached from the growth surface observed in phase contrast images.

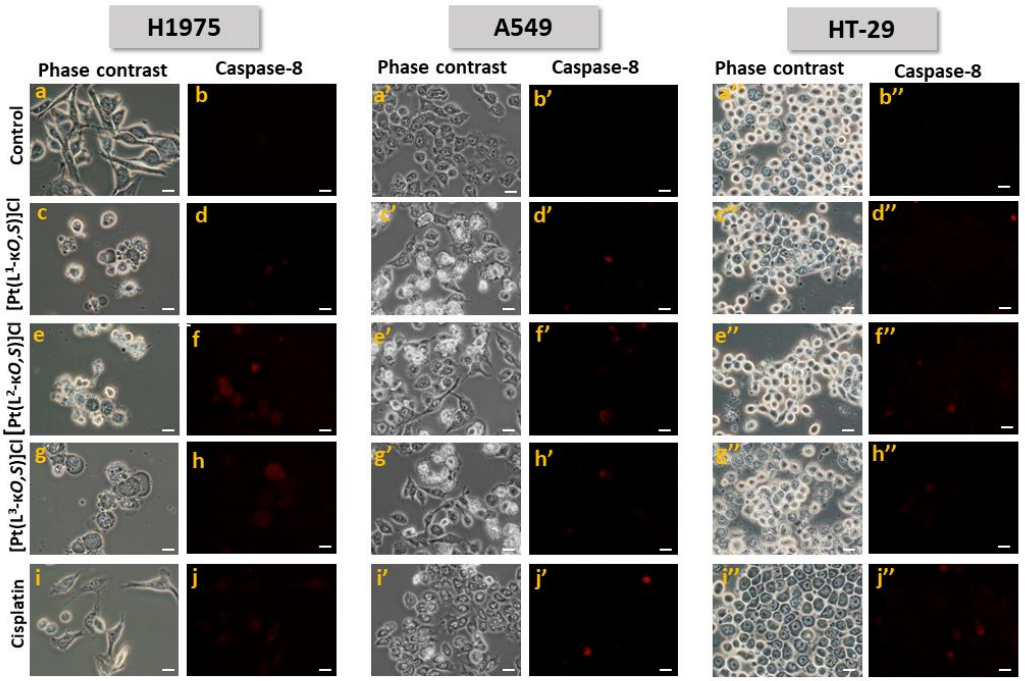


Figure 3.9: Photomicrographs of H1975, A549, and HT-29 cells showing the absence of caspase-8 activity after an 18-hour treatment with platinum complexes and cisplatin. *H1975 and HT-29 cells were treated with 3 µM of [Pt(dmp)(L^1-κO,S)]Cl, [Pt(dmp)(L^2-κO,S)]Cl, [Pt(dmp)(L^3-κO,S)]Cl complexes and 15 µM cisplatin while A549 cells were treated with 5 µM of [Pt(dmp)(L^1-κO,S)]Cl, [Pt(dmp)(L^2-κO,S)]Cl, [Pt(dmp)(L^3-κO,S)]Cl complexes and 25 µM cisplatin. Panels a-b, a'-b' and a''-b'' shows the control cells without red fluorescence. Images were captured with Olympus DP72 digital camera. Magnification 400X; scalebar: 20 µm.*

HT-29 cells showed no indication of caspase-8 activation following an 18 hour treatment with the three active platinum complexes and cisplatin, indicated by the absence of the red fluorescence signal (*Figure 3.9*, *panel a''- j''*).

The lack of caspase-8 activity suggests that platinum complexes and cisplatin do not trigger apoptotic cell death through the extrinsic signalling pathway (death receptor-mediated) in the examined cell lines following an 18-hour exposure.

Instead, this points to the possibility that apoptosis may be initiated via the intrinsic (mitochondria-mediated) apoptotic pathway.

3.3.8 Measurement of the mitochondrial membrane potential ($\Delta\psi_m$) in H1975, A549 and HT-29 cells

Mitochondrial membrane potential (MMP) is an important parameter for assessing mitochondrial function. Healthy cells with normal functioning mitochondria, have a high MMP ($\Delta\psi m$), described as a hyperpolarization state (Sivandzade, Bhalerao and Cucullo, 2019). This high $\Delta\psi m$ is indicative of an intact mitochondria membrane that is efficient in generating energy. The early stages of apoptosis are associated with a loss of mitochondrial function and one of the notable features of this process is a decrease in $\Delta\psi m$, referred to as depolarization.

In this study, the effect of active platinum complexes on $\Delta\psi_m$ of H1975, A549 and HT-29 cells was determined by detecting the presence of J aggregates (red-orange/yellow fluorescence) and J monomers (green fluorescence) to distinguish between healthy non-apoptotic cells (appear red/orange/yellow) and unhealthy apoptotic cells with compromised mitochondrial membrane (appear green). Cisplatin and staurosporine were used as positive controls. Staurosporine is a non-selective kinase inhibitor that induces apoptosis (Lock *et al.*, 1997) Results are shown by representative photomicrographs in *Figure 3.10, Figure 3.11*, and *Figure 3.12* for H1975, A549 and HT-29 cells respectively.

In the H1975 control cells, the yellow/orange fluorescence, indicate the presence of J-aggregates (*Figure 3.10, panel a*). Treatment with [Pt(dmp)(L^1-κ*O,S*)]Cl, [Pt(dmp)(L^2-κ*O,S*)]Cl, [Pt(dmp)(L^3-κ*O,S*)]Cl, cisplatin and staurosporine in H1975 cells resulted in a near complete loss of MMP as indicated by the intense green fluorescence of J-monomers (*Figure 3.10, panel b, c, d, e and f*).

H1975 cells treated with staurosporine (*Figure 3.10, panel e*), were similar to the control cells, indicative of intact MMP. Cisplatin-treated cells showed intense green fluorescence (*panel c*), similar to the platinum complexes. This similarity indicates

a loss of mitochondrial membrane potential (MMP), suggesting compromised mitochondrial function attributed to increased permeability.

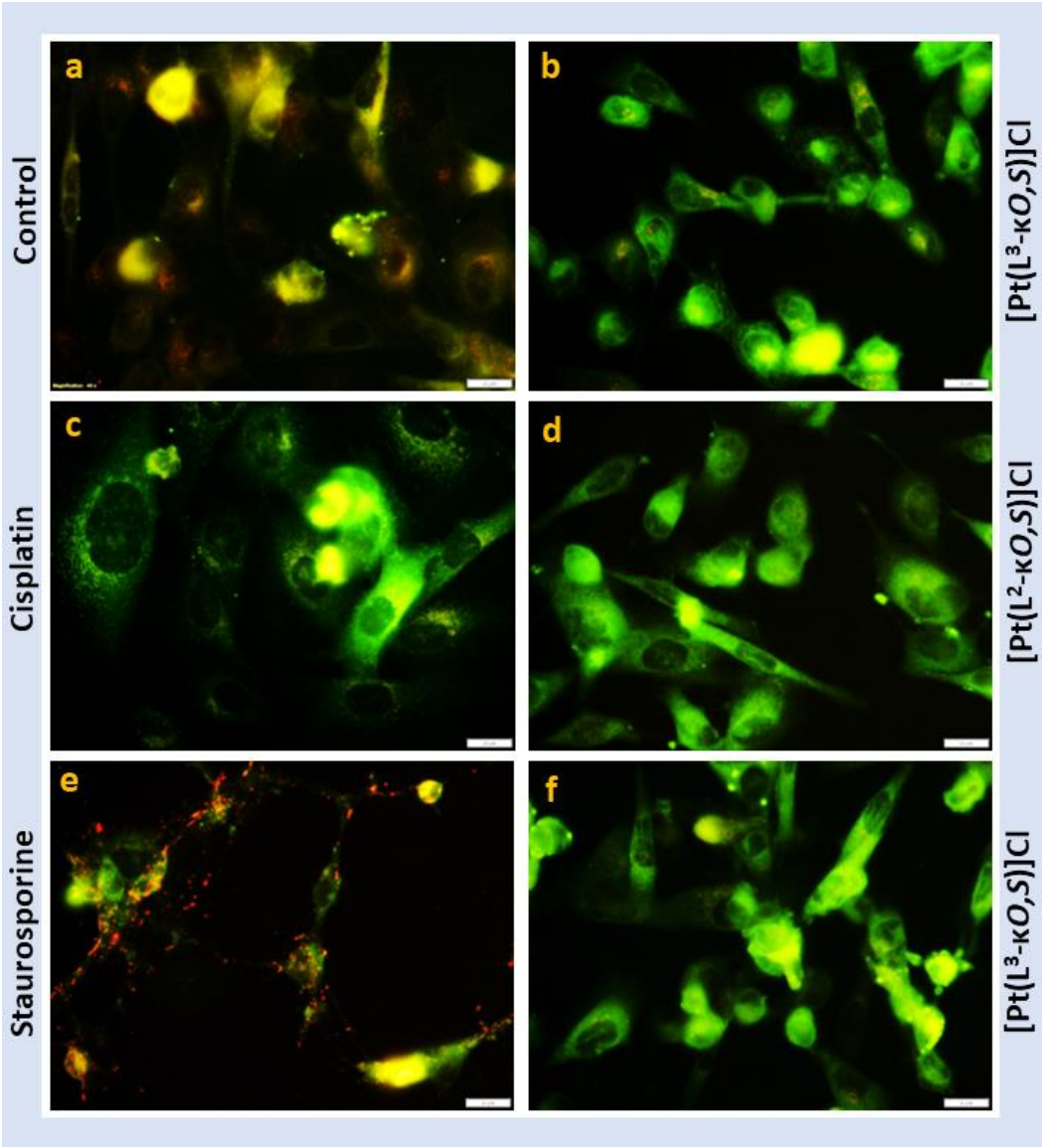


Figure 3.10: Effects of platinum complexes, cisplatin and staurosporine on mitochondrial membrane potential in H1975 cells. *Cells were treated with 3 µM of [Pt(dmp)(L^1-κO,S)]Cl, [Pt(dmp)(L^2-κO,S)]Cl, [Pt(dmp)(L^3-κO,S)]Cl complexes, 15 µM cisplatin and the positive control staurosporine (200 nM) for 18 hours and exposed to the JC-1 reagent for 30 minutes. Images were captured with the Olympus DP72 digital camera detect the presence of J-aggregates (yellow/red-orange) and JC-1 monomers (green). (Magnification 400X; Scalebar: 20 µm). Panel a shows the untreated control cells while panels b-f show treated cells.*

In A549 cells, the control cells appeared granular and showed yellow/orange fluorescence indicative of the presence of J- aggregates (*Figure 3.11, panel a*). Both the positive controls, cisplatin and staurosporine had a granular appearance similar to that of the control cells. They also demonstrated an intense green fluorescence, which suggests the presence of J monomers. Cells treated with platinum complexes; [Pt(dmp)(L^1-κ*O,S*)]Cl, [Pt(dmp)(L^2-κ*O,S*)]Cl and [Pt(dmp)(L^3-κ*O,S*)]Cl showed green fluorescence, indicative of the loss of MMP and a loss of the structural integrity of the mitochondria. (*Figure 3.11, panels b, d and f*).

The HT-29 control cells showed healthy mitochondria displaying yellow/orange fluorescence, indicated by the presence of J aggregates (*Figure 3.12, panel a*). All treated cells including cisplatin and staurosporine showed the green fluorescence in cells, indicative of a state of depolarization and a loss of MMP (*Figure 3.12, panel b, c, d, e),* with the exception of cells treated with [Pt(dmp)(L^3-κ*O,S*)]Cl (*panel f*), where J-aggregates were still observed in some cells. This may have indicated a slower response of HT-29 cells to [Pt(dmp)(L^3-κ*O,S*)]Cl, compared to the other two platinum complexes.

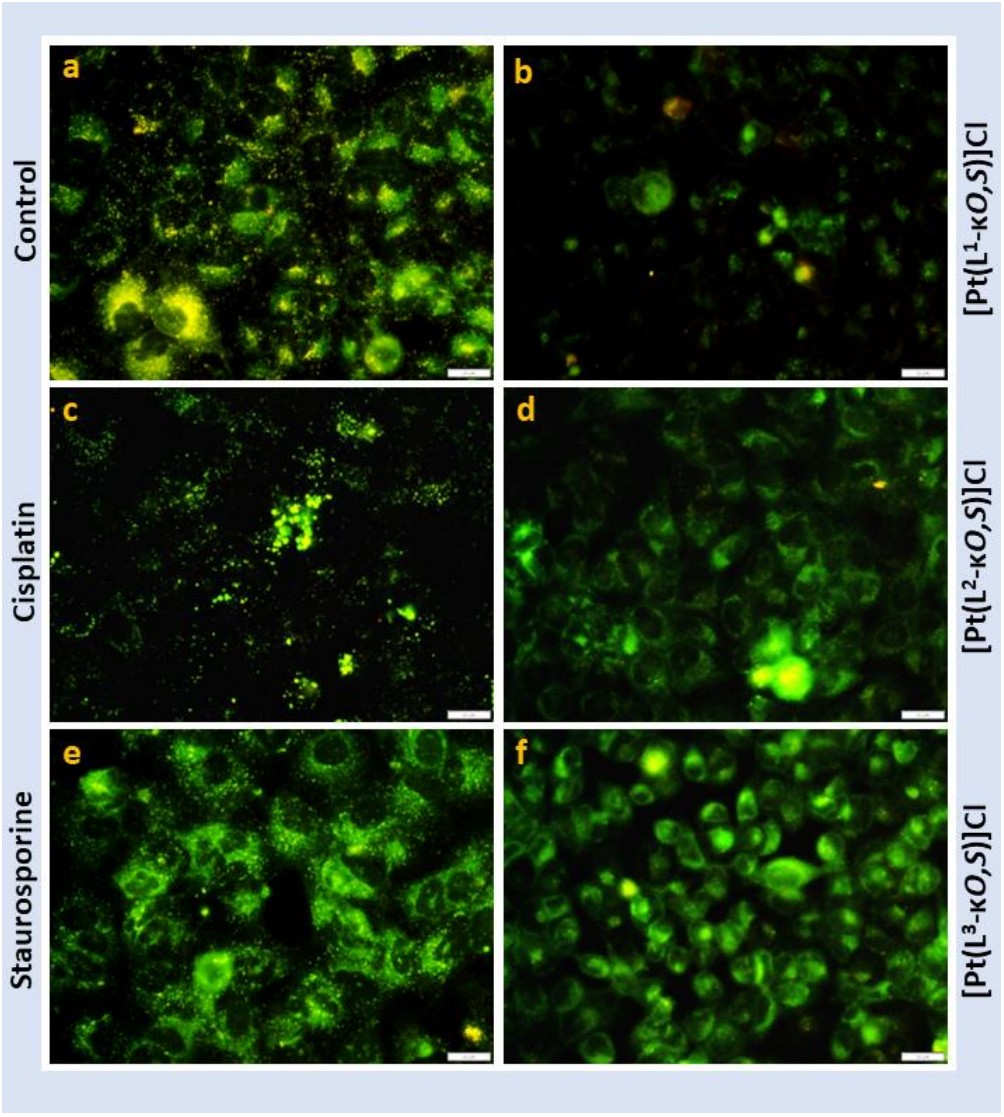


***Figure 3.11**: **Effects of platinum complexes on mitochondrial membrane potential in A549 cells.** Cells were treated with 5 µM of [Pt(dmp)(L^1-κO,S)]Cl, [Pt(dmp)(L^2-κO,S)]Cl, [Pt(dmp)(L^3-κO,S)]Cl complexes, 25 µM cisplatin and 200 nM staurosporine (positive control) for 18 hours and exposed to JC-1 reagent for 30 minutes . Images were captured with the Olympus DP72 digital camera (Magnification 400X; Scalebar: 20 µm). Panel a shows the untreated control cells while panels b-f shows treated cells. J-aggregates were distinguishable by their yellow/red-orange fluorescence, whereas JC-1 monomers were characterized by their green fluorescence.*

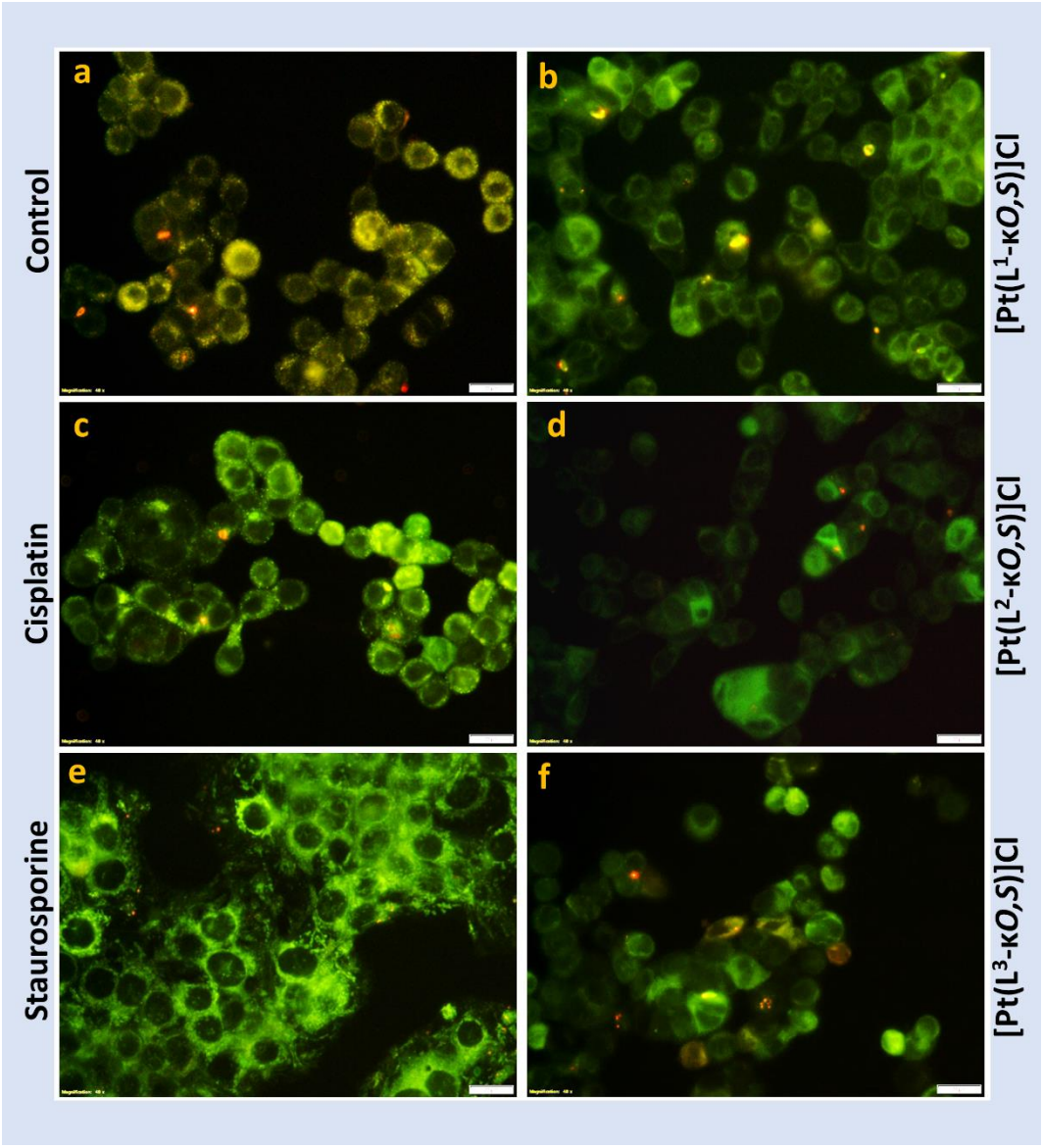


***Figure 3.12**: **Effects of platinum complexes, cisplatin and staurosporine on mitochondrial membrane potential in HT-29 cells.** Cells were treated with 3 µM of [Pt(dmp)(L^1-κO,S)]Cl, [Pt(dmp)(L^2-κO,S)]Cl, [Pt(dmp)(L^3-κO,S)]Cl complexes, 15 µM cisplatin and 200 nM staurosporine for 18 hours and exposed to JC-1 reagent for 30 minutes. Images were captured using Olympus DP72 digital camera and overlayed to detect the presence of J-aggregate and JC-1 monomers. (Magnification 400X; Scalebar: 20 µm). Panel a shows the untreated control cells while panels b-f shows treated cells.*

3.3.9 Measurement of Reactive Oxygen Species (ROS) in cancer cells

Reactive oxygen species (ROS) are short-lived oxygen containing molecules that are rapidly cleared within the cell by antioxidant enzymes. Oxidative stress is regarded as a time-dependent event, that may occur early in the cell death process (Ludke *et al.*, 2017; Yang *et al.*, 2018). Therefore, a 4-hour treatment period was used as the optimal duration for assessing ROS levels after exposing the test complexes to the cell lines used in this study. High levels of ROS are known to damage proteins, nucleic acids, lipids, membranes, and other cellular organelles, ultimately causing cell cycle arrest and activating cell death mechanisms such as apoptosis.

The induction of oxidative stress by platinum complexes was measured using CellROX™ Deep Red Reagent (C10422, Invitrogen). Results are shown by *Table 3.4* and representative photomicrographs in *Appendix B, Figure B7* for H1975, *Figure B8* for A549 and *Figure B9* for HT-29 cells respectively.

Table 3.4: A summary of the percentage of cells showing the elevated ROS levels in H1975, A549 and HT-29 cells after a 4 hour treatment with [Pt(dmp)(L^n-κO,S)]Cl complexes, cisplatin and tertiary-butylhydroperoxide.

Treatment	ROS positive cells (%)		
	H1975	A549	HT-29
Control	49.1	0.0	0.0
[Pt(dmp)(L^{1}κ*O,S*)]Cl	87.3	12.6	89.7
[Pt(dmp)(L^{2}κ*O,S*)]Cl	51.7	98.2	59.6
[Pt(dmp)(L^{3}κ*O,S*)]Cl	34.2	2.3	40.4
Cisplatin	80.4	66.7	82.9
tBHP	100	21.5	100

Following treatment with 3 µM of [Pt(dmp)(L^1-κ*O,S*)]Cl, [Pt(dmp)(L^2-κ*O,S*)]Cl, [Pt(dmp)(L^3-κ*O,S*)]Cl, 15 µM cisplatin and 20 µM tertiary-butylhydroperoxide (tBHP) for a period of 4 hours, an increase in the red fluorescence was observed in H1975 cells compared to the untreated control cells (*Table 3.4).* Untreated control cells showed low levels of ROS indicated by the 49.1% of cells showing the bright red staining. Since cancer cells are reported to have increased levels of ROS compared to normal cells, it was not unexpected to observe the bright red signal in the untreated control of this lung cancer cell line (Hyun, 2020; Nakamura and Takada, 2021; Shah and Rogoff, 2021). The positive control, tBHP showed a maximal response of ROS generation with 100% of cells displaying the red fluorescence. This high level of ROS indicated that tBPH was an effective oxidative stress inducer in H1975 cells, serving its purpose as a positive control. Amongst the three platinum complexes tested, [Pt(dmp)(L^1-κ*O,S*)]Cl caused the highest increase in ROS levels (87.3%) followed by [Pt(dmp)(L^2-κ*O,S*)]Cl (51.7%), while [Pt(dmp)(L^3-κ*O,S*)]Cl had lower levels of ROS (34%) compared to the control cells (49%) (*Table 3.4*). This indicated that [Pt(dmp)(L^3-κ*O,S*)]Cl was the least active inducer of oxidative stress in H1975 cells. Cisplatin showed red staining in 80.4% of H1975 cells, indicative of elevated ROS levels (*Table 3.4*).

In A549 cells, the untreated control cells did not show any red fluorescence, while the positive controls, tBHP and cisplatin displayed red fluorescence in some cells, indicating ROS induction (*Table 3.4*). [Pt(dmp)(L^1-κ*O,S*)]Cl caused a minor increase in ROS levels in a small percentage of A549 cells (12.6%) compared to both positive controls (cisplatin (66.7%) and tBHP (21.5%). Cells treated with [Pt(dmp)(L^2-κ*O,S*)]Cl showed high ROS levels in 98.2% of cells, as evidenced by the intense red fluorescence observed in cells (*Table 3.4*; *Figure B8, panel i*). Interestingly, phase-contrast images showed the formation of large cytoplasmic vacuoles in 100% of cells treated with [Pt(dmp)(L^2-κ*O,S*)]Cl, suggesting a potential correlation between the formation of these vacuoles and oxidative stress in this cancer cell line (*Figure B8, panel g-i*). The complex [Pt(dmp)(L^3-κ*O,S*)]Cl did not induce meaningful ROS generation, as indicated by the absence of the red staining

in cells (2.3%), making it the least effective in causing oxidative stress in A549 cells (*Table 3.4*).

The positive controls, cisplatin (82.9%) and tBHP (100%), increased levels of ROS in HT-29 cells as indicated by the intensity of red fluorescence, signifying elevated oxidative stress in HT-29 cells at the time of assessment (*Table 3.4*).

Among the three tested platinum complexes, [Pt(dmp)(L^1-κ*O,S*)]Cl (89.7%) was the most effective inducer of oxidative stress in HT-29 cells, followed by [Pt(dmp)(L^2-κ*O,S*)]Cl (59.6%) and [Pt(dmp)(L^3-κ*O,S*)]Cl (40.4%) (*Table 3.4*). While [Pt(dmp)(L^2-κ*O,S*)]Cl and [Pt(dmp)(L^3-κ*O,S*)]Cl induced less oxidative stress compared to cisplatin (82.9%), [Pt(dmp)(L^1-κ*O,S*)]Cl yielded similar results to cisplatin, albeit with slightly lower intensity. The increase in ROS levels in HT-29 cells confirmed that platinum complexes were able to induce oxidative stress, suggesting that they promote cancer cell death over cancer cell survival.

[Pt(dmp)(L^2-κ*O,S*)]Cl treated cells that appeared to have just completed mitosis showed increased ROS intensity, indicating higher ROS levels compared to other cells in the field (*Figure B9, panel i*). This is consistent with observations made in literature where mitotic cells showed elevated ROS levels, attributed to the increased metabolic demand during cell proliferation (Havens *et al.*, 2006; Patterson *et al.*, 2019). In contrast, cells treated with [Pt(dmp)(L^3-κ*O,S*)]Cl displayed a lower ROS signal, evident through decreased red fluorescence intensity in 40.4% of cells compared to the other two active platinum complexes and the positive controls.

3.3.10 Haemoxygenase-1 (HMOX1/HO-1/HSP32) expression in cancer cells

HO-1, a member of the heat shock protein family, also referred to as HSP32, plays a major role in regulating excessive amounts of reactive oxygen species (ROS). High ROS levels reflect the extent of oxidative stress in cells and the need for regulation to protect cells against death. Thus, the increased ROS levels induced by

platinum complexes prompted an assessment of HO-1 expression through immunofluorescence assay. In this assay, an increase in intensity of green fluorescence indicated increased HO-1 expression in the cell.

3.3.10.1 HO-1 expression in H1975 cells

Compared to the control cells and cisplatin (*Figure 3.13, panels b and* j), the platinum complexes increased the expression of HO-1 in H1975 cells (*Figure 3.13, panels d, f and h*). The low intensity of the green fluorescence in most of the control cells suggests that the baseline expression of HO-1 in H1975 cells is low and localized to the nucleus. Exposure to platinum complexes synthesized in this work triggered an increased HO-1 expression (*Figure 3.13, panels d, f and h*). The green fluorescence appeared to be more intense and localised in the nucleus as it was less intense in the cytoplasm. Phase contrast images showed that healthy cells that adhered to the growth surface had a lower green fluorescence intensity, in contrast to the cells that were detached from the surface (*panel c, e, and g*). The latter group displayed a higher HO-1 signal in the nucleus. Cisplatin did not show any superior expression of HO-1 in H1975 cells compared to the three active platinum complexes, this was indicated by the low intensity of the green fluorescence relative to that of platinum complexes (*panel j*).

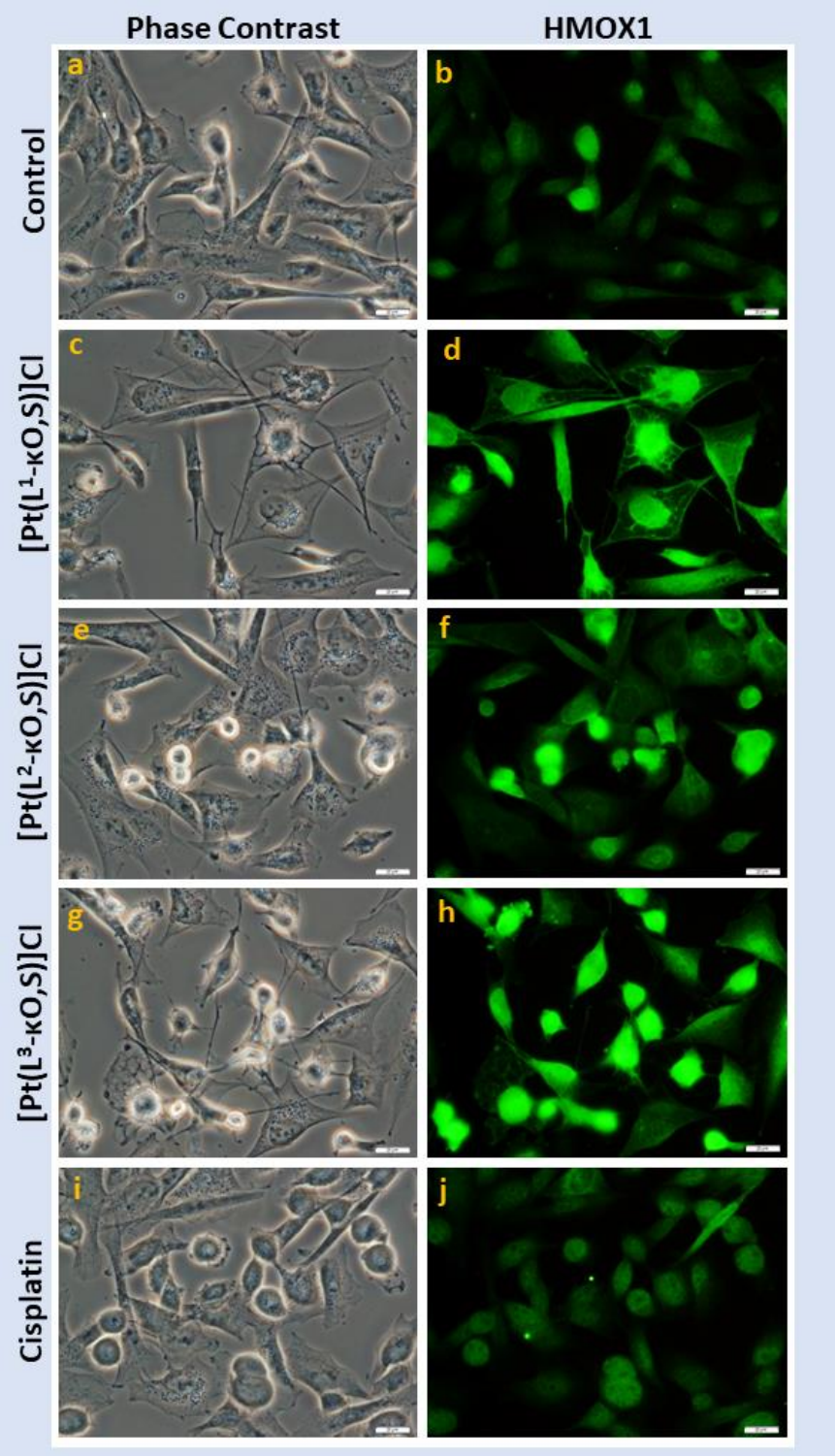


Figure 3.13: Effects of platinum complexes and cisplatin on the expression level of HO-1 in H1975 cells. *Cells were treated with 3 µM of [Pt(dmp)(L^1-κO,S)]Cl, [Pt(dmp)(L^2-κO,S)]Cl, [Pt(dmp)(L^3-κO,S)]Cl complexes and 15 µM of cisplatin for 18 hours. Green fluorescence indicates the presence of HO-1. Cells were viewed with an Olympus BX41 epifluorescence microscope and images captured with a DP72 camera. (Magnification 400X; Scalebar: 20 µm).*

3.3.10.2 HO-1 expression in A549 cell

The untreated control cells and the positive control; cisplatin showed a low HO-1 expression in 100% of A549 cells indicated by the low intensity of the green fluorescence (*Figure 3.14, panels b and j*). Cisplatin-treated cells displayed a more evenly distributed intensity throughout both the cell cytoplasm and nucleus, indicating that HO-1 was found in both the nucleus and cytoplasm of A549 cells.

[Pt(dmp)(L^1-κ*O,S*)]Cl increased the expression of HO-1 in A549 cells as observed by the increased intensity of the green fluorescence in 100% of cells (*Figure 3.14, panel d*). Cells exhibiting prominent cytoplasmic vacuoles displayed reduced HO-1 signal in the cytoplasm, with an accompanying increase in signal within the nucleus (*panel d*). Cells treated with [Pt(dmp)(L^2-κ*O,S*)]Cl and [Pt(dmp)(L^3-κ*O,S*)]Cl showed increased levels of HO-1 fluorescence, similar to what was observed in [Pt(dmp)(L^1-κ*O,S*)]Cl-treated cells.

Similar to H1975 cells, A549 cells that appeared to be detaching from the growth surface displayed a higher intensity of the HO-1 fluorescence compared to the adhered cells, this was more evident in cells treated with [Pt(dmp)(L^2-κ*O,S*)]Cl (*panel e-f*). These may have been evidence of an increased response to oxidative stress in detaching cells compared to adhered cells.

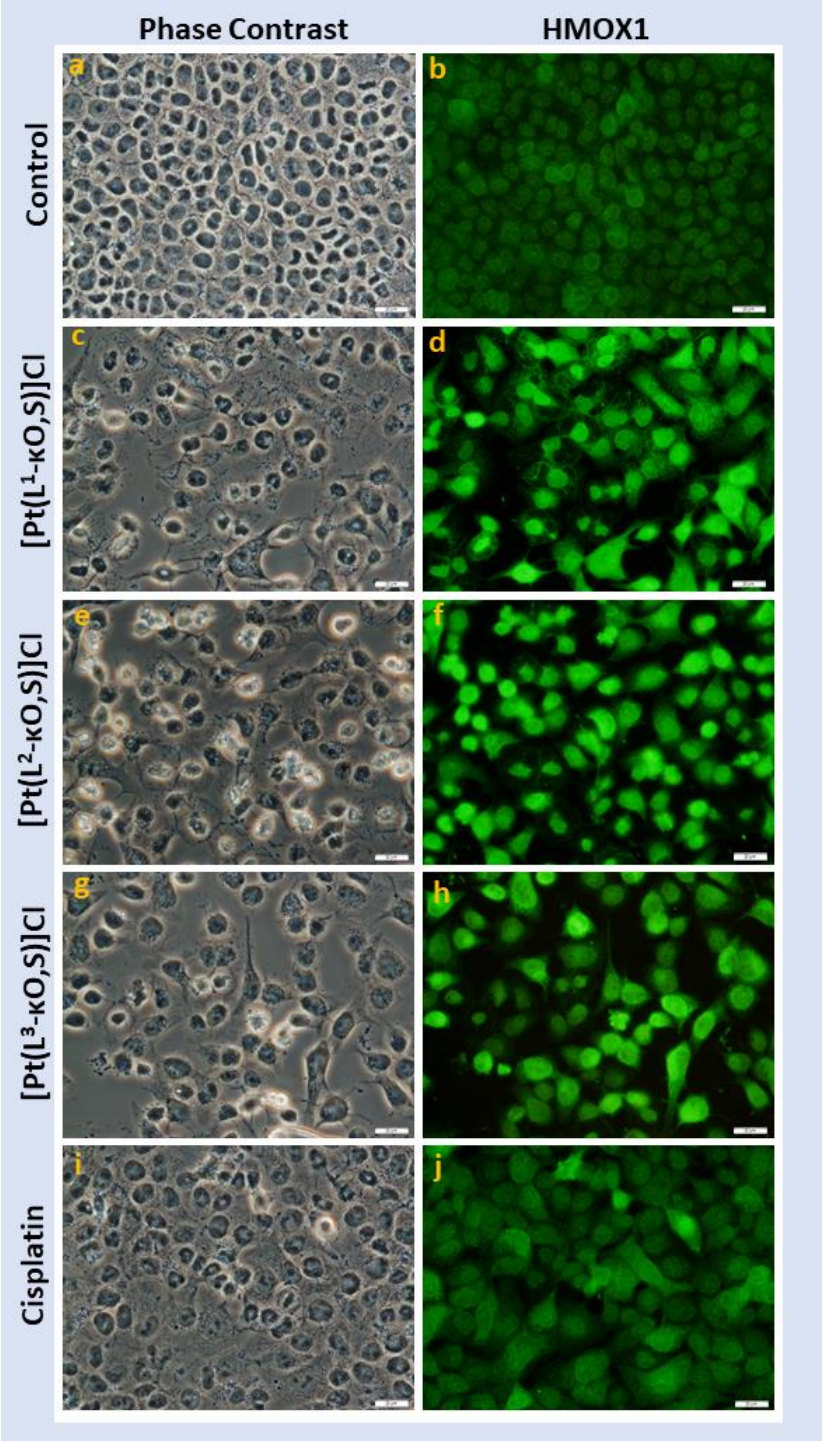


***Figure 3.14**: **Effects of platinum complexes and cisplatin on the expression level of HO-1 in A549 cells.** Cells were treated with 5 µM of [Pt(dmp)(L^1-κO,S)]Cl, [Pt(dmp)(L^2-κO,S)]Cl, [Pt(dmp)(L^3-κO,S)]Cl complexes and 25 µM of cisplatin for 18 hours. Green fluorescence indicates the presence of HO-1. Cells were viewed with an Olympus BX41 epifluorescence microscope and images captured with a DP72 camera. (Magnification 400X; Scalebar: 20 µm).*

3.3.10.3 HO-1 expression in HT-29 cells

The expression of HO-1 was evaluated in HT-29 cells and results are shown by the representative photomicrographs in *Figure 3.15*. The untreated control cells showed a low baseline expression of HO-1 (*Figure 3.15, panel b*). All three platinum complexes increased HO-1 expression, with [Pt(dmp)(L^3-κ*O,S*)]Cl being the most effective (*Figure 3.15, panel h*). This was closely followed by [Pt(dmp)(L^1-κ*O,S*)]Cl (*panel d*) and [Pt(dmp)(L^2-κ*O,S*)]Cl (*panel f*). Cisplatin showed an increased expression of HO-1, similar to [Pt(dmp)(L^2-κ*O,S*)]Cl treated cells, with a high intensity in the nucleus and low intensity in the cytoplasm (*panel j*).

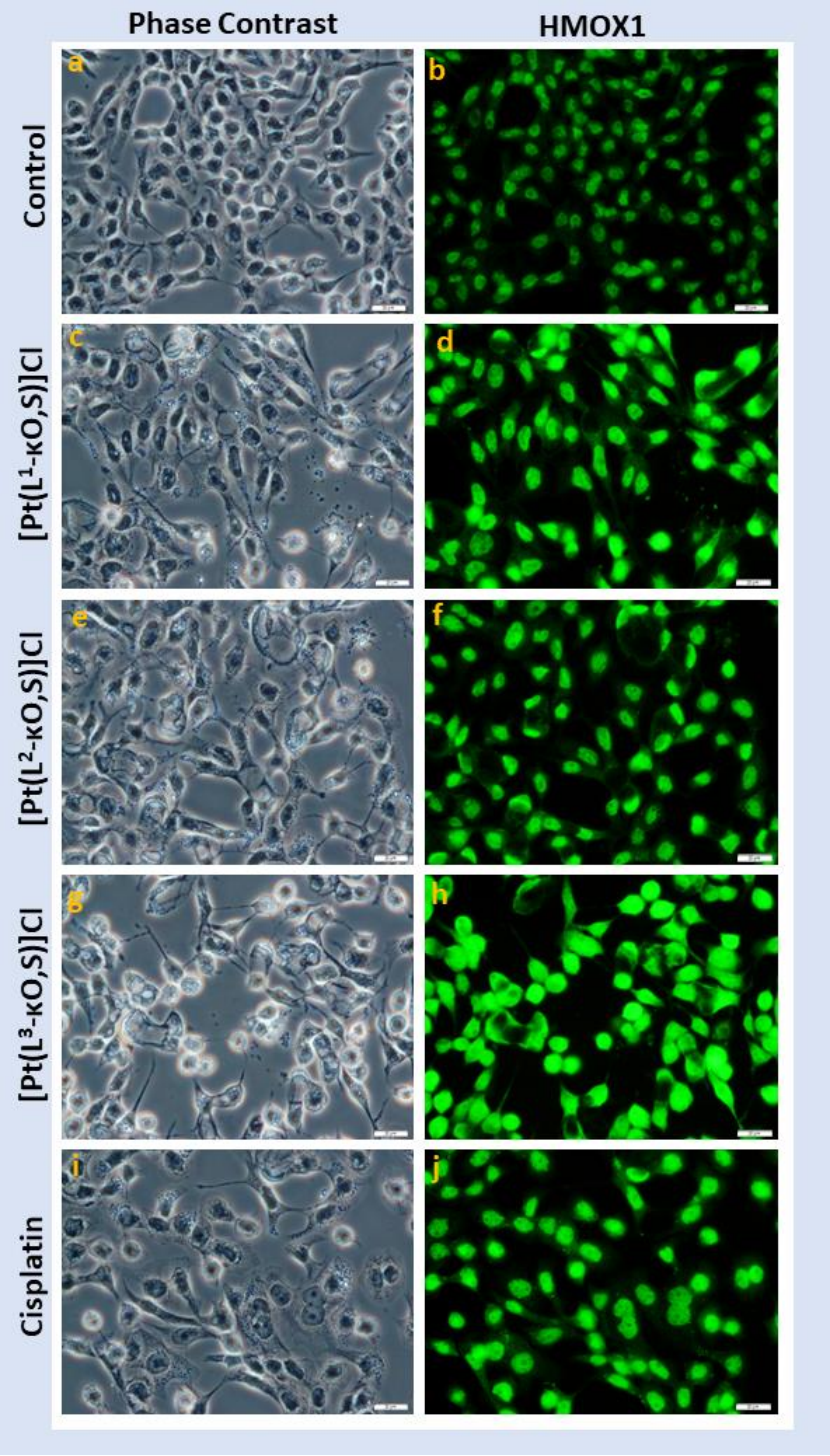


***Figure 3.15**: **Effects of platinum complexes and cisplatin on the expression level of HO-1 in HT-29 cells.** Cells were treated with 3 µM of [Pt(dmp)(L^1-κO,S)]Cl, [Pt(dmp)(L^2-κO,S)]Cl, [Pt(dmp)(L^3-κO,S)]Cl complexes and 15 µM of cisplatin for 18 hours and viewed with an Olympus BX41 epifluorescence microscope and images captured with DP72 camera. (Magnification 400X; Scalebar: 20 µm). Green fluorescence indicates the presence of HO-1.*

3.3.11 The effect of platinum complexes on p21 expression in cancer cell

P21 is a cyclin-dependent kinase inhibitor that plays a pivotal role in controlling the progression of cell division through cell cycle checkpoints by ensuring that new cells contain authentic copies of parent DNA (Waga *et al.*, 1994; Kreis *et al.*, 2019). An increase in the expression of nuclear p21 is a useful marker for the evaluation of DNA damage in cells and can be correlated to the initiation of intrinsic apoptosis (Fujiwara *et al.*, 2008; Mohapatra *et al.*, 2012).

Cancer cells were treated with active platinum complexes and evaluated for p21 expression by immunofluorescence assay using a p21 antibody. Results are shown by *Table 3.5* as well the representative photomicrographs in Appendix B *Figure B10, Figure B11 and Figure B12* for H1975, A549 and HT-29 cells respectively. The nuclear expression of p21 was visualized by merging Hoechst images with p21 images, indicated by a bright green fluorescent signal.

Table 3.5: The percentage of cells showing the expression of nuclear p21 following an 18 hour treatment with platinum complexes and cisplatin. *The percentage of cells with intense and low p21 signals are highlighted in the columns.*

Treatment	H1975			A549			HT-29		
	p21 signal (%)								
	p21 cells	intense	low	p21 cells	intense	low	p21 cells	intense	low
Control	86	36	50	54	19	35	0	0	0
[Pt(dmp)(L^1κ*O,S*)]	100	75	25	100	78	22	66	26	40
[Pt(dmp)(L^2κ*O,S*)]	100	67	33	92	55	37	65	23	42
[Pt(dmp)(L^3κ*O,S*)]	100	89	11	85	70	15	75	46	29
Cisplatin	65	2	62	90	44	47	0	0	0

In H1975 control cells, 50% of cells exhibited low-intensity green fluorescence for p21, while 36% displayed an intense p21 signal (*Table 3.5*), signifying lower p21 expression in control cells. The platinum complexes; [Pt(dmp)(L^1-κ*O,S*)]Cl,

[Pt(dmp)(L^2-κ*O,S*)]Cl, and [Pt(dmp)(L^3-κ*O,S*)]Cl) increased nuclear p21 expression compared to both the untreated control and cisplatin-treated cells. All three platinum complexes induced p21 expression in 100% of cells, with [Pt(dmp)(L^3-κ*O,S*)]Cl showing the highest response (89% intense p21 signal). [Pt(dmp)(L^2-κ*O,S*)]Cl had the lowest percentage of cells with an intense positive p21 signal, indicating a slower response. In contrast, cisplatin-treated cells had a reduced percentage of p21-positive cells (65%), with only 2% displaying intense p21 signals (*Table 3.5*). This further showed the superior induction of p21 response to DNA damage by platinum complexes compared to cisplatin in H1975 cells.

The untreated control of A549 cells showed 54% of the cells expressing p21 with 19% of the total cell population showing an intense p21 signal localized in the cell nucleus while 35% of cells showed a low p21 signal, indicating a low response to DNA damage in A549 cells (*Table 3.5*). Both the platinum complexes and cisplatin led to nearly 100% of cells inducing p21 expression (*Table 3.5*). The percentage of A549 cells with an intense fluorescent signal increased from 19% in the control cells to 78%, 55% and 70% for [Pt(dmp)(L^1-κ*O,S*)]Cl, [Pt(dmp)(L^2-κ*O,S*)]Cl and [Pt(dmp)(L^3-κ*O,S*)]Cl respectively (*Table 3.5*). Cisplatin was able to induce p21 expression in 90% of cells, with only 44% of the cells showing an intense p21 fluorescence, a response not observed in the H1975 or HT-29 cell lines.

The untreated control cells showed no p21 signal, indicating the absence of p21 expression in HT-29 cells (*Table 3.5*). Platinum complexes increased p21 expression, with [Pt(dmp)(L^1-κ*O,S*)]Cl and [Pt(dmp)(L^2-κ*O,S*)]Cl being the least effective in inducing p21 since they both showed a lower percentage of cells with an intense p21 signal (26% and 23%) compared and [Pt(dmp)(L^3-κ*O,S*)]Cl (*Table 3.5*). [Pt(dmp)(L^3-κ*O,S*)]Cl caused the highest p21 expression, with 46% of the cells showing an intense p21 expression. Compared to H1975 and A549 cells, HT-29 cells showed a lower response of the intense p21expression.

3.4 Discussion

In this study, the cytotoxic effects of nine [Pt(diimine)(L^n-κ*O*,*S*)]Cl complexes on the cell viability of H1975, A549 and HT-29 cancer cell lines were determined using an MTT assay after a 48 hour treatment. Complexes bearing the 5,6-dimethyl-1,10-phenanthroline (dmp) ligand showed promising results and were identified as active compounds from the series. Following this, their IC_{50} values were determined and compared to that of the well-known platinum drug, cisplatin. In order to determine the mechanism of cell death, initial investigations on cell morphology indicated that the complexes induce apoptotic cell death. This regulated cell death mechanism was further investigated by employing several markers of apoptotic cell death.

3.4.1 Platinum complexes are cytotoxic to H1975, A549 and HT-29 cancer cells

All nine [Pt(diimine)(L^n-κ*O*,*S*)]Cl complexes were cytotoxic at 50 µM as they inhibited cell growth between 92% and 99.4% across the three cancer cell lines. A qualitative structure-activity relationship at 5 µM concentration showed that diimine ligand variations, particularly dmp, significantly influenced the activity of platinum complexes. The presence of two methyl substituents at positions 5 and 6 of a phenanthroline ligand enhanced the cytotoxic activity of [Pt(dmp)(L^n-κ*O*,*S*)]Cl complexes, aligning with literature observations (Brodie, Collins and Aldrich-Wright, 2004). The results highlight the superior activity of complexes bearing the methyl-substituted phen ligand compared to the unsubstituted phen and bulkier dpq ligand. At 5 µM, the cytotoxicity of the free diimine ligands (phen, dmp, and dpq) showed that dmp exhibited superior cytotoxicity compared to phen and dpq in all three cancer cell lines. This trend aligns with the observations made in the platinum complexes.

Disubstituted acylthiourea ligands had varying cytotoxic effects on platinum complexes across three cancer cell lines. The complexes containing *N*,*N*-di(butyl)-*N*′-benzoylthiourea (HL^1) and *N*,*N*-di(butyl)-*N*′-pivaloylthiourea (HL^3) were the most cytotoxic, in contrast to *N*,*N*-di(butyl)-*N*′-acetylthiourea (HL^2). This trend was consistent with the observed superior activity of HL^1 (70.5%) and HL^3 (89.6%)

compared to HL^2 (94.4%) against H1975 cells (*Appendix B, Table B2*). Based on these findings, we speculate that the R^1 substituent on the acylthiourea ligand must be aromatic or bulky, possessing increased van der Waals forces and a lipophilic nature. This would facilitate the entry of complexes through cell membranes to access potential target molecules within the cell.

It is worth noting that the cell viability of these ligands (acylthiourea and diimines) was higher than those of the respective platinum complexes, indicating that platinum complexes were more active than the respective free ligands.

Further investigation into the IC_{50} values of the three active platinum (II) complexes [Pt(dmp)(L^1-κ*O*,*S*)]Cl, [Pt(dmp)(L^2-κ*O*,*S*)]Cl, and [Pt(dmp)(L^3-κ*O*,*S*)]Cl at 48 hour treatment confirmed that these platinum complexes showed superior anti-cancer activity compared to cisplatin. These IC_{50} values ranged from 0.68 to 2.23 µM falling within the clinically relevant low micromolar range (below 5 µM). HT-29 cells were the most sensitive to the test compounds while H1975 cells were the least responsive. Similar to literature, H1975 cells are reported to be resistant to treatment as they possess multiple mutations in the epidermal growth factor receptor (EGFR) and TP53 genes (Tang *et al.*, 2016; Zhang *et al.*, 2019). Further investigations to elucidate the mechanism of action of these complexes were conducted.

Cell morphology studies showed that platinum complexes synthesized in this study induced morphological changes consistent with apoptotic cell death to a greater extent than cisplatin. These changes included nuclei fragmentation, indicative of late apoptosis, and the formation of large cytoplasmic vacuoles, suggesting cellular stress. A higher percentage of apoptotic nuclei was observed in A549 cells, followed by H1975 cells and lastly, HT-29 cells. Necrosis was not observed, as evidenced by the absence of bright propidium iodide (PI) staining.

3.4.2 Platinum complexes caused the externalization of PS and increase annexin-V binding indicating the induction of apoptosis

The exposure of PS on the external surface cell membrane is a feature of early apoptosis and is detected by the binding of fluorescence labelled annexin-V to PS

(Demchenko, 2013; Lee *et al.*, 2013). Platinum complexes were able to induce PS translocation to outer cell membranes to various extents in H1975, A549 and HT-29 cells. Additionally, the uptake of propidium iodide (PI) shown by red staining in combination with annexin V (AV) binding was indicative of cells with compromised plasma membranes after exposure to test compounds, thus confirming the induction of late apoptosis or secondary necrosis. Secondary necrosis, a regulated form of cell death, is triggered after apoptotic cell death completion when cells are not promptly cleared by phagocytes. It is characterized by osmotic cell swelling, lysis, and subsequent leakage of cell contents, resulting in tissue injury and inflammation. Detection of secondary necrosis often involves positive staining for AV and PI making it challenging to distinguish between late apoptotic and secondary necrotic cells (Rogers *et al.*, 2017).

Platinum complexes induced late-apoptosis/secondary necrosis in H1975 cells compared to cisplatin, which mainly caused early apoptotic cells after 18 hour treatment. This may have shown the slower response of H1975 cells to cisplatin compared to the three platinum complexes in this cell line. Platinum complexes induced early apoptosis in A549 cells compared to H1975 and HT-29 cells. Cisplatin showed varying effects, showing a lower activity in H1975 and HT-29 compared to platinum complexes.

The results confirmed the ability of platinum complexes to cause PS exposure in all three cell lines, H1975, A549, and HT-29, providing evidence for apoptosis induction. In order to definitively determine that platinum complexes induce apoptosis, additional apoptotic assays such as an increase in caspase-3/7 activity are important for verification.

3.4.3 Platinum complexes increase caspase-3/7 activity in H1975, A549 and HT-29 cells

Apoptosis can be executed via either the intrinsic or extrinsic signalling pathway, both involving the activation of caspases (Pfeffer and Singh, 2018; Shlomovitz, Speir and Gerlic, 2019). Caspases are enzymes (cysteine aspartyl-specific proteases) that cleave proteins after aspartate residues (Asp/D) in the amino acid sequence (Thornberry and Lazebnik, 1998; Shi, 2004). They are synthesized in their

inactive monomeric form (procaspases) and require dimerization or cleavage to be activated (Shi, 2004). Dimerization is facilitated by binding adaptor proteins to specific regions in the procaspases to trigger a cascade that causes the controlled degradation of cells (apoptosis).

The activation of caspase-3/7 is considered a late apoptotic event. Active caspase-3/7, cleaves various downstream substrates, including the inhibitor of caspase-activated DNAse (ICAD), resulting in the activation of caspase-activated DNAse (CAD) (McIlwain, Berger and Mak, 2013; Eskandari and Eaves, 2022). The activation of CAD induces chromatin condensation and DNA fragmentation (Eskandari and Eaves, 2022). Therefore, the increase in caspase-3/7 activity serves as an indicator of apoptotic cell death.

In this study, the ability of the platinum complexes and cisplatin to induce caspase-3/7 activity were evaluated in H1975, A549 and HT-29 cancer cell lines after a 24-hour treatment period using fluorescence microscopy. The three platinum complexes; [Pt(dmp)(L^1-κ*O*,*S*)]Cl, [Pt(dmp)(L^2-κ*O*,*S*)]Cl and [Pt(dmp)(L^3-κ*O*,*S*)]Cl were able to induce caspase-3/7 activity across the three cancer cell lines [Pt(dmp)(L^1-κ*O*,*S*)]Cl was the most effective inducer of caspase-3/7 activity in all three cancer cells lines compared to the other two platinum complexes and cisplatin. [Pt(dmp)(L^1-κ*O*,*S*)]Cl caused the highest percentage of cells with active caspase-3/7 in A549 cells (91.4%), followed by HT-29 cells (54.5%) and H1975 cells (33.7%).

This observation highlights variations in the susceptibility of each cell line to the different platinum complexes, with A549 being the most predisposed to caspase-3/7 activation compared to H1975 and HT-29 cells as shown. Based on the examination of photomicrographs, it was noted that cells displaying no evident response to caspase-3/7 activity remained firmly attached to the cell surface, with no signs of detachment. This suggests that these cells may have been responding slowly to the complexes, still been in the early stages of the cell death process compared to A549 cells. The increase in caspase-3/7 activity observed across the three cancer cell lines indicate that all three platinum complexes cause cell death by apoptosis.

Since the activation of caspase-3/7 alone cannot specifically identify the apoptotic signalling pathway that is initiated. Additional studies, including the assessment of caspase-8 and caspase-9 activation, are necessary to differentiate between the intrinsic and extrinsic pathways, respectively. Therefore, to determine if cell death was caused by the intrinsic pathway or extrinsic pathway, the effect of platinum complexes and cisplatin on caspase-8 activity was investigated.

3.4.4 The effect of platinum complexes on caspase-8 activity

Caspase-8 is classified as an initiator caspase and its activation is caused by the binding of death ligands, including Fas ligand (FasL), Tumour Necrosis Factor-alpha (TNF-α), or TNF-related apoptosis-inducing ligand (TRAIL), to their corresponding death receptors, which are on the external surface of the cell membrane. When these ligands bind to their respective receptors, such as Fas (CD95), TNF receptor 1 (TNF R1), and TRAIL receptors (DR4 and DR5), they trigger receptor clustering, forming the Death-Inducing Signalling Complex (DISC) (Wang and El-Deiry, 2003; Elmore, 2007). DISC is responsible for activating procaspase-8 to active caspase-8. Active caspase-8 in turn activates the effector caspases, caspase-3 and caspase-7 (McIlwain, Berger and Mak, 2013).

All three platinum complexes and cisplatin were poor activators of caspase-8 across the three cancer cells lines, H1975, A549 and HT-29 after an 18-hour treatment period. This was indicated by the lack of bright red fluorescence in cells, suggesting that the complexes did not induce any meaningful caspase-8 activity. Based on these results, it can be concluded that platinum complexes do not induce apoptosis through the extrinsic pathway.

3.4.5 Markers of apoptosis

According to literature, metal complexes can cause an overproduction of reactive oxygen species, resulting in the disruption of mitochondria through increasing mitochondrial membrane permeability and/or cause DNA damage, subsequently inducing apoptosis through the intrinsic pathway (Abdolmaleki *et al.*, 2023).

Therefore, the induction of apoptosis via the intrinsic pathway was explored by evaluating the effect of platinum complexes on ROS generation/levels, mitochondrial membrane permeability and the expression of oxidative stress response proteins as well as DNA damage response proteins.

3.4.6 Platinum complexes cause a loss of MMP in H1975, A549 and HT-29 cells

Mitochondrial membrane potential (MMP) represents the difference in electric potential across the mitochondrial membrane. MMP/$\Delta\psi_m$ loss is considered an early event in the activation of intrinsic apoptosis, occurring before caspase-9 (Wang and Youle, 2009). This event is attributed to the opening of mitochondrial permeability pores, causing a subsequent loss of the electrochemical gradient (Sivandzade, Bhalerao and Cucullo, 2019). This enables the release of pro-apoptotic proteins such as cytochrome c, Apoptosis-Inducing Factor (AIF), Smac/DIABLO, HTRA2/Omi, and Endonuclease G, which in turn facilitates the formation of an apoptosome complex, ultimately leading to the activation of procaspase-9 into caspase-9 (Suhaili *et al.*, 2017; Zorova *et al.*, 2018). Therefore, $\Delta\psi_m$ serves as an important indicator of mitochondrial function and overall cell health because mitochondria play a fundamental role in the apoptotic processes of cells.

JC-1 is a lipophilic, cationic charged dye that enters accumulates in the mitochondria of healthy cells to form J-aggregates. This is because in healthy cells, there is a strong electrochemical gradient due to the highly negative charge inside the mitochondria. This gradient promotes the movement of cations into the mitochondria through the mitochondrial membrane. In apoptotic cells, the JC-1 dye does not accumulate in the mitochondria; instead, it persists in its monomeric form, known as J monomers.

The untreated control cells showed cells with healthy mitochondria across the three cancer cell lines as indicated by the presence of the yellow/red-orange fluorescence due to presence of J aggregates in the mitochondria of these cells. The positive

controls, cisplatin and staurosporine caused a near complete loss of MMP in A549 (*Figure 3.11*) cells HT-29 cells (*Figure 3.12*) indicated by the increased green fluorescence and the lack of yellow/red-orange fluorescence observed. H1975 cells showed a near complete loss of MMP in cisplatin treated cells while staurosporine treated cells showed red-orange fluorescence, indicative of the presence of cells with intact mitochondrial membrane (*Figure 3.10*).

Similar to the positive controls, all three platinum complexes caused a loss of MMP, as evidenced by the presence of the green fluorescence in nearly 100% of cells across all three cancer cell lines (*Figure 3.10, Figure 3.11 and Figure 3.12, panels b, d, and f*). This is associated with the loss of mitochondrial membrane integrity and function, promoting the induction of intrinsic apoptosis.

Therefore, the loss of MMP induced by platinum complexes provided evidence for the induction of apoptosis through the intrinsic pathway. Given that MMP alone does not exclusively signify the induction of intrinsic apoptosis, it was important to assess oxidative stress in conjunction with internal stressors such as DNA damage, which can be evaluated by examining the expression of DNA damage response proteins (i.e p21) and eventually, caspase-9 activity (Galluzzi *et al.*, 2008; Deavall *et al.*, 2012).

3.4.7 Platinum complexes induce oxidative stress

Reactive oxygen species include radicals such as superoxide anion ($O_2^{-\bullet}$), hydroxyl ($OH^{\bullet}$), peroxyl ($RO_2^{\bullet}$) as well as non-radicals such as hydrogen peroxide (H_2O_2), organic peroxides (ROOH) and nitric oxide (NO) (Abdal Dayem *et al.*, 2017). ROS are mainly generated in the electron transport chain on the inner mitochondrial membrane during oxidative phosphorylation where ATP is generated from oxygen and sugar molecules (Zhao *et al.*, 2019). The mitochondria plays an important role in cellular metabolism and serves as both a source and a target of (ROS) (Suski *et al.*, 2012). ROS are essential for cell homeostasis and have a dual role that depends on their concentration level in cells. At low to moderate levels, ROS acts as signalling molecules that promote cell proliferation, invasion and angiogenesis (promoting tumour progression) whereas at high levels, ROS causes oxidative

stress that damages proteins, lipids and nucleic acids, leading to apoptosis (Abdal Dayem *et al.*, 2017; Perillo *et al.*, 2020).

The imbalance between the generation and elimination of ROS can lead cells into either oxidative stress or reductive stress. Many chemotherapeutic drugs including anthracyclines (doxorubicin, epirubicin, and daunorubicin), camptothecins (topotecan and irinotecan) and alkylating agents (cisplatin, carboplatin, and oxaliplatin) have previously been reported to increase ROS in cancer cells causing oxidative stress and apoptotic cell death (Chen *et al.*, 2018; Jian *et al.*, 2020).

The effect of platinum complexes; [Pt(dmp)(L^1-κ*O,S*)]Cl, [Pt(dmp)(L^2-κ*O,S*)]Cl, [Pt(dmp)(L^3-κ*O,S*)]Cl along with positive controls; cisplatin and tertiary-butylhydroperoxide (TBHP) on ROS production was measured after a 4-hour treatment period of the three cancer cell lines. This duration was selected because ROS are short-lived and highly reactive, necessitating a time-dependent evaluation. TBHP is a ROS inducer, that forms t-butoxyl radicals upon reaction with haemoglobin, initiating peroxidation and disrupting membranes by increasing their permeability (Kučera *et al.*, 2014; Akhtar *et al.*, 2020). In comparison to untreated control cells, platinum complexes were able to increase ROS levels in A549 and HT-29 cells, while H1975 cells showed the intrinsic ROS in their untreated cells. This was not unexpected since cancer cells have higher levels of ROS compared to normal cells, making cells more sensitive and susceptible to oxidative stress (Reczek and Chandel, 2017; Nakamura and Takada, 2021). Studies have shown that basal levels of ROS are important for biological activities and can promote protumourigenic signalling, facilitating cancer cell proliferation, differentiation and adaptation to hypoxia (Mittler, 2017; Reczek and Chandel, 2017). However, an increase in these ROS level can induce oxidative stress, initiating cell death.

The complex, [Pt(dmp)(L^1-κ*O,S*)]Cl was the most effective inducer of ROS in H1975 and HT-29 cells. In contrast, [Pt(dmp)(L^2-κ*O,S*)]Cl was the most effective ROS inducer in A549 cells and displayed prominent cytoplasmic vacuoles, as evident in phase-contrast images (*Figure B8, panel i*). This observation implies a correlation between the presence of cytoplasmic vacuoles and oxidative stress. In

HT-29 cells, increased ROS levels were also observed in mitotic cells, suggestive of increased metabolic activity.

The results indicate that the platinum complexes cause oxidative stress in H1975, A549, and HT-29 cells. Interestingly, the structural difference among these complexes appears to be associated with their ability to induce ROS formation. [Pt(dmp)(L^2-κ*O,S*)]Cl displayed a higher sensitivity to the A549 cells whereas [Pt(dmp)(L^1-κ*O,S*)]Cl was most effective in H1975 and HT-29 cells while [Pt(dmp)(L^3-κ*O,S*)]Cl was the least effective across the three cancer cell lines.

Although ROS is associated with intrinsic apoptosis, some research has also shown that excessive ROS generation can link to the extrinsic pathway of apoptosis by activating death receptors like Fas, TRAIL-R1/2, and TNF R1 (Nakamura and Takada, 2021). However, this study's findings indicated a lack of caspase-8 activity, suggesting the induction of intrinsic apoptosis.

An increase in ROS causes increased expression levels of stress response antioxidant enzymes, including NAD(P)H quinone dehydrogenase 1, haemoxygenase-1 (HO-1), thioredoxin reductase 1, superoxide dismutase, glutathione peroxidase and catalase, which serve to protect cancer cells from excessive ROS (Ma, 2013; Nakamura and Takada, 2021). Therefore, the effect of the platinum complexes on the expression of HO-1 was investigated.

3.4.8 Platinum complexes increased the expression of HO-1

HO-1 is known as a cytoprotective enzyme that responds to oxidative stress. HO-1 protein degrades toxic haem into free ferrous iron (Fe^{2+}) biliverdin, and carbon monoxide (Huan Wang *et al.*, 2023). Biliverdin is later converted into bilirubin, and both possess anti-oxidative properties that counteract ROS and prevent cell death.

Platinum complexes increased the expression level of HO-1 in H1975, A549 and HT-29 cells as shown by the increase in green fluorescence (*Figure 3.13, Figure 3.14 and Figure 3.15).* In contrast, cisplatin, had varying effects on HO-1 expression in different cell lines. It suppressed HO-1 expression in the lung cancer cell lines, H1975 and A549 but increased expression in HT-29 cells. The

differences observed in HO-1 expression levels may be attributed to the distinct characteristics of each cell line and the innate degree of oxidative stress of each cell line. Importantly, a lower HO-1 signal may suggest a reduced ability of cells to protect themselves from the harmful effects of oxidative stress and increased susceptibility to death (Lin *et al.*, 2007). The increase in HO-1 expression observed after treatment with platinum complexes, further confirms that these complexes induce oxidative stress in cancer cell lines, thereby promoting the initiation of ROS-induced apoptosis.

Recent studies suggests that the increased expression or enzymatic activity of HO-1 contributes to apoptosis resistance and triggers protective autophagy, a process linked to the development of chemoresistance. This implies that inhibiting HO-1 in various cancers may reverse chemoresistance or enhance chemosensitivity (Huan Wang *et al.*, 2023).

The catalytic activity of HO-1 has been demonstrated to be affected by its subcellular localization. Hence, it is imperative to examine the cellular localization of HO-1 in cells to determine or speculate on its potential role, drawing insights from existing literature. Previous studies have demonstrated that the full-length (32 kDa) HO-1 is primarily synthesized and located in the endoplasmic reticulum (ER), with potential translocation to the mitochondria, cytoplasm or nucleus where it serves different functions that are not clearly understood (Chiang, Chen and Chang, 2021). The nuclear translocation has been associated a loss of its catalytic function while cytoplasmic localization (mitochondrial, ER) is associated its full function and cell survival (tumour progression) (Dunn *et al.*, 2014; Chiang, Chen and Chang, 2021; Mascaró *et al.*, 2021). This may be attributed to the fact that HO-1 can be cleaved from the smooth ER membrane, resulting in a 28 KDa truncated form found predominantly in the nucleus while full length HO-1 is found in the cytoplasm (Lin *et al.*, 2007).

HO-1 expression was localised in both the cytoplasm and nucleus, with a particularly intense signal in the nucleus. This intriguing observation warrants further investigation to determine the implication of HO-1 expression in these cell lines.

Based on literature, the nuclear translocation of HO-1 is highly associated with the cancer progression in many types of cancer (i.e head and neck squamous cell carcinomas and lung cancers), contributing to chemotherapeutic resistance (Chiang, Chen and Chang, 2021). However, on another study, a correlation between a high nuclear HO-1 expression and poor overall cancer survival was observed in prostate cancer (Wegiel *et al.*, 2013). The mechanism by which HO-1 exerts its anti-apoptotic effects is not completely understood and requires further investigations.

High ROS levels (oxidative stress) are known to trigger cell death by damaging cell membranes, proteins and DNA (Kleih *et al.*, 2019). Therefore, the effect of platinum complexes on DNA damage was evaluated by examining the expression and localization of the DNA damage response protein, p21.

3.4.9 Platinum complexes increased the expression of p21

The induction of DNA damage by platinum complexes was investigated using an immunofluorescence assay using a p21 antibody.

A baseline p21 expression was observed in untreated control cells of both H1975 and A549 lung cancer cell lines. All three platinum complexes; [Pt(dmp)(L^1-κ*O*,*S*)]Cl, [Pt(dmp)(L^2-κ*O*,*S*)]Cl and [Pt(dmp)(L^3-κ*O*,*S*)]Cl were able to increase the nuclear expression of p21across the three cancer cell lines (H1975, A549 and HT-29). The upregulation of p21 expression, observed after the administration of platinum complexes surpassed that in cisplatin-treated cells. This suggests that the complexes induced DNA damage, potentially activating the DNA damage response. Overall, the complex [Pt(dmp)(L^3-κ*O*,*S*)]Cl consistently showed increased levels of nuclear p21 expression in H1975 and HT-29 cells while [Pt(dmp)(L^1-κ*O*,*S*)]Cl caused the highest percentage of cells with an intense p21 signal (*Table 3.6*) Compared to H1975 and A549 cells, cisplatin did not increase p21 expression in HT-29 cells. This could be attributed to mutations in p53 in HT-29 cells, which may have decreased the ability of the cells to induce p21 expression (Macleod *et al.*, 1995; Wang *et al.*, 2020).

While there seemed to be some variability in the activation of p21 among the cell lines, this could be attributed to the fact that p21 measurements were taken at a single time point and concentration across the different cell lines. The inability of cisplatin to induce p21 expression may have been due to the poor sensitivity of these cell lines to cisplatin. It is worth noting that cisplatin is unstable in aqueous environment, and this may have limited the extent of DNA damage it could have caused.

P21 has a dual role depending on where it is located within the cell. When located in the nucleus, p21 exhibits pro-apoptotic properties by binding to cyclin-dependent kinases Cdk1 and Cdk2 to prevent cells with damaged DNA from entering the S phase of the cycle where DNA synthesis takes place, for cells that are already in the S phase when DNA damaged occurs, p21 prevents the completion of DNA synthesis by inhibiting enzymes at the replication fork.

The increased expression of the DNA damage response protein, p21 indicate that the platinum complexes cause DNA damage across the three cancer cell lines., causing cell cycle arrest. These results therefore confirm DNA damaged as the trigger source for intrinsic apoptosis.

3.5 In summary

A qualitative structure-activity analysis identified platinum complexes with the dmp ligand as the most cytotoxic in the series, prompting their selection for evaluation against lung cancer cell lines (H1975 and A549) and a colorectal cancer cell line (HT-29). The three most potent platinum complexes, [Pt(dmp)(L^1-κ*O*,*S*)]Cl, [Pt(dmp)(L^2-κ*O*,*S*)]Cl, and [Pt(dmp)(L^3-κ*O*,*S*)]Cl, had low IC_{50} values across the three cell lines; ranging between 0.68 - 2.28 µM after a 48-hour treatment, whereas cisplatin had higher IC_{50} values ranging from 12.5 to 19.4 µM. HT-29 cells were the most sensitive to these platinum complexes with IC_{50} values below 1 µM.

Evaluation of cell morphology showed that platinum complexes caused nuclear fragmentation, suggestive of apoptotic cell death, which was further confirmed by

increased annexin-V binding and caspase-3/7 activation. The absence of caspase-8 activity in all three cancer cell lines indicated that these platinum complexes do not induce apoptosis via the extrinsic apoptotic pathway.

The active complexes induced oxidative stress by increasing the cellular ROS levels and disrupting the integrity of the mitochondrial membrane, as evident by the loss of MMP. This indicates that platinum complexes caused mitochondria damage, which facilitates the release of pro-apoptotic factors (i.e cytochrome c) associated with the induction of intrinsic apoptosis.

Given that oxidative stress leads to an increased expression of antioxidant enzymes such as HO-1 to regulate ROS levels, the effect of platinum complexes on HO-1 expression was evaluated. Elevated levels of HO-1 expression provided further evidence of oxidative stress induction by platinum complexes. HO-1 was detected in both the cytoplasm and the cell nucleus of these cancer cell lines. This requires further investigation since cytoplasmic expression is associated with functional HO-1, which regulate ROS effectively, while nuclear expression is associated with the loss of HO-1 function/ or reduced enzymatic activity. Further investigation to elucidate the role of HO-1 expression in these cancer cells is required, since its implications on tumour progression, chemoresistance, and the induction of cell death remains unclear. The increased nuclear expression of the DNA damage response protein, p21, suggests that DNA might be a target of these complexes.

These findings support the notion that these platinum complexes cause ROS-induced cell death by activating intrinsic apoptosis. The data presented here demonstrate the superiority of the [Pt(dmp)(L^n-κ*O*,*S*)]Cl complexes over cisplatin.

Given the evidence of cell death through the intrinsic apoptotic pathway, an apoptotic regulatory proteome array was used to further investigate the cellular response to these potent platinum complexes as presented in chapter 4.

Chapter 4: Evaluation of the effect of platinum complexes on the expression of apoptosis-associated proteins in cancer cells

4.1 Introduction

Cancer cells thrive by evading regulated forms of cell death such as apoptosis. Thus, exploring the expression patterns of apoptotic proteins in cancer cells offers a means to further investigate the fundamental factors contributing to cancer pathogenesis and identifying potential therapeutic targets. Chemotherapeutic agents that cause the upregulation of pro-apoptotic proteins or downregulation of anti-apoptotic proteins are important in treating cancer as this can effectively promote regulated cell death and hinder tumour progression (Chen, Zeng and Zhou, 2018; Carneiro and El-Deiry, 2020).

Conventional methods for studying the expression level of multiple proteins (i.e single analyte immunoassays and western blotting) are time-consuming, labour-intensive, and expensive. A multiplex antibody array enables cost-effective, timesaving and sample-efficient detection of numerous proteins simultaneously. By examining the expression levels of both anti-apoptotic and pro-apoptotic proteins, conclusions can be drawn and potential new targets can be identified.

In this chapter, the effect of the two most active platinum complexes; [Pt(dmp)(L^1-κ*O*,*S*)]Cl and [Pt(dmp)(L^3-κ*O*,*S*)]Cl and the positive control, cisplatin, on the expression level of apoptotic regulatory proteins were evaluated on the two human lung cancer cell lines (H1975 & A549) and the colorectal cancer cell line HT-29 using an apoptosis proteome array.

4.1.1 An overview of important apoptosis-associated proteins and their role in apoptosis

Intrinsic apoptosis is controlled by the Bcl-2 family proteins that can be anti- or pro-apoptotic. (Tzifi *et al.*, 2012). In the intrinsic pathway, cytochrome c is released from damaged mitochondria, binds to an apoptotic protease activating factor-1 molecule (APAF-1), and an inactive "initiator" caspase; procaspase-9, forming a complex known as the apoptosome (Shakeri, Kheirollahi and Davoodi, 2017). This activation of caspase-9 leads to the activation of executioner caspases (caspases-3 and -7), causing the cell morphology and biochemical changes characteristic of apoptosis.

The extrinsic pathway operates independently of mitochondria. It is triggered by death receptors like Fas, TRAIL, and the tumour necrosis factor (TNF) receptor family of proteins located on the cell membrane. This pathway directly activates the caspase cascade by recruiting the initiator caspase-8 within a complex known as the death-inducing signalling complex (DISC) (Elmore, 2007).

4.1.2 The Bcl-2 family of proteins

The B-cell lymphoma 2 (Bcl-2) family of proteins play an important role in apoptosis. The pro- and anti-apoptotic members of the Bcl-2 protein family can be distinguished by the presence of up to four relatively short sequence motifs called Bcl-2 homology domains (BH1, BH2, BH3 and BH4) (Youle and Strasser, 2008; Hardwick and Soane, 2013). All Bcl-2 proteins contain at least one conserved Bcl-2 homology domains. The anti-apoptotic members (Bcl-2, Bcl-xL, and Mcl-1) has four domains (BH1-BH4) and inhibit the pro-apoptotic Bcl-2 members. The BH3 domain is prevalent in pro-apoptotic members such as Bad, Bik/Nbk, Blk, Bid, Hrk/DP5, Bim/Bod, Bmf, Noxa, Puma/Bbc-3 BID and BIM, or the multidomain; Bax, Bak, Bcl-xS, Bok/Mtd and Bcl-GL (Bouillet and Strasser, 2002; Peña-Blanco and García-Sáez, 2018). The proteins; Bad, Bik, Bmf, Hrk, Noxa, and Puma fall under a class of Bcl-2 proteins (pro-apoptotic) that regulate Bax/Bak oligomerization/activation.

Pro-apoptotic proteins i.e Bax/Bak exert their function by undergoing conformational changes causing mitochondrial outer membrane permeabilization (MOMP) to various proteins and inducing mitochondria to fragment into smaller units (Peña-Blanco and García-Sáez, 2018). This enables the release of cytochrome c and other apoptotic proteins such as Apoptosis Inducing Factor (AIF), Smac/DIABLO, HTRA2/Omi and Endonuclease G from the mitochondria into the cytosolic space of the cell. Cytochrome c in the cytosol is essential for the activation of caspase-9 and facilitates the successful assembly of the apoptosome with pro-caspase-9, which in turn activates the effector caspase-3, leading to apoptosis. BID is the unique BH3-only pro-apoptotic Bcl-2 member, as it interconnects death receptor (extrinsic apoptosis) stimulation to intrinsic apoptosis (Tzifi *et al.*, 2012). BID is activated to truncated BID (tBID) by caspase-8 induced cleavage following death receptor stimulation and thereafter, tBID is translocated to the mitochondria to activate Bax and Bak, thus increasing mitochondria permeability.

Anti-apoptotic Bcl-2 protein members inhibit intrinsic (mitochondria-mediated) apoptosis. They directly bind and inhibit pro-apoptotic Bcl-2 members preventing the release of cytochrome c and other apoptotic factors from the mitochondria into the cytosolic space of the cell (Kuwana *et al.*, 2005; Hardwick and Soane, 2013). Bcl-2 is known to bind and inactivate Bax thereby preventing Bax/Bak oligomerization and other pro-apoptotic proteins to inhibit apoptosis (Wang and El-Deiry, 2003; Tzifi *et al.*, 2012).

4.1.3 Death receptor proteins

Death receptor proteins are cell surface/transmembrane proteins that regulate apoptosis, via the extrinsic pathway(Green, 2022). These include tumour necrosis factor (TNF) family proteins, which is comprised of TNF-receptor 1 and 2 (TNF R1/DR4 and TNF R2/DR5), TNF-related apoptosis inducing ligand receptors 1- 4 (TRAIL-R1 to TRAIL-R4), First apoptotic signal receptor protein (Fas), apoptosis-inducing ligands/binding proteins;(TRAIL, Fas Ligand) and adaptor proteins; (FADD, TRADD). Fas-associated death domain (FADD) is an adaptor molecule that recruits pro-caspase-8 and activates it into caspase-8, whereas TNF-receptor-

associated death domain (TRADD) modulates cell-survival by binding to and stabilizing inhibitors of apoptosis (cIAP-1 and cIAP-2) (Gentle *et al.*, 2011). TRAIL initiates apoptosis through engagement of its death receptors (Wang and El-Deiry, 2003). There are five receptors for TRAIL, including membrane-bound death receptors DR4/TRAIL-R1, DR5/TRAIL-R2, DcR1/TRAIL-R3/TRID, DcR2 /TRAIL-R4/TRUNDD and the soluble receptor osteoprotegerin (OPG) (Wang and El-Deiry, 2003; Pimentel, Zhou and Wu, 2023). TRAIL R1 and TRAIL R2 death receptors are known to possess conserved death domain (DD) motifs while the other three TRAIL receptors act as decoys on their ability to inhibit TRAIL induced apoptosis (Wang and EL-Deiry, 2003).

Some cells express Fas or TNF receptors which can cause apoptosis via ligand binding and protein cross-linking (Elmore, 2007). TRAIL or Fas ligand binding to their specific receptors, triggers clustering and activation of the receptor via dimerization or trimerization. This clustering leads to the formation of the Death Inducing Signal Complex (DISC) by recruiting the adaptor protein FADD, which in turn binds to the cytoplasmic domain using DD associations. The DISC then binds to procaspase-8 (or procaspase-10), leading to a proteolytic activation of caspase-8, which in turn cleaves and activates caspase-3, ultimately causing apoptotic cell death.

4.1.4 Tumour suppressor protein p53

The tumour suppressor protein p53, has many functions, which include the initiation of cell cycle arrest, induction of apoptosis, DNA repair and differentiation (Haolan Wang *et al.*, 2023). In response to cellular stress such as DNA damage, the p53 protein accumulates within the cell nucleus, where it carries out its pro-apoptotic role. p53 exerts its transcriptional or pro-apoptotic function by undergoing chemical modifications such as phosphorylation or acetylation (Ozaki and Nakagawara, 2011). Phosphorylation at Ser-15, Ser-20 and Ser-46 on the NH_2-terminal converts latent p53 to its active form (Piette, Neel and Maréchal, 1997). Additionally, phosphorylation of p53 at the COOH terminal of Ser-392 by casein kinase II enhances its DNA binding activity (Herrmann, Kraiss and Montenarh,

1991). The ability of p53 to bind to DNA is closely linked to its role as a tumour suppressor (Ozaki and Nakagawara, 2011). Activated p53 cause cell cycle arrest, allowing for DNA repair and/or apoptosis. This prevents the division of cells with damaged DNA by activation of target genes (i.e p21) involved in facilitating cell cycle arrest.

p53 initiates apoptosis by stimulating the expression of some Bcl-2 family proteins such as Bax and BH3 only proteins. Alternatively, p53 can also bind to one or more of the anti-apoptotic proteins (e.g Bcl-xL), preventing them from inhibiting Bax/Bak activation and its associated mitochondrial pore formation, thus facilitating the release of cytochrome c and other pro-apoptotic factors from the mitochondria (Chipuk *et al.*, 2003; Papaliagkas *et al.*, 2007).

Over 50% of human cancers carry loss of function mutations in p53 gene and in some cases, cancer cells with these p53 mutations become resistant to chemotherapy. In normal cells, p53 is maintained at low levels through ubiquitin/proteasome-dependent protein degradation by a RING-finger type E3 ubiquitin protein ligase MDM2 (murine double minute 2) (Ozaki and Nakagawara, 2011). However, in cancer cells, mutant p53 escapes MDM2-mediated proteasomal degradation, accumulates to high levels and loses its tumour suppressor function (Scian *et al.*, 2004).

4.1.5 Cell cycle protein p21Cip1/Waf1/CDKN1A

One of the p53-target gene products; $p21^{CIP1/Waf1}$ (Cdk-interacting protein/wild-type p53-activated fragment 1) protein, plays a central role in cell cycle progression, DNA repair and apoptosis (Haolan Wang *et al.*, 2023). p21 is an inhibitor of cyclin-dependent kinases (CDKs), which regulates the progression of the cell cycle. In response to DNA damage or cellular stress, p21 is increased and cell cycle arrest induced.

Nuclear localization of p21 is associated with its pro-apoptotic response to DNA damage and cytoplasmic localization of p21 causes the inhibition of multiple pro-apoptotic proteins such as pro-caspase-3, caspase-8, caspase-10, apoptosis signal-

regulating kinase 1 and stress-activated protein kinase (Abbas *et al*, 2009; Kreis *et al*, 2015; Kreis *et al*, 2019).

4.1.6 Heat shock proteins

Heat shock proteins (HSPs), are a group of molecular chaperones that play central roles in cellular stress responses and protein homeostasis. HSPs protect cells against oxidative stress, hypoxia and inflammatory stimuli, thus preventing cell death. The HSP protein family is highly conserved and classified based on their molecular weights, mainly including large HSPs; HSP90, HSP70, HSP60, HSP40 and small HSPs such as HSP27/HSPB1 (Hu *et al.*, 2022). Their primary function is to facilitate protein folding, transport and prevent the aggregation of misfolded or damaged proteins, which are harmful to cells (Saibil, 2013; Hu *et al.*, 2022). Additionally, HSPs can regulate inflammation, oxidative stress and other cellular processes to protect cells from various stressors. Increased levels of HSPs indicate of cellular stress and a required intervention to allow cell survival.

HSP27 and HSP70 are known to inhibit caspase-dependent apoptosis and promote tumour growth (Vidyasagar, Wilson and Djamali, 2012; Dubey *et al.*, 2015). In the murine L929 cell line, HSP27 was found to inhibit extrinsic apoptosis by blocking the Fas mediated cell death and intrinsic apoptosis by blocking procaspase-3/7 activation (Dubey *et al.*, 2015). HSP70 directly suppresses intrinsic apoptosis by associating with APAF-1 and blocking the assembly of the apoptosome complex and activation of pro-caspase-9 (Beere *et al.*, 2000). HSP60 is a key chaperone and plays an essential role in the transport and folding of mitochondrial proteins. Its expression is increased in different types of cancer and is associated with cell survival (Ghosh *et al.*, 2008; Caruso Bavisotto *et al.*, 2020).

Haemoxygenase-1 (HO-1) and haem oxygenase-2 (HO-2) are HSPs (HSP32 cognates) that have cytoprotective functions beyond protein folding. HO-1 and HO-2 are isozymes that catalyse the same reaction, which is to degrade haem into carbon monoxide (CO), free ferrous iron (Fe^{2+}) and biliverdin. Biliverdin is further converted into bilirubin, a potent antioxidant (Roach, Wagner and Hackett, 2011).

SPs have become important targets for therapeutic interventions and drug development in multiple areas of medicine.

4.1.7 Inhibitors of apoptosis (IAPs)

IAPs are a family of proteins that have been conserved throughout evolution and possess a common baculovirus inhibitor of apoptosis protein repeat (BIR) domain. BIR domains are versatile domains involved in protein-protein interactions, capable of binding numerous proteins and directly inhibiting caspases (Mace, Shirley and Day, 2010) . These proteins include XIAP, cIAP-1, cIAP-2, livin and survivin and they function to inhibit apoptosis by binding to the active site of caspases (proteolytic enzymes that initiate and execute apoptosis). IAPS are selective towards specific caspases, and the expression of a specific IAP will therefore inhibit a specific caspase (Sing *et al*, 2022). XIAP inhibits apoptosis by directly binding to the active site of initiator caspase-9 and executioner caspase-3 and caspase-7, inhibiting both the intrinsic and extrinsic apoptotic pathways (Scott *et al.*, 2005). cIAP-1 and cIAP-2 are E3 ubiquitin ligases (E3) causing ubiquitination of various target proteins, including caspases. causing their degradation (Scott *et al.*, 2005; Eckelman and Salvesen, 2006). Additionally, these proteins are recognized for their participation in the modulation of the NF-κB (nuclear factor-kappa B) signalling pathway. NF-κB, a transcription factor essential for promoting cell survival and preventing apoptosis, is subject to regulatory influences from cIAP-1 and cIAP-2 (Verzella *et al.*, 2020). Other members of the IAPs such as livin and survivin possess one BIR domain and are selective for caspase-9 (Singh *et al.*, 2022).

The overexpression of IAPs is often observed in cancer cells, contributing to their ability to evade cell death and promote tumour growth. Suppressing the anti-apoptotic effects IAPs makes it possible to potentially restore the apoptotic process and promote the elimination of cancer cells.

4.1.8 Smac/DIABLO and HTRA2/Omi

The second mitochondria derived activator of caspases also known as the direct inhibitor of apoptosis-binding protein with low pI (Smac/DIABLO) and a serine protease, HTRA2/Omi are both pro-apoptotic proteins found in the intermembrane space of the mitochondria (Yang *et al.*, 2003; Martinez-Ruiz *et al.*, 2008; Kaur *et al.*, 2019). These proteins are released into the cytosol through mitochondria pores mediated by Bax/Bak activation and directly bind and inhibit IAPs. This prevents IAPs from binding to the active site of their respective caspases, thus promoting apoptosis (Martinez-Ruiz *et al.*, 2008; Pandey *et al.*, 2022).

4.1.9 Insulin-like Growth Factors (IGFs) and IGF-Binding Proteins (IGFBPs)

Insulin-like Growth Factor (IGFs) are peptides that play an important role in cell growth, development, and metabolism (Jogie-Brahim, Feldman and Oh, 2009; LeRoith, Holly and Forbes, 2021). The two main types of IGFs are IGF-1 and IGF-2. They are structurally similar to insulin and interact with cell surface receptors to mediate their effects. IGFs promote cell survival by activating signalling pathways, such as the PI3K/Akt pathway, which promotes cell survival and inhibits apoptosis (Zhang *et al.*, 2018). IGFs can suppress the activation of pro-apoptotic proteins by preventing the release of cytochrome c from mitochondria, thereby inhibiting the initiation of apoptotic pathways.

Insulin-like Growth Factor 1 Receptor (IGF1R) is a transmembrane receptor located on the cell surface and it is activated by IGF-1 binding. Activation of IGF1R triggers a cascade of signalling pathways that stimulate cell growth.

4.1.9.1 IGF-Binding Proteins (IGFBPs)

Insulin-like growth factor binding proteins (IGFBPs) are a group of six proteins (IGFBP-1 to IGFBP-6) that modulate the activity of insulin-like growth factors (IGFs). IGFBPs can either enhance or inhibit the binding of IGFs to their receptors, influencing the balance between pro-survival and pro-apoptotic signals

(Brahmkhatri, Prasanna and Atreya, 2015). By sequestering IGFs, IGFBPs extend their half-life and impact the activation of survival pathways like PI3K/Akt.

IGFBPs, such as IGFBP-2 and IGFBP-5, can potentiate IGF signalling, while IGFBP-1 and IGFBP-4 inhibit it by sequestering IGFs. IGFBP-3 and IGFBP-6 possess pro-apoptotic properties, directly inducing apoptosis independently of IGFs(Jogie-Brahim, Feldman and Oh, 2009). These IGFBPs can interact with cell surface receptors or intracellular signalling molecules, triggering apoptotic pathways. IGFBP-3 is the most abundant IGFBP in circulation, and it forms a ternary complex with IGF-1 or IGF-2. IGFBP-3 can interact with the tumour suppressor protein p53, modulating its activity and influencing apoptotic pathways, this effect was presumed to make IGFBP-3 have a protective role against the potentially carcinogenic effects of IGF-I (Rajah, Valentinis and Cohen, 1997; Grimberg, 2000). IGFBP-4 binds to both IGF-1 and IGF-2 with high affinity and inhibits their actions. IGFBP-6 is involved in fetal growth, cell proliferation, and apoptosis regulation. The interplay between IGFBPs, IGFs, and other signalling molecules determines cell survival or apoptosis outcomes.

4.2 Experimental

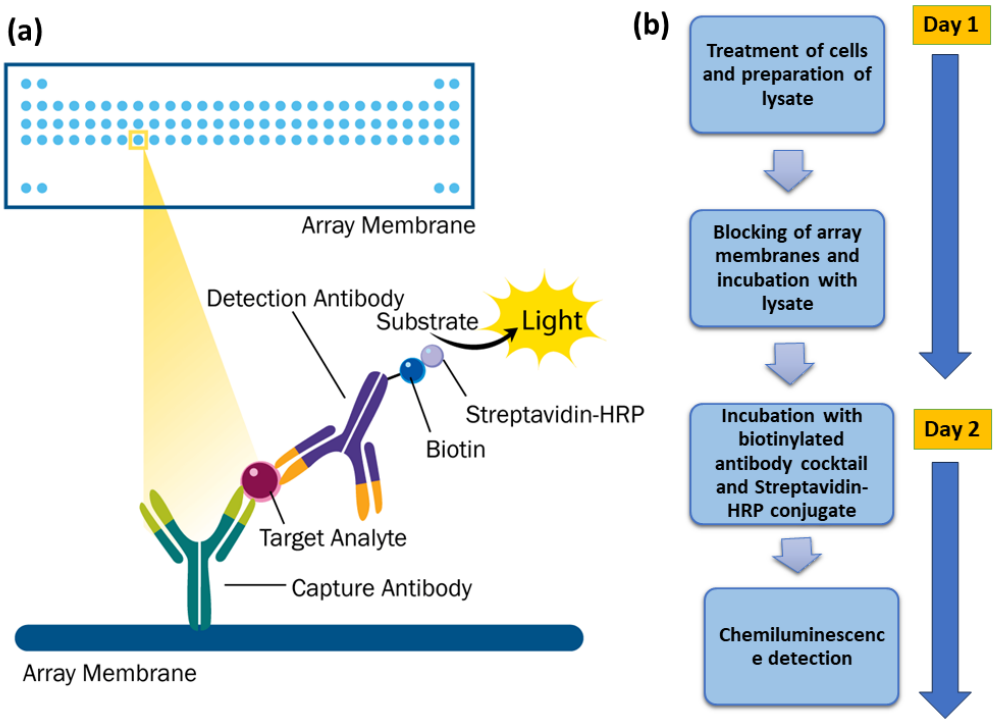
The effect of platinum complexes on the expression level of apoptotic-regulatory proteins was investigated against two human lung epithelial cancer cell lines; A549 & H1975 as well as a colorectal cancer cell line, HT-29 using two human apoptosis proteome array kits purchased from R&D systems and RayBiotech respectively. HT-29 cells were evaluated using the Proteome Profiler Human Apoptosis Array Kit (ARY009, R&D Systems, Whitehead Scientific, Cape Town, South Africa). The kit allowed a simultaneous evaluation of 35 apoptosis-associated proteins in duplicate and contained four nitrocellulose membranes spotted with capture antibodies. A549 and H1975 were evaluated using the RayBio® C-Series Human Apoptosis Antibody Array C1 kit (AAH-APO-1-8, RayBiotech, BIOCOM BIOTECH AFRICA, South Africa). The kit allowed a simultaneous evaluation of 43 apoptosis-associated proteins in duplicate and contained a total of eight antibody arrays; of which four were used per cell line. A change to the RayBiotech array kit

was made since it was more cost-effective and detected 43 proteins instead of the 35 proteins by the R&D systems.

The two most active platinum complexes; [Pt(dmp)(L^1-κ*O*,*S*)]Cl and [Pt(dmp)(L^3-κ*O*,*S*)]Cl were selected for evaluation with the proteome arrays and cisplatin was used as a positive control. The concentration of platinum complexes and treatment period used in this proteome array were carefully considered. Cells were closely monitored for morphological changes to ensure cells were not dead before cell harvesting and protein isolation. Each cell lines were treated with concentrations equivalent to the IC_{80} values of each test compound for 18 hours. Lysates were prepared in the presence of a protease inhibitor cocktail (cOmplete™ Protease Inhibitor Cocktail, Roche, South Africa).

4.2.1 Human apoptotic proteome array

The human apoptotic proteome array consists of an array of antibodies (capture antibodies) immobilized on a solid support (nitrocellulose membranes), which acts to bind the specific protein (antigen) in the lysate. A cocktail of biotinylated detection antibodies is used to detect the immobilized proteins on the capture antibodies, and their signal is amplified using a streptavidin-horseradish peroxidase conjugated antibody that binds to biotin on the biotinylated detection antibody. Streptavidin has a very high affinity for biotin. The enzyme activity of the horseradish peroxidase causes the emission of light when exposed to chemiluminescent detection reagents and this is detected with the CCD camera of the BIO-Rad ChemiDoc instrument (*Scheme 4.1*). The intensity of the protein signal (dark spot) on the membrane corresponds to the amount of bound target protein.



***Scheme 4.1**: **Summary of the principle and general procedure of the proteome array** (a) the array membranes are immobilized with "capture" antibody which bind the target protein (antigen) found in lysate samples during incubation. The detection antibody-biotin and streptavidin-HRP enhance the signal of the bound protein under chemiluminescent light during detection. (b) The experiment was completed in two days following the steps described. The scheme was adapted from R&D system protocol (R&D Systems, 2016).*

4.2.2 Treatment of cells

Cells were grown in 75 cm^3 cell culture flasks at a density of 7 x 10^6 cells per flask and allowed to adhere on the growth surface overnight. Cells were then treated with concentrations equivalent to IC_{80} values of the platinum complexes; [Pt(dmp(L^1-κ*O*,*S*)]Cl, [Pt(dmp(L^3-κ*O*,*S*)]Cl and cisplatin for 18 hours while the untreated control was incubated with 20 mL complete media. Following this, cells were viewed with phase contrast microscope to observe any changes in cell morphology, thereafter the cell media was carefully removed from each flask. Floating cells were harvested by collecting the media into centrifuge tubes and centrifuging for 5 minutes at 1500 rpm, decanting the supernatant. The adhered cells from each flask were washed with 1X PBS and harvested using sterilized cell scrapers.

4.2.3 Lysate preparation

Cell lysates were prepared by solubilizing each cell sample pellet with 1 mL of freshly prepared 1X Lysis Buffer, to which half a tablet of the protease inhibitor cocktail was added to prevent protein degradation and ensure optimal yield. The cell lysates were vigorously resuspended to break up DNA which made the suspension viscous. This was followed by incubation on a rocking platform for 30 minutes at 4°C. Following this, lysates were centrifuged at 14 000 rpm for 5 minutes at 4°C and the supernatants were transferred to sterile 1.5 mL microcentrifuge tubes and stored on ice. The protein concentration for each lysate sample was determined using the Bradford assay. Reagents were kept on ice throughout the experiment and all reagents were freshly prepared as specified in *Table 4.1* (R&D Systems and Raybiotech protocol) before usage.

Table 4.1: List of reagents and their preparation as described by the Proteome Profiler™ Human Apoptosis Array Kit (ARY009, R&D Systems) for HT-29 cell lines and the RayBio® C-Series Human Apoptosis Antibody Array C1 kit for lung cancer cell lines A549 and H1975 respectively.

Reagent/s	**Preparation (*R&D Systems*)**	**Preparation (*RayBio® C-Series*)**
1X Lysis Buffer	Added half of protease inhibitor cocktail tablet to 10 mL of 1X Lysis Buffer 17	1X Cell Lysis Buffer was prepared by diluting 10 mL of 2X lysis buffer concentrate with 10 mL of deionized water (1:1).
Protease Inhibitor Cocktail	-	60 µL of 1X cell lysis buffer was added into a vial of protease inhibitor cocktail
Biotinylated Antibody Cocktail (BAC)	-	Added 150 µL of blocking buffer into a BAC vial to resuspend the antibody. Mixed gently and transferred the reagent into a tube with 1.8 mL blocking buffer
1X Wash Buffer concentrate.	Dilute 40 mL of 25X Wash Buffer concentrate into	Dilute 20X Wash Buffer I concentrate to 1X by

	960 mL of deionized water	adding 10 mL of it into 190 mL of water (200 mL) Dilute 20X Wash Buffer II concentrate the same.
1X Array Buffer 2/3	Dilute 5X Array Buffer 2 to 1X by adding 2 mL into 8 mL of Array Buffer 3	-
Detection Antibody Cocktail	One vial of Detection Antibody Cocktail (~15 µl) was reconstituted in 100 µl deionized water	-
1X Streptavidin-HRP	Dilute Streptavidin-HRP in 1X Array Buffer 2/3 (1:2000)	10 µl of 1000X Streptavidin-HRP was diluted in 9 990 µL blocking buffer (10 mL)
Chemi reagent mix	A 1:1 mixture of Chemi reagent 1 and 2 was prepared to a final volume of 2 mL and covered in foil to protect from light	A 1:1 mixture of Detection Buffer C and D was prepared to a final volume of 2 mL and covered with foil

Note: The components and concentration of the various buffers and chemi reagents are propriety information.

4.2.4 Protein quantification (Bradford assay)

The Bradford assay was used to determine the concentration of proteins in each lysate sample. Lysates were diluted 10X with Milli-Q deionized water to minimize interference of detergents (Bradford, 1976). Following the protein determination, each lysate sample was prepared to a final amount of 400 µg protein in a total volume of 2 mL adjusted using array buffer 1 (R&D system) or blocking buffer (Raybiotech) and kept on ice. Each array membrane was incubated with the same 400 µM protein prepared form each treatment.

4.2.5 Preparation of membrane arrays (HT-29)

Four nitrocellulose membrane arrays each containing a duplicate of 35 different capture antibodies were placed into a 4-Well Multi-dish and blocked for 1 hour with 2 mL of Array blocking Buffer 1 on a rocking platform at room temperature. Following this 2 mL of each lysate, containing 400 µg of protein each were prepared, and added to each membrane. This was incubated overnight on a rocking

platform shaker at 4 °C. This allowed proteins to bind to capture antibodies on the arrays.

On the following day, each membrane was washed with 20 mL 1X Wash Buffer for 10 minutes on a rocking platform shaker to remove any unbound proteins. This was followed by incubation with the Detection Antibody Cocktail, diluted with 1.5 mL of 1X Array Buffer 2/3 and incubated for one hour on a rocking platform shaker. Thereafter, the arrays were washed as previously described with 20 mL 1X Wash Buffer. This was followed by a 30-minute incubation of the membranes with 2 mL of 1:2000 Streptavidin-HRP conjugate on a rocking platform shaker at room temperature.

Following the washing step, the array membranes were then incubated with 1 mL of the prepared chemiluninesence reagent mix for 1 minute. The chemiluminescence signal was detected using a BIO-Rad ChemiDoc™ Imager and analyzed using the BIO-RAD Image Lab Software Version 5.2.1 to quantify the intensities of each protein duplicate into pixel density.

The membrane array map of capture proteins in the Proteome Profiler™ Human Apoptosis Array kit (R&D Systems) showing proteins coordinates is shown in *Figure 4.1* and *Table 4.2* below.

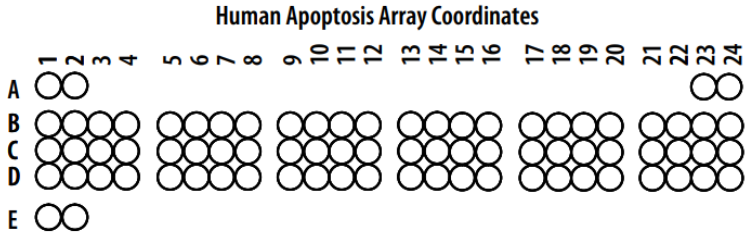


***Figure 4.1**: Coordinates of 35 human apoptosis target proteins, reference spot (positive control) and PBS (negative control) spotted in duplicates on each of the four-nitrocellulose membrane array from R&D system.*

***Table 4.2**: **The proteome array map (R&D Systems) for HT-29 cells**. An outline of 35 capture proteins (duplicate) detected using the Proteome Profiler™ Human Apoptosis Array Kit (R&D Systems).*

Coordinates	Target/Control	Coordinates	Target/Control
A1, A2	Reference spots	**C13, C14**	HO-2/HMOX-2
A23, A24	Reference spots	**C15, C16**	HSP27
B1, B2	Bad	**C17, C18**	HSP60
B3, B4	Bax	**C19, C20**	HSP70
B5, B6	Bcl-2	**C21, C22**	HTRA2/Omi
B7, B8	Bcl-x	**C23, C24**	Livin
B9, B10	Pro-Caspase-3	**D1, D2**	PON2
B11, B12	Cleaved Caspase-3	**D3, D4**	P21/cip1/cdkn1a
B13, B14	Catalase	**D5, D6**	P27/Kip1
B15, B16	cIAP-1	**D7, D8**	Phospho-p53 (S15)
B17, B18	cIAP-2	**D9, D10**	Phospho-p53 (S46)
B19, B20	Claspin	**D11, D12**	Phospho-p53 (S392)
B21, B22	Clusterin	**D13, D14**	Phospho-Rad17 (S635)
B23, B24	Cytochrome c	**D15, D16**	SMAC/DIABLO
C1, C2	Trail R1/DR4	**D17, D18**	Survivin
C3, C4	TRAIL R2/DR5	**D19, D20**	TNF R1
C5, C6	FADD	**D21, D22**	XIAP
C7, C8	Fas/TNFRSF6/CD95	**D23, D24**	PBS (Negative Control)
C9, C10	HIF-1α	**E1, E2**	Reference spots
C11, C12	HO-1/HMOX-1		

4.2.6 Preparation of membrane arrays (H1975 and A549)

Four nitrocellulose membranes, each carrying 43 unique capture antibodies, were incubated with blocking buffer and incubated with the prepared cell lysate as previously stated (section 4.2.5).

Thereafter, lysates were aspirated from each well one at a time and membranes were washed three times with 2 mL of Wash Buffer I and twice with 2 mL of 1X Wash Buffer II at five-minute intervals on a rocking platform shaker to ensure removal of any unbound proteins. The membranes were then incubated with 1.8 mL of the diluted BAC for 2 hours on a rocking platform shaker at room temperature and thereafter washed as described above. Following this, each membrane was incubated with 2 mL of freshly diluted 1:2000 streptavidin-HRP on rocking platform shaker for 2 hours at room temperature. on a rocking platform followed by a washing step as described above.

Each membrane was then placed on a plastic sheet and incubated with 500 µl of the prepared detection buffer mixture for two minutes at room temperature. Excess detection reagent was blotted, the membranes were sandwiched with plastic sheets and detected as described above (section 4.2.5).

The membrane array map of capture proteins in the RayBio® C-Series Human Apoptosis Antibody Array C1 kit is shown in *Table 4.3*.

Table 4.3: The proteome array map (RayBiotech) for A549 and H1975 cells. *The map shows coordinates of 43 apoptosis capture proteins in duplicate.*

Antibody		A	B	C	D	E	F	G
	1	POS	POS	NEG	NEF	BLANK	BLANK	Bad
	2							
	3	CD40	CD40 ligand	cIAP-2	CytoC	DR6	Fas	Fas Ligand
	4							
	5	IGFBP-1	IGFBP-2	IGFBP-3	IGFBP-4	IGFBP-5	IGFBP-6	IGF-1R
	6							
	7	TNF-RII	TNF-alpha	TNF-beta	TRAIL-R1	TRAIL-R2	TRAIL-R3	TRAIL-R4
	8							

Antibody		H	I	J	K	L	M	N
	1	Bax	Bcl-2	Bcl-w	BID	BIM	Caspase -3	Caspase -8
	2							
	3	BLANK	HSP27	HSP60	HSP70	HTRA2	IGF-1	IGF-2
	4							
	5	Livin	p21	p27	p53	Smac/DIABLO	Survivin	TNF-RI
	6							
	7	XIAP	BLANK	BLANK	NEG	NEG	NEG	POS
	8							

Changes in the expression level of apoptotic-regulatory proteins after treatment with platinum complexes are herein reported. The signal (dots) on membrane arrays were correlated to the expression level of proteins and quantified as arbitrary units depicting pixel density.

The data was further statistically analyzed on GraphPad prism software, version 5 using one-way analysis of variance (ANOVA) (95% confidence interval, $p<0.05$) to test if there was a significant difference between the means of the signals, followed by a Dunnett's Multiple Comparison post-hoc test The probability values indicated that the difference between the means were either non-significant (ns), poorly significant ($p<0.05$) *, significant ($p<0.01$) ** or highly significant ($p<0.001$) *** as presented by their respective star signs on each table. The baseline expression level of proteins was categorized according to *Table 4.4*.

***Table 4.4*: Baseline expression level of apoptotic protein (pixel density) in HT-29, H1975 and A549 cells.**

Baseline expression level	Pixel density range (HT-29)	Pixel density range (H1975 & A549)
Very low	0 - 50 000	0 - 100 000
Low	50 000 – 200 000	100 000 – 200 000
Moderate	200 000 – 400 000	200 000 – 400 000
Moderate high	400 000 – 600 000	400 000 – 600 000
High	600 000 – 900 000	600 000 – 900 000
Very high	900 000 or greater	900 000 or greater

4.3 Results

The results were expressed as the percentage change in expression levels relative to the untreated negative control (baseline expression) (*Table 4.5, Table 4.6 and Table 4.7*).

4.3.1 Apoptosis-associated proteins in HT-29 cells

The expression level of apoptotic-regulatory proteins in HT-29 cells following treatment with concentration equivalent to the IC_{80} value of [Pt(dmp)(L^1-κ*O,S*]Cl, [Pt(dmp)(L^3-κ*O,S*)]Cl and cisplatin are shown *Figure 4.2*. A percentage change greater than 20% was considered to be meaningful.

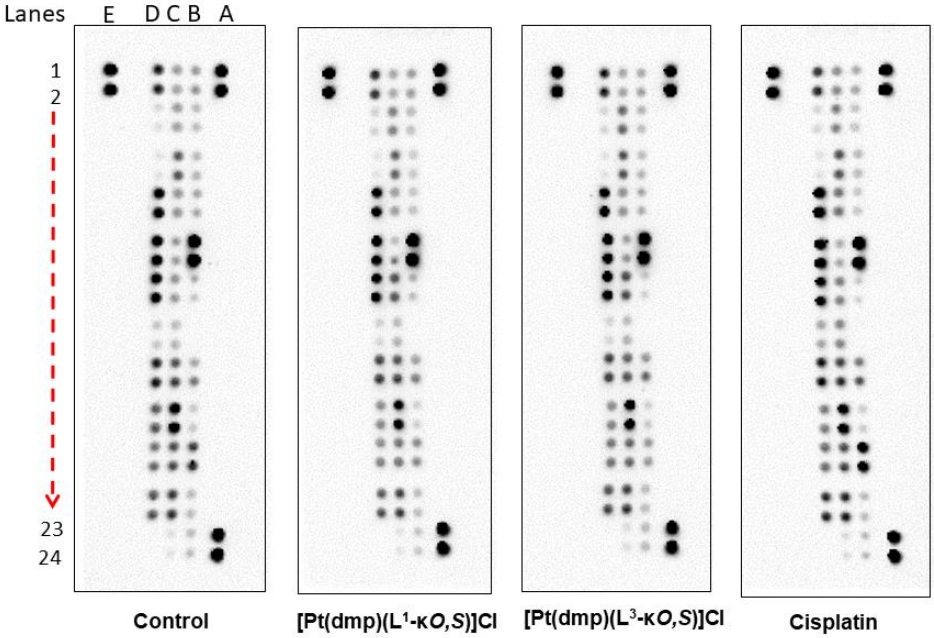


Figure 4.2: Chemiluminescent signals of the apoptosis array membranes (R&D Systems) showing the effect of the platinum complexes and cisplatin in HT-29 cells*. Each membrane array was incubated with 400 ug protein. Cells were treated with* 2.0 µM of [Pt(dmp)(L^1-κ*O,S*]Cl, 1.3 µM of [Pt(dmp)(L^3-κ*O,S*)]Cl and 20 µM cisplatin *for 18 hours. Chemiluminescence was detected with the BIO-RAD ChemiDoc MP Imager.*

***Table 4.5**: The expression level of apoptotic proteins and the percentage change in HT-29 cells after an 18 hour treatment with concentration equivalent to IC_{80} values of [Pt(dmp)(L^1-κO,S)]Cl, [Pt(dmp)(L^3-κO,S)]Cl and cisplatin. The data is reported as percentage change measured relative to the untreated control cells.*

Apoptotic protein	Baseline expression Level	[Pt(dmp)(L^1-κ*O,S*)]Cl		[Pt(dmp)(L^3-κ*O,S*)]Cl		Cisplatin	
		Change (%)	sign	Change (%)	sign	Change (%)	sign
Bad	Moderate	-2.7	ns	-19.6	***	-26.9	***
Bax	Moderate	+12.2	ns	+8.9	ns	-7.8	ns
Bcl-2	Moderate	-13.0	*	-6.4	ns	+1.0	ns
Bcl-x	Moderate	-21.7	***	-5.7	ns	-34.7	***
Procaspase-3	High	+5.9	ns	+2.0	ns	-6.7	ns
Cleaved Caspase-3	Low	+19.4	*	-3.6	ns	-28.5	*
Cytochrome c	Moderate	-14.3	***	+15.4	***	-14.2	***
XIAP	High	-18.6	**	+15.8	*	+8.0	ns
cIAP-1	Moderate	+9.0	ns	+22.7	ns	+23.7	ns
cIAP-2	Moderate	+3.4	ns	+21.4	**	-16.2	*
Survivin	Moderate	-33.0	***	-34.0	***	-30.4	***
Livin	Low	-20.3	***	+8.4	ns	-6.6	ns
Smac/DIABLO	High	-12.8	*	-14.7	*	+1.5	ns
HTRA2/Omi	High	-13.0	*	-1.0	ns	-0.2	ns
HIF-1α	Moderate	-15.3	ns	+1.0	ns	-30.7	*
Heamoxygenase 1	Moderate	+78.4	***	+88.3	***	+15.2	*
Heamoxygenase 2	Moderate	+2.9	ns	-1.7	ns	+68.1	***
HSP27	High	-0.37	ns	-2.31	ns	+2.80	ns
HSP60	Very high	-15.1	**	-7.3	ns	-10.9	*
HSP70	High	-22.0	***	-10.3	***	-3.6	**
Clusterin	Moderate	-14.1	***	+2.1	ns	-27.3	***
PON-2	High	-10.7	***	-7.7	**	-15.5	***
TRAIL-R1	Moderate	-9.6	*	-9.3	*	+13.3	**
TRAIL-R2	Moderate	+23.5	***	+52.7	***	+15.4	***
FADD	High	-9.2	**	-5.7	ns	-1.0	ns
Fas/TNFRSF6/CD95	Moderate	-12.9	**	+1.8	ns	+23.1	***
TNF RI/TNFRSF1A	Moderate	-19.4	**	-2.7	ns	-2.8	ns
Phospho-p53 (S15)	Very high	-5.7	ns	-3.9	ns	+12.9	**
Phospho-p53 (S46)	Very high	-4.9	ns	-2.5	ns	+5.3	ns
Phospho-p53 (S392)	Very high	-1.1	ns	+3.6	*	-7.9	***
Phospho-Rad17 (S635)	Moderate	-18.4	***	-8.0	*	+53.6	***
p21/CIP1/CDKN1A	Low	+25.2	**	+23.9	**	+6.8	ns
p27/Kip1	Low	-5.1	ns	+19.9	ns	+0.4	ns
Claspin	High	-46.1	***	-49.0	***	+40.7	***

*Note: The positive (+) sign indicates an increase in protein expression, whilst the negative (–) sign indicates a decrease. The data was statistically analysed using one-way ANOVA (non-parametric test), followed by Dunnett's Multiple Comparison test) which compared the pixel density of treated cells to those of the control for each protein. Legend: ***(p<0.001) highly significant, **(p<0.01) significant, * (p<0.05) poorly significant, ns non-significant.*

4.3.1.1 Haemoxygenase proteins and heat shock proteins

In HT-29 control cells, the cytoprotective proteins haemoxygenase-1 (HO-1) and haem oxygenase-2 (HO--2) showed a moderate expression, with HO-1 being higher than HO-2. Both platinum complexes; [Pt(dmp)(L^1-κ*O,S*)]Cl and [Pt(dmp)(L^3-κ*O,S*)]Cl significantly increased the expression of HO-1 by 78.4% (p<0.001) and 88.3 (p<0.001) respectively, whereas cisplatin poorly increased its expression by 15.2% (p<0.05) (*Table 4.5*). Changes in the expression level of HO-2/HMOX2 by both platinum complexes were non-significant. In contrast, cisplatin caused a significant increase of 68.1% (p<0.001) in the expression of HO-2 (*Table 4.5*).

The anti-apoptotic heat shock proteins; HSP27, HSP60 and HSP70 were highly expressed in HT-29 control cells. The complex [Pt(dmp)(L^1-κ*O,S*)]Cl significantly decreased HSP70 expression by 22.0% (p<0.001) in HT-29 cells (*Table 4.5*). No meaningful changes were observed in the expression level of HSP27 and HSP60 after treatment with platinum complexes and cisplatin.

4.3.1.2 The expression of Bcl-2 family proteins and cytochrome c

Expression of four members of the Bcl-2 family of proteins were determined, Bad and Bax are pro-apoptotic proteins, whilst Bcl-2 and Bcl-x were anti-apoptotic proteins. All four proteins were moderately expressed in HT-29 control cells. The complex; [Pt(dmp)(L^3-κ*O,S*)]Cl and cisplatin decreased the expression of Bad by 19.6 (p<0.001) and 26.9 (p<0.001) respectively, whereas [Pt(dmp)(L^1-κ*O,S*)]Cl caused no meaningful change in its expression level (*Table 4.5*). There were no significant changes in the expression of the pro-apoptotic protein Bax (*Table 4.5).*

The expression level of Bcl-2 was low in HT-29 cells and not significantly affected by the complexes and cisplatin. [Pt(dmp)(L^1-κ*O,S*)]Cl decreased Bcl-x expression by 21.7% (p<0.001) whilst cisplatin decreased its expression by 34.7% (p<0.001).Complex [Pt(dmp)(L^3-κ*O,S*)]Cl caused no meaningful change in the expression level of neither Bcl-2 nor Bcl-x proteins.

4.3.1.3 The expression of procaspase-3 and cleaved caspase-3

Active caspase-3 plays a crucial role as one of the executioner caspases in the final stages of triggering apoptosis through both the intrinsic and extrinsic pathways (Sagar *et al.*, 2010). The inactive procaspase-3 was highly expressed in HT-29 control cells, while cleaved caspase-3 levels were low (*Table 4.5*). Both [Pt(dmp)(L^1-κ*O,S*)]Cl, [Pt(dmp)(L^3-κ*O,S*)]Cl and cisplatin caused no significant changes in the expression of procaspase-3 as shown in *Table 4.5*. [Pt(dmp)(L^1-κ*O,S*)]Cl increased the expression of cleaved caspase-3 by 19.4% whereas cisplatin decreased its the expression of by 28.5% (p<0.05).

4.3.1.4 The expression of death receptor proteins

The death receptor proteins, tumour necrosis factor receptor 1 (TNF RI/TNFRSF1A), Fas-associated death domain (FADD), Fas, TRAIL-R1 and TRAIL-R2 were included in the array. TNF R1 was moderately expressed in HT-29 untreated control cells (*Figure 4.2*, *Table 4.5*) and complex [Pt(dmp)(L^1-κ*O,S*)]Cl decreased its expression level by 19.4% (p<0.01) while [Pt(dmp)(L^3-κ*O,S*)]Cl and cisplatin showed no meaningful changes (*Table 4.5*).

FADD was highly expressed in HT-29 untreated control cells (*Figure 4.2*, *Table 4.5*) with no-meaningful changes observed for the various treatments. Fas/TNFRSF6/CD95 was moderately expressed in untreated control cells (*Figure 4.2, Table 4.5*) and not affected by the platinum complexes whilst cisplatin increased Fas expression by 23.1% (p<0.001).

TRAIL R1/DR4 and TRAIL R2/DR5 are transmembrane proteins that trigger apoptosis by facilitating the activation of pro-caspase-8. Both TRAIL R1/DR4 and TRAIL R2/DR5 were moderately expressed in HT-29 control cells (*Table 4.5*) and none of the treatments caused a meaningful change in the expression of TRAIL R1 (*Table 4.6*).

In contrast, platinum complexes caused a significant increase in the expression of TRAIL-R2 relative to the untreated control cells and cisplatin. The complex [Pt(dmp)(L^1-κ*O,S*)]Cl increased its expression by 23.5% (p<0.001) whereas

[Pt(dmp)(L^3-κ*O,S*)]Cl showed an increase of 52.7% (p<0.001) relative to the control (*Table 4.5*). Cisplatin caused a smaller increase of 15.4% (p<0.001) in comparison to the two complexes (*Table 4.5*).

4.3.1.5 The expression of tumour suppressor protein p53 and cell cycle proteins; $p21^{Cip1}$, $p27^{Kip1}$, phospho-Rad17 and claspin

The proteome array included phosphorylated forms of the tumour suppressor protein p53 at various serine residues; phospho-p53 (S15), phospho-p53 (S46) and phospho-p53 (S392). All three proteins were highly expressed in HT-29 control cells (*Table 4.6*). Neither of the two platinum complexes and cisplatin caused meaningful changes in the expression level of phospho-p53 (S15), phospho-p53 (S46) and (S392) respectively (*Table 4.5*).

The cell cycle regulatory proteins that inhibit cyclin dependent kinases, $p21^{Cip1/CDKN1A}$ and $p27^{Kip1}$ were poorly expressed in control cells (*Figure 4.2*). Whilst no meaningful changes were observed in the expression of p27, the two complexes [Pt(dmp)(L^1-κ*O,S*)]Cl and [Pt(dmp)(L^3-κ*O,S*)]Cl increased the expression level of p21 protein by 25.2% *(*p<0.01), and 23.9% (p<0.01). Cisplatin caused no significant change in p21 expression. The array results confirm the immunofluorescence data.

The phospho-Rad 17 protein was moderately expressed in HT-29 control cells. Treatment with [Pt(dmp)(L^1-κ*O,S*)]Cl decreased the expression of phospho-Rad17 by 18.4% (p<0.001) and [Pt(dmp)(L^3-κ*O,S*)]Cl decreased its expression by 8% (p<0.05) (*Figure 4.5*). These changes were considered not meaningful. In contrast, cisplatin significantly increased the expression of phospho-Rad 17 by 53.6% (p<0.001) (*Figure 4.5, Table 4.5*).

Both [Pt(dmp)(L^1-κ*O,S*)]Cl and [Pt(dmp)(L^3-κ*O,S*)]Cl caused a significant decrease in the expression of claspin, with decreases of 46.1% (p<0.001) and 49.0% (p<0.001) respectively. In contrast, cisplatin significantly increased the expression level of claspin by 40.7% (p<0.001) in HT-29 cells.

4.3.1.6 The expression of inhibitors of apoptosis (IAPs)

The IAPs included the X-linked inhibitor of apoptosis protein (XIAP), cIAP-1, cIAP-2, survivin and livin. XIAP was moderately expressed in the HT-29 control cells (*Figure 4.2*). Although not deemed to be meaningful, the complex; [Pt(dmp)(L^1-κ*O,S*)]Cl decreased XIAP expression by 18.6% whereas [Pt(dmp)(L^3-κ*O,S*)]Cl caused an increase of 15.8% ($p<0.05$) in expression (*Table 4.5*) . Cisplatin caused no meaningful change in the expression of XIAP.

The cIAP-1 protein was moderately expressed in the untreated control cells. The complex, [Pt(dmp)(L^1-κ*O,S*)]Cl caused no meaningful change in cIAP-1 expression whilst [Pt(dmp)(L^3-κ*O,S*)]Cl and cisplatin increased the expression level of cIAP-1 protein by 22.7% and 23.7% respectively. Similar to cIAP-1, cIAP-2 was moderately expressed in HT-29 control cells (*Figure 4.2, Table 4.5)*. [Pt(dmp)(L^1-κ*O,S*)]Cl did not cause any meaningful change in cIAP-2 expression whereas the complex [Pt(dmp)(L^3-κ*O,S*)]Cl increased cIAP-2 expression by 21.4% ($p<0.01$) whilst cisplatin only decreased its expression by 16.2% ($p<0.05$).

Survivin is also an inhibitor of apoptosis that was moderately expressed in control cells. Both platinum complexes; [Pt(dmp)(L^1-κ*O,S*)]Cl and [Pt(dmp)(L^3-κ*O,S*)]Cl significantly decreased the expression level of survivin in HT-29 cells by 33.0% ($p<0.001$) 34.0% and 30.4% ($p<0.001$) respectively (*Table 4.5*).

Livin was poorly expressed in HT-29 control cells, thus the small changes in the expression of this protein were considered not to be meaningful.

4.3.1.7 The expression of Smac/DIABLO and HTRA2/Omi proteins

Smac/DIABLO and HTRA2/Omi are pro-apoptotic proteins that inhibit the activity of IAPs, preventing them from inhibiting apoptosis. Both Smac/DIABLO and HTRA2/Omi were highly expressed in HT-29 control cells. The percentage changes observed in the expression of Smac/DIABLO and HTRA2/omi in response to platinum complexes were considered not to be meaningful.

4.3.2 Apoptosis-associated proteins in A549 cells

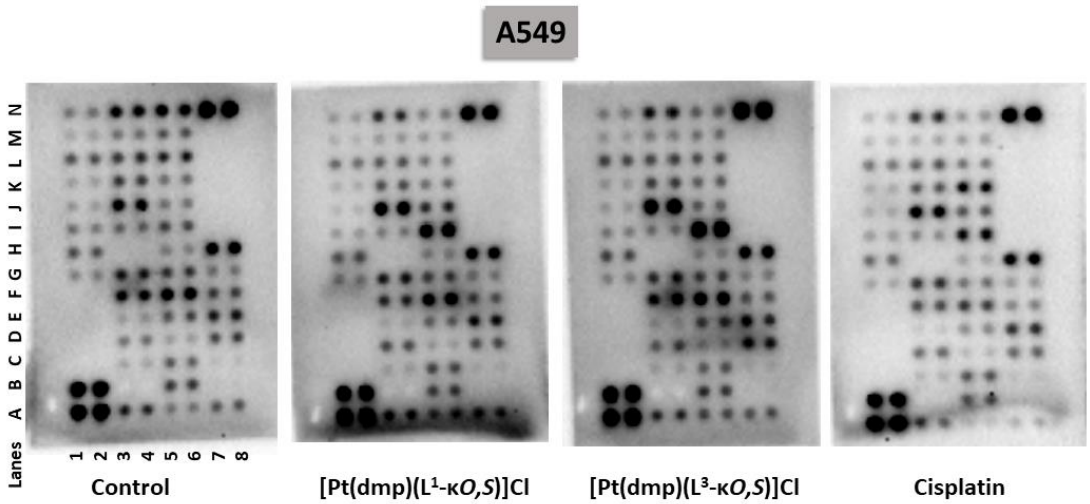


Figure 4.3 Chemiluminescent signals of the apoptosis array membranes (RayBiotech) showing the effect of the platinum complexes and cisplatin in A549 cells*. Each membrane array was incubated with 400 ug protein.* Cells were treated with 2 µM of [Pt(dmp)(L^1-κ*O,S*]Cl, 2.5 µM of [Pt(dmp)(L^3-κ*O,S*)]Cl and 25 µM cisplatin *for 18 hours. . Chemiluminescence was detected with the BIO-RAD ChemiDoc MP Imager.*

***Table 4.6**: The expression level of apoptotic proteins in A549 cells and the percentage change caused by treatment with concentration equivalent IC_{80} values of [Pt(dmp)(L^1-κO,S)]Cl, [Pt(dmp)(L^3-κO,S)]Cl and cisplatin for 18 hours. The data is reported as percentage change measured relative to the untreated control cells.*

Apoptotic protein	Baseline expression Level	[Pt(dmp)(L^1-κO,S)]Cl		[Pt(dmp)(L^3-κO,S)]Cl		Cisplatin	
		Change (%)	sign	Change (%)	sign	Change (%)	sign
Bad	Low	-1.4	ns	-35.5	*	-40.7	**
Bax	Moderate	+10.0	ns	-4.7	ns	+2.9	ns
Bcl-2	Low	-33.9	**	-10.0	ns	-29.7	**
BID	Low	-37.6	***	-32.8	***	-21.2	*
BIM	Moderate	-29.1	**	+12.3	ns	-21.3	*
Caspase-3	Low	-37.6	*	+1.4	ns	-17.3	ns
Caspase-8	Low	-30.0	**	-9.1.	ns	-38.9	***
Cytochrome c	Moderate	+20.7	ns	+10.7	ns	+27.3	ns
XIAP	High	0.9	ns	+10.9	*	0.0	ns
cIAP-2	Low	-45.8	***	-36.3	***	-26.3	***
Survivin	Moderate L	-62.9	***	-35.5	***	-40.9	***
Livin	Low	+66.1	***	-142.3	***	-19.6	*
Smac/DIABLO	Moderate	-45.2	***	-23.9	***	-41.6	***
HTRA2/Omi	Moderate	-12.9	*	-17.3	*	-21.7	***
HSP27	Moderate	-30.1	*	+5.8	ns	-40.3	**
HSP60	High	-39.7	***	-63.8	***	+4.3	ns
HSP70	Moderate h	-22.1	***	-15.1	***	-35.4	***
CD40	Moderate	-21.0	***	+7.2	***	nd-	nd-
Fas	High	-40.5	*	+42.9	*	-39.7	*
Fas Ligand	Moderate	-50.6	***	-16.1	ns	-29.8	*
TNF R1	Moderate	-72.4	***	-62.3	***	-71.1	***
TNF R2	Moderate	-37.7	***	+2.8	ns	nd	nd
TRAIL R1	Moderate	-5.1	ns	+48.7	**	+13.6	ns
TRAIL R2	Moderate	+15.6	ns	+47.8	**	+44.1	**
TRAIL R3	Moderate	+26.6	*	-6.1	ns	-25.6	ns
TRAIL R4	Moderate	-3.2	ns	-38.8	**	-11.8	ns
p53	Moderate	-19.9	**	+2.8	ns	+89.9	***
p21/CIP1/CDKN1A	High	+189.1	***	+282.6	***	+52.5	***
p27/Kip1	Moderate	+80.7	***	+51.6	***	+35.1	**
IGF 1	Low	-46.7	***	-23.5	***	-37.8	***
IGF 2	Mod high	-25.2	***	-22.7	***	-7.3	*
IGFBP-1	Low	+26.0	***	+84.6	***	nd	nd
IGFBP-2	Moderate	-26.0	**	-2.0	ns	-2.0	ns
IGFBP-3	Moderate	-14.8	**	-27.9	***	+23.0	***
IGFBP-4	Low	-35.1	ns	+133.8	***	-26.7	ns
IGFBP-5	Moderate	-3.7	ns	+68.4	**	+3.3	ns
IGFBP-6	High	+28.2	**	+38.3	***	-40.7	***
IGF-1 R	Mod high	-10.4	ns	-5.8	ns	-34.6	***

Note: The positive (+) sign indicates an increase in protein expression, whilst the negative (-) sign indicates a decrease. nd: not detected. The data was statistically analysed using one-way ANOVA (non-parametric),

*followed by Dunnett's Multiple Comparison test) which compared the pixel density of experimental means to those of the control for each protein. Legend: ***(p<0.001) highly significant, **(p<0.01) significant, * (p<0.05) poorly significant, ns non-significant.*

4.3.2.1 The expression of Bcl-2 family proteins

Members of the Bcl-2 protein family evaluated in this proteome array, included the pro-apoptotic Bad, Bax, BID, BIM and anti-apoptotic members Bcl-2 and Bcl-w. The baseline expression of Bcl-w was too low and changes could not be quantified accurately. The pro-apoptotic Bad and BID were poorly expressed in A549 control cells while Bax and BIM were moderately expressed in A549 control cells (*Figure 4.3; Table 4.6*). The complex [Pt(dmp)(L^1-κ*O,S*)]Cl caused non-significant changes in the expression of Bad relative to the control whereas [Pt(dmp)(L^3-κ*O,S*)]Cl and cisplatin further suppressed the expression of Bad by 35.5% (p<0.05) and 40.7 (p<0.01) respectively (*Table 4.6*). No meaningful changes were observed in the expression of Bax (*Table 4.6*).

BID and BIM directly activate Bax/Bak. BID was poorly expressed in A549 control cells while BIM was moderately expressed in A549 control cells. Both platinum complexes [Pt(dmp)(L^1-κ*O,S*)]Cl, [Pt(dmp)(L^3-κ*O,S*)]Cl and cisplatin decreased the expression of BID by 37.6%, 32.8% (p<0.001) and 21.2% (p<0.05) respectively (*Table 4.6*). [Pt(dmp)(L^1-κ*O,S*)]Cl and cisplatin decreased the expression of BIM by 29.1% (p<0.01) and 21.3% (p<0.01) respectively, whilst the other complex, [Pt(dmp)(L^3-κ*O,S*)]Cl did not cause any meaningful change in the expression BIM (*Table 4.6*).

Expression of anti-apoptotic Bcl-2 was low in control cells. [Pt(dmp)(L^1-κ*O,S*)]Cl and cisplatin caused a significant decrease in the expression of anti-apoptotic Bcl-2 by 33.9% (p<0.01) and 29.7% (p<0.01) respectively, whilst [Pt(dmp)(L^3-κ*O,S*)]Cl caused no meaningful change in Bcl-2 expression (*Table 4.6*). The proteins with a low baseline expression on the A549 cells (Bad, BIM, Bcl-2) were considered to have not played a major role in the apoptotic cell death of this cell line.

4.3.2.2 The expression of caspase-3 and caspase-8

The array indicated that caspase-3 and caspase-8 were poorly expressed in A549 control cells (*Figure 4.2*). Treatment with [Pt(dmp)(L^1-κ*O,S*)]Cl decreased caspase-3 expression by 37.6% ($p<0.05$) whereas [Pt(dmp)(L^3-κ*O,S*)]Cl and cisplatin caused no significant changes in its expression (*Table 4.6*). The expression of caspase-8 was decreased by [Pt(dmp)(L^1-κ*O,S*)]Cl and cisplatin at 30% ($p<0.01$) and 38.9% ($p<0.001$) respectively (*Table 4.6*). [Pt(dmp)(L^3-κ*O,S*)]Cl did not cause any significant changes in the expression level of caspase-8 (*Table 4.6*).

4.3.2.3 The expression of death receptor proteins

Baseline expression of death receptor proteins; TNF R1 and TNF R2 were moderate in untreated control cells. The effect of platinum complexes [Pt(dmp)(L^1-κ*O,S*)]Cl, [Pt(dmp)(L^3-κ*O,S*)]Cl and cisplatin resulted in a significant decrease of TNF R1 expression by 72.4% ($p<0.001$), 62.3% ($p<0.001$) and 71.1% respectively. [Pt(dmp)(L^1-κ*O,S*)]Cl significantly decreased the expression of TNF R2 by 37.7% ($p<0.001$) whilst [Pt(dmp)(L^3-κ*O,S*)]Cl caused no significant change. The effect of cisplatin on the expression of TNF R2 could not be quantified accurately.

TRAIL R1, TRAIL R2, TRAIL R3 and TRAIL R4 were moderately expressed in the untreated A549 control cells. [Pt(dmp)(L^1-κ*O,S*)]Cl and cisplatin caused non-significant changes in the expression of TRAIL R1,but [Pt(dmp)(L^3-κ*O,S*)]Cl increased TRAIL R1 expression by 48.7% ($p<0.01$). [Pt(dmp)(L^3-κ*O,S*)]Cl and cisplatin increased TRAIL R2 expression by 47.8% ($p<0.01$) and 44.1% ($p<0.01$) respectively. The expression of TRAIL-R3 was increased by 26.6% ($p<0.05$) by the complex [Pt(dmp)(L^1-κ*O,S*)]Cl. [Pt(dmp)(L^3-κ*O,S*)]Cl decreased the expression of TRAIL-R4 by 38.3% ($p<0.01$). Beyond these effects, no meaningful changes were observed in the expression of TRAIL R3 and TRAIL R4.

The moderately expressed of Fas ligand was decreased by platinum complexes [Pt(dmp)(L^1-κ*O,S*)]Cl and cisplatin by 50.6% ($p<0.001$) and 29.8 ($p<0.05$) respectively (*Table 4.6*). Fas protein was highly expressed in A549 control cells, [Pt(dmp)(L^1-κ*O,S*)]Cl and cisplatin decreased the expression of Fas by 40.5% and

39.7% (p<0.05) whereas [Pt(dmp)(L^3-κ*O,S*)]Cl increased its expression by 42.9% (p<0.05) (*Table 4.6*).

The protein CD40 was moderately expressed in A549 control cells. [Pt(dmp)(L^1-κ*O,S*)]Cl significantly decreased the expression of CD40 by 21% (p<0.001) while a 7.2% increase caused by [Pt(dmp)(L^1-κ*O,S*)]Cl was considered to be insignificant (*Table 4.6*).

4.3.2.4 The expression of p53, p21 and p27

p53 was moderately expressed in A549 control cells. The complex, [Pt(dmp)(L^1-κ*O,S*)]Cl decreased the expression of p53 by 19.9% (p<0.01) while [Pt(dmp)(L^3-κ*O,S*)]Cl did not cause any significant change in its expression. In contrast, cisplatin significantly increased the expression of p53 by 89.9% (p<0.001) (*Table 4.6*).

The cyclin dependent kinase inhibitor and DNA damage response protein, p21 was highly expressed in A549 control cells. Platinum complexes; [Pt(dmp)(L^1-κ*O,S*)]Cl significantly increased the expression of p21 protein by 189.1% (p<0.001) with [Pt(dmp)(L^3-κ*O,S*)]Cl causing an increase of 282.6% (p<0.001) respectively. Cisplatin caused a smaller increase in the expression of p21 (52.5% (p<0.001) compared to the two platinum complexes investigated (*Table 4.6*).

The tumour suppressor protein p27 was moderately expressed in A549 control cells. Both platinum complexes; [Pt(dmp)(L^1-κ*O,S*)]Cl and [Pt(dmp)(L^3-κ*O,S*)]Cl increased p27 expression by 80.7% (p<0.001) and 51.6% (p<0.001) respectively. Cisplatin caused the least increase of 35.1 (p<0.001) when compared to the two platinum complexes, similar to p21 protein.

4.3.2.5 The expression of heat shock proteins

Heat shock proteins; HSP27 and HSP70 were moderately expressed in A549 control cells whilst HSP60 was highly expressed (*Figure 4.3*; *Table 4.6*). The complex, [Pt(dmp)(L^1-κ*O,S*)]Cl and cisplatin decreased HSP27 expression by 30.1% (p<0.05) and 40.3% (p<0.01) respectively, whilst [Pt(dmp)(L^3-κ*O,S*)]Cl caused no meaningful change in the expression of HSP27 (*Table 4.6*). [Pt(dmp)(L^1-

κ*O,S*)]Cl and [Pt(dmp)(L^3-κ*O,S*)]Cl significantly increased the expression of HSP60 by 39.7% (p<0.001) and 63.8% (p<0.001) respectively while cisplatin caused no meaningful changes (*Table 4.6*). Both platinum complexes [Pt(dmp)(L^1-κ*O,S*)]Cl, [Pt(dmp)(L^3-κ*O,S*)]Cl and cisplatin were able to significantly decrease the expression of HSP70 by 22.1% (p<0.001), 15.1% (p<0.001) and 35.4% (p<0.001) respectively (*Table 4.6*).

4.3.2.6 The expression of IAPs)

The IAPs evaluated in this proteome array included XIAP, cIAP-1, survivin and livin. XIAP was highly expressed in A549 control cell. No significant changes were observed in the expression of XIAP after treatment with platinum complexes and cisplatin (*Table 4.6*).

cIAP-2 and livin were poorly expressed in control cells while survivin was moderately expressed (*Figure 4.6*). The complexes [Pt(dmp)(L^1-κ*O,S*)]Cl, [Pt(dmp)(L^3-κ*O,S*)]Cl and cisplatin were able to significantly decrease the expression of cIAP-2 by 45.8%, 36.3% and 26.3% (p<0.001) as well as survivin by 62.9%, 35.5% and 40.9% (p<0.001) respectively (*Table 4.6*). The expression of livin was decreased by [Pt(dmp)(L^3-κ*O,S*)]Cl and cisplatin while [Pt(dmp)(L^1-κ*O,S*)]Cl increased its expression by 66.1% (p<0.001). A significant decrease in the expression of these IAPs by both platinum complexes was indicative of their ability to supress IAPs function, thus promoting apoptosis induction in A549 cells.

4.3.2.7 The expression of Smac/DIABLO and HTRA2/omi

The pro-apoptotic Smac/DIABLO and HTRA2/omi were moderately expressed in A549 control cells (*Table 4*.6). Both platinum complexes and cisplatin caused a significant decrease in their expression level in A549 cells. The complexes, [Pt(dmp)(L^1-κ*O,S*)]Cl and [Pt(dmp)(L^3 -κ*O,S*)]Cl decreased the expression of Smac/DIABLO by 45.2% (p<0.001) and 23.9% (p<0.001) in A549 respectively. Cisplatin also decreased the expression of Smac/DIABLO by 41.6% (p<0.001) in A549 cells. The effect of platinum complexes on HTRA2/omi were considered not

meaningful (>20%), however, cisplatin decreased its expression by 21.7% (p<0.01).

4.3.2.8 The expression of IGFs and IGFBPs

The Insulin-like Growth Factors 1 (IGF 1) was poorly expressed in A549 control cells whereas IGF 2 was highly expressed (*Table 4.6*). Platinum complexes and cisplatin caused a significant decrease in the expression level of both proteins relative to the untreated control cells. [Pt(dmp)(L^1-κ*O,S*)]Cl and [Pt(dmp)(L^3-κ*O,S*)]Cl decreased IGF 1 expression by 46.7% and 23.5% (p<0.001) as well as IGF-2 by 25.2% and 22.7% (p<0.001) respectively. Cisplatin–decreased the expression level of IGF-1 by 37.8% (p<0.001) and did not induce a meaningful change in IGF-2 expression (*Table 4.6*).

The effect of platinum complexes and cisplatin on the expression of six Insulin-like growth factor binding proteins (IGFBP 1- 6) varied. These proteins are pro-apoptotic since they prevent IGFs from exerting their pro-survival effects on cancer cells. Thus, the ability of platinum complexes to increase the expression of IGFBP proteins is considered to aid the inhibition of cell proliferation.

IGFBP-1 expression was low in the untreated control cells (*Table 4.6*). Platinum complexes were able to cause a significant increase the expression level of IGFBP-1 with [Pt(dmp)(L^3-κ*O,S*)]Cl showing the highest increase of 84.6% (p<0.001) and [Pt(dmp)(L^1-κ*O,S*)]Cl only increasing it by 26% (p<0.001).

[Pt(dmp)(L^3-κ*O,S*)]Cl significantly decreased IGFBP-3 expression by 27.9% (p<0.001). In contrast, cisplatin increased the expression of IGFBP-3 by 23.0% (p<0.001). The expression of IGFBP-4 showed no significant changes except for an increase induced by [Pt(dmp)(L^3-κ*O,S*)]Cl, elevating its expression by 133%. The complex, [Pt(dmp)(L^3-κ*O,S*)]Cl increased IGFBP-5 expression by 68.4% (p<0.01). IGFBP-6 was highly expressed in A549 control cells. Both platinum complexes, [Pt(dmp)(L^1-κ*O,S*)]Cl and [Pt(dmp)(L^3-κ*O,S*)]Cl significantly increased the expression of IGFBP-6 by 28.2% (p<0.01) and 38.3% (p<0.001)

respectively. Cisplatin had an opposite effect where it significantly decreased IGFBP-6 expression by 40.7% (p<0.001).

Insulin-like growth factor 1 receptor (IGF 1R), a transmembrane receptor located on the cell surface is activated when IGF-1 binds to it. The two platinum complexes [Pt(dmp)(L^1-κ*O,S*)]Cl and [Pt(dmp)(L^3-κ*O,S*)]Cl, did not show any significant effect on the expression of IGF1R, however, cisplatin significantly decreased its expression by 34.6% (p<0.001), consistent with the observed decrease in IGF-1 expression

The activation of IGF 1R triggers a cascade of signalling pathways that regulate cell growth, proliferation, differentiation, and survival. Thus, a decrease in the expression of IGF 1R by cisplatin, as well as IGF-1 and IGF-2 decrease by platinum complexes, promotes cell death rather than cell survival in A549 cell lines.

4.3.3 Apoptosis-associated proteins in H1975 cells

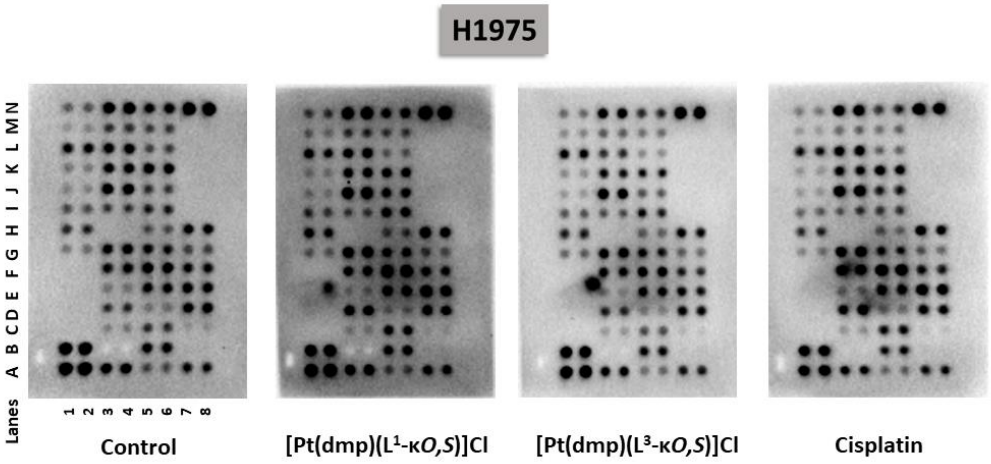


***Figure 4.4**: **Chemiluminescent signals of the apoptosis array membranes (RayBiotech) showing the effect of the platinum complexes and cisplatin in H1975 cells**. Each membrane array was incubated with 400 ug protein.* Cells were treated with 3 µM [Pt(dmp)(L^1-κ*O,S*]Cl, 2.6 µM [Pt(dmp)(L^3-κ*O,S*]Cl and 30 µM cisplatin *for 18 hours. Chemiluminescence was detected with the BIO-RAD ChemiDoc MP Imager.*

***Table 4.7**: The expression level of apoptotic proteins in H1975 cells and the percentage change caused by treatment with concentration equivalent IC_{80} values of [Pt(dmp)(L^1-κO,S)]Cl, [Pt(dmp)(L^3-κO,S)]Cl and cisplatin for 18 hours.* *The data is reported as percentage change measured relative to the untreated control cells.*

Apoptotic protein	Baseline expression Level	[Pt(dmp)(L^1-κ*O,S*)]Cl		[Pt(dmp)(L^3-κ*O,S*)]Cl		Cisplatin	
		Change (%)	sign	Change (%)	sign	Change (%)	sign
Bad	Low	+20.4	***	-20.8	***	-17.5	***
Bax	Low	+55.5	***	-1.5	ns	-12.7	***
Bcl-2	Low	+34.6	***	-31.9	***	-12.1	***
BID	Low	+8.6	ns	-12.8	ns	-28.1	**
BIM	Moderate	-29.6	**	-29.7	**	-27.6	**
Caspase-3	Very low	+11.4	ns	+15.3	ns	-19.0	ns
Caspase-8	Moderate	+28.3	***	-31.9	***	-26.6	***
Cytochrome c	Moderate	+23.0	*	-2.3	ns	+34.7	**
XIAP	Mod High	+31.6	***	-30.3	***	-11.5	**
cIAP-2	Moderate	-4.3	ns	-14.4	**	-26.2	***
Survivin	Moderate	-17.0	**	-30.6	***	-28.1	***
Livin	Moderate	+65.7	***	-2.3	ns	+6.4	ns
Smac/DIABLO	Moderate	-52.3	***	-61.1	***	-36.6	**
HTRA2/Omi	Mod High	-41.2	***	-44.2	***	-19.9	***
HSP27	Moderate	+8.0	ns	-23.6	**	+8.7	ns
HSP60	Mod High	+34.8	***	-9.0	**	+7.6	**
HSP70	Moderate	-4.6	*	-28.6	***	-14.7	***
CD40	Mod High	+35.2	***	-34.2	***	-33.0	***
Fas	Mod High	+21.1	***	+0.8	ns	+27.8	***
Fas Ligand	Mod High	+20.4	***	-17.5	***	-0.2	ns
TNF R1	Mod High	+16.5	***	-31.2	***	-25.0	***
TNF R2	Moderate	+35.3	**	-31.4	**	-24.5	*
TRAIL R1	Mod High	+31.3	***	-21.7	***	-13.9	**
TRAIL R2	Mod High	+46.9	***	-31.7	***	+3.1	ns
TRAIL R3	Mod High	+29.6	***	-29.6	***	-24.8	***
TRAIL R4	Moderate	+29.5	***	-20.7	***	-16.9	***
p53	Mod High	+2.3	ns	-40.6	***	-16.6	***
$p21^{CIP1/CDKN1A}$	Moderate	+38.9	***	-26.9	***	-13.0	**
p27/Kip1	Moderate	+14.4	**	-17.4	**	+0.5	ns
IGF 1	Low	-12.0	*	-20.3	***	-28.6	***
IGF 2	Mod High	+20.3	***	-32.6	***	-14.0	***
IGFBP-1	Moderate	+40.6	***	-34.2	***	-18.5	**
IGFBP-2	Mod High	-8.3	***	-37.5	***	-31.1	***
IGFBP-3	Moderate	+23.4	***	-17.9	***	+1.1	ns
IGFBP-4	Moderate	+34.6	***	-20.0	**	+6.2	ns
IGFBP-5	Mod high	+37.9	***	-4.9	ns	+29.3	***
IGFBP-6	Mod high	+43.7	***	-20.5	***	+10.1	***
IGF-1 R	Mod high	+4.3	**	-21.0	***	-18.9	**

4.3.3.1 The expression of Bcl-2 family proteins and cytochrome c

The baseline expression level of pro-apoptotic Bad, Bax and BID were low in H1975 cells (*Figure 4.4, Table 4.7*). [Pt(dmp)(L^1-κ*O,S*)]Cl increased the expression of Bad by 20.4% and Bax by 55.5% ($p<0.001$) while [Pt(dmp)(L^3-κ*O,S*)]Cl decreased the expression of Bad by 20.8% ($p<0.001$). Both platinum complexes and cisplatin supressed the expression of BIM by 29.6%, 29.7% and 27.6% ($p<0.01$) respectively. Cisplatin did not cause any meaningful changes in the expression of Bad and Bax in this cell line, indicating the superior effect of [Pt(dmp)(L^1-κ*O,S*)]Cl. BIM was moderately expressed in H1975 control cells. [Pt(dmp)(L^1-κ*O,S*)]Cl, [Pt(dmp)(L^3-κ*O,S*)]Cl and cisplatin decreased the expression of BIM by 29.6% , 29.7%, 27.6% ($p<0.01$) respectively.

The anti-apoptotic Bcl-2 protein was significantly suppressed by [Pt(dmp)(L^3-κ*O,S*)]Cl (31.9%) while [Pt(dmp)(L^1-κ*O,S*)]Cl increased its expression by 34.6% with cisplatin causing non-meaningful changes.

Cytochrome c was moderately expressed in H1975 control cells and the complex, [Pt(dmp)(L^1-κ*O,S*)]Cl and cisplatin increased its expression by 23% and 34.7% ($p<0.001$) respectively.

4.3.3.2 The expression of caspase-3 and caspase-8

The baseline expression level of caspase-3 was very low in H1975 cells and both platinum complexes and cisplatin caused non-significant changes in its expression following treatment. Caspase-8 was moderately expressed in the H1975 control cells. [Pt(dmp)(L^1-κ*O,S*)]Cl increased the expression of caspase-8 by 28.3% ($p<0.001$) while [Pt(dmp)(L^1-κ*O,S*)]Cl and cisplatin decreased its expression by 31.9% and 26.6% ($p<0.001$) respectively.

4.3.3.3 The expression of death receptor proteins

The baseline expression level of CD40, Fas and Fas ligand were moderately high in H1975 cells. [Pt(dmp)(L^1-κ*O,S*)]Cl increased the expression of CD40 by 35.2% ($p<0.001$) while [Pt(dmp)(L^3-κ*O,S*)]Cl and cisplatin decreased its expression by

34.2% and 33% (p<0.001) respectively. The expression of Fas receptor was increased by [Pt(dmp)(L^1-κ*O,S*)]Cl and cisplatin (p<0.001) while [Pt(dmp)(L^3-κ*O,S*)]Cl did not cause any meaningful change. Only [Pt(dmp)(L^1-κ*O,S*)]Cl was able to increase the expression of Fas ligand.

The baseline expression of TNF R1 was moderate high while that of TNF R2 was moderate in H1975 cells. The complex [Pt(dmp)(L^3-κ*O,S*)]Cl and cisplatin decreased the expression of TNF R1 by 31.2% and 25% (p<0.001)and TNF R2 by 31.4% and 24.5% respectively. [Pt(dmp)(L^1-κ*O,S*)]Cl increased the expression of TNF R2 by 35.3%.

The baseline expression of TRAIL R1, TRAIL R2 and TRAIL R3 were moderately high while that of TRAIL R4 was moderate in H1975 cells. [Pt(dmp)(L^1-κ*O,S*)]Cl increased the expression of TRAIL R2 by 46.9% while [Pt(dmp)(L^3-κ*O,S*)]Cl decreased it by 31.7% (p<0.001). The complex, [Pt(dmp)(L^1-κ*O,S*)]Cl increased the expression of TRAIL R1, TRAIL R2, TRAIL R3, TRAIL R4 by 31.3%, 46.9%, 29.6% and 29.5% respectively while [Pt(dmp)(L^3-κ*O,S*)]Cl decreased their expression by 21.7%, 31.7%, 29.6% and 20.7% respectively. These findings suggest that the structural differences between the complexes result in opposing effects in H1975 cells.

4.3.3.4 The expression of p53, p21 and p27

In H1975 control cells, p53 showed a moderate baseline expression level (*Table 4.7*). However, [Pt(dmp)(L^3-κ*O,S*)]Cl reduced p53 expression by 40.6% (p<0.001), while [Pt(dmp)(L^1-κ*O,S*)]Cl and cisplatin did not elicit significant changes in p53 expression. The expression of p21 was significantly increased by [Pt(dmp)(L^1-κ*O,S*)]Cl, demonstrating a 38.9% increase (p<0.001), and no substantial changes were observed in the expression of p27.

4.3.3.5 The expression of HSPs

In H1975 control cells, the expression of HSP27 and HSP70 was moderate, whereas HSP60 showed a higher expression compared to both HSPs. The complex

[Pt(dmp)(L^3-κ*O,S*)]Cl was able to significantly decrease the expression of HSP27 and HSP70 while [Pt(dmp)(L^1-κ*O,S*)]Cl and cisplatin did not cause any meaningful changes in the expression of either of the two HSPs. [Pt(dmp)(L^1-κ*O,S*)]Cl increased HSP60 expression by 34.8% (p<0.001).

4.3.3.6 The expression of IAPs

The baseline expression level of XIAP was moderate high in H1975 cells while that of cIAP-2, survivin and livin was moderate (*Table 4.7*). XIAP expression was significantly suppressed by [Pt(dmp)(L^3-κ*O,S*)]Cl, decreasing it by 30.3% (p<0.001) while [Pt(dmp)(L^1-κ*O,S*)]Cl increased its expression by 31.6% (p<0.001). Neither platinum complex caused meaningful changes in cIAP-2 expression, whereas cisplatin suppressed its expression by 26.2%. Furthermore, both [Pt(dmp)(L^3-κ*O,S*)]Cl and cisplatin significantly decreased the expression of survivin by 30.6% and 28.1% (p<0.001), respectively.

4.3.3.7 The expression of Smac/DIABLO and HTRA2/omi

Smac/DIABLO and HTRA2/omi were moderately expressed in H1975 control cells (*Table 4.7*). Both platinum complexes and cisplatin suppressed the expression of Smac/DIABLO by 52.3%, 61.1% (p<0.001) and 36.6% (p<0.01) [Pt(dmp)(L^1-κ*O,S*)]Cl and [Pt(dmp)(L^3-κ*O,S*)]Cl decreased the expression of HTRA2/omi by 41.2% and 44.2% (p<0.001) in H1975 cells while cisplatin decreased it by 19.9%. The decrease in Smac/DIABLO and HTRA2/omi were much higher than those observed in A549 cells.

4.3.3.8 The expression of IGF and IGFBPs

The baseline expression level of IGF 1 was low in H1975 control cells while that of IGF 2 was moderate high (*Table 4.7*). [Pt(dmp)(L^3-κ*O,S*)]Cl and cisplatin were able to decrease the expression of IGF 1 by 20.3% and 28.6% (p<0.001) respectively. [Pt(dmp)(L^3-κ*O,S*)]Cl significantly decreased the expression of IGF 2

by 32.6% while [Pt(dmp)(L^1-κ*O,S*)]Cl increased its expression by 20.3%. Cisplatin did not cause any meaningful change in IGF 2 expression.

The baseline expression level of IGFBP-1, IGFBP-3 and IGFBP-4 was moderate in H1975 cells while that of IGFBP-2, IGFB-5 and IGFBP-6 was moderate high. The complex [Pt(dmp)(L^1-κ*O,S*)]Cl caused a significant increase in the expression of IGFBP-1, IGFBP-3, IGFBP -4, IGFBP-5 and IGFBP-6 while [Pt(dmp)(L^3-κ*O,S*)]Cl decreased IGFBP-1, IGFBP-2, IGFBP 4, and IGFBP-6 while causing no meaningful changes in the expression of IGFBP-5. [Pt(dmp)(L^1-κ*O,S*)]Cl and cisplatin increased the expression of IGFBP-5 by 37.9% and 29.3% respectively.

IGF-1 R was moderately expressed in the H1975 control cells, [Pt(dmp)(L^3-κ*O,S*)]Cl and cisplatin decreased its expression by 21% and 18.9% respectively. [Pt(dmp)(L^3-κ*O,S*)]Cl caused a non-meaningful change in IGF-1 R expression.

The differential expression of IGFBP proteins by [Pt(dmp)(L^1-κ*O,S*)]Cl and [Pt(dmp)(L^3-κ*O,S*)]Cl may be attributed to the structural differences, with [Pt(dmp)(L^1-κ*O,S*)]Cl being more susceptible to inhibit cancer cell survival by favouring the increase in IGFBP proteins.

4.4 Discussion

Following the evaluation of apoptotic cell death by platinum complexes in HT-29, A549 and H1975 cancer cells, the proteome array provided data on the expression levels of important apoptosis-associated regulatory proteins. The proteome array kits used for HT-29 and lung cancer cell lines (A549 and H1975) featured common apoptotic regulatory proteins categorized into pro-apoptotic proteins, anti-apoptotic proteins and cell cycle proteins (*Table 4.8*).

The common pro-apoptotic proteins between the two proteomic kits included two members of the Bcl-2 family (Bad, Bax), cytochrome c, caspase-3, death receptor proteins (TNF R1, Fas, TRAIL R1, TRAIL R2), Smac/DIABLO and HTRA2/OMI. The anti-apoptotic proteins included the inhibitors of apoptosis (XIAP, survivin and livin), heat shock proteins (HSP27, HSP60 and HSP70) as well as the Bcl-2 protein.

Common cell cycle proteins included the tumour suppressor proteins; p53, p27 and p21.

Table 4.8: A summary and comparison of the percentage change in expression of commonly evaluated apoptotic-regulatory proteins in HT-29, A549 and H1975 cell lines respectively.

Apoptotic protein / Baseline expression	**HT-29**	**A549**	**H1975**	**Comment(s)**
Pro-apoptotic proteins				
Bad	Moderate	Low	Moderate	Bad expression was decreased in HT-29 and A549 cells, but varied in H1975 cells
[Pt(dmp)(L^1-κO,S)]Cl	*-2.7*	*-1.4*	+20.4	
[Pt(dmp)(L^3-κO,S)]Cl	-19.6	-35.5	-20.8	
Cisplatin	-26.9	-40.7	-17.5	
Bax	Moderate	Moderate	Moderate	Bax expression was non-significantly affected in all three cell lines, PtL1 increased in H1975 cells
[Pt(dmp)(L^1-κO,S)]Cl	*+12.2*	*+10.0*	+55.5	
[Pt(dmp)(L^3-κO,S)]Cl	*+8.9*	*-4.7*	*-1.5*	
Cisplatin	*-7.8*	*+2.9*	-12.7	
Cytochrome c	Moderate	Moderate	Moderate	Cyc c expression was significantly increased in H1975 cells
[Pt(dmp)(L^1-κO,S)]Cl	-14.3	*+20.7*	+23.0	
[Pt(dmp)(L^3-κO,S)]Cl	+15.4	*+10.7*	*-2.3*	
Cisplatin	-14.2	*+27.3*	+34.7	
Caspase-3	Low	Low	Low	HT-29 data presents expression of cleaved caspase-3
[Pt(dmp)(L^1-κO,S)]Cl	+19.4	-37.6	*+11.4*	
[Pt(dmp)(L^3-κO,S)]Cl	*-3.6*	*+1.4*	*+15.3*	
Cisplatin	-28.5	*-17.3*	*-19.0*	
TNF R1	Moderate	Moderate	Mod high	TNF R1 was significantly supressed in A549 cells
[Pt(dmp)(L^1-κO,S)]Cl	-19.4	-72.4	+16.5	
[Pt(dmp)(L^3-κO,S)]Cl	*-2.7*	-62.3	-31.2	
Cisplatin	*-2.8*	-71.1	-25.0	
Fas	Moderate	High	Mod high	Fas expression varied across the three cell lines, increased in H1975 cells
[Pt(dmp)(L^1-κO,S)]Cl	*-12.9*	-40.5	+21.1	
[Pt(dmp)(L^3-κO,S)]Cl	*+1.8*	+42.9	*+0.8*	
Cisplatin	+23.1	-39.7	+27.8	
TRAIL R1	Moderate	Moderate	Mod high	TRAIL R1 expression was in differentially expressed by two different complexes in A549 and H1975
[Pt(dmp)(L^1-κO,S)]Cl	-9.6	*-5.1*	+31.3	
[Pt(dmp)(L^3-κO,S)]Cl	-9.3	+48.7	-21.7	
Cisplatin	+13.3	*+13.6*	-13.9	
TRAIL R2	Moderate	Moderate	Mod high	TRAIL R2 was significantly increased in HT-29 cells
[Pt(dmp)(L^1-κO,S)]Cl	+23.5	*-15.6*	+46.9	
[Pt(dmp)(L^3-κO,S)]Cl	+52.7	+47.8	-31.7	

Cisplatin	+15.4	*+44.1*	+3.1	
Smac/DIABLO	High	Moderate	Moderate	Smac expression was suppressed across the three cancer cell lines
[Pt(dmp)(L^1-κO,S)]Cl	-12.8	-45.2	-52.3	
[Pt(dmp)(L^3-κO,S)]Cl	-14.7	-23.9	-61.1	
Cisplatin	*+1.5*	-41.6	-36.6	
HTRA2/omi	High	Moderate	Mod High	HTRA2/Omi expression was not meaningful in HT-29 cells but suppressed in H1975 and A549 cells
[Pt(dmp)(L^1-κO,S)]Cl	-13.0	*-12.9*	-41.2	
[Pt(dmp)(L^3-κO,S)]Cl	*-1.0*	-17.3	-44.2	
Cisplatin	*-0.2*	-21.7	-19.9	
Anti-apoptotic proteins				
Bcl-2	Moderate	Low	Moderate	Bcl-2 expression was non-significant in HT-29 cells, suppressed in A549 and varied in H1975 cells
[Pt(dmp)(L^1-κO,S)]Cl	*-13.0*	-33.9	+34.6	
[Pt(dmp)(L^3-κO,S)]Cl	*-6.4*	*-10.0*	-31.9	
Cisplatin	*+1.0*	-29.7	-12.1	
HSP27	High	Moderate	Moderate	HSP27 was suppressed or insignificant across the three cell lines
[Pt(dmp)(L^1-κO,S)]Cl	*-0.4*	-30.1	*+8.0*	
[Pt(dmp)(L^3-κO,S)]Cl	*-2.3*	*+5.8*	-23.6	
Cisplatin	*+2.8*	-40.3	*+8.7*	
HSP60	Very high	High	Mod high	HSP60 expression level was increased in A549 cells
[Pt(dmp)(L^1-κO,S)]Cl	-15.1	+39.7	+34.8	
[Pt(dmp)(L^3-κO,S)]Cl	*-7.3*	+63.8	-9.0	
Cisplatin	-10.9	*+4.3*	+7.6	
HSP70	High	Mod high	Moderate	Pt complexes suppressed HSP70 across the three cancer cell lines
[Pt(dmp)(L^1-κO,S)]Cl	-22.0	-22.1	*-4.6*	
[Pt(dmp)(L^3-κO,S)]Cl	-10.3	-15.1	-28.6	
Cisplatin	*-3.6*	-35.4	-14.7	
Survivin	Moderate	Moderate	Moderate	Both Pt complexes and cisplatin suppressed survivin across the three cancer cell lines
[Pt(dmp)(L^1-κO,S)]Cl	-33.0	-62.9	-17.0	
[Pt(dmp)(L^3-κO,S)]Cl	-34.0	-35.5	-30.6	
Cisplatin	-30.4	-40.9	-28.1	
Livin	Low	Low	Moderate	Livin baseline expression was decreased in HT-29 cells
[Pt(dmp)(L^1-κO,S)]Cl	-20.3	+66.1	+65.7	
[Pt(dmp)(L^3-κO,S)]Cl	*+8.4*	*+142.3*	*-2.3*	
Cisplatin	*-6.6*	-19.6	*+6.4*	
XIAP	High	High	Mod high	XIAP varied in H1975 and non-significant in HT-29 and A549 cells
[Pt(dmp)(L^1-κO,S)]Cl	-18.6	*+0.9*	+31.6	
[Pt(dmp)(L^3-κO,S)]Cl	+15.8	+10.9	-30.3	
Cisplatin	*+8.0*	*0*	-11.5	
cIAP-2	Moderate	Low	Low	cIAP-2 was suppressed in A549 and H1975 cells but varied in HT-29
[Pt(dmp)(L^1-κO,S)]Cl	*+3.4*	-45.8	*-4.3*	
[Pt(dmp)(L^3-κO,S)]Cl	+21.4	-36.3	-14.4	
Cisplatin	-16.2	-26.3	-26.2	
Cell cycle proteins				

p21	Low	High	Moderate	p21 was significantly increased in A549 cells
[Pt(dmp)(L^1-κO,S)]Cl	+25.2	+189.1	+38.9	
[Pt(dmp)(L^3-κO,S)]Cl	+23.9	+282.6	-26.9	
Cisplatin	*+6.8*	+52.5	-13.0	
p27	Low	Moderate	Moderate	p27 expression was significantly increased in A549 cells and not significant in HT-29 cells
[Pt(dmp)(L^1-κO,S)]Cl	*-5.1*	+80.7	+14.4	
[Pt(dmp)(L^3-κO,S)]Cl	*+19.9*	+51.6	-17.4	
Cisplatin	*+0.4*	+35.1	*+0.5*	
p53	Very high	Moderate	Mod high	p53 expression non-significant in H1975 and decreased in A59 cells, cisplatin increased its expression in A549 cells
[Pt(dmp)(L^1-κO,S)]Cl	-	*-19.9*	*+2.3*	
[Pt(dmp)(L^3-κO,S)]Cl	-	*+2.8*	-40.6	
Cisplatin	-	+89.9	-16.6	

*Note: Italicised values were statistically non-significant according to one-way ANOVA, and the Dunnet's post hoc test. * Mod high refers to moderate high baseline expression level. Three forms of phosphorylated p53 were evaluated in HT-29 cells.*

4.4.1 Bad, Bax, Bcl-2 and cytochrome c

Bad can be both pro-and anti-apoptotic as it is indirectly promotes apoptosis by inhibiting anti-apoptotic members of the Bcl-2 proteins family such as Bcl-2 and Bcl-xL, thereby allowing the pro-apoptotic members to trigger the apoptotic pathway (Howells *et al.*, 2011). Phosphorylation of Bad by kinases is linked to its anti-apoptotic effects, rendering it unable to fulfill its pro-apoptotic function. Consequently, this allows free Bcl-2 to inhibit Bak/Bax-mediated apoptosis (Howells *et al.*, 2011).

Across the three cancer cell lines, [Pt(dmp)(L^3-κ*O*,*S*)]Cl and cisplatin decreased Bad expression, with the exception of [Pt(dmp)(L^1-κ*O*,*S*)]Cl, which increased the expression of Bad in H1975 cells.

Bax is a pro-apoptotic Bcl-2 proteins that functions together with Bak to induce intrinsic apoptosis by undergoing conformational changes that lead to mitochondrial outer membrane permeabilization (MOMP). This results in increased mitochondrial permeability, facilitating the release of cytochrome c and other apoptotic proteins such as Apoptosis Inducing Factor (AIF), Smac/DIABLO, HTRA2/Omi and Endonuclease G from the mitochondria into the cytosol (Peña-Blanco and García-Sáez, 2018).

No meaningful changes were observed in the expression of Bax across the three cancer cell lines except for a significant increase caused by [Pt(dmp)(L^1-κ*O*,*S*)]Cl in H1975 cells, similarly to Bad. This indicates that in H1975 cells, [Pt(dmp)(L^1-κ*O*,*S*)]Cl was able to promote apoptosis by increasing the expression of Bad and Bax.

Given the low baseline expression of Bcl-2 in all three the cells lines, the changes in expression level observed although statistically significant was not considered to be meaningful.

Treatment with platinum complexes and cisplatin did not cause any meaningful change in the expression of cytochrome c in HT-29 and A549 cells, indicating that cytochrome c did not play a significant role in the cell death of these cell lines. [Pt(dmp)(L^1-κ*O*,*S*)]Cl significantly increased the expression of cytochrome c in H1975 cells while cisplatin showed a superior increase of cytochrome c in H1975 cells, suggesting that cytochrome c is important in this cell line and likely contributes towards the formation of the apoptosome, facilitating intrinsic apoptosis.

4.4.2 Caspase-3 and cleaved caspase-3

Caspase-3 is an effector caspase that plays an important role in the final stages of triggering apoptosis. Caspasse-3 activation is considered a late event in apoptosis and its activation does not distinguish between the intrinsic and extrinsic pathways (Sagar *et al.*, 2010).

In HT-29 cells, both the inactive (pro-caspase-3) and active form of caspase-3 (cleaved casapse-3) were evaluated in the proteome array while only pro-caspase-3 was measured in A549 and H1975 cells. In HT-29 cells the baseline expression level of procaspase-3 was high while cleaved caspase-3 level was low.

Platinum complexes caused no significant changes in the expression of procaspase-3 or cleaved caspase-3 respectively in HT-29 cells. [Pt(dmp)(L^1-κ*O*,*S*)]Cl showed a small increase in cleaved caspase-3 expression, consistent with the moderate increase in caspse-3/7 activity observed in chapter 3. Similarly, changes in the

expression level of inactive caspase-3 in A549 and H1975 cells were also statistically non-significant, not meaningful due to the low baseline expression level, except for a small decrease by [Pt(dmp)(L^1-κ*O*,*S*)]Cl in A549 cells, suggesting a possible activation of caspase-3.

The lack of significant changes in cleaved caspase-3 levels in HT-29, and the lack of a meaningful decrease in the expression of inactive caspase-3 in A549 and H1975 observed in this proteome array, could be attributed to the short treatment period used to obtain the proteome arrays .It is possible that the caspase 3 response would be more obvious after a longer exposure period of the cells to the various treatments. It is important to note that the arrays are detecting expression levels and not caspase-3 enzyme activity.

4.4.3 Platinum complexes increased the expression of TRAIL R2

Overall, the platinum complexes decreased or caused non-significant changes in the expression of TNF R1, Fas/TNFRSF6/CD95, FADD and TRAIL R1/DR4 in HT-29 cells. In A549 and H1975 cells, the expression of TNF R1 was significantly decreased by both platinum complexes and cisplatin with the exception of [Pt(dmp)(L^1-κ*O*,*S*)]Cl which increased its expression in H1975. This decrease suggests a lack of activation of the extrinsic apoptotic pathway, aligning with the previously observed absence of caspase-8 activity in HT-29 cells (chapter 3, section 3.3.3.2).

In contrast, platinum complexes significantly increased the expression of TRAIL R2 in HT-29 cells. The observed increase in the expression of TRAIL R2 by both [Pt(dmp)(L^1-κ*O*,*S*)]Cl and [Pt(dmp)(L^3-κ*O*,*S*)]Cl was superior to that of cisplatin and indicated that these platinum complexes may also trigger apoptotic cell death via the TRAIL induced extrinsic pathway to a certain extent in HT-29 cells.

Platinum complexes caused a differential expression of TRAIL R2 as well as other death receptor proteins (TRAIL R3, TRAIL R4, TNF R1, TNF R1 and Fas) in H1975. [Pt(dmp)(L^1-κ*O*,*S*)]Cl caused an increase while [Pt(dmp)(L^3-κ*O*,*S*)]Cl decreased its expression. The opposite was true for A549 cells, where [Pt(dmp)(L^3-

κ*O*,*S*)]Cl was shown to moderately increase the expression of TRAIL R1, and TRAIL R2. Cisplatin did not cause any meaningful changes in TRAIL R2 expression in both H1975 and A549 cells but decreased the expression of other death receptor proteins. The implications of increased TRAIL R2 expression across the three cancer cells lines is unclear as caspase-8 activity was not observed.

4.4.4 Platinum complexes decreased the expression of HSPs

Heat shock proteins; HSP27, HSP60 and HSP70 are molecular chaperones that protect cells against oxidative stress, hypoxia and inflammatory stimuli thus preventing cell death and promoting cell survival (Hu *et al.*, 2022). HSP27 and HSP70 possess anti-apoptotic properties. HSP27 blocks the activation of caspase-3/7, while HSP70 is known to inhibit the activation of intrinsic apoptosis by preventing the assembly of Apaf-1 into forming an apoptosome complex, important for the activation of pro-caspase-9 into caspase-9 (Beere *et al.*, 2000).

The baseline expression of HSP27 and HSP70 was high in HT-29 cells and moderate in A549 and H1975 cells. Platinum complexes did not cause any meaningful changes in HSP27 expression in HT-29 cells but were able to decrease its expression in A549 and H1975. The expression of HSP70 was suppressed by platinum complexes and cisplatin in all three cancer cells lines although cisplatin caused a higher decrease in A549 cells. HSP60 is a molecular chaperone found in the mitochondria and cytosol of cells. A high expression of HSP60 is important for cancer progression since HSP60 expression is associated with apoptosis resistance. The baseline expression level of HSP60 was high in HT-29 and A549 but moderate in H1975 cells. Platinum complexes caused a less significant decrease in HSP60 expression in HT-29 cells, while a significant increase was observed in A549 cells. [Pt(dmp)(L^1-κ*O*,*S*)]Cl increased HSP60 expression in H1975. The increase in HSP60 expression is not preferred as it is associated with cancer cell survival.

The ability of platinum complexes to inhibit the expression of HSP27 and HSP70 in these cancer cell lines; HT-29, A549 and H1975 suggests that the complexes drive the induction of apoptosis, preventing the inhibition of caspase-3/7 and

caspase-9 activation by these proteins, which is important for the treatment of cancer.

4.4.5 Platinum complexes decreased the expression of IAPs

Inhibitor of apoptosis are a family of intracellular anti-apoptotic proteins that act by binding and inhibiting caspases. All IAP proteins are characterized by the presence of one to three baculovirus IAP repeat (BIR) domains, which are zinc-binding regions that mediate protein-protein interactions. IAPs (XIAP, cIAP-1, cIAP-2, livin and survivin) function to inhibit apoptosis by either binding to the active site of caspases via their BIR domains or indirectly through protein-protein interactions and by modulating the levels of other proteins (Lau and Pratt, 2012). Several IAP family members are upregulated in various human cancers, correlating with an unfavourable prognosis.

XIAP inhibits both the intrinsic and extrinsic apoptotic pathways apoptosis by directly binding to the active site of initiator caspase-9 and executioner caspase-3/7 (Scott *et al.*, 2005; Parrish, Freel and Kornbluth, 2013; Zumbrägel *et al.*, 2017). The baseline expression level of XIAP was high in HT-29 cells and moderately high in A549 and H1975 cells. [Pt(dmp)(L^3-κ*O*,*S*)]Cl and cisplatin were able to significantly suppress the expression of XIAP in H1975 cells, whereas [Pt(dmp)(L^1-κ*O*,*S*)]Cl decreased its expression in HT-29 cells.

The baseline expression of cIAP-2 was moderate in HT-29 and H1975 cells but low in A549. The platinum complexes significantly suppressed the expression of cIAP-2 in A549 and H1975 favouring apoptosis.

Survivin is the smallest member of the IAPS that inhibits caspase activation indirectly by interacting with XIAP. It is known to be overexpressed in nearly all human tumours and transformed cell lines but is rarely present in normal tissues (Kasof and Gomes, 2001). Survivin was moderately expressed in the three cell lines. However, its expression was significantly decreased by the two platinum complexes and cisplatin across all three cancer cell lines. The ability of platinum

complexes to suppress its expression in all three cancer cell lines is associated with their ability to favour the induction of apoptosis.

Livin is an IAP that interacts by binding to and inhibiting caspase-3, caspase-7, and caspase-9 as well as the pro-apoptotic protein Smac/DIABLO, thereby impeding their pro-apoptotic functions. Livin had low baseline expression in the three cancer cell lines. Consequently, changes in the expression of livin following treatment with platinum complexes showed an increase in A549 cells and H1975 cells while a decrease was observed in HT-29 cells suggesting livin to be a stress response protein.

4.4.6 Smac/DIABLO and HTRA2/Omi

Smac/DIABLO and HTRA2/Omi are pro-apoptotic proteins that function by competitively binding to IAPs on their respective BIR domains, disrupting their ability to inhibit caspases to promote apoptosis. This enables the activation of caspases, leading to apoptosis (Yang *et al.*, 2003). Smac/DIABLO has a high affinity for XIAP as it directly binds and inhibits XIAP from blocking caspase-3/7 as well as caspase-9 activation (Martinez-Ruiz *et al.*, 2008).

Similar to Smac/DIABLO, HTRA2/Omi binds and inhibits XIAP, and directly cleaves various IAPs (Yang et al., 2003; Suzuki et al., 2004; Hu et al., 2019). The baseline expression levels of Smac/DIABLO and HTRA2/Omi were high in HT-29 cells but moderate in A549 and H1975 cells. Platinum complexes and cisplatin did not induce meaningful changes in the expression of these proteins in HT-29, whereas a significant decrease was observed in A549 and H1975 cells. The lack of change and decreased expression of these proteins suggests that they did not play a major role in apoptosis which would be by preventing IAPs from binding to caspases in these cancer cell lines. Since the XIAP was highly expressed in untreated HT-29, A549 and H1975 cells with non-meaningful changes observed following treatment with platinum complexes and cisplatin, it is suspected that XIAP may have inhibited caspase activation to a certain extent in these cell lines, consistent with the observed moderate increase in caspase-3/7 activity instead of a high activity especially in HT-29 and H1975 cells (chapter 3).

4.4.7 The expression of cell cycle proteins; p21, p27 and p53

4.4.7.1 Platinum complexes increased the expression of p21

In response to a variety of cellular stresses such as DNA damage, p21 is induced to accumulate in the cell nucleus to exert its pro-apoptotic function. Both platinum complexes significantly increased the expression of p21 in HT-29 and A549 cells but varied in H1975 cells, where [Pt(dmp)(L^1-κ*O*,*S*)]Cl caused an increase while [Pt(dmp)(L^3-κ*O*,*S*)]Cl supressed p21 expression. A major increase was observed in A549 cells compared to HT-29 and H1975 cells. Immunofluorescence evaluation on p21 expression showed that platinum complexes caused an increase in nuclear expression of p21 in all three cancer cell lines, thus providing evidence that DNA may be a target of these complexes (Peega *et al.*, 2021). The interaction between platinum complexes and the DNA target molecule was therefore important to investigate based on this evidence. The upregulation of p21 by platinum complexes promotes cell cycle arrest to allow DNA repair and/or induce apoptosis to prevent the division of cells with serious DNA damage.

4.4.7.2 The expression of p53 in HT-29, A549 and H1975 cells

In HT-29 cells, the expression level of three phosphorylated forms of p53 at serine sites (phospho-p53(S15), phospho-p53(S46) and phospho-p53(S392) was detected whereas the proteome array used for A549 and H1975 cells included normal p53. Phosphorylation of p53 is a post translational modifications caused by active kinases on serine residues, protecting p53 from being degraded by its negative regulator, E3 ubiquitin-protein ligase MDM2 protein (Meek and Anderson, 2009; Alfadul *et al.*, 2023). p53 largely exists in its non-phosphorylated form, considered to be inactive "since it can be inhibited by MDM2 (Alfadul *et al.*, 2023). All three phosphorylated p53 were highly expressed in HT-29 control cells. Neither the platinum complexes nor cisplatin induced significant changes in the expression levels of all three phosphorylated forms of p53. This indicated that both these complexes and cisplatin had no meaningful impact on the expression of these phosphorylated p53. The high baseline expression of p53 in HT-29 cells can be

attributed to the fact that p53 is mutated in HT-29 cells (Anaya-Eugenio *et al.*, 2020). This is associated with a gain of function mutation that drives cell proliferation and is not affected by treatment with platinum complexes.

The baseline expression level of the tumour suppressor protein, p53 was moderate in A549 cells and moderately high in H1975 cells. In A549 cells, [Pt(dmp)(L^3-κ*O,S*)]Cl caused a significant decrease in p53 expression, in contrast to cisplatin which increased p53 levels. The increase was indicative of the accumulation of p53 in A549 cells following treatment with cisplatin. The increase in p53 is a normal response to DNA damage and therefore the response is indicative of cisplatin induced DNA damage.

4.4.7.3 The expression of p27

P27 is a tumour suppressor protein that is associated with the DNA damage response. It is classified as an inhibitor of cyclin-dependent kinases (CDK), which controls the cell cycle. P27 arrests cells in the G1 phase by inhibiting cyclin dependent kinase 2 which is essential for the transition to the S phase, where DNA replication and repair takes place before proceeding to G2 phase in the cell cycle. It's function is influenced by its cellular location and phosphorylation status (Lee and Kim, 2009). P27 has contradicting roles by acting as a tumour suppressor as well as a pro-tumourigenic oncogene. In cancer cells, p27 is downregulated, and a strong inverse correlation exists between tumour progression and p27 levels.

Platinum complexes caused no significant changes in the expression of p27 in HT-29 cells. In H1975 cells, the changes caused by the platinum complexes were not considered to be meaningful. However, in A549 cells, both complexes and cisplatin significantly increased p27 expression. The increased expression of p27 following exposure to platinum complexes is associated with its function as a tumour suppressor, preventing cells from dividing in response to DNA damage.

Furthermore, the observed increase in p27 warrants additional investigation into its cellular localization since nuclear p27 is known to function as a tumour suppressor, inhibiting tumour growth and promoting apoptosis while cytoplasmic p27 serves as

an oncogene, promoting tumour progression (Lee and Kim, 2009; Crivellaro *et al.*, 2016).

4.4.8 Other important apoptosis-associated proteins in HT-29 cells

The proteins; HMOX-1, HMOX-2, claspin, phosphorylated forms of p53, phospho-Rad17 and cIAP-1 were only evaluated in HT-29 cells whilst, caspase-8, death receptor proteins (TNF R2, TRAIL R3, TRAIL R4) and insulin-like growth factor proteins (IGF 1, IGF 2, IGF-1R and a range of IGFBP 1-6 were included in the proteome array of lung cancer cell lines; A549 and H1975 cells.

4.4.8.1 Phospho-RAD17

Phosphorylated Rad17, is a cell cycle protein that participates in checkpoint-mediated cell cycle arrest (G(2)/M) in response to DNA damage or inhibition of DNA replication (Wang *et al.*, 2006; Marechal and Zou, 2013). RAD17 is phosphorylated by ATR, the primary kinase sensing DNA damage during S phase leading to the activation of p53 (Fischer, Dang and DeCaprio, 2018).

In HT-29 control cells, phospho-RAD17 showed a moderate expression. Platinum complexes caused non meaningful changes in the expression of phosphor-RAD17, while cisplatin significantly increased its expression (*Table 4.6*). The increase in phospho-RAD17 is indicative of an increased response to DNA damage, caused by cisplatin compared to platinum complexes in this cell line.

The binding of RAD17 to claspin is crucial for the cellular response to genotoxic stress (Wang *et al.*, 2006).

4.4.8.2 Platinum complexes supress claspin expression

Claspin is an important adaptor protein in the cell cycle process that plays a role in protecting and maintaining intact DNA (Azenha, Lopes and Martins, 2017). Claspin was highly expressed in HT-29 control cells. Both [Pt(dmp)(L^1-κ*O*,*S*)]Cl and [Pt(dmp)(L^3-κ*O*,*S*)]Cl caused a significant decrease in the expression of claspin

while in contrast, cisplatin significantly increased its expression level by almost the same amount. The overexpression of claspin has previously been shown to protect cells from replication stress and promote tumour progression in a checkpoint independent manner (Bianco *et al.*, 2019; Cai *et al.*, 2021). Claspin is usually expressed at higher levels in cancer cells compared to normal cells, as observed in untreated HT-29 cells. Therefore, the ability of platinum complexes to significantly decrease the expression of claspin in HT-29 is considered a pro-apoptotic effect, inhibiting its tumour progression role, showing the desired outcome as opposed to the effect caused by cisplatin in further upregulating its expression. Further investigations of claspin and its role as the potential target in this cell line are required.

4.4.8.3 Platinum complexes increased the expression of HO-1n HT-29 cells

Table 4.9: The expression level of HO-1 in HT-29 cells

HT-29	**HO-1**
Baseline expression level	**Moderate**
[Pt(dmp)(L^1-κ*O,S*)]Cl	+78.4
[Pt(dmp)(L^3-κ*O,S*)]Cl	+88.3
Cisplatin	+15.2

HO-1 is an antioxidant enzyme that protect cells against oxidative stress (Chiang, Chen and Chang, 2021). It regulates inflammation, apoptosis, cell proliferation, and angiogenesis in prostate cancer (Ben-Eltriki *et al.*, 2023). An elevated cellular level of HO-1 is an indicator of oxidative stress. An increase in HO-1 expression in HT-29 cells following treatment with platinum complexes is considered a response towards maintaining ROS levels, promoting cell survival (Ben-Eltriki *et al.*, 2023). Additionally, the increase of HO-1 is associated with chemoresistance and tumour progression (Dubey *et al.*, 2015; Chiang, Chen and Chang, 2021; Mascaró *et al.*, 2021).

The proteome array data showed that the platinum complexes significantly increased HO-1 expression in HT-29 cells (*Table 4.9*), correlating with oxidative stress as shown by increase ROS levels in HT-29 cells after a 4 hour treatment (chapter 3, section 3.3.8). The increased HO-1 expression in the proteome array supports the results observed in immunofluorescence assay. Immunofluorescence analysis in chapter 3 showed an increased expression of HO-1 across the three cancer cell lines. HO-1 expression was localised in both the cytoplasm and nucleus, with a particularly intense signal in the nucleus.

4.4.9 Other important apoptosis-associated proteins in A549 and H1975 cells.

4.4.9.1 Caspase-8 expression varied in H1975 cells

Casapse-8 is an initiator caspase involved the activation of extrinsic apoptosis. The Ray biotech proteome array included the inactive form of caspase-8. Changes in the expression level of caspase-8 in A549 cells was considered not meaningful since the baseline expression level was low and both platinum complexes and cisplatin did not cause any meaningful changes in its expression. However, in H1975 cells, [Pt(dmp)(L^3-κ*O*,*S*)]Cl and cisplatin decreased the expression of caspase-8 while [Pt(dmp)(L^1-κ*O*,*S*)]Cl showed increased its expression. The differential expression of caspase-8 could potentially indicate distinct effects between the two complexes, suggesting they may operate through different mechanisms or have varied effects within the same cell line.

4.4.9.2 Platinum complexes decreased the expression of BID and BIM

BID and BIM are pro-apoptotic members of the Bcl-2 family of proteins as they both promote Bax/Bak oligomerization, causing intrinsic apoptosis. In addition truncated BID also stimulates death receptor-mediated apoptosis and links extrinsic apoptosis and intrinsic apoptosis by causing the cleavage of caspase-8 (Tzifi *et al.*, 2012).

Both platinum complexes and cisplatin suppressed the expression of BID and BIM in both A549 and H1975 cells. The low baseline expression level of BID in both A549 and H1975 indicated that BID does not have an important role in the apoptotic process in these cell lines. The suppression caused by the platinum complexes and cisplatin although statistically significant was not meaningful.

The baseline expression level of BIM was moderate in both A549 and H1975 cells. Platinum complexes and cisplatin significantly suppressed the expression level BIM in both these cancer cell lines, except for [Pt(dmp)(L^3-κ*O,S*)]Cl , which caused non-significant change. A decrease in BIM expression suggest that this protein did not play a major role in inducing apoptosis in these cell lines.

4.4.9.3 Platinum complexes suppress the expression of IGFs

The binding of IGF1 to its receptor IGF1R on the cell surface promotes cell survival by triggering the activation of phosphoinositide 3-kinase (PI3K/AKT) pathway and blocks apoptosis by phosphorylation and inhibition of proapoptotic proteins such as Bad (Wang and Sun, 2002; Galvan *et al.*, 2003). IGF-1 and IGF-2 inhibit apoptosis and promote cell survival in various processes (Zhang *et al.*, 2018).

Both platinum complexes and cisplatin significantly supressed the expression of IGF-1 and IGF-2 in A549 cells whereas in H1975 cells, [Pt(dmp)(L^3-κ*O,S*)]Cl and cisplatin significantly decreased the expression of IGF-2, with [Pt(dmp)(L^3-κ*O,S*)]Cl causing a greater decrease than cisplatin. The observed reduction in the expression of IGF-1 and IGF-2 in both cell lines provides evidence that this effect is not random, but rather suggest that these complexes may play a role in inducing apoptosis by inhibiting the expression of IGFs.

IGFs can indirectly inhibit the activation of pro-apoptotic proteins (i.e Bad), through phosphorylation, preventing the release of cytochrome c from mitochondria, thereby blocking the initiation of intrinsic apoptotic pathway (Gilmore *et al.*, 2002; Galvan *et al.*, 2003).

IGF-IR expression was significantly suppressed by [Pt(dmp)(L^3-κ*O,S*)]Cl in H1975 cells while only cisplatin decreased its expression in A549 cells. Platinum

complexes did not cause any significant change in the expression of IGF-R1 in A549 cells.

Previous studies have indicated that elevated IGF-IR expression in neuroblastoma cells increases their resistance to chemotherapy induced apoptosis (Van Golen, Castle and Feldman, 2000). Consequently, the absence of change or reduction in the expression of this protein in A549 and H1975 cells after exposure to platinum complexes is presumed to prevent IGF-1R from exerting its function from preventing apoptosis.

4.4.9.4 Platinum complexes caused a differential expression of IGFBPs

IGFBPs bind to IGFs with an equal or greater affinity than the IGF1 receptor and are thus important regulators of IGF signalling. Binding to an IGFBP increases the half-life of IGF in the circulation and blocks its potential binding to the insulin receptor (Allard and Duan, 2018).

The effect of platinum complexes and cisplatin on the expression of six insulin-like growth factor binding proteins (IGFBP 1-6) varied. These are pro-apoptotic proteins since they prevent IGFs from exerting their pro-survival effects on cancer cells.

Both platinum complexes caused a significant increase the expression level of IGFBP-1 and IGFBP-6 in A549 cells. Cisplatin had an opposite effect where it significantly decreased IGFBP-6 in A549 cells, indicating the superior effect of platinum complexes to decrease the survival of these cancer cell.

IGFBP-3 expression was significantly increased by [Pt(dmp)(L^1-κ*O*,*S*)]Cl in H1975 but was decreased in A549 cell by both complexes. In contrast, cisplatin increased the expression of IGFBP-3 in A549 cells.

The effects of platinum complexes on IGFBP and role in apoptosis requires further investigation, especially regarding the mechanism of the increase.

4.5 In summary

The proteome arrays provided a means to evaluate the effect of platinum complexes on the expression of apoptosis-associated proteins in the three cell lines used in this study. Platinum complexes significantly increased the expression of HO-1, TRAIL R2, p21 and significantly decreased the expression of survivin, HSP70 and claspin in HT-29 cells. The increase in HO-1 levels was correlated to the cell's response to oxidative stress, while the upregulation of p21 was associated with the response to DNA damage. This correlation aligns with the findings of the increased expression of HO-1 and p21 observed by the immunofluorescence assay. An increase in the expression TRAIL R2 suggested possible induction of the extrinsic apoptotic pathway, however, further investigations in the mechanism by which extrinsic apoptosis may be induced is required since caspase-8 activation was not observed. The observed effect of platinum complexes in inhibiting claspin expression in HT-29 cells, in contrast to the upregulation induced by cisplatin, provides supporting evidence for their role in reducing tumourigenesis, potentially triggered by claspin overexpression in HT-29 cells. This implies a preference for apoptosis induction and suggests an inhibitory effect on tumour progression.

All three cell lines, HT-29, A549 and H1975 showed a suppression of the anti-apoptotic protein, survivin, following treatment with the platinum complexes. The downregulation of IGF-1 and IGF-2 and the anti-apoptotic heat shock proteins; HSP27 and HSP70 by either of the platinum complexes in H1975 cells suggested that these platinum complexes created and environment favourable for the induction of mitochondrial-mediated apoptosis.

Based on the evidence from the proteome arrays in combination with studies conducted in chapter-3, platinum complexes caused oxidative stress, indicated by increased ROS levels and increased HO-1 expression. This led to DNA damage as observed by the increase in p21 expression and mitochondrial stress, evidenced by mitochondrial outer membrane permeability, which triggers the intrinsic apoptosis.

Chapter 5: DNA binding studies with active platinum complexes

5.1 Introduction

Deoxyribonucleic acid (DNA) is the primary target for many chemotherapeutic agents. Metal-based drugs such as cisplatin, exert their anti-cancer effects by binding irreversibly to the DNA and inhibiting DNA replication and transcription (Dasari and Bernard Tchounwou, 2014). Diimine ligands including 1,10-phenanthroline derivatives, have been previously shown to bind to DNA via non-covalent interactions. This is attributed to their planar aromatic nature enabling interactions with DNA base pairs through DNA intercalation and hydrophobic interactions (Pages *et al.*, 2015; Sánchez-González and Gil, 2021). This binding causes damage to DNA and triggers cell death through apoptosis (Devi *et al.*, 2017; Boros, Dyson and Gasser, 2020). Therefore, understanding DNA–complex interactions is important for drug development and determining the potential mechanism of action behind their therapeutic effects, and predicting their potential side effects.

DNA interactions with registered drugs and test compounds can be broadly categorized into two major groups; covalent binding and non-covalent binding. Covalent binding permanently alters the DNA structure through irreversible coordination with the DNA while non-covalent binding is reversible and can be further categorized into three major subgroups being; electrostatic interactions, intercalation and groove binding (Rehman *et al.*, 2015; García-Ramos *et al.*, 2017).

The DNA binding mode of the two most potent platinum complexes; [Pt(dmp)(L^1-κ*O*,*S*)]Cl and [Pt(dmp)(L^3-κ*O*,*S*)]Cl were investigated by employing the following techniques; electrophoretic mobility shift assay (gel electrophoresis), thermal degradation analysis, circular dichroism and electronic absorption titrations. The aim was to investigate the effect of platinum complexes on DNA mobility, melting temperature, and conformation as well as to determine their DNA binding affinity.

5.2 Experimental

5.2.1 Chemicals and solvents

Chemicals and analytical grade solvents were purchased from Sigma-Aldrich and Merck (South Africa). The pUC57 plasmid DNA and calf thymus DNA sodium salt (ctDNA) were purchased from Sigma–Aldrich Chemicals. A stock solution of ctDNA was freshy prepared upon experimental usage. ctDNA was carefully weighed and dissolved in the appropriate buffer solution as per experiment (TA, TBS or PBS). The mixture was gently agitated overnight at 120 rpm to ensure thorough dissolution and homogeneity. The concentration of the solution was determined spectrophotometrically at 260 nm using a molar extinction coefficient ε =13 200 M^{-1} cm^{-1}). Additionally, the absence of proteins in the prepared DNA solution was confirmed by measuring the ratio of absorbance at 260 nm to that at 280 nm (260/280 nm). The obtained ratio was found to be 1.8, indicating that the DNA was pure and free from any protein contamination.

5.2.2 Electrophoretic Mobility Shift Assay

5.2.2.1 Background and principle of the assay

The Electrophoretic Mobility Shift Assay (EMSA) is a rapid and sensitive separation technique extensively used to investigate protein-nucleic acid interactions. In more recent applications, EMSA has been utilized to study interactions between potential drug molecules and nucleic acids. This assay involves subjecting a mixture of molecules, such as compound-nucleic acid complexes to an electric field over a short period, causing them to migrate through a non-denaturing gel matrix (agarose or polyacrylamide gel). The resulting pattern of mobility shifts in the gel provides valuable information about the interactions and binding affinities between the molecules under investigation (Fried and Crothers, 1981; Garner and Revzin, 1981; Ream, Lewis and Lewis, 2016).

Interactions between DNA and metal complexes have been studied using gel electrophoresis. The mobility of DNA in the presence of metal complexes can either be enhanced or hindered, depending on the size, charge, and interaction of the metal complex with DNA. A metal complex with a high affinity for DNA, characterized

by a high charge and large size, slows down the mobility of DNA in the gel. In contrast, free unbound DNA migrates at a faster rate.

5.2.2.2 Experiment procedure

Gel electrophoresis experiments were carried out in triplicate using hand-cast 1.25% agarose gels prepared in a Mini-Sub-Cell GT® Agarose Gel Electrophoresis System (Bio-Rad) by dissolving 437.5 mg Type 1 Agarose (e.g. Sigma-Aldrich product 6013) with 37 mL of 1x Tris-acetate buffer (TA) (40 mM Tris, 20 mM acetate, pH 7.6) (Sigma-Aldrich, Johannesburg). The solution was placed in a microwave for 1-2 minutes and cooled to 60 ℃. The gel was poured into a level casting tray and allowed to set for 30 minutes at room temperature. A standard 0.75 mm, 15-well comb was used to form sample loading wells in the gel. [Pt(dmp)(L^1-κ*O,S*)]Cl and [Pt(dmp)(L^2-κ*O,S*)]Cl samples for EMSA were prepared in 10% DMSO TA buffer to total volume of 10 uL and incubated at 37 ℃ for 30 minutes before the addition of a 2 µl of loading dye (Sigma product no. G 7654; 0.25% (w/v) bromophenol blue, 0.25%(w/v) xylene cyanole FF, 40% (w/v) sucrose in water). Samples were loaded into each well as 6 uL aliquots with 12.5ng of DNA per lane on the gels. The gel was run at 75 V for 90 minutes and stained with an Ethidium Bromide solution (0.5 mg/L in) for 30 minutes and thereafter washed for 20 minutes. The gels were visualized using a G:Box Chemi XRQ gel doc system (Syngene) with mid-wave transillumination and a UV filter (GeneSys 1.4.6.0).

A shift in the position of the discrete bands of DNA-complex was compared to the negative control (free pUC57 DNA) and used to indicate the presence of an interaction. The obtained results were compared with positive controls for DNA intercalation (ethidium bromide) and minor groove binding (Hoechst-33258) to analyze and make experimental predictions about the potential binding mode of platinum complexes.

5.2.3 DNA thermal degradation

Thermal degradation or denaturation of DNA is the dissociation of double-stranded DNA into single-stranded DNA due to the breaking of hydrogen bonds between base pairs upon exposure to increasing temperature. The temperature at which 50%

of the double-stranded DNA is converted into single-stranded DNA is referred to as the melting temperature (T_m) (Devi *et al.*, 2017).

The melting temperature of DNA is highly dependent on the stability of the double helix. The binding of small molecules can either stabilize or destabilize the DNA helix based on their mode of binding causing conformational changes in the DNA structure. T_m is indicative of the binding affinity of the complex to the DNA target; therefore, an increase in the melting temperature indicates a higher binding affinity as the energy required to break the bond between the complex and DNA is high. Thus, the T_m of destabilized DNA is decreased relative to the free unbound DNA helix.

The base pairs in ds-DNA are stable and stacked inside the double helix at lower temperatures. As the temperature increases, the DNA undergoes denaturation, and the ds-DNA structure starts to unwind, leading to the formation of single-stranded DNA (ss-DNA). This transition to single-stranded form at higher temperatures increases absorbance, causing a hyperchromic shift. The increase in absorbance occurs because the base pairs in the DNA are no longer restricted by hydrogen bonds, leading to a change in the optical properties of the DNA solution.

5.2.3.1 Experiment procedure

Samples were prepared in 1X Tris-acetate buffer (40 mM Tris-acetate, pH 7.6) containing 10% (v/v) DMSO to solubilize the complexes. A stock solution of calf thymus DNA (ctDNA) was freshly prepared in Tris-acetate buffer and its concentration was measured spectroscopically at 260 nm using a molar extinction coefficient of 13200 M^{-1} cm^{-1} per base pair.

DNA thermal denaturation experiments were recorded in triplicate on a Jasco J-1500 Circular Dichroism Spectrometer using a 1.00 cm path length quartz cell, with concentrations of the ctDNA and platinum complexes at 100 µM and 2.5 µM respectively. The absorbance of ctDNA. was monitored at a wavelength of 260 nm due to the π–π* transition of the four base pairs; against increasing temperature. Measurements at 260 nm and 600 nm were recorded at 5 °C intervals between 25 °C and 50 °C, and 1 °C intervals between 50 °C and 95 °C. The data were corrected

and normalized, and the temperature at which 50 % of the DNA was denatured was determined from the resultant graph.

5.2.4 Circular dichroism

5.2.4.1 Background and principle of the experiment

Circular dichroism (CD) is a spectroscopic technique that is used to investigate the structural and optical properties of molecules. It involves the interaction of chiral molecules with circularly polarized light. Chiral molecules selectively absorb one direction of circularly polarized light, generating a CD spectrum. This technique offers valuable insights into the structural conformations of molecules, especially in biomolecules such as proteins and nucleic acids (Kypr *et al.*, 2009; Rodger, 2013).

A CD spectrum is obtained by measuring the difference in the absorption of left and right circularly polarized light (LCP and RCP) by chiral molecules as a function of wavelength. The difference in absorption is known as circular dichroism and is described by the following equations:

$$CD = \Delta A(\lambda) = A_L(\lambda) - A_R(\lambda) \qquad (Eq\ 1)$$

$$\Delta A\ (\lambda) = (\varepsilon_L - \varepsilon_R)Cl \qquad (Eq\ 2, Beer\ lambert\ law)$$

Where ΔA is the difference in absorbance; ε_l and ε_r are molar extinction coefficients of left and right circularly polarized light, C is the molar concentration and l is the path length.

CD was used to investigate changes in DNA conformation following exposure to platinum complexes. The interaction of molecules with DNA has the potential to modify the helical structure of the ds-DNA helix, leading to the transitions into various established or less characterized configurations. The three widely acknowledged DNA conformations are A-DNA, B-DNA, and Z-DNA.

Calf thymus DNA is a recognized example of a B-DNA (right-handed double helix), the most common form of DNA found in living cells since its structural discovery in 1953 (Watson and Crick, 1953; Kypr *et al.*, 2009). The binding of

various compounds to DNA can induce conformational changes, leading to the adoption of the A-form configuration (right-handed double helix, similar to the B-DNA but with a shorter and more compact helical structure), Z-form (left-handed double helical structure), triplexes (three-stranded DNA), quadruplexes (four-stranded DNA) and other lees characterized conformations (Rosu *et al.*, 2002; Chang, Chen and Hou, 2012).

The determination of the helical structure is conducted experimentally through CD spectra where variations in both sign and shape are observed on the spectra when comparing B-DNA with A-DNA or Z-DNA (Miyahara, Nakatsuji and Sugiyama, 2013). The CD spectrum of B-DNA is comprised of positive and negative bands within the 200-300 nm region due to the helical arrangement of the bases. Markers of B-DNA include four major bands at 210 nm (negative band), 220 nm (positive band), 245 nm (negative band) and 275 nm (positive band). The positive band at around 275 nm is attributed to base stacking while the negative band at 245 is attributed to the helicity of DNA. These bands shift depending on the structural arrangement of the DNA base pairs and direction of the helical structure within the DNA molecule.

The CD spectrum of A-DNA is characterized by a dominant positive band at around 260 nm and a negative band at 210 nm (Kypr *et al.*, 2009). The transition from B-form to A-form is fast and accompanied by an increase in the intensity of the 260 nm band and a decrease in the intensity of the band at 210 nm band. The CD spectrum of the Z-form DNA nearly shows an inversion of the B-form DNA with a negative band around 290 nm and a positive band at ~260 nm as well a deep negative band at 205 nm (Kypr *et al.*, 2009)

5.2.4.2 Experimental procedure

A stock solution of calf thymus DNA (ctDNA) was prepared in PBS (pH 7.4). The stock solutions of platinum complexes were prepared in acetonitrile and diluted using PBS to final test concentrations (25 µM, 50 µM, 100 µM and 200 µM). Acetonitrile was used instead to of DMSO to avoid spectroscopic interference since DMSO displays peaks at ~250 nm.

CD measurements were performed on a Jasco-1500 magnetic circular dichroism spectropolarimeter and carried out in triplicates using 1.0 cm quartz cuvettes. The ctDNA concentration was used at 100 µM and each spectrum was measured in triplicates from 200 - 500 nm and recorded at 37 °C. Platinum complexes [Pt(dmp)(L^1-κ*O*,*S*)]Cl and [Pt(dmp)(L^3-κ*O*,*S*)]Cl were prepared at four different concentrations of 25 µM, 50 µM, 100 µM and 200 µM resulting in respective ratios of [Pt(dmp)(L^n-κ*O*,*S*)]/[ctDNA] (r) equal to 0.25, 0.5, 1, and 2.

The CD spectra of platinum complexes were obtained by plotting the data points (Wavelength vs CD) on Origin software version 8. CD spectra of EB and HS were obtained for comparison purposes from separate experiments conducted in the lab.

5.2.5 Electronic absorption titration spectroscopy

5.2.5.1 Background and principle of the experiment

Electronic absorption spectroscopy is a sensitive and effective technique for determining the binding affinity of metal complexes to DNA. Changes in the electronic absorption spectrum are correlated to the type of interaction between the metal complex and DNA upon titration with DNA (Jomová *et al.*, 2019). Metal complexes normally display specific bands (peaks) within the UV-visible region of the absorption spectrum, this may be due to ligand-metal charge transfer, d-d transitions or π-π* transition within the complex. These bands are therefore used to characterize the complexes and changes in one of the bands can be monitored in the presence of the DNA molecule to determine the binding affinity.

A strong intercalative interaction between the metal complex and DNA is characterized by a decrease in the absorbance of the complex (hypochromism) and a shift to either a higher or lower wavelength (bathochromic/red or hypsochromic/blue shift) (Topala *et al*, 2014, Paitandi *et al*, 2018). Major or minor groove binding of metal complexes to DNA are characterized by an increase in the absorbance of the complex (hyperchromism). Significant changes in the spectrum are associated with the extent and strength of metal complex-DNA interactions and the binding affinity can be quantified by calculating the binding constant (K_b).

The DNA binding constant of metal complexes is calculated using the modified Benesi-Hilderbrand equation:

$$\frac{[DNA]}{\varepsilon_a - \varepsilon_f} = \frac{[DNA]}{\varepsilon_b - \varepsilon_f} + \frac{1}{K_b}\left(\varepsilon_b - \varepsilon_f\right) \qquad (Eq\ 3)$$

where ε_a, ε_f and ε_b is the molar extinction coefficient of the apparent absorbance at a given concentration of complex ($A_{observed}$/[Complex]), free metal complex, and fully bound metal complex respectively. The constant K_b is given by the ratio of the slope to intercept of a linear plot of [DNA]/ε_a-ε_b versus [DNA].

5.2.5.2 Experimental procedure

The electronic absorption spectra were recorded at 37 °C with a Specord 210® Plus (Analytik Jena) double-beam spectrometer equipped with a Scientific water-bath for temperature control during titration. Spectroscopic titrations were performed in triplicate in 1X Tris-buffered saline (pH 7.6) containing 10% (v/v) DMSO to solubilize the complexes. A stock solution of ctDNA was freshly prepared in 1X TBS and its concentration was established spectroscopically at 260 nm using a molar extinction coefficient of 13200 M^{-1} cm^{-1} per base pair. The titration involved the addition of increasing amounts of ctDNA (0 – 100 µM) into a fixed concentration (40 µM) of the platinum complex, [Pt(dmp)(L^1-κ*O*,*S*)]Cl in a quartz cuvette with a pathlength of 1 cm. The [Pt(dmp)(L^1-κ*O*,*S*)]Cl absorption band was monitored at 280 nm, spectral changes at 280 nm would indicate the interaction of the platinum complex with ctDNA. The DNA background absorbance was corrected by adding DNA to both sample and reference with each dilution. This ensured that there was no interference from the DNA band. The experiment was repeated at least three times.

5.3 Results and Discussion

5.3.1 Electrophoretic Mobility Shift Assay

The obtained results were compared with positive controls for DNA intercalation (ethidium bromide) and minor groove binding (Hoechst-33258) to analyze and make experimental predictions about the potential binding mode of platinum complexes (*Figure 5.1* and *Figure 5.2*).

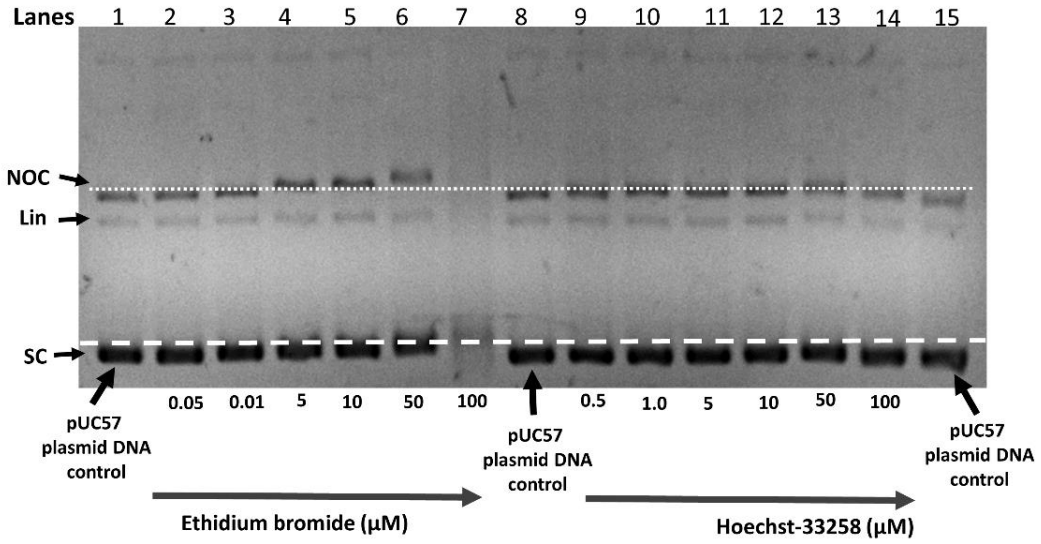


Figure 5.1: EMSA gel showing the effects of the interaction of Ethidium Bromide (EB) and Hoechst-33258 (HS) with pUC57 plasmid DNA. *Gel electrophoresis was performed on a 1.25% agarose gel prepared in TA buffer. Each lane was loaded with 12.5 ng of DNA in the presence of a range of EB and HS concentrations. Increasing concentrations of EB and HS (ranging from 0.05 to 100 μM)*

The gel image of pUC57 plasmid DNA in the absence and presence of increasing concentration of a DNA intercalator (EB) and minor groove binder (HS) showed a shift in DNA bands indicative of DNA interaction (*Figure 5.1*). It is important to note that upon migration on the gel matrix, pUC57 plasmid DNA separates into the supercoiled DNA (SC), nicked open circular DNA (NOC), linear DNA (Lin). The gel analysis shows the two minor bands of NOC and Lin, while the main band for SC migrated further down the gel (*Figure 5.1*).

Ethidium bromide (EB) showed retardation of the supercoiled SC DNA band with increasing concentration (*Figure 5.1, Lane 2-7*). The gel showed a dose-related retardation of supercoiled plasmid DNA from as little as 5 µM of EB compared to the control (*Figure 5.1, Lane 4*). As the concentration was increased to 50 µM, the retardation in the mobility of DNA bands became more prominent (*Figure 5.1, Lane 5-6).* At a higher concentration of 100 µM, complete precipitation of DNA was observed, indicated by a smear in Lane 7.

Hoescht-33258 (HS) showed minor changes in the mobility of DNA within a range of 0.05 – 50 µM relative to the control (*Figure 5.1, Lane 9-3*). A higher concentration of HS was required to affect the electrophoretic mobility of DNA since significant changes in the mobility of supercoiled and NOC DNA bands were observed at 100 µM (*Figure 5.1, Lane 14*). HS appeared to have enhanced the mobility of SC and NOC DNA bands at 100 µM. This is because HS tends to not significantly affect the size of the DNA as it binds outside the DNA duplex (Comings, 1975). The effect of platinum complexes on the electrophoretic mobility of DNA was compared to that of EB and HS as positive controls for DNA intercalation and groove binding.

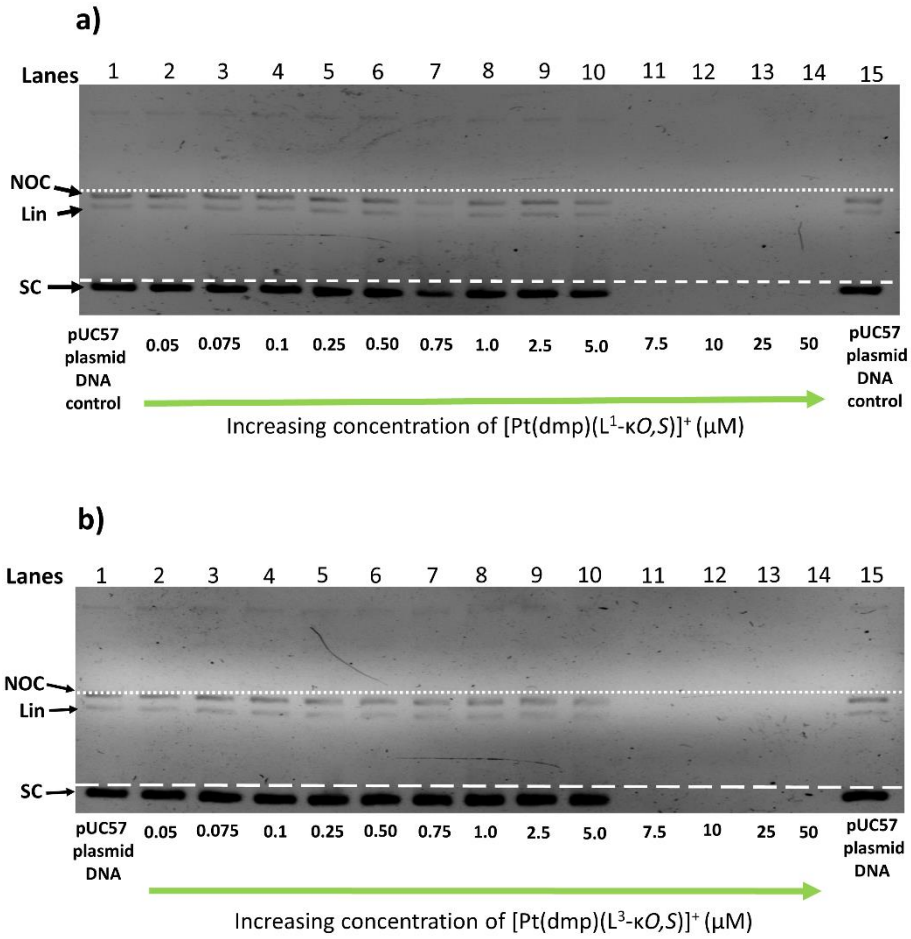


***Figure 5.2**: EMSA gel of pUC57 plasmid DNA in presence of increasing concentrations of a) [Pt(dmp)(L[1]-κO,S)]Cl and b) [Pt(dmp)(L[3]-κO,S)]Cl (0.05 - 50 μM).* *Each lane was loaded with 12.5 ng of pUC57 DNA with the complexes dissolved in TA buffer. The plasmid bands were visualized with ethidium bromide.*

A shift in the electrophoretic mobility of pUC57 plasmid DNA was observed in the presence of platinum complexes, indicative of an interaction with DNA. The observed gel images showed an enhancement in the mobility of the supercoiled band in the presence of [Pt(dmp)(L^1-κ*O,S*)]Cl and [Pt(dmp)(L^3-κ*O,S*)]Cl respectively compared to the control which contained free pUC57 plasmid DNA (*Figure 5.2 a and b*). The DNA-interaction was observed at a concentration of 0.25 μM for [Pt(dmp)(L^1-κ*O,S*)]Cl and 0.075 μM for [Pt(dmp)(L^3-κ*O,S*)]Cl respectively. This indicated that a very low concentration of each platinum complex was required to affect the structure of the DNA enough to enhance its mobility.

Therefore, this experiment suggested that both platinum complexes were likely to act as groove binders, similar to HS, which also showed an enhancement of DNA mobility, albeit at a higher concentration (100 μM).

The complex; [Pt(dmp)(L^3-κ*O,S*)]Cl showed an enhanced mobility of DNA at significantly lower concentrations compared to [Pt(dmp)(L^1-κ*O,S*)]Cl, indicating a higher binding affinity of the former complex for DNA. This may be attributed to the structural differences in the acylthiourea ligands within the complexes, where the smaller tertiary butyl substituent (HL^3) enhances binding over the bulkier aromatic ring benzoyl substituent (HL^1). The hydrophobic nature of the benzoyl group in HL^1 is thought to hinder optimal interaction with the negatively charged DNA backbone, while the less bulky tertiary butyl group is more favourable for external DNA binding.

Concentrations of [Pt(dmp)(L^1-κ*O,S*)]Cl and [Pt(dmp)(L^3-κ*O,S*)]Cl above 5 μM resulted in complete disappearance of the DNA bands. This was possibly due to massive cleavage of the DNA, the plasmid DNA running off the gel or precipitation for [Pt(dmp)(L^1-κ*O,S*)]Cl and [Pt(dmp)(L^3-κ*O,S*)]Cl respectively (*Figure 5.1, Lane 11-14*). No additional cleavage products were noted on the gels as the intensities of the two minor bands (NOC and Lin) did not increase with an increase in concentration of the complexes.

It is important to note that this experiment does not take into account the complexities of cells as it was conducted directly using DNA solution in the presence of test complexes.

5.3.2 DNA thermal degradation

The difference between the melting temperature of free ctDNA (T_{mDNA}) and the melting temperature of ctDNA in the presence of the platinum complexes ($T_{mDNA\text{-}complex}$) was evaluated and compared to the corresponding differences observed with the positive controls EB (intercalator) and HS (groove binder).

$$\Delta T_m = T_{mDNA-complex} - T_{mDNA} \qquad (Eq\ 4)$$

A smaller change in T_{mDNA} (less than 5 ℃) has been previously correlated with electrostatic interactions and groove binding whereas a larger change, typically falling within the range of 5 to 10 ℃ has been considered to be evidence of intercalation.

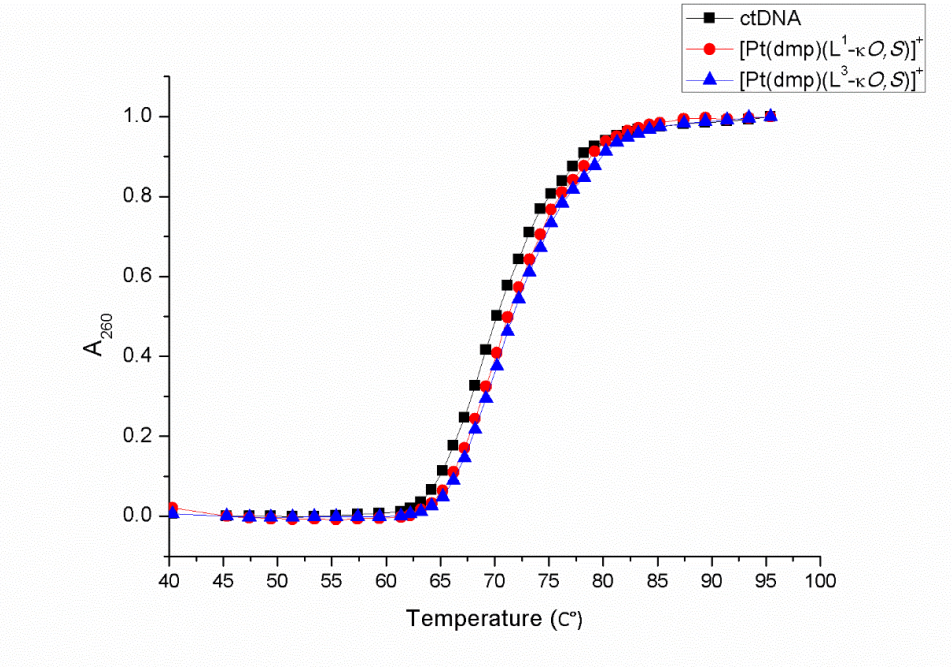


***Figure 5.3**: **Melting curves of ctDNA in the absence and presence of [Pt(dmp)(L^1-κO,S)]Cl and [Pt(dmp)(L^3-κO,S)]Cl complexes**. Fixed concentrations of 100 µM ctDNA and 2.5 µM of each platinum complex were prepared in TA buffer (pH 7.6) and subjected to increasing temperatures between 25°C and 95 °C with the absorbance measured at 260 nm.*

***Table 5.1: Melting temperature of ctDNA (*100 µM*) in the absence and presence* 2.5 µM *[Pt(dmp)(L^1-κO,S)]Cl and [Pt(dmp)(L^3-κO,S)]Cl* respectively.**

DNA denaturation samples	T_m (℃)	ΔT
ctDNA	70.2	-
ctDNA-[Pt(dmp)(L^1-κ*O,S*)]Cl	71.2	1.0
ctDNA-[Pt(dmp)(L^3-κ*O,S*)]Cl	71.7	1.5

DNA thermal degradation analysis showed an increase in the melting temperature of ctDNA from 70.2 °C to 71.2 °C upon the addition of 2.5 μM [Pt(dmp)(L^1-κ*O,S*)]Cl (*Figure 5.3; Table 5.1*). The +1.0 °C increase was indicative of the strengthening of the hydrogen bonds between the DNA strands since more heat energy was required to disrupt these bonds. The melting temperature for ctDNA in the presence of 2.5 μM [Pt(dmp)(L^3-κ*O,S*)]Cl increased to 71.7 °C, showing an increase of 1.5°C from free ctDNA alone. This +1.5 °C increase also indicated a strengthening of the hydrogen bonds between the DNA base pairs upon interaction with the [Pt(dmp)(L^3-κ*O,S*)]Cl complex.

When comparing these findings with results obtained for EB and HS in separate experiments conducted within the lab, a temperature change of +6.78 °C and +0.57 °C at a concentration of 25 μM respectively aligns with the proposed binding mode, consistent with observations from gel electrophoresis.

This data supplies additional evidence that [Pt(dmp)(L^1-κ*O,S*)]Cl and [Pt(dmp)(L^3-κ*O,S*)]Cl act as groove binders. The larger change in the melting temperature of DNA, exceeding 5 °C, is indicative of intercalation, whereas smaller changes below 5 °C have been previously associated with groove binding. Similar to the gel electrophoresis results, [Pt(dmp)(L^3-κ*O,S*)]Cl demonstrated an increased binding affinity to DNA compared to [Pt(dmp)(L^1-κ*O,S*)]Cl, as evidenced by a the smaller increase of 0.5 °C in ΔT_m.

5.3.3 Circular dichroism

The CD spectra of free ctDNA and ctDNA in the presence of the two platinum complexes at 25, 50, 100 and 200 μM was measured. The CD spectrum of ctDNA alone showed a B-form configuration with four peaks within the 200 nm - 300 wavelength (*Figure 5.4*, black line). These peaks were observed at 210 nm (negative), 220 nm (positive), 246 nm (negative) and 274 nm (positive) which align with the literature-reported bands at 245 nm (negative) and 275 nm (positive). In the presence of 25 μM [Pt(dmp)(L^1-κ*O,S*)]Cl complex, the CD spectra displayed four peaks with the same sign at 210 nm (negative), 222 nm (positive), 247 nm (negative), and 275 nm (positive) (*Figure 5.4, red line*).

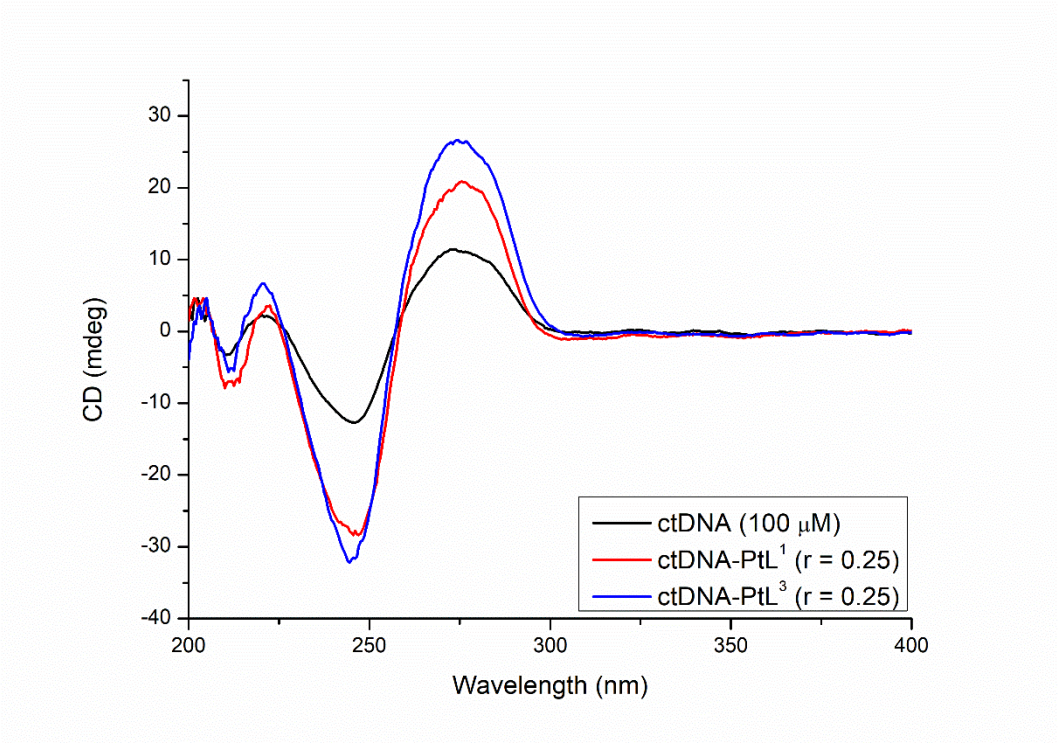


Figure 5.4: CD spectrum of ctDNA (100 μM) and the effect of the platinum complexes on the spectrum. *ctDNA in the absence and presence of 25 μM [Pt(dmp)(L^1-κO,S)]Cl (red line) and [Pt(dmp)(L^3-κO,S)]Cl (blue line).*

Similarly, the [Pt(dmp)(L^3-κ*O*,*S*)]Cl complex showed peaks at 210 nm (negative), 220 nm (positive), 245 nm (negative), and 274 nm (positive) respectively (*Figure 5.4, blue line*).

Analysis of these spectra indicated that both [Pt(dmp)(L^1-κ*O*,*S*)]Cl and [Pt(dmp)(L^3-κ*O*,*S*)]Cl complexes did not induce significant changes in the B-conformation of DNA. The major peaks in the CD spectra were maintained, with minor shifts that were not substantial enough to suggest a change in DNA conformation. Thus, it can be concluded that the DNA retained its B-conformation following interaction with both platinum complexes.

Previous studies have indicated that electrostatic interactions and groove binding with DNA have a minimal impact on the position and intensity of the bands associated with base stacking (275 nm) and helicity (245 nm). However, an

intercalative interaction tends to enhance the intensities of both bands (Paitandi *et al.*, 2018)

In the case of platinum complexes; [Pt(dmp)(L^1-κ*O,S*)]Cl and [Pt(dmp)(L^3-κ*O,S*)]Cl examined in this study, an increase in the intensities of both the 245 nm and 275 bands was observed at a concentration of 25 µM (complex: DNA r = 0.25). This suggests that there was an intercalative interaction occurring between the complexes and base pairs of ctDNA at this concentration. However, as the concentration of the complexes was increased to 50 µM, 100 µM, and 200 µM, with complex/DNA ratios of 0.5, 1, and 2) respectively, DNA precipitation occurred, resulting in a significant reduction in the intensity of the 275 nm peak (Erxleben, 2017).

The presence of an induced circular dichroism (ICD) signal within the optical transition region of achiral metal complexes serves as evidence for DNA binding (Hong *et al.*, 2018). Intercalators typically exhibit negative induced CD signals or very small positive signals upon binding to DNA while groove binders are known to result in significant positive induced CD signal (Rodger, 2013).

The absorption maxima of unbound [Pt(dmp)(L^1-κ*O,S*)]Cl was observed at 280 nm with a small negative band at a complex-to-DNA ratio of 0.25 (*Figure 5.4*, red). However, as the concentrations of the complex were increased (r = 0.5, 1, 2), a more prominent negative induced CD signal appeared at 280 nm, correlating to intercalative binding (*Figure C1*, *Appendix*). The other complex, [Pt(dmp)(L^3-κ*O,S*)]Cl, did not show a distinctive induced band. Instead, [Pt(dmp)(L^3-κ*O,S*)]Cl caused a greater increase in the intensity of the DNA band compared to [Pt(dmp)(L^1-κ*O,S*)]Cl complex at r = 0.25 (25 µM), indicative of stronger interaction (*Figure 5.4*, blue line).

5.3.4 Electronic absorption titration spectroscopy

The binding affinity of the complex [Pt(dmp)(L^1-κ*O,S*)]Cl to DNA was investigated using UV-vis electronic absorption titration spectroscopy. A fixed concentration of the complex (40 µM) was titrated by gradually increasing the

amount of ctDNA (0 – 100 µM). The concentration of ctDNA was established spectroscopically at a wavelength of 260 nm using a molar extinction coefficient of 13200 M^{-1} cm^{-1} per base pair.

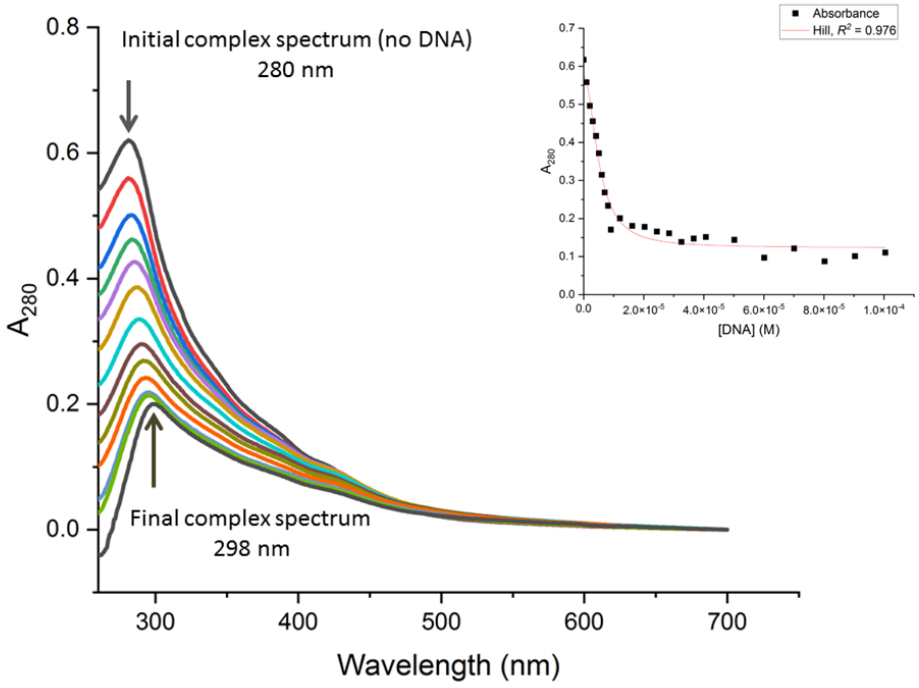


***Figure 5.5**: **Electronic absorption spectrum of [Pt(dmp)(L¹-κO,S)]Cl complex in the absence and presence of increasing concentrations of ctDNA.** The spectra were recorded at a fixed concentration of 40 µM for the complex, while ctDNA concentrations ranged from 0 to 100 µM at 37˚C in 1X Tris Buffered Saline containing. The plot illustrates a hypochromic shift (insert: decreasing absorbance) and bathochromic shift (shift to higher wavelengths from 280 to 298 nm) of the complexes with increasing [ctDNA].*

The absorption spectrum of [Pt(dmp)(L^1-κ*O*,*S*)]Cl showed maxima band at 280 nm which rapidly decreased in intensity upon increasing concentration of ctDNA (*Figure 5.5*). Furthermore, a small shift to a higher wavelength of 298 nm was observed. These changes were classified as a hypochromic and bathochromic/red-shift respectively, indicative of an intercalative interaction between the DNA and [Pt(dmp)(L^1-κ*O*,*S*)]Cl complex. A red shift is indicative of the stabilization of the DNA duplex.

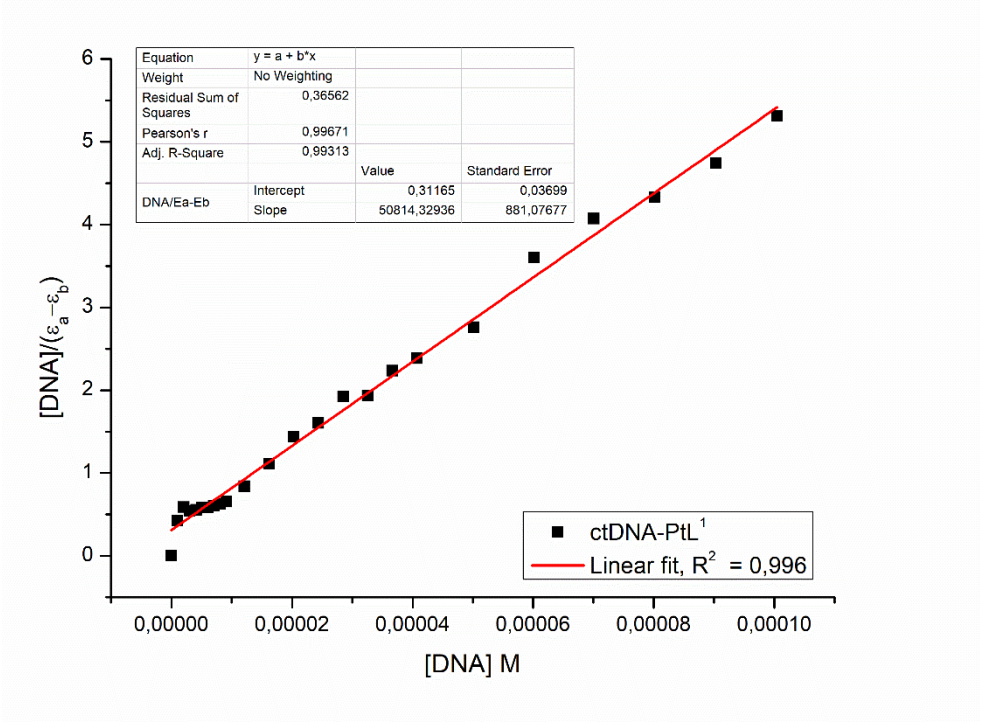


***Figure 5.6**: Representative plot of [DNA] versus [DNA]/(ε_a − ε_f) for the titration of the [Pt(dmp)(L^1-κO,S)]Cl complex with ctDNA.*

The DNA binding affinity of the [Pt(dmp)(L^1-κ*O*,*S*)]Cl complex to ctDNA was explored by determining the intrinsic binding constant (K_b) value from a plot of [DNA] versus [DNA]/ε_a-ε_f using eq 3 (*Figure 5.6*). The binding constant was calculated by the ratio of the slope ($1/\varepsilon_b$-ε_f) to intercept ($1/K_b(\varepsilon_b$-ε_f) and was found to be of 2.06 x 10^5 M^{-1}. The K_b value was relatively high, within the same order of magnitude as the classical intercalators such as ethidium bromide (1.23 x10^5) and methylene blue (3.3 x 10^5), indicative of a strong binding affinity to ctDNA (Garbett, Hammond and Graves, 2004; Karami *et al.*, 2018; Rohini *et al.*, 2018).

The analysis of the other platinum complex, [Pt(dmp)(L^3-κ*O*,*S*)]Cl could not be attained due to solubility issues as the complex precipitated in the buffer solution during the experiment, thus a uniform spectrum was not maintained.

5.4 In summary

The DNA binding mode of two platinum complexes [Pt(dmp)(L^1-κ*O*,*S*)]Cl and [Pt(dmp)(L^3-κ*O*,*S*)]Cl was investigated using electrophoretic mobility shift assay, DNA thermal degradation analysis, circular dichroism and electronic absorption titration. The obtained results indicated that the complexes interact with the DNA molecule via two possible binding modes; groove binding and intercalation. The electrophoretic mobility shift assay showed enhancement of DNA mobility upon exposure to increasing concentrations of [Pt(dmp)(L^1-κ*O*,*S*)]Cl and [Pt(dmp)(L^3-κ*O*,*S*)]Cl complexes; with significant changes observed at low concentrations of 0.25 μM and 0.075 μM respectively. This observation was consistent with that of the well-known DNA minor groove binder, Hoechst-32258, which showed significant enhanced mobility of the plasmid DNA at higher concentrations, 100 μM, indicating the superior activity of the platinum complex by showing a similar shift at much lower concentrations. This observation indicated that both platinum complexes act as groove binders at low concentrations (<5 μM).

Thermal degradation analysis showed an increase of 1.0 °C and 1.5 °C in the melting temperature of ctDNA in the presence of [Pt(dmp)(L^1-κ*O*,*S*)]Cl and [Pt(dmp)(L^3-κ*O*,*S*)]Cl complexes respectively. This small change was indicative of groove binding, as it does not cause major changes in the size and length of DNA molecule.

Circular dichroism confirmed that the structure of B-DNA was maintained in the presence of both platinum complexes. An increase in the intensity of the 260 nm DNA band at a complex/DNA ratio of 0.25 indicated that the complexes had stabilized the DNA base pairs through intercalation.

The intrinsic binding constant (K_b) value for [Pt(dmp)(L^1-κ*O*,*S*)]Cl determined by electronic absorption titration was found to be $2.06 \times 10^5\ M^{-1}$, suggestive of a strong binding affinity to ctDNA, comparable to that of an intercalator, ethidium bromide. A decrease in absorbance at 280 nm for [Pt(dmp)(L^1-κ*O*,*S*)]Cl band upon titration (hypochromic shift) was indicative of intercalation. The binding constant for [Pt(dmp)(L^3-κ*O*,*S*)]Cl was not obtained due to solubility issues. The binding affinity of platinum complexes was presumed to be influence by the structural

variations on the ancillary ligands (*N*,*N*-dibutyl-*N'*-acylthiourea), since the complex bearing HL^3 (a small alkyl/tertiary butyl substituent on the R^1) showed stronger binding compared to the complexes bearing HL^1 (an aromatic/benzoyl substituent on R^1).

Chapter 6: Summary and Conclusion

While platinum-based drugs like cisplatin, carboplatin, and oxaliplatin have made significant contributions to cancer treatment, their drawbacks, characterized by poor stability in aqueous solutions and severe adverse effects resulting from their covalent binding to DNA, prompted a search for of alternative platinum complexes with potential non-covalent DNA interactions. This study aimed to synthesize, characterize and evaluate the anticancer activity of platinum complexes with the formula; [Pt(diimine)(L^n-κ*O*,*S*)]Cl, where the disubstituted acylthiourea ligands coordinate in a bidentate fashion to the platinum center, through the sulfur and oxygen donor atoms. The anticancer activity was evaluated in two lung and a colorectal cancer cell lines. In addition to this, the effect of active platinum complexes on the mode of cell death, apoptotic protein profile and interaction with DNA was evaluated.

6.1 Synthesis and characterization of platinum complex; [Pt(diimine)(*N*,*N*-dialky-*N'*-acylthiourea)]Cl

Disubstituted acylthiourea ligands were successfully synthesized following the previously established one-pot synthesis method where an acyl chloride was added in dissolved potassium thiocyanate, followed by dropwise addition of an appropriate diamine ligand in anhydrous acetone. A total of nine acylthiourea ligand were successfully synthesized and characterized with yields ranging between 62 - 96%.

A range of first and second generation platinum complexes bearing both the unsubstituted 1,10-phenanthroline as well as 5,6-dimethyl-1,10-phenanthroline were successfully synthesized by reacting the prepared platinum precursor, $PtCl_2$(diimine) with the appropriate *N*,*N*-alkyl-*N'*-acylthiourea in acetonitrile, in the presence of a weak base. The synthesis of complexes bearing -arylthiourea ligand, where R^1 is an aromatic group such as benzoyl (HL^1, HL^5 and HL^8) or 1-napthoyl

(HL^4 and HL^7) was achieved using a 5% binary water/acetonitrile solvent system. The synthesis followed a stepwise reaction method, where the disubstituted thiourea ligand was carefully added dropwise into a dilute suspension of the appropriate metal precursor in excess sodium acetate base. This facilitated *in situ* deprotonation of the acylthiourea ligand, enabling coordination to the platinum center through the sulfur and oxygen donor atoms. As a result, the desired cationic [Pt(diimine)(L^n-κ*O*,*S*)]Cl complex was formed as the major product with high yields ranging from 67% to 92%.

The first-generation complexes included the three biologically active chelate [Pt(dmp)(L^1-κ*O*,*S*)]Cl, [Pt(dmp)(L^2-κ*O*,*S*)]Cl and [Pt(dmp)(L^3-κ*O*,*S*)]Cl. The second generation of this class of square planar platinum(II) complexes was prepared with a variations on the alkyl chain (diethyl) and acyl group (1-napthoyl, pivaloyl, benzoyl) of the *N*,*N*-dialkyl-*N*'-acylthiourea ligands against dmp and phen ligands.

The chemical structures of both ligands and complexes were determined using a comprehensive set of characterization techniques. ^{1}H and ^{13}C NMR spectroscopy provided insights into the molecular composition and connectivity of the compounds. Infrared spectroscopy was employed to identify functional groups based on their vibrational frequencies, offering valuable information about the chemical bonds present. Mass spectrometry allowed for precise determination of molecular weights and confirmed the identity of the synthesized compounds. Elemental analysis further contributed to the characterization, providing quantitative data on the elemental composition of the ligands and complexes. Collectively, these characterization techniques ensured a thorough and accurate understanding of the chemical structures of the synthesized compounds.

6.2 Platinum complexes are cytotoxic to lung and colorectal cancer cells

A series of first generation [Pt(diimine)(L^n-κ*O*,*S*)]Cl complexes were evaluated for their cytotoxicity at 50 µM and 5 µM using an MTT cell viability assay against

H1975, A549 and HT-29 cells and three active complexes were identified. The IC_{50} values of three most active platinum complexes; [Pt(dmp)(L^1-κ*O*,*S*)]Cl, [Pt(dmp)(L^2-κ*O*,*S*)]Cl and [Pt(dmp)(L^3-κ*O*,*S*)]Cl was thereafter determined alongside that of the positive control, cisplatin. The IC_{50} values were in the low micromolar range 0.68 -2.28 μM indicating that these complexes would be active at clinically relevant concentrations. HT-29 cells were the most sensitive compared to the H1975 and A549 cells.

6.3 Platinum complexes induce intrinsic apoptosis in HT-29 and H1975 and A549 cells

The cytotoxicity of platinum complexes was investigated in HT-29, H1975 and A549 cells. Evaluation of the effect of platinum complexes on the cell morphology of these cancer cells showed changes indicative of cell stress and apoptotic cell. These included the formation of cytoplasmic vacuoles as well as nuclear fragmentation.

The translocation of phosphatidylserine on the cell outer cell membrane after treatment with platinum complexes was indicative of early and late stages of apoptotic cell death across the three-cancer cell line. Furthermore, the moderate increase in caspase-3 activity across the three cancer cell lines confirmed that apoptosis was the main mode of cell death.

Increased ROS generation after treatment with platinum complexes indicated the complexes induced oxidative stress. The lack of caspase-8 activity suggested that cell death does not occur via the extrinsic pathway, while the loss of mitochondrial membrane potential (MMP) indicated that intrinsic apoptosis was induced. Since oxidative stress causes damage to membranes, DNA and proteins, the three active platinum complexes where therefore confirmed to initiate cell death via a stress-induced intrinsic apoptotic pathway.

Further analysis through immunofluorescence assays showed an increase in the protein expression of HO-1, which provided further evidence of oxidative stress induction by platinum complexes while an increase in the nuclear expression of p21

protein indicated DNA damage as the trigger for intrinsic apoptosis, also highlight DNA as the molecular target.

Further investigation into the increased nuclear expression of HO-1 is required since its implications on tumour progression, chemoresistance, and the induction of cell death remains unclear.

6.4 The effect of active platinum complexes on the expression of apoptosis-associated proteins in HT-29, A549 and H1975 cells

The proteome arrays provided evidence that platinum complexes; [Pt(dmp)(L^1-κ*O*,*S*)]Cl and [Pt(dmp)(L^3-κ*O*,*S*)]Cl significantly increased the expression level HO-1/HMOX1/HSP32 expression in HT-29 cells, correlating with the results observed with immunofluorescence. Increased HO-1 expression further confirmed the induction of oxidative stress by platinum complexes in these cancer cells lines, which was showed superior response compared to cisplatin.

An increased expression level of the death receptor TRAIL R2/DR5 suggests potential activation of both extrinsic and intrinsic apoptotic pathways, despite the absence of caspase-8 activation, warranting further investigation.

Claspin, a cell cycle protein associated with protecting cells from replication stress and promoting tumour progression, emerged as a potential target. Cisplatin increased claspin expression in HT-29 cells, while both platinum complexes suppressed its expression, suggesting their superior role in inhibiting tumour progression compared to cisplatin.

A major increase in the expression level of p21 was observed in A549 cells, aligning with a higher caspase-3/7 activity and increased apoptosis observed in cell morphology evaluation of this cell line compared to H1975 and HT-29 cells. In all three cancer cell lines evaluated (HT-29, A549, and H1975), platinum complexes led to a decrease of anti-apoptotic proteins that inhibit apoptosis, specifically survivin and HSP70, providing evidence of their involvement in promoting cell death through apoptosis.

6.5 DNA Binding Studies

The interaction of the two most potent platinum complexes, [Pt(dmp)(L^1-κ*O*,*S*)]Cl and [Pt(dmp)(L^3-κ*O*,*S*)]Cl, with the DNA target molecule was investigated using multiple techniques: Electrophoretic mobility shift assay (EMSA), DNA melting temperature analysis and spectroscopic methods including circular dichroism (CD) and electronic absorption titration spectroscopy.

EMSA gels showed enhanced mobility for both complexes across the gel suggestive of groove binding, indicating interaction with DNA. DNA melt curves showed a slight increase of +1℃ and 1.5℃ for [Pt(dmp)(L^1-κ*O*,*S*)]Cl and [Pt(dmp)(L^3-κ*O*,*S*)]Cl, respectively, suggesting groove-binding rather than intercalation.

Circular dichroism indicated that the complexes did not alter the B-DNA confirmation. However, an increase in DNA band intensity at a complex/DNA ratio of 0.25 suggested stabilization of DNA base pairs through intercalation. [Pt(dmp)(L^3-κ*O*,*S*)]Cl demonstrated superior binding affinity throughout the DNA binding techniques employed, indicating stronger binding compared to [Pt(dmp)(L^1-κ*O*,*S*)]Cl. The intrinsic binding constant (K_b) for [Pt(dmp)(L^1-κ*O*,*S*)]Cl, determined by electronic absorption titration spectroscopy, was found to be 2.06×10^5 M^{-1}, indicative of robust binding affinity to ctDNA comparable to that of the DNA intercalator, ethidium bromide.

6.6 Conclusion

This study identified [Pt(dmp)(L^1-κ*O*,*S*)]Cl, [Pt(dmp)(L^2-κ*O*,*S*)]Cl, and [Pt(dmp)(L^3-κ*O*,*S*)]Cl as active complexes against lung cancer cell lines (H1975, A549) and colorectal cancer cell line (HT-29), with IC_{50} values showing superior activity compared to cisplatin. The low micromolar IC_{50} values suggest the potential for achieving complete cell death at clinically relevant and acceptable concentration ranges. These platinum complexes activated the intrinsic apoptotic pathway, supported by evidence confirming DNA damage and oxidative stress, leading to mitochondrial membrane disruption and activation of caspase-3/7. This resulted in morphological changes consistent with apoptotic cell death, mainly

indicated by nuclear fragmentation and chromatin condensation. The complexes significantly reduced the expression of the anti-apoptotic protein survivin across the three cancer cell lines and increased the levels of the pro-apoptotic protein p21, serving as inducers of apoptotic cell death. Studies confirming the high-affinity interaction with DNA indicated that DNA is the target of these platinum complexes.

6.7 Future work

Future investigations will focus on evaluating the efficacy of second-generation [Pt(dmp)(L^n-κ*O*,*S*)]Cl complexes. Building on the observed higher DNA binding affinity of [Pt(dmp)(L^3-κ*O*,*S*)]Cl compared to [Pt(dmp)(L^1-κ*O*,*S*)]Cl, modifications in the alkyl chain of disubstituted acylthiourea ligands, while maintaining pivaloyl/tertiary butyl on the acyl group (R^1), will be explored. Additionally, variations such as incorporating sugar moieties or amino acids instead of long alkyl chains and substituting chlorine as the counterion will be investigated to enhance aqueous solubility and cellular uptake.

Further studies will involve stability tests, alternative methods to obtain crystalline forms of the complexes and the integration of drug delivery systems such as nanoparticles or polymers. These approaches aim to target cancer cells and not normal cells. In-depth investigations will also include determining the selectivity index in non-cancer cell lines. In addition to this, the effect of active platinum complexes on caspase-9 activation will be evaluated to further validate intrinsic apoptosis as the mechanism of cell death induced in lung and colorectal cancer cells.

In vivo studies in a comprehensive animal model (i.e nude mice) will provide insights into safety, toxicity profiles and pharmacokinetics/pharmacodynamics, addressing limitations associated with *in vitro* studies and accounting for mammalian body responses. These findings are critical for future applications.

In vitro combination studies with HO-1 inhibitors will elucidate the role of (HO-1) in response to cell stress and the validation of complex effects on protein expression levels will be carried out through western blot analyses.

To further understand complex-DNA interactions, *in silico* studies will be employed to confirm the DNA binding mode under physiological conditions. Competition studies with intercalators and groove-binders will validate the mechanism of action.

References

Abdal Dayem, A. *et al.* (2017) 'The Role of Reactive Oxygen Species (ROS) in the Biological Activities of Metallic Nanoparticles', *International Journal of Molecular Sciences*, 18(1), p. 120. Available at: https://doi.org/10.3390/ijms18010120.

Abdolmaleki, S. *et al.* (2023) 'Cytotoxicity and mechanism of action of metal complexes: An overview', *Toxicology*, 492, p. 153516. Available at: https://doi.org/10.1016/j.tox.2023.153516.

Adan, A., Kiraz, Y. and Baran, Y. (2016) 'Cell Proliferation and Cytotoxicity Assays', *Current Pharmaceutical Biotechnology*, 17(14), pp. 1213–1221. Available at: https://doi.org/10.2174/1389201017666160808160513.

Akhtar, S. *et al.* (2020) 'ROS-induced oxidative damage in lymphocytes ex vivo/in vitro from healthy individuals and MGUS patients: protection by myricetin bulk and nanoforms', *Archives of Toxicology*, 94(4), pp. 1229–1239. Available at: https://doi.org/10.1007/s00204-020-02688-4.

Aleksić, M.M. and Kapetanović, V. (2014) 'An overview of the optical and electrochemical methods for detection of DNA - drug interactions', *Acta Chimica Slovenica*, 61(3), pp. 555–573.

Alessio, E. and Messori, L. (2019) 'NAMI-A and KP1019/1339, Two Iconic Ruthenium Anticancer Drug Candidates Face-to-Face: A Case Story in Medicinal Inorganic Chemistry', *Molecules*, 24(10), p. 1995. Available at: https://doi.org/10.3390/molecules24101995.

Alfadul, S.M. *et al.* (2023) 'Metal-Based Anticancer Complexes and p53: How Much Do We Know?', *Cancers*, 15(10), p. 2834. Available at: https://doi.org/10.3390/cancers15102834.

Ali, A.A., McCrudden, C.M. and McCarthy, H.O. (2017) 'Evaluation of the Impact of Nitric Oxide on Resistance to Platinum-Based Chemotherapeutics', in *Nitric Oxide as a Chemosensitizing Agent*. Elsevier, pp. 71–90. Available at: https://doi.org/10.1016/B978-0-12-811020-1.00005-3.

Allard, J.B. and Duan, C. (2018) 'IGF-Binding Proteins: Why Do They Exist and Why Are There So Many?', *Frontiers in Endocrinology*, 9, p. 117. Available at: https://doi.org/10.3389/fendo.2018.00117.

Almaqwashi, A.A. *et al.* (2016) 'Mechanisms of small molecule–DNA interactions probed by single-molecule force spectroscopy', *Nucleic Acids Research*, 44(9), pp. 3971–3988. Available at: https://doi.org/10.1093/nar/gkw237.

Anaya-Eugenio, G.D. *et al.* (2020) 'Tumor suppressor p53 independent apoptosis in HT-29 cells by auransterol from Penicillium aurantiacobrunneum',

Biomedicine & Pharmacotherapy, 127, p. 110124. Available at: https://doi.org/10.1016/j.biopha.2020.110124.

Atale, N. *et al.* (2014) 'Cell-death assessment by fluorescent and nonfluorescent cytosolic and nuclear staining techniques', *Journal of Microscopy*, 255(1), pp. 7–19. Available at: https://doi.org/10.1111/jmi.12133.

Azenha, D., Lopes, M.C. and Martins, T.C. (2017) 'Claspin functions in cell homeostasis—A link to cancer?', *DNA Repair*, 59, pp. 27–33. Available at: https://doi.org/10.1016/j.dnarep.2017.09.002.

Bagnoli, M., Canevari, S. and Mezzanzanica, D. (2010) 'Cellular FLICE-inhibitory protein (c-FLIP) signalling: A key regulator of receptor-mediated apoptosis in physiologic context and in cancer', *The International Journal of Biochemistry & Cell Biology*, 42(2), pp. 210–213. Available at: https://doi.org/10.1016/j.biocel.2009.11.015.

Baskar, R. *et al.* (2012) 'Cancer and Radiation Therapy: Current Advances and Future Directions', *International Journal of Medical Sciences*, 9(3), pp. 193–199. Available at: https://doi.org/10.7150/ijms.3635.

Beere, H.M. *et al.* (2000) 'Heat-shock protein 70 inhibits apoptosis by preventing recruitment of procaspase-9 to the Apaf-1 apoptosome', *Nature Cell Biology*, 2(8), pp. 469–475. Available at: https://doi.org/10.1038/35019501.

Ben-Eltriki, M. *et al.* (2023) 'Pharmacological Significance of Heme Oxygenase 1 in Prostate Cancer', *Current Issues in Molecular Biology*, 45(5), pp. 4301–4316. Available at: https://doi.org/10.3390/cimb45050273.

Bianco, J.N. *et al.* (2019) 'Overexpression of Claspin and Timeless protects cancer cells from replication stress in a checkpoint-independent manner', *Nature Communications*, 10(1), p. 910. Available at: https://doi.org/10.1038/s41467-019-08886-8.

Boros, E., Dyson, P.J. and Gasser, G. (2020) 'Classification of Metal-Based Drugs according to Their Mechanisms of Action', *Chem*, 6(1), pp. 41–60. Available at: https://doi.org/10.1016/j.chempr.2019.10.013.

Bouillet, P. and Strasser, A. (2002) 'BH3-only proteins — evolutionarily conserved proapoptotic Bcl-2 family members essential for initiating programmed cell death', *Journal of Cell Science*, 115(8), pp. 1567–1574. Available at: https://doi.org/10.1242/jcs.115.8.1567.

Bradford, M.M. (1976) 'A rapid and sensitive method for the quantitation of microgram quantities of protein utilizing the principle of protein-dye binding', *Analytical Biochemistry*, 72(1–2), pp. 248–254. Available at: https://doi.org/10.1016/0003-2697(76)90527-3.

Brahmkhatri, V.P., Prasanna, C. and Atreya, H.S. (2015) 'Insulin-like growth factor system in cancer: novel targeted therapies', *BioMed Research*

International, 2015, p. 538019. Available at: https://doi.org/10.1155/2015/538019.

Brauchle, E. *et al.* (2014) 'Cell death stages in single apoptotic and necrotic cells monitored by Raman microspectroscopy', *Scientific Reports*, 4(1), p. 4698. Available at: https://doi.org/10.1038/srep04698.

Brodie, C.R., Collins, J.G. and Aldrich-Wright, J.R. (2004) 'DNA binding and biological activity of some platinum(ii) intercalating compounds containing methyl-substituted 1,10-phenanthrolines', *Dalton Transactions*, (8), p. 1145. Available at: https://doi.org/10.1039/b316511f.

Brown, A., Kumar, S. and Tchounwou, P.B. (2019) 'Cisplatin-Based Chemotherapy of Human Cancers', *Journal of Cancer Science & Therapy*, 11(4), p. 97.

Bucevičius, J., Lukinavičius, G. and Gerasimaitė, R. (2018) 'The Use of Hoechst Dyes for DNA Staining and beyond', *Chemosensors*, 6(2), p. 18. Available at: https://doi.org/10.3390/chemosensors6020018.

Cai, C. *et al.* (2021) '*Claspin* Overexpression Promotes Tumor Progression and Predicts Poor Clinical Outcome in Prostate Cancer', *Genetic Testing and Molecular Biomarkers*, 25(2), pp. 131–139. Available at: https://doi.org/10.1089/gtmb.2020.0226.

Carneiro, B.A. and El-Deiry, W.S. (2020) 'Targeting apoptosis in cancer therapy', *Nature Reviews Clinical Oncology*, 17(7), pp. 395–417. Available at: https://doi.org/10.1038/s41571-020-0341-y.

Caruso Bavisotto, C. *et al.* (2020) 'Hsp60 Post-translational Modifications: Functional and Pathological Consequences', *Frontiers in Molecular Biosciences*, 7, p. 95. Available at: https://doi.org/10.3389/fmolb.2020.00095.

Chang, Y.-M., Chen, C.K.-M. and Hou, M.-H. (2012) 'Conformational Changes in DNA upon Ligand Binding Monitored by Circular Dichroism', *International Journal of Molecular Sciences*, 13(3), pp. 3394–3413. Available at: https://doi.org/10.3390/ijms13033394.

Chen, L., Zeng, Y. and Zhou, S.-F. (2018) 'Role of Apoptosis in Cancer Resistance to Chemotherapy', in Y. Tutar (ed.) *Current Understanding of Apoptosis*. Rijeka: IntechOpen. Available at: https://doi.org/10.5772/intechopen.80056.

Chen, P. *et al.* (2018) 'Mechanisms and Disease Pathogenesis Underlying Metal-Induced Oxidative Stress', *Oxidative Medicine and Cellular Longevity*, 2018, pp. 1–3. Available at: https://doi.org/10.1155/2018/7612172.

Cheng, Y. *et al.* (2019) 'Randomized controlled trial of lobaplatin plus etoposide vs. cisplatin plus etoposide as first-line therapy in patients with extensive-stage

small cell lung cancer', *Oncology Letters* [Preprint]. Available at: https://doi.org/10.3892/ol.2019.10125.

Chiang, S.-K., Chen, S.-E. and Chang, L.-C. (2021) 'The Role of HO-1 and Its Crosstalk with Oxidative Stress in Cancer Cell Survival', *Cells*, 10(9), p. 2401. Available at: https://doi.org/10.3390/cells10092401.

Chipuk, J.E. *et al.* (2003) 'Pharmacologic activation of p53 elicits Bax-dependent apoptosis in the absence of transcription', *Cancer Cell*, 4(5), pp. 371–381. Available at: https://doi.org/10.1016/S1535-6108(03)00272-1.

Cmielová, J. and Rezáčová, M. (2011) 'p21Cip1/Waf1 protein and its function based on a subcellular localization [corrected]', *Journal of Cellular Biochemistry*, 112(12), pp. 3502–3506. Available at: https://doi.org/10.1002/jcb.23296.

Comings, D.E. (1975) 'Mechanisms of chromosome banding: VIII. Hoechst 33258-DNA interaction', *Chromosoma*, 52(3), pp. 229–243. Available at: https://doi.org/10.1007/BF00332113.

Crivellaro, S. *et al.* (2016) 'The non-genomic loss of function of tumor suppressors: an essential role in the pathogenesis of chronic myeloid leukemia chronic phase', *BMC Cancer*, 16(1), p. 314. Available at: https://doi.org/10.1186/s12885-016-2346-6.

Crowley, L.C. *et al.* (2016) 'Measuring Cell Death by Propidium Iodide Uptake and Flow Cytometry', *Cold Spring Harbor Protocols*, 2016(7), p. pdb.prot087163. Available at: https://doi.org/10.1101/pdb.prot087163.

Cunha, B.N. *et al.* (2020) 'Selective Coordination Mode of Acylthiourea Ligands in Half-Sandwich Ru(II) Complexes and Their Cytotoxic Evaluation', *Inorganic Chemistry*, 59(7), pp. 5072–5085. Available at: https://doi.org/10.1021/acs.inorgchem.0c00319.

Dasari, S. and Bernard Tchounwou, P. (2014) 'Cisplatin in cancer therapy: Molecular mechanisms of action', *European Journal of Pharmacology*, 740, pp. 364–378. Available at: https://doi.org/10.1016/j.ejphar.2014.07.025.

Dasari, S. and Tchounwou, P.B. (2014) 'Cisplatin in cancer therapy: molecular mechanisms of action', *European Journal of Pharmacology*, 740, pp. 364–378. Available at: https://doi.org/10.1016/j.ejphar.2014.07.025.

De Vitto, H., Valencia, J.P. and Radosevich, J.A. (2018) 'General View of the Cytoplasmic and Nuclear Features of Apoptosis', in J. Radosevich (ed.) *Apoptosis and Beyond*. 1st edn. Wiley, pp. 1–12. Available at: https://doi.org/10.1002/9781119432463.ch1.

Deavall, D.G. *et al.* (2012) 'Drug-Induced Oxidative Stress and Toxicity', *Journal of Toxicology*, 2012, pp. 1–13. Available at: https://doi.org/10.1155/2012/645460.

Debela, D.T. *et al.* (2021) 'New approaches and procedures for cancer treatment: Current perspectives', *SAGE Open Medicine*, 9, p. 205031212110343. Available at: https://doi.org/10.1177/20503121211034366.

Demchenko, A.P. (2013) 'Beyond annexin V: fluorescence response of cellular membranes to apoptosis', *Cytotechnology*, 65(2), pp. 157–172. Available at: https://doi.org/10.1007/s10616-012-9481-y.

Denton, D. and Kumar, S. (2019) 'Autophagy-dependent cell death', *Cell Death & Differentiation*, 26(4), pp. 605–616. Available at: https://doi.org/10.1038/s41418-018-0252-y.

Devi, C.S. *et al.* (2017) 'Analytical Techniques Used to Detect DNA Binding Modes of Ruthenium(II) Complexes with Extended Phenanthroline Ring', *Journal of Fluorescence*, 27(6), pp. 2119–2130. Available at: https://doi.org/10.1007/s10895-017-2151-x.

Di Pietro, M.L. *et al.* (2021) 'Ru(II)-Dppz Derivatives and Their Interactions with DNA: Thirty Years and Counting', *Applied Sciences*, 11(7), p. 3038. Available at: https://doi.org/10.3390/app11073038.

Douglass, I.B. and Dains, F.B. (1934) 'The Preparation and Hydrolysis of Mono- and Disubstituted Benzoylthioureas [1]', *Journal of the American Chemical Society*, 56(6), pp. 1408–1409. Available at: https://doi.org/10.1021/ja01321a061.

Dubey, A. *et al.* (2015) 'Heat shock proteins: a therapeutic target worth to consider', *Veterinary World*, 8(1), pp. 46–51. Available at: https://doi.org/10.14202/vetworld.2015.46-51.

Dunn, L.L. *et al.* (2014) 'New Insights into Intracellular Locations and Functions of Heme Oxygenase-1', *Antioxidants & Redox Signaling*, 20(11), pp. 1723–1742. Available at: https://doi.org/10.1089/ars.2013.5675.

Eckelman, B.P. and Salvesen, G.S. (2006) 'The Human Anti-apoptotic Proteins cIAP1 and cIAP2 Bind but Do Not Inhibit Caspases', *Journal of Biological Chemistry*, 281(6), pp. 3254–3260. Available at: https://doi.org/10.1074/jbc.M510863200.

Egan, T.J. *et al.* (2004) 'In Vitro Antimalarial Activity of a Series of Cationic 2,2'-Bipyridyl- and 1,10-Phenanthrolineplatinum(II) Benzoylthiourea Complexes', *Journal of Medicinal Chemistry*, 47(11), pp. 2926–2934. Available at: https://doi.org/10.1021/jm031132g.

Elmore, S. (2007) 'Apoptosis: A Review of Programmed Cell Death', *Toxicologic Pathology*, 35(4), pp. 495–516. Available at: https://doi.org/10.1080/01926230701320337.

Erxleben, A. (2017) 'Investigation of Non-covalent Interactions of Metal Complexes with DNA in Cell-free Systems', *CHIMIA*, 71(3), p. 102. Available at: https://doi.org/10.2533/chimia.2017.102.

Eskandari, E. and Eaves, C.J. (2022) ‘Paradoxical roles of caspase-3 in regulating cell survival, proliferation, and tumorigenesis’, *Journal of Cell Biology*, 221(6), p. e202201159. Available at: https://doi.org/10.1083/jcb.202201159.

Fares, J. *et al.* (2020) ‘Molecular principles of metastasis: a hallmark of cancer revisited’, *Signal Transduction and Targeted Therapy*, 5(1), p. 28. Available at: https://doi.org/10.1038/s41392-020-0134-x.

Ferlay, J. *et al.* (2021) ‘Cancer statistics for the year 2020: An overview’, *International Journal of Cancer*, 149(4), pp. 778–789. Available at: https://doi.org/10.1002/ijc.33588.

Fischer, M., Dang, C.V. and DeCaprio, J.A. (2018) ‘Control of Cell Division’, in *Hematology*. Elsevier, pp. 176–185. Available at: https://doi.org/10.1016/B978-0-323-35762-3.00017-2.

Fisher, D.M. *et al.* (2007) ‘Chiral Platinum(II) Metallointercalators with Potent in vitro Cytotoxic Activity’, *ChemMedChem*, 2(4), pp. 488–495. Available at: https://doi.org/10.1002/cmdc.200600211.

Fried, M. and Crothers, D.M. (1981) ‘Equilibria and kinetics of lac repressor-operator interactions by polyacrylamide gel electrophoresis’, *Nucleic Acids Research*, 9(23), pp. 6505–6525. Available at: https://doi.org/10.1093/nar/9.23.6505.

Fujiwara, K. *et al.* (2008) ‘Pivotal Role of the Cyclin-dependent Kinase Inhibitor p21WAF1/CIP1 in Apoptosis and Autophagy’, *Journal of Biological Chemistry*, 283(1), pp. 388–397. Available at: https://doi.org/10.1074/jbc.M611043200.

Fulda, S. and Debatin, K.-M. (2006) ‘Extrinsic versus intrinsic apoptosis pathways in anticancer chemotherapy’, *Oncogene*, 25(34), pp. 4798–4811. Available at: https://doi.org/10.1038/sj.onc.1209608.

Galluzzi, L. *et al.* (2008) ‘Viral control of mitochondrial apoptosis’, *PLoS pathogens*, 4(5), p. e1000018. Available at: https://doi.org/10.1371/journal.ppat.1000018.

Galluzzi, L. *et al.* (2018) ‘Molecular mechanisms of cell death: recommendations of the Nomenclature Committee on Cell Death 2018’, *Cell Death & Differentiation*, 25(3), pp. 486–541. Available at: https://doi.org/10.1038/s41418-017-0012-4.

Galvan, V. *et al.* (2003) ‘Type 1 Insulin-like Growth Factor Receptor (IGF-IR) Signaling Inhibits Apoptosis Signal-regulating Kinase 1 (ASK1)’, *Journal of Biological Chemistry*, 278(15), pp. 13325–13332. Available at: https://doi.org/10.1074/jbc.M211398200.

Garbett, N.C., Hammond, N.B. and Graves, D.E. (2004) ‘Influence of the Amino Substituents in the Interaction of Ethidium Bromide with DNA’, *Biophysical*

Journal, 87(6), pp. 3974–3981. Available at: https://doi.org/10.1529/biophysj.104.047415.

García-Ramos, J.C. *et al.* (2017) 'Metal-Based Drug-DNA Interactions', *Journal of the Mexican Chemical Society*, 57(3). Available at: https://doi.org/10.29356/jmcs.v57i3.213.

Garner, M.M. and Revzin, A. (1981) 'A gel electrophoresis method for quantifying the binding of proteins to specific DNA regions: application to components of the Escherichia coli lactose operon regulatory system', *Nucleic Acids Research*, 9(13), pp. 3047–3060. Available at: https://doi.org/10.1093/nar/9.13.3047.

Gentle, I.E. *et al.* (2011) 'In TNF-stimulated Cells, RIPK1 Promotes Cell Survival by Stabilizing TRAF2 and cIAP1, which Limits Induction of Non-canonical NF-κB and Activation of Caspase-8', *Journal of Biological Chemistry*, 286(15), pp. 13282–13291. Available at: https://doi.org/10.1074/jbc.M110.216226.

Ghosh, J.C. *et al.* (2008) 'Hsp60 Regulation of Tumor Cell Apoptosis', *Journal of Biological Chemistry*, 283(8), pp. 5188–5194. Available at: https://doi.org/10.1074/jbc.M705904200.

Gibson, D. (2002) 'Drug–DNA interactions and novel drug design', *The Pharmacogenomics Journal*, 2(5), pp. 275–276. Available at: https://doi.org/10.1038/sj.tpj.6500133.

Gilmore, A.P. *et al.* (2002) 'Activation of BAD by Therapeutic Inhibition of Epidermal Growth Factor Receptor and Transactivation by Insulin-like Growth Factor Receptor', *Journal of Biological Chemistry*, 277(31), pp. 27643–27650. Available at: https://doi.org/10.1074/jbc.M108863200.

Grawe, G.F. *et al.* (2022) 'Ruthenium(II)-diphosphine complexes containing acylthiourea ligands are effective against lung and breast cancers', *Dalton Transactions*, 51(4), pp. 1489–1501. Available at: https://doi.org/10.1039/D1DT02851K.

Green, D.R. (2022) 'The Death Receptor Pathway of Apoptosis', *Cold Spring Harbor Perspectives in Biology*, 14(2), p. a041053. Available at: https://doi.org/10.1101/cshperspect.a041053.

Grimberg, A. (2000) 'p53 and IGFBP-3: Apoptosis and Cancer Protection', *Molecular Genetics and Metabolism*, 70(2), pp. 85–98. Available at: https://doi.org/10.1006/mgme.2000.3008.

Hajibabaie, F., Abedpoor, N. and Mohamadynejad, P. (2023) 'Types of Cell Death from a Molecular Perspective', *Biology*, 12(11), p. 1426. Available at: https://doi.org/10.3390/biology12111426.

Hanahan, D. and Weinberg, R.A. (2000) 'The Hallmarks of Cancer', *Cell*, 100(1), pp. 57–70. Available at: https://doi.org/10.1016/S0092-8674(00)81683-9.

Hanahan, D. and Weinberg, R.A. (2011) 'Hallmarks of Cancer: The Next Generation', *Cell*, 144(5), pp. 646–674. Available at: https://doi.org/10.1016/j.cell.2011.02.013.

Hardwick, J.M. and Soane, L. (2013) 'Multiple Functions of BCL-2 Family Proteins', *Cold Spring Harbor Perspectives in Biology*, 5(2), pp. a008722–a008722. Available at: https://doi.org/10.1101/cshperspect.a008722.

Havens, C.G. *et al.* (2006) 'Regulation of Late G_1/S Phase Transition and APC^{Cdh1} by Reactive Oxygen Species', *Molecular and Cellular Biology*, 26(12), pp. 4701–4711. Available at: https://doi.org/10.1128/MCB.00303-06.

Herrmann, C.P., Kraiss, S. and Montenarh, M. (1991) 'Association of casein kinase II with immunopurified p53', *Oncogene*, 6(5), pp. 877–884.

Hissler, M. *et al.* (2000) 'Platinum diimine complexes: towards a molecular photochemical device', *Coordination Chemistry Reviews*, 208(1), pp. 115–137. Available at: https://doi.org/10.1016/S0010-8545(00)00254-X.

Hong, A. *et al.* (2018) 'Isomer-Specific Induced Circular Dichroism Spectroscopy of Jet-Cooled Phenol Complexes with (−)-Methyl L -Lactate', *The Journal of Physical Chemistry Letters*, 9(3), pp. 476–480. Available at: https://doi.org/10.1021/acs.jpclett.7b03241.

Howells, C.C. *et al.* (2011) 'The Bcl-2-associated death promoter (BAD) lowers the threshold at which the Bcl-2-interacting domain death agonist (BID) triggers mitochondria disintegration', *Journal of Theoretical Biology*, 271(1), pp. 114–123. Available at: https://doi.org/10.1016/j.jtbi.2010.11.040.

Hu, C. *et al.* (2022) 'Heat shock proteins: Biological functions, pathological roles, and therapeutic opportunities', *MedComm*, 3(3). Available at: https://doi.org/10.1002/mco2.161.

Hu, Y. *et al.* (2019) 'Omi/HtrA2 Protease Associated Cell Apoptosis Participates in Blood-Brain Barrier Dysfunction', *Frontiers in Molecular Neuroscience*, 12, p. 48. Available at: https://doi.org/10.3389/fnmol.2019.00048.

Hyun, D.-H. (2020) 'Insights into the New Cancer Therapy through Redox Homeostasis and Metabolic Shifts', *Cancers*, 12(7), p. 1822. Available at: https://doi.org/10.3390/cancers12071822.

Im, K. *et al.* (2019) 'An Introduction to Performing Immunofluorescence Staining', in W.H. Yong (ed.) *Biobanking*. New York, NY: Springer New York (Methods in Molecular Biology), pp. 299–311. Available at: https://doi.org/10.1007/978-1-4939-8935-5_26.

Ishiguro, K. *et al.* (2014) 'Distinct mechanisms of cell-kill by triapine and its terminally dimethylated derivative Dp44mT due to a loss or gain of activity of their copper(II) complexes', *Biochemical Pharmacology*, 91(3), pp. 312–322. Available at: https://doi.org/10.1016/j.bcp.2014.08.006.

Jian, Z. *et al.* (2020) 'Oxidative stress, apoptosis and inflammatory responses involved in copper-induced pulmonary toxicity in mice', *Aging*, 12(17), pp. 16867–16886. Available at: https://doi.org/10.18632/aging.103585.

Jogie-Brahim, S., Feldman, D. and Oh, Y. (2009) 'Unraveling Insulin-Like Growth Factor Binding Protein-3 Actions in Human Disease', *Endocrine Reviews*, 30(5), pp. 417–437. Available at: https://doi.org/10.1210/er.2008-0028.

Johnstone, T.C., Pil, P.M. and Lippard, S.J. (2015) 'Cisplatin and Related Drugs☆', in *Reference Module in Biomedical Sciences*. Elsevier, p. B9780128012383987403. Available at: https://doi.org/10.1016/B978-0-12-801238-3.98740-3.

Johnstone, T.C., Suntharalingam, K. and Lippard, S.J. (2016) 'The Next Generation of Platinum Drugs: Targeted Pt(II) Agents, Nanoparticle Delivery, and Pt(IV) Prodrugs', *Chemical Reviews*, 116(5), pp. 3436–3486. Available at: https://doi.org/10.1021/acs.chemrev.5b00597.

Jomová, K. *et al.* (2019) 'A Switch between Antioxidant and Prooxidant Properties of the Phenolic Compounds Myricetin, Morin, 3′,4′-Dihydroxyflavone, Taxifolin and 4-Hydroxy-Coumarin in the Presence of Copper(II) Ions: A Spectroscopic, Absorption Titration and DNA Damage Study', *Molecules*, 24(23), p. 4335. Available at: https://doi.org/10.3390/molecules24234335.

Jonker, D. *et al.* (2006) 'Role of oxaliplatin combined with 5-fluorouracil and folinic acid in the first- and second-line treatment of advanced colorectal cancer', *Current Oncology (Toronto, Ont.)*, 13(5), pp. 173–184.

Jung, S., Jeong, H. and Yu, S.-W. (2020) 'Autophagy as a decisive process for cell death', *Experimental & Molecular Medicine*, 52(6), pp. 921–930. Available at: https://doi.org/10.1038/s12276-020-0455-4.

Kamiloglu, S. *et al.* (2020) 'Guidelines for cell viability assays', *Food Frontiers*, 1(3), pp. 332–349. Available at: https://doi.org/10.1002/fft2.44.

Kangara, E.F. *et al.* (2019) 'Conformational analysis and potential anticancer activity of [Pt(phen)(L1-κ *S*) $_2$] studied by single crystal X-ray diffraction and variable temperature ^{1} H and ^{195} Pt NMR spectroscopy', *New Journal of Chemistry*, 43(9), pp. 3665–3672. Available at: https://doi.org/10.1039/C8NJ06010J.

Karami, K. *et al.* (2018) 'Synthesis and characterization of two new trans palladium (II) complexes containing benzylamine ligand: DNA/BSA interactions, molecular docking and in vitro cytotoxic activity', *Inorganica Chimica Acta*, 471, pp. 797–807. Available at: https://doi.org/10.1016/j.ica.2017.02.027.

Kari, S. *et al.* (2022) 'Programmed cell death detection methods: a systematic review and a categorical comparison', *Apoptosis*, 27(7–8), pp. 482–508. Available at: https://doi.org/10.1007/s10495-022-01735-y.

Kasof, G.M. and Gomes, B.C. (2001) ‘Livin, a Novel Inhibitor of Apoptosis Protein Family Member’, *Journal of Biological Chemistry*, 276(5), pp. 3238–3246. Available at: https://doi.org/10.1074/jbc.M003670200.

Katerji, M., Filippova, M. and Duerksen-Hughes, P. (2019) ‘Approaches and Methods to Measure Oxidative Stress in Clinical Samples: Research Applications in the Cancer Field’, *Oxidative Medicine and Cellular Longevity*, 2019, pp. 1–29. Available at: https://doi.org/10.1155/2019/1279250.

Kaur *et al.* (2019) ‘Extracellular HtrA2 Induces Apoptosis in Human Umbilical Vein Endothelial Cells’, *International Journal of Molecular Sciences*, 20(21), p. 5446. Available at: https://doi.org/10.3390/ijms20215446.

Kemp, S. *et al.* (2007) ‘The effect of ancillary ligand chirality and phenanthroline functional group substitution on the cytotoxicity of platinum(II)-based metallointercalators’, *Journal of Inorganic Biochemistry*, 101(7), pp. 1049–1058. Available at: https://doi.org/10.1016/j.jinorgbio.2007.04.009.

Kerr, J.F.R., Wyllie, A.H. and Currie, A.R. (1972) ‘Apoptosis: A Basic Biological Phenomenon with Wideranging Implications in Tissue Kinetics’, *British Journal of Cancer*, 26(4), pp. 239–257. Available at: https://doi.org/10.1038/bjc.1972.33.

Khalid, N. and Azimpouran, M. (2023) ‘Necrosis’, in *StatPearls*. Treasure Island (FL): StatPearls Publishing. Available at: http://www.ncbi.nlm.nih.gov/books/NBK557627/ (Accessed: 20 December 2023).

Kleih, M. *et al.* (2019) ‘Direct impact of cisplatin on mitochondria induces ROS production that dictates cell fate of ovarian cancer cells’, *Cell Death & Disease*, 10(11), p. 851. Available at: https://doi.org/10.1038/s41419-019-2081-4.

Koch, K.R. (2001) ‘New chemistry with old ligands: N-alkyl- and N,N-dialkyl-N′-acyl(aroyl)thioureas in co-ordination, analytical and process chemistry of the platinum group metals’, *Coordination Chemistry Reviews*, 216–217, pp. 473–488. Available at: https://doi.org/10.1016/S0010-8545(01)00337-X.

Kominami, K. *et al.* (2012) ‘The molecular mechanism of apoptosis upon caspase-8 activation: Quantitative experimental validation of a mathematical model’, *Biochimica et Biophysica Acta (BBA) - Molecular Cell Research*, 1823(10), pp. 1825–1840. Available at: https://doi.org/10.1016/j.bbamcr.2012.07.003.

Kreis *et al.* (2019) ‘Function of p21 (Cip1/Waf1/CDKN1A) in Migration and Invasion of Cancer and Trophoblastic Cells’, *Cancers*, 11(7), p. 989. Available at: https://doi.org/10.3390/cancers11070989.

Kroemer, G. *et al.* (2009) ‘Classification of cell death: recommendations of the Nomenclature Committee on Cell Death 2009’, *Cell Death & Differentiation*, 16(1), pp. 3–11. Available at: https://doi.org/10.1038/cdd.2008.150.

Kučera, O. *et al.* (2014) 'The Effect of *tert* -Butyl Hydroperoxide-Induced Oxidative Stress on Lean and Steatotic Rat Hepatocytes *In Vitro*', *Oxidative Medicine and Cellular Longevity*, 2014, pp. 1–12. Available at: https://doi.org/10.1155/2014/752506.

Kuwana, T. *et al.* (2005) 'BH3 Domains of BH3-Only Proteins Differentially Regulate Bax-Mediated Mitochondrial Membrane Permeabilization Both Directly and Indirectly', *Molecular Cell*, 17(4), pp. 525–535. Available at: https://doi.org/10.1016/j.molcel.2005.02.003.

Kypr, J. *et al.* (2009) 'Circular dichroism and conformational polymorphism of DNA', *Nucleic Acids Research*, 37(6), pp. 1713–1725. Available at: https://doi.org/10.1093/nar/gkp026.

Lapasam, A. and Kollipara, M.R. (2020) 'A survey of crystal structures and biological activities of platinum group metal complexes containing *N* -acylthiourea ligands', *Phosphorus, Sulfur, and Silicon and the Related Elements*, 195(10), pp. 779–804. Available at: https://doi.org/10.1080/10426507.2020.1764956.

Lau, R. and Pratt, M.A.C. (2012) 'The Opposing Roles of Cellular Inhibitor of Apoptosis Proteins in Cancer', *ISRN Oncology*, 2012, pp. 1–5. Available at: https://doi.org/10.5402/2012/928120.

Lee, J. and Kim, S.S. (2009) 'The function of p27 ^{KIP1} during tumor development', *Experimental and Molecular Medicine*, 41(11), p. 765. Available at: https://doi.org/10.3858/emm.2009.41.11.102.

Lee, S.-H. *et al.* (2013) 'Phosphatidylserine exposure during apoptosis reflects bidirectional trafficking between plasma membrane and cytoplasm', *Cell Death & Differentiation*, 20(1), pp. 64–76. Available at: https://doi.org/10.1038/cdd.2012.93.

LeRoith, D., Holly, J.M.P. and Forbes, B.E. (2021) 'Insulin-like growth factors: Ligands, binding proteins, and receptors', *Molecular Metabolism*, 52, p. 101245. Available at: https://doi.org/10.1016/j.molmet.2021.101245.

Lin, Q. *et al.* (2007) 'Heme Oxygenase-1 Protein Localizes to the Nucleus and Activates Transcription Factors Important in Oxidative Stress', *Journal of Biological Chemistry*, 282(28), pp. 20621–20633. Available at: https://doi.org/10.1074/jbc.M607954200.

Liu, Y. *et al.* (2021) 'Molecular mechanisms of chemo- and radiotherapy resistance and the potential implications for cancer treatment', *MedComm*, 2(3), pp. 315–340. Available at: https://doi.org/10.1002/mco2.55.

Lock, R.B. *et al.* (1997) 'Potentiation of etoposide-induced apoptosis by staurosporine in human tumor cells is associated with events downstream of

DNA-protein complex formation', *Cancer Chemotherapy and Pharmacology*, 39(5), pp. 399–409. Available at: https://doi.org/10.1007/s002800050590.

Lucaciu, R.L. *et al.* (2022) 'Metallo-Drugs in Cancer Therapy: Past, Present and Future', *Molecules*, 27(19), p. 6485. Available at: https://doi.org/10.3390/molecules27196485.

Ludke, A. *et al.* (2017) 'Time course of changes in oxidative stress and stress-induced proteins in cardiomyocytes exposed to doxorubicin and prevention by vitamin C', *PloS One*, 12(7), p. e0179452. Available at: https://doi.org/10.1371/journal.pone.0179452.

Ma, Q. (2013) 'Role of Nrf2 in Oxidative Stress and Toxicity', *Annual Review of Pharmacology and Toxicology*, 53(1), pp. 401–426. Available at: https://doi.org/10.1146/annurev-pharmtox-011112-140320.

Mace, P.D., Shirley, S. and Day, C.L. (2010) 'Assembling the building blocks: structure and function of inhibitor of apoptosis proteins', *Cell Death & Differentiation*, 17(1), pp. 46–53. Available at: https://doi.org/10.1038/cdd.2009.45.

Macleod, K.F. *et al.* (1995) 'p53-dependent and independent expression of p21 during cell growth, differentiation, and DNA damage.', *Genes & Development*, 9(8), pp. 935–944. Available at: https://doi.org/10.1101/gad.9.8.935.

Mandal, R. *et al.* (2020) 'Caspase-8: The double-edged sword', *Biochimica Et Biophysica Acta. Reviews on Cancer*, 1873(2), p. 188357. Available at: https://doi.org/10.1016/j.bbcan.2020.188357.

Marechal, A. and Zou, L. (2013) 'DNA Damage Sensing by the ATM and ATR Kinases', *Cold Spring Harbor Perspectives in Biology*, 5(9), pp. a012716–a012716. Available at: https://doi.org/10.1101/cshperspect.a012716.

Martinez-Ruiz, G. *et al.* (2008) 'Role of Smac/DIABLO in cancer progression', *Journal of Experimental & Clinical Cancer Research*, 27(1), p. 48. Available at: https://doi.org/10.1186/1756-9966-27-48.

Mascaró, M. *et al.* (2021) 'Nuclear Localization of Heme Oxygenase-1 in Pathophysiological Conditions: Does It Explain the Dual Role in Cancer?', *Antioxidants*, 10(1), p. 87. Available at: https://doi.org/10.3390/antiox10010087.

Mbeje, N.P., Ginindza, T.G. and Jafta, N. (2021) 'Establishing and Evaluating Cancer Surveillance System in KwaZulu-Natal, South Africa', *Cancer Informatics*, 20, p. 117693512110299. Available at: https://doi.org/10.1177/11769351211029967.

McIlwain, D.R., Berger, T. and Mak, T.W. (2013) 'Caspase Functions in Cell Death and Disease', *Cold Spring Harbor Perspectives in Biology*, 5(4), pp. a008656–a008656. Available at: https://doi.org/10.1101/cshperspect.a008656.

McKeage, M.J. (2001) ‘Lobaplatin: a new antitumour platinum drug’, *Expert Opinion on Investigational Drugs*, 10(1), pp. 119–128. Available at: https://doi.org/10.1517/13543784.10.1.119.

Meek, D.W. and Anderson, C.W. (2009) ‘Posttranslational Modification of p53: Cooperative Integrators of Function’, *Cold Spring Harbor Perspectives in Biology*, 1(6), pp. a000950–a000950. Available at: https://doi.org/10.1101/cshperspect.a000950.

van Meerloo, J., Kaspers, G.J.L. and Cloos, J. (2011) ‘Cell sensitivity assays: the MTT assay’, *Methods in Molecular Biology (Clifton, N.J.)*, 731, pp. 237–245. Available at: https://doi.org/10.1007/978-1-61779-080-5_20.

Mitrea, D.G. and Cîrcu, V. (2021) ‘Synthesis and characterization of novel acylthiourea compounds used in ions recognition and sensing in organic media’, *Spectrochimica Acta Part A: Molecular and Biomolecular Spectroscopy*, 258, p. 119860. Available at: https://doi.org/10.1016/j.saa.2021.119860.

Mittler, R. (2017) ‘ROS Are Good’, *Trends in Plant Science*, 22(1), pp. 11–19. Available at: https://doi.org/10.1016/j.tplants.2016.08.002.

Miyahara, T., Nakatsuji, H. and Sugiyama, H. (2013) ‘Helical Structure and Circular Dichroism Spectra of DNA: A Theoretical Study’, *The Journal of Physical Chemistry A*, 117(1), pp. 42–55. Available at: https://doi.org/10.1021/jp3085556.

Mohapatra, P. *et al.* (2012) ‘Quinacrine-Mediated Autophagy and Apoptosis in Colon Cancer Cells Is Through a p53- and p21-Dependent Mechanism’, *Oncology Research Featuring Preclinical and Clinical Cancer Therapeutics*, 20(2), pp. 81–91. Available at: https://doi.org/10.3727/096504012X13473664562628.

Morgan, G.T. and Burstall, F.H. (1934) ‘323. Researches on residual affinity and co-ordination. Part XXXV. 2 : 2′ : 2″-Tripyridylplatinum salts’, *J. Chem. Soc.*, 0(0), pp. 1498–1500. Available at: https://doi.org/10.1039/JR9340001498.

Mosmann, T. (1983) ‘Rapid colorimetric assay for cellular growth and survival: application to proliferation and cytotoxicity assays’, *Journal of Immunological Methods*, 65(1–2), pp. 55–63. Available at: https://doi.org/10.1016/0022-1759(83)90303-4.

Nakamura, H. and Takada, K. (2021) ‘Reactive oxygen species in cancer: Current findings and future directions’, *Cancer Science*, 112(10), pp. 3945–3952. Available at: https://doi.org/10.1111/cas.15068.

Neidle, S. (2001) ‘DNA minor-groove recognition by small molecules (up to 2000)’, *Natural Product Reports*, 18(3), pp. 291–309. Available at: https://doi.org/10.1039/a705982e.

Ng, N.S. *et al.* (2018) ‘The in vitro renal cell toxicity of some unconventional anticancer phenanthroline-based platinum(II) complexes’, *Journal of Inorganic*

Biochemistry, 179, pp. 97–106. Available at: https://doi.org/10.1016/j.jinorgbio.2017.11.021.

Novoa-Ramírez, C.S. *et al.* (2023) 'Biological activity of mixed chelate copper(II) complexes, with substituted diimine and tridentate Schiff bases (NNO) and their hydrogenated derivatives as secondary ligands: Casiopeína's fourth generation', *Journal of Inorganic Biochemistry*, 242, p. 112097. Available at: https://doi.org/10.1016/j.jinorgbio.2022.112097.

Ovadje, P. *et al.* (2011) 'Selective induction of apoptosis through activation of caspase-8 in human leukemia cells (Jurkat) by dandelion root extract', *Journal of Ethnopharmacology*, 133(1), pp. 86–91. Available at: https://doi.org/10.1016/j.jep.2010.09.005.

Ozaki, T. and Nakagawara, A. (2011) 'Role of p53 in Cell Death and Human Cancers', *Cancers*, 3(1), pp. 994–1013. Available at: https://doi.org/10.3390/cancers3010994.

Pages, B.J. *et al.* (2014) 'Synthesis and analysis of the anticancer activity of platinum(II) complexes incorporating dipyridoquinoxaline variants', *Dalton Trans.*, 43(41), pp. 15566–15575. Available at: https://doi.org/10.1039/C4DT02133A.

Pages, B.J. *et al.* (2015) 'Metal complex interactions with DNA', *Dalton Transactions*, 44(8), pp. 3505–3526. Available at: https://doi.org/10.1039/C4DT02700K.

Pages, B.J. *et al.* (2018) 'Combining the platinum(II) drug candidate kiteplatin with 1,10-phenanthroline analogues', *Dalton Transactions*, 47(7), pp. 2156–2163. Available at: https://doi.org/10.1039/C7DT04108J.

Paitandi, R.P. *et al.* (2018) 'Pyrazole appended quinoline-BODIPY based arene ruthenium complexes: their anticancer activity and potential applications in cellular imaging', *Dalton Transactions*, 47(48), pp. 17500–17514. Available at: https://doi.org/10.1039/C8DT02947D.

Pandey, S.K. *et al.* (2022) 'Non-apoptotic activity of the mitochondrial protein SMAC/Diablo in lung cancer: Novel target to disrupt survival, inflammation, and immunosuppression', *Frontiers in Oncology*, 12, p. 992260. Available at: https://doi.org/10.3389/fonc.2022.992260.

Papaliagkas, V. *et al.* (2007) 'The proteins and the mechanisms of apoptosis: a mini-review of the fundamentals', *Hippokratia*, 11(3), pp. 108–113.

Parrish, A.B., Freel, C.D. and Kornbluth, S. (2013) 'Cellular Mechanisms Controlling Caspase Activation and Function', *Cold Spring Harbor Perspectives in Biology*, 5(6), pp. a008672–a008672. Available at: https://doi.org/10.1101/cshperspect.a008672.

Patterson, J.C. *et al.* (2019) 'ROS and Oxidative Stress Are Elevated in Mitosis during Asynchronous Cell Cycle Progression and Are Exacerbated by Mitotic Arrest', *Cell Systems*, 8(2), pp. 163-167.e2. Available at: https://doi.org/10.1016/j.cels.2019.01.005.

Pedrosa, P. *et al.* (2018) 'Inorganic Coordination Chemistry: Where We Stand in Cancer Treatment?', in T. Akitsu (ed.) *Basic Concepts Viewed from Frontier in Inorganic Coordination Chemistry*. IntechOpen. Available at: https://doi.org/10.5772/intechopen.80233.

Peega, T. *et al.* (2021) 'Synthesis and evaluation of the anticancer activity of [Pt(diimine)(*N* , *N* -dibutyl- *N* ′-acylthiourea)] $^{+}$ complexes', *Dalton Transactions*, 50(34), pp. 11742–11762. Available at: https://doi.org/10.1039/D1DT01385H.

Peña-Blanco, A. and García-Sáez, A.J. (2018) 'Bax, Bak and beyond — mitochondrial performance in apoptosis', *The FEBS Journal*, 285(3), pp. 416–431. Available at: https://doi.org/10.1111/febs.14186.

Perillo, B. *et al.* (2020) 'ROS in cancer therapy: the bright side of the moon', *Experimental & Molecular Medicine*, 52(2), pp. 192–203. Available at: https://doi.org/10.1038/s12276-020-0384-2.

Pfeffer, C. and Singh, A. (2018) 'Apoptosis: A Target for Anticancer Therapy', *International Journal of Molecular Sciences*, 19(2), p. 448. Available at: https://doi.org/10.3390/ijms19020448.

Piette, J., Neel, H. and Maréchal, V. (1997) 'Mdm2: keeping p53 under control', *Oncogene*, 15(9), pp. 1001–1010. Available at: https://doi.org/10.1038/sj.onc.1201432.

Pimentel, J.M., Zhou, J.-Y. and Wu, G.S. (2023) 'The Role of TRAIL in Apoptosis and Immunosurveillance in Cancer', *Cancers*, 15(10), p. 2752. Available at: https://doi.org/10.3390/cancers15102752.

Plutín, A.M. *et al.* (2016) 'Anti- Mycobacterium tuberculosis activity of platinum(II)/ N , N -disubstituted- N ′-acyl thiourea complexes', *Inorganic Chemistry Communications*, 63, pp. 74–80. Available at: https://doi.org/10.1016/j.inoche.2015.11.020.

Puyo, S., Montaudon, D. and Pourquier, P. (2014) 'From old alkylating agents to new minor groove binders', *Critical Reviews in Oncology/Hematology*, 89(1), pp. 43–61. Available at: https://doi.org/10.1016/j.critrevonc.2013.07.006.

Rajah, R., Valentinis, B. and Cohen, P. (1997) 'Insulin-like Growth Factor (IGF)-binding Protein-3 Induces Apoptosis and Mediates the Effects of Transforming Growth Factor-β1 on Programmed Cell Death through a p53- and IGF-independent Mechanism', *Journal of Biological Chemistry*, 272(18), pp. 12181–12188. Available at: https://doi.org/10.1074/jbc.272.18.12181.

Ream, J.A., Lewis, L.K. and Lewis, K.A. (2016) 'Rapid agarose gel electrophoretic mobility shift assay for quantitating protein: RNA interactions', *Analytical Biochemistry*, 511, pp. 36–41. Available at: https://doi.org/10.1016/j.ab.2016.07.027.

Reczek, C.R. and Chandel, N.S. (2017) 'The Two Faces of Reactive Oxygen Species in Cancer', *Annual Review of Cancer Biology*, 1(1), pp. 79–98. Available at: https://doi.org/10.1146/annurev-cancerbio-041916-065808.

Rehman, S.U. *et al.* (2015) 'Studying non-covalent drug–DNA interactions', *Archives of Biochemistry and Biophysics*, 576, pp. 49–60. Available at: https://doi.org/10.1016/j.abb.2015.03.024.

Renehan, A.G. (2001) 'What is apoptosis, and why is it important?', *BMJ*, 322(7301), pp. 1536–1538. Available at: https://doi.org/10.1136/bmj.322.7301.1536.

Roach, R.C., Wagner, P.D. and Hackett, P.H. (2011) *Hypoxia: from genes to the bedside*. New York: Springer.

Roberts, D.L. *et al.* (2001) 'The Inhibitor of Apoptosis Protein-Binding Domain of Smac Is Not Essential for Its Proapoptotic Activity', *Journal of Cell Biology*, 153(1), pp. 221–228. Available at: https://doi.org/10.1083/jcb.153.1.221.

Rodger, A. (2013) 'DNA-Ligand Circular Dichroism', in G.C.K. Roberts (ed.) *Encyclopedia of Biophysics*. Berlin, Heidelberg: Springer Berlin Heidelberg, pp. 484–486. Available at: https://doi.org/10.1007/978-3-642-16712-6_636.

Rogers, C. *et al.* (2017) 'Cleavage of DFNA5 by caspase-3 during apoptosis mediates progression to secondary necrotic/pyroptotic cell death', *Nature Communications*, 8(1), p. 14128. Available at: https://doi.org/10.1038/ncomms14128.

Rohini, G. *et al.* (2018) 'Biological evaluation, DNA/protein-binding aptitude of novel dibenzosuberene appended palladium (II)-thiourea complexes: Biological evaluation of novel palladium(II)-thiourea complexes', *Applied Organometallic Chemistry*, 32(12), p. e4567. Available at: https://doi.org/10.1002/aoc.4567.

Rosenberg, B. (1978) 'Platinum Complexes for the Treatment of Cancer', *Interdisciplinary Science Reviews*, 3(2), pp. 134–147. Available at: https://doi.org/10.1179/030801878791926119.

Rosenberg, B., Van Camp, L. and Krigas, T. (1965) 'Inhibition of Cell Division in Escherichia coli by Electrolysis Products from a Platinum Electrode', *Nature*, 205(4972), pp. 698–699. Available at: https://doi.org/10.1038/205698a0.

Rosu, F. *et al.* (2002) 'Triplex and quadruplex DNA structures studied by electrospray mass spectrometry', *Rapid Communications in Mass Spectrometry*, 16(18), pp. 1729–1736. Available at: https://doi.org/10.1002/rcm.778.

Saeed, A. *et al.* (2019) 'Current developments in chemistry, coordination, structure and biological aspects of 1-(acyl/aroyl)-3- (substituted)thioureas: advances Continue …', *Journal of Sulfur Chemistry*, 40(3), pp. 312–350. Available at: https://doi.org/10.1080/17415993.2018.1551488.

Saeed, A., Flörke, U. and Erben, M.F. (2014) 'A review on the chemistry, coordination, structure and biological properties of 1-(acyl/aroyl)-3-(substituted) thioureas', *Journal of Sulfur Chemistry*, 35(3), pp. 318–355. Available at: https://doi.org/10.1080/17415993.2013.834904.

Sagar, J. *et al.* (2010) 'Lowering the apoptotic threshold in colorectal cancer cells by targeting mitochondria', *Cancer Cell International*, 10(1), p. 31. Available at: https://doi.org/10.1186/1475-2867-10-31.

Saibil, H. (2013) 'Chaperone machines for protein folding, unfolding and disaggregation', *Nature Reviews Molecular Cell Biology*, 14(10), pp. 630–642. Available at: https://doi.org/10.1038/nrm3658.

Sánchez-González, Á. and Gil, A. (2021) 'Elucidating the intercalation of methylated 1,10-phenanthroline with DNA: the important weight of the CH/H interactions and the selectivity of CH/π and CH/n interactions', *RSC Advances*, 11(3), pp. 1553–1563. Available at: https://doi.org/10.1039/D0RA07646E.

Sarkar, S. *et al.* (2013) 'Cancer Development, Progression, and Therapy: An Epigenetic Overview', *International Journal of Molecular Sciences*, 14(10), pp. 21087–21113. Available at: https://doi.org/10.3390/ijms141021087.

Schwartz, L.M. (2021) 'Autophagic Cell Death During Development – Ancient and Mysterious', *Frontiers in Cell and Developmental Biology*, 9, p. 656370. Available at: https://doi.org/10.3389/fcell.2021.656370.

Scian, M.J. *et al.* (2004) 'Tumor-derived p53 mutants induce oncogenesis by transactivating growth-promoting genes', *Oncogene*, 23(25), pp. 4430–4443. Available at: https://doi.org/10.1038/sj.onc.1207553.

Scott, F.L. *et al.* (2005) 'XIAP inhibits caspase-3 and -7 using two binding sites: evolutionarily conserved mechanism of IAPs', *The EMBO Journal*, 24(3), pp. 645–655. Available at: https://doi.org/10.1038/sj.emboj.7600544.

Seaman, J.E. *et al.* (2016) 'Cacidases: caspases can cleave after aspartate, glutamate and phosphoserine residues', *Cell Death & Differentiation*, 23(10), pp. 1717–1726. Available at: https://doi.org/10.1038/cdd.2016.62.

Shah, M.A. and Rogoff, H.A. (2021) 'Implications of reactive oxygen species on cancer formation and its treatment', *Seminars in Oncology*, 48(3), pp. 238–245. Available at: https://doi.org/10.1053/j.seminoncol.2021.05.002.

Shakeri, R., Kheirollahi, A. and Davoodi, J. (2017) 'Apaf-1: Regulation and function in cell death', *Biochimie*, 135, pp. 111–125. Available at: https://doi.org/10.1016/j.biochi.2017.02.001.

Shi, Y. (2004) ‘Caspase activation, inhibition, and reactivation: a mechanistic view’, *Protein Science: A Publication of the Protein Society*, 13(8), pp. 1979–1987. Available at: https://doi.org/10.1110/ps.04789804.

Shlomovitz, I., Speir, M. and Gerlic, M. (2019) ‘Flipping the dogma – phosphatidylserine in non-apoptotic cell death’, *Cell Communication and Signaling*, 17(1), p. 139. Available at: https://doi.org/10.1186/s12964-019-0437-0.

Singh, V. *et al.* (2022) ‘Apoptosis and Pharmacological Therapies for Targeting Thereof for Cancer Therapeutics’, *Sci*, 4(2), p. 15. Available at: https://doi.org/10.3390/sci4020015.

Sirajuddin, M., Ali, S. and Badshah, A. (2013) ‘Drug–DNA interactions and their study by UV–Visible, fluorescence spectroscopies and cyclic voltametry’, *Journal of Photochemistry and Photobiology B: Biology*, 124, pp. 1–19. Available at: https://doi.org/10.1016/j.jphotobiol.2013.03.013.

Sivandzade, F., Bhalerao, A. and Cucullo, L. (2019) ‘Analysis of the Mitochondrial Membrane Potential Using the Cationic JC-1 Dye as a Sensitive Fluorescent Probe’, *BIO-PROTOCOL*, 9(1). Available at: https://doi.org/10.21769/BioProtoc.3128.

Sperandio, S., de Belle, I. and Bredesen, D.E. (2000) ‘An alternative, nonapoptotic form of programmed cell death’, *Proceedings of the National Academy of Sciences*, 97(26), pp. 14376–14381. Available at: https://doi.org/10.1073/pnas.97.26.14376.

Strekas, T.C. *et al.* (1995) ‘Characterization of copper(i) and copper(ii) complexes of a bis-diimine coordinated to ruthenium(ii) and their interaction with calf thymus DNA’, *Journal of Coordination Chemistry*, 34(1), pp. 77–85. Available at: https://doi.org/10.1080/00958979508024305.

Suhaili, S.H. *et al.* (2017) ‘Mitochondrial outer membrane permeabilization: a focus on the role of mitochondrial membrane structural organization’, *Biophysical Reviews*, 9(4), pp. 443–457. Available at: https://doi.org/10.1007/s12551-017-0308-0.

Sung, H. *et al.* (2021) ‘Global Cancer Statistics 2020: GLOBOCAN Estimates of Incidence and Mortality Worldwide for 36 Cancers in 185 Countries’, *CA: A Cancer Journal for Clinicians*, 71(3), pp. 209–249. Available at: https://doi.org/10.3322/caac.21660.

Suski, J.M. *et al.* (2012) ‘Relation Between Mitochondrial Membrane Potential and ROS Formation’, in C.M. Palmeira and A.J. Moreno (eds) *Mitochondrial Bioenergetics*. Totowa, NJ: Humana Press (Methods in Molecular Biology), pp. 183–205. Available at: https://doi.org/10.1007/978-1-61779-382-0_12.

Suzuki, Y. *et al.* (2004) 'Mitochondrial protease Omi/HtrA2 enhances caspase activation through multiple pathways', *Cell Death & Differentiation*, 11(2), pp. 208–216. Available at: https://doi.org/10.1038/sj.cdd.4401343.

Tang, Z.-H. *et al.* (2016) 'Characterization of osimertinib (AZD9291)-resistant non-small cell lung cancer NCI-H1975/OSIR cell line', *Oncotarget*, 7(49), pp. 81598–81610. Available at: https://doi.org/10.18632/oncotarget.13150.

Thornberry, N.A. and Lazebnik, Y. (1998) 'Caspases: enemies within', *Science (New York, N.Y.)*, 281(5381), pp. 1312–1316. Available at: https://doi.org/10.1126/science.281.5381.1312.

Todorov, L. and Kostova, I. (2023) 'Recent Trends in the Development of Novel Metal-Based Antineoplastic Drugs', *Molecules*, 28(4), p. 1959. Available at: https://doi.org/10.3390/molecules28041959.

Tower, J. (2015) 'Programmed cell death in aging', *Ageing Research Reviews*, 23, pp. 90–100. Available at: https://doi.org/10.1016/j.arr.2015.04.002.

Tyagi, P., Gahlot, P. and Kakkar, R. (2008) 'Structural aspects of the anti-cancer drug oxaliplatin: A combined theoretical and experimental study', *Polyhedron*, 27(18), pp. 3567–3574. Available at: https://doi.org/10.1016/j.poly.2008.08.025.

Tzifi, F. *et al.* (2012) 'The Role of BCL2 Family of Apoptosis Regulator Proteins in Acute and Chronic Leukemias', *Advances in Hematology*, 2012, pp. 1–15. Available at: https://doi.org/10.1155/2012/524308.

Van Golen, C.M., Castle, V.P. and Feldman, E.L. (2000) 'IGF-I receptor activation and BCL-2 overexpression prevent early apoptotic events in human neuroblastoma', *Cell Death & Differentiation*, 7(7), pp. 654–665. Available at: https://doi.org/10.1038/sj.cdd.4400693.

Verzella, D. *et al.* (2020) 'Life, death, and autophagy in cancer: NF-κB turns up everywhere', *Cell Death & Disease*, 11(3), p. 210. Available at: https://doi.org/10.1038/s41419-020-2399-y.

Vidyasagar, A., Wilson, N.A. and Djamali, A. (2012) 'Heat shock protein 27 (HSP27): biomarker of disease and therapeutic target', *Fibrogenesis & Tissue Repair*, 5(1), p. 7. Available at: https://doi.org/10.1186/1755-1536-5-7.

Waga, S. *et al.* (1994) 'The p21 inhibitor of cyclin-dependent kinases controls DNA replication by interaction with PCNA', *Nature*, 369(6481), pp. 574–578. Available at: https://doi.org/10.1038/369574a0.

Wang, C. and Youle, R.J. (2009) 'The Role of Mitochondria in Apoptosis', *Annual Review of Genetics*, 43(1), pp. 95–118. Available at: https://doi.org/10.1146/annurev-genet-102108-134850.

Wang, Huan *et al.* (2023) 'Cytoprotective Role of Heme Oxygenase-1 in Cancer Chemoresistance: Focus on Antioxidant, Antiapoptotic, and Pro-Autophagy

Properties', *Antioxidants*, 12(6), p. 1217. Available at: https://doi.org/10.3390/antiox12061217.

Wang, Haolan *et al.* (2023) 'Targeting p53 pathways: mechanisms, structures, and advances in therapy', *Signal Transduction and Targeted Therapy*, 8(1), p. 92. Available at: https://doi.org/10.1038/s41392-023-01347-1.

Wang, J. and Lenardo, M.J. (2000) 'Roles of caspases in apoptosis, development, and cytokine maturation revealed by homozygous gene deficiencies', *Journal of Cell Science*, 113(5), pp. 753–757. Available at: https://doi.org/10.1242/jcs.113.5.753.

Wang, J.-Q. *et al.* (2015) 'A Randomized Controlled Trial Comparing Clinical Outcomes and Toxicity of Lobaplatin- Versus Cisplatin-Based Concurrent Chemotherapy Plus Radiotherapy and High-Dose-Rate Brachytherapy for FIGO Stage II and III Cervical Cancer', *Asian Pacific Journal of Cancer Prevention*, 16(14), pp. 5957–5961. Available at: https://doi.org/10.7314/APJCP.2015.16.14.5957.

Wang, L. *et al.* (2020) 'Function of p21 and its therapeutic effects in esophageal cancer (Review)', *Oncology Letters*, 21(2), p. 136. Available at: https://doi.org/10.3892/ol.2020.12397.

Wang, S. and El-Deiry, W.S. (2003) 'TRAIL and apoptosis induction by TNF-family death receptors', *Oncogene*, 22(53), pp. 8628–8633. Available at: https://doi.org/10.1038/sj.onc.1207232.

Wang, X. *et al.* (2006) 'Rad17 Phosphorylation Is Required for Claspin Recruitment and Chk1 Activation in Response to Replication Stress', *Molecular Cell*, 23(3), pp. 331–341. Available at: https://doi.org/10.1016/j.molcel.2006.06.022.

Wang, Y. and Sun, Y. (2002) 'Insulin-Like Growth Factor Receptor-1 as an Anti-Cancer Target: Blocking Transformation and Inducing Apoptosis', *Current Cancer Drug Targets*, 2(3), pp. 191–207. Available at: https://doi.org/10.2174/1568009023333863.

Watson, J.D. and Crick, F.H.C. (1953) 'Molecular Structure of Nucleic Acids: A Structure for Deoxyribose Nucleic Acid', *Nature*, 171(4356), pp. 737–738. Available at: https://doi.org/10.1038/171737a0.

Weber, G.F. (2015) 'DNA Damaging Drugs', in Weber, G. F., *Molecular Therapies of Cancer*. Cham: Springer International Publishing, pp. 9–112. Available at: https://doi.org/10.1007/978-3-319-13278-5_2.

Wegiel, B. *et al.* (2013) 'Carbon Monoxide Expedites Metabolic Exhaustion to Inhibit Tumor Growth', *Cancer Research*, 73(23), pp. 7009–7021. Available at: https://doi.org/10.1158/0008-5472.CAN-13-1075.

Wheate, N.J. *et al.* (2007a) 'Novel platinum(ii)-based anticancer complexes and molecular hosts as their drug delivery vehicles', *Dalton Transactions*, (43), p. 5055. Available at: https://doi.org/10.1039/b704973k.

Wheate, N.J. *et al.* (2007b) 'Novel platinum(ii)-based anticancer complexes and molecular hosts as their drug delivery vehicles', *Dalton Transactions*, (43), p. 5055. Available at: https://doi.org/10.1039/b704973k.

Wheate, N.J. *et al.* (2010) 'The status of platinum anticancer drugs in the clinic and in clinical trials', *Dalton Transactions*, 39(35), p. 8113. Available at: https://doi.org/10.1039/c0dt00292e.

Wu, Y.-S. *et al.* (2005) 'Intercalation into the DNA double helix and in vivo biological activity of water-soluble planar [Pt(diimine)(N,N-dihydroxyethyl-N′-benzoylthioureato)]+Cl− complexes: A study of their thermal stability, their CD spectra and their gel mobility', *Archives of Biochemistry and Biophysics*, 440(1), pp. 28–37. Available at: https://doi.org/10.1016/j.abb.2005.05.022.

Yang, H. *et al.* (2018) 'The role of cellular reactive oxygen species in cancer chemotherapy', *Journal of Experimental & Clinical Cancer Research*, 37(1), p. 266. Available at: https://doi.org/10.1186/s13046-018-0909-x.

Yang, Q.-H. *et al.* (2003) 'Omi/HtrA2 catalytic cleavage of inhibitor of apoptosis (IAP) irreversibly inactivates IAPs and facilitates caspase activity in apoptosis', *Genes & Development*, 17(12), pp. 1487–1496. Available at: https://doi.org/10.1101/gad.1097903.

Youle, R.J. and Strasser, A. (2008) 'The BCL-2 protein family: opposing activities that mediate cell death', *Nature Reviews Molecular Cell Biology*, 9(1), pp. 47–59. Available at: https://doi.org/10.1038/nrm2308.

Zahra, U. *et al.* (2022) 'Recent trends in chemistry, structure, and various applications of 1-acyl-3-substituted thioureas: a detailed review', *RSC Advances*, 12(20), pp. 12710–12745. Available at: https://doi.org/10.1039/D2RA01781D.

Zhang, M. *et al.* (2018) 'Insulin-like growth factor 1/insulin-like growth factor 1 receptor signaling protects against cell apoptosis through the PI3K/AKT pathway in glioblastoma cells', *Experimental and Therapeutic Medicine* [Preprint]. Available at: https://doi.org/10.3892/etm.2018.6336.

Zhang, Y. *et al.* (2019) 'p53 sensitizes chemoresistant non-small cell lung cancer via elevation of reactive oxygen species and suppression of EGFR/PI3K/AKT signaling', *Cancer Cell International*, 19(1), p. 188. Available at: https://doi.org/10.1186/s12935-019-0910-2.

Zhao, R. *et al.* (2019) 'Mitochondrial electron transport chain, ROS generation and uncoupling (Review)', *International Journal of Molecular Medicine* [Preprint]. Available at: https://doi.org/10.3892/ijmm.2019.4188.

Zorova, L.D. *et al.* (2018) 'Mitochondrial membrane potential', *Analytical Biochemistry*, 552, pp. 50–59. Available at: https://doi.org/10.1016/j.ab.2017.07.009.

Zumbrägel, F.K. *et al.* (2017) 'Survivin does not influence the anti-apoptotic action of XIAP on caspase-9', *Biochemical and Biophysical Research Communications*, 482(4), pp. 530–535. Available at: https://doi.org/10.1016/j.bbrc.2016.11.094.

Kotzé I. A. *et al.* (2009). 'Self-Association of [Pt^{II}(1,10-Phenanthroline)(*N*-pyrrolidyl-*N*-(2,2- dimethylpropanoyl)thiourea)]$^{+}$ and Non-Covalent Outer-Sphere Complex Formation with Fluoranthene through π–Cation Interactions: A High Resolution ^{1}H and DOSY NMR Study', *European Journal of Inorganic Chemistry*, 200, pp. 1626–1633.

Kangara, E.F., (2019). Synthesis and characterisation of novel [Pt^{II}(phen)(L^{n}-κS)$_2$] complexes: Exploring rare monodentate coordination of disubstituted acylthioureato ligands. PhD thesis. University of the Witwatersrand. 1-145.

Magwaza, R. N., (2017). Synthesis and characterization of novel [Pt(diimine)(acylthiourea)]$^{+}$ complexes as potential anticancer agents and exploring the use of Sulphobutyl-ether- β -cyclodextrin and surfactant micelles as a drug delivery system, MSc, University of the Witwatersrand, 1-120.

Appendix A: Chapter 2

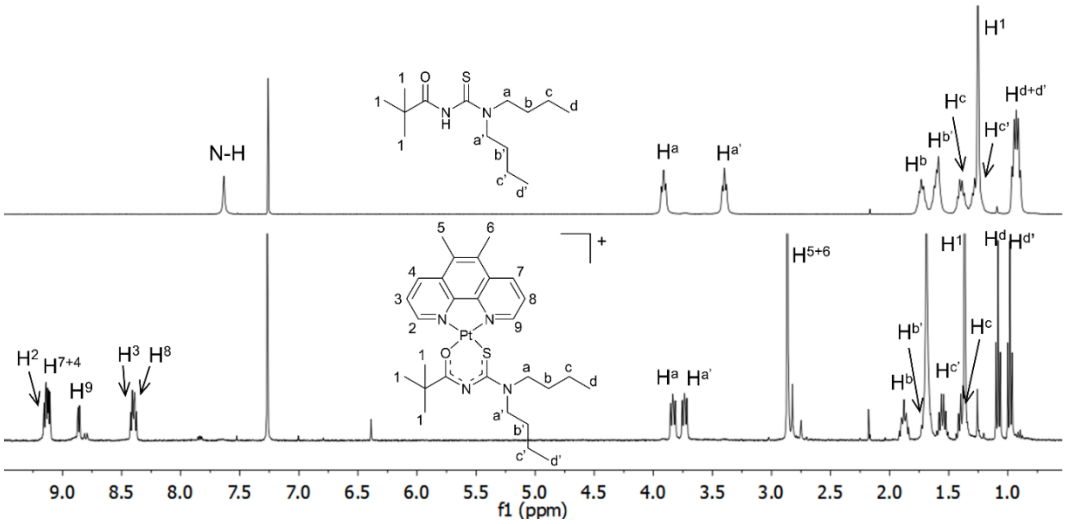


***Figure A1**: Stacked 1D ^{1}H-NMR spectra of N,N-dibutyl-N'-pivaloylthiourea ligand with [Pt(dmp)(L^{3}-κO,S)]$^{+}$ complex in chloroform-d at 300K with all assignments showing a shift in the proton signals (aliphatic region) upon complexation. Spectra shows pure ligand and complex structure obtained, with residual water and acetone signal observed at 1.59 and 2.17 ppm.*

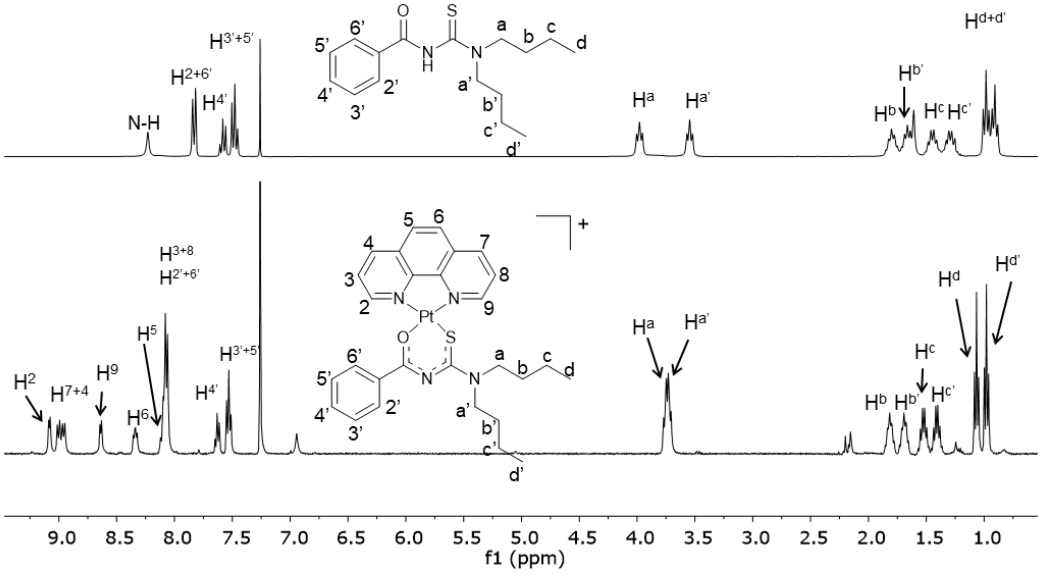


***Figure A2**: Stacked 1D ^{1}H-NMR spectra of N,N-dibutyl-N'-1-benzoylthiourea ligand with [Pt(phen)(L^{1}-κO,S)]$^{+}$ complex in chloroform-d at 300K with all assignments showing a shift in the proton signals (aliphatic region) upon complexation.*

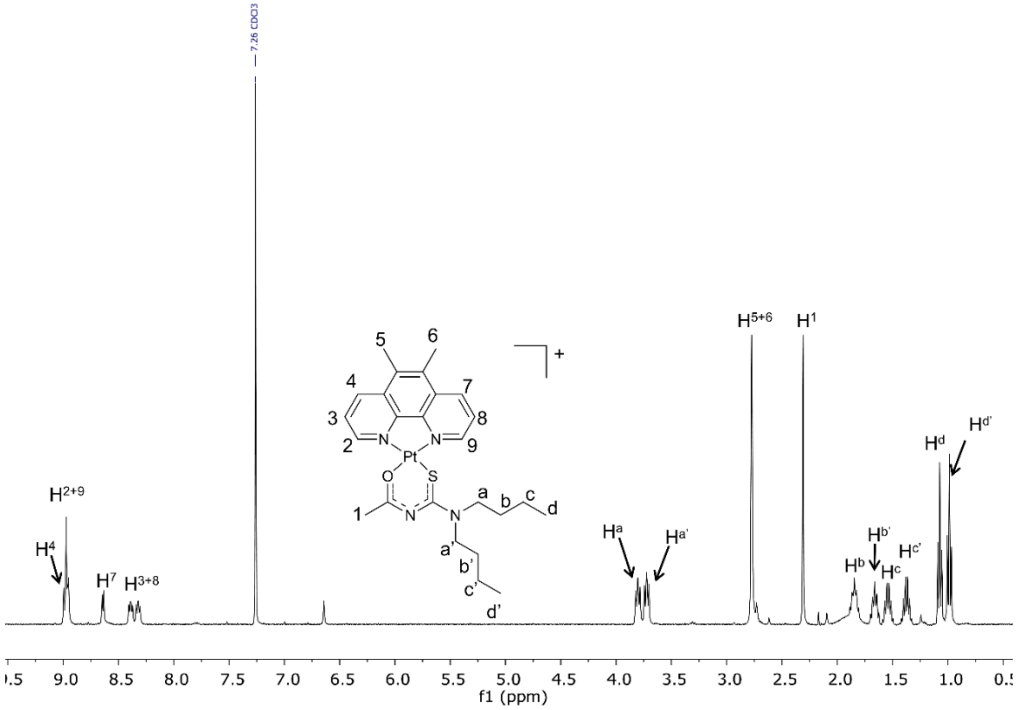


***Figure A3**: Assigned ^{1}H-NMR spectra of [Pt(dmp)(L^{2}-κO,S)]$^{+}$ complex in chloroform-d at 300K.*

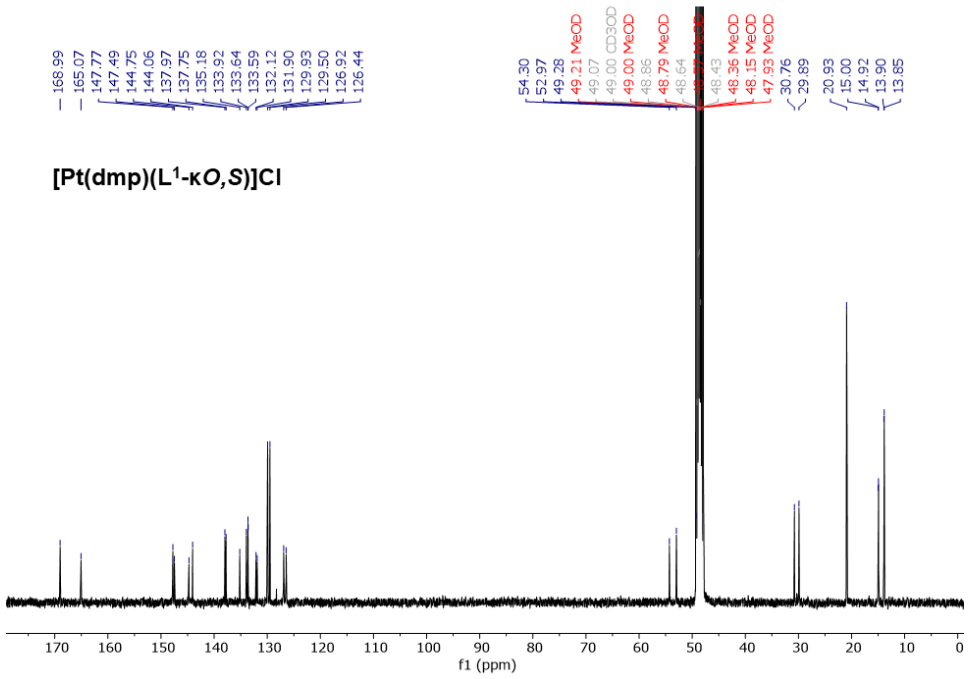


***Figure A4**: ^{13}C NMR spectrum of [Pt(dmp)(L^{1}-κO,S)]$^{+}$ complex in methanol-d$_4$ at 300K.*

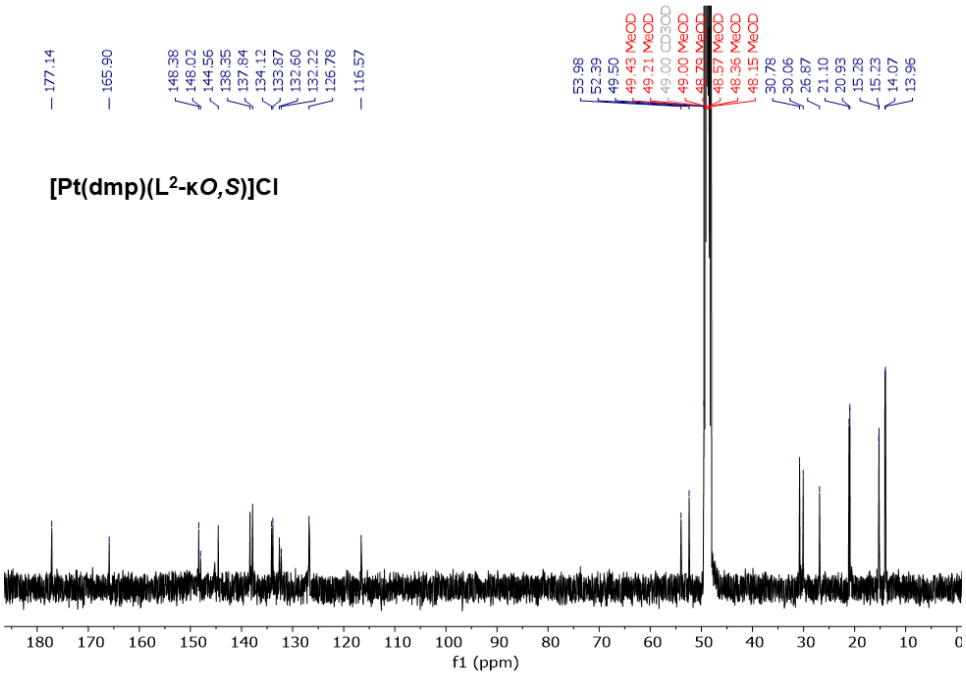


***Figure A5**: ^{13}C NMR spectrum of $[Pt(dmp)(L^2\text{-}\kappa O,S)]^+$ complex in methanol-d_4 at 300K.*

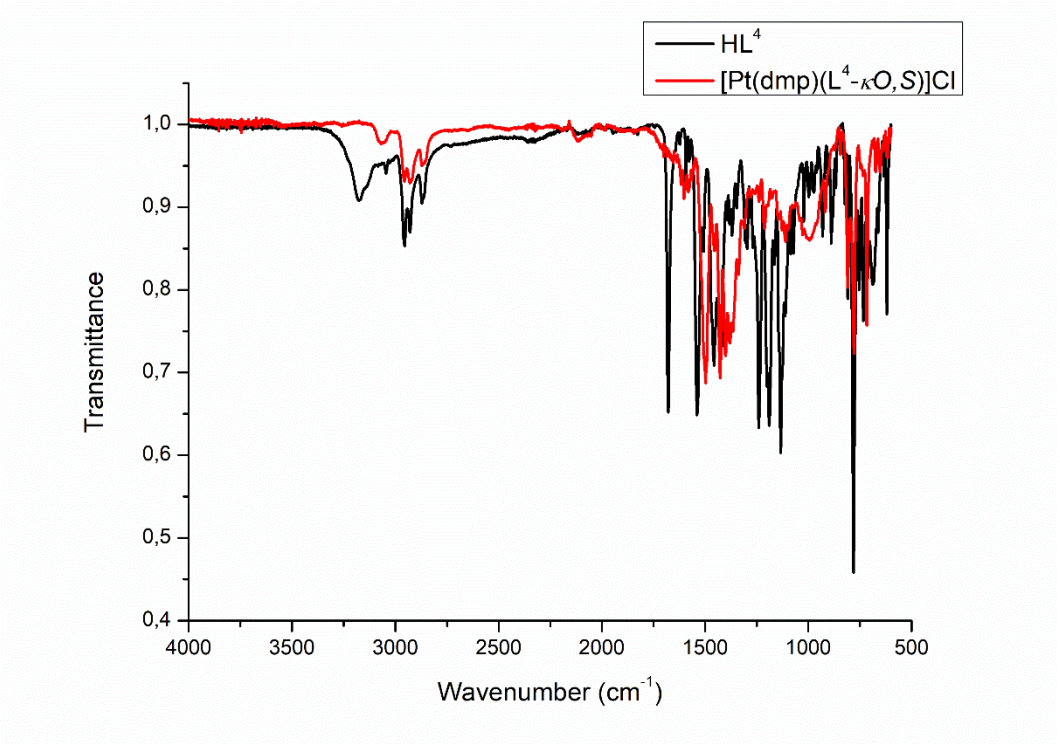


***Figure A6:** Infra-red spectrum of HL^4 stacked alongside that of $[Pt(dmp)(L^4\text{-}\kappa O,S)]Cl$ complex.*

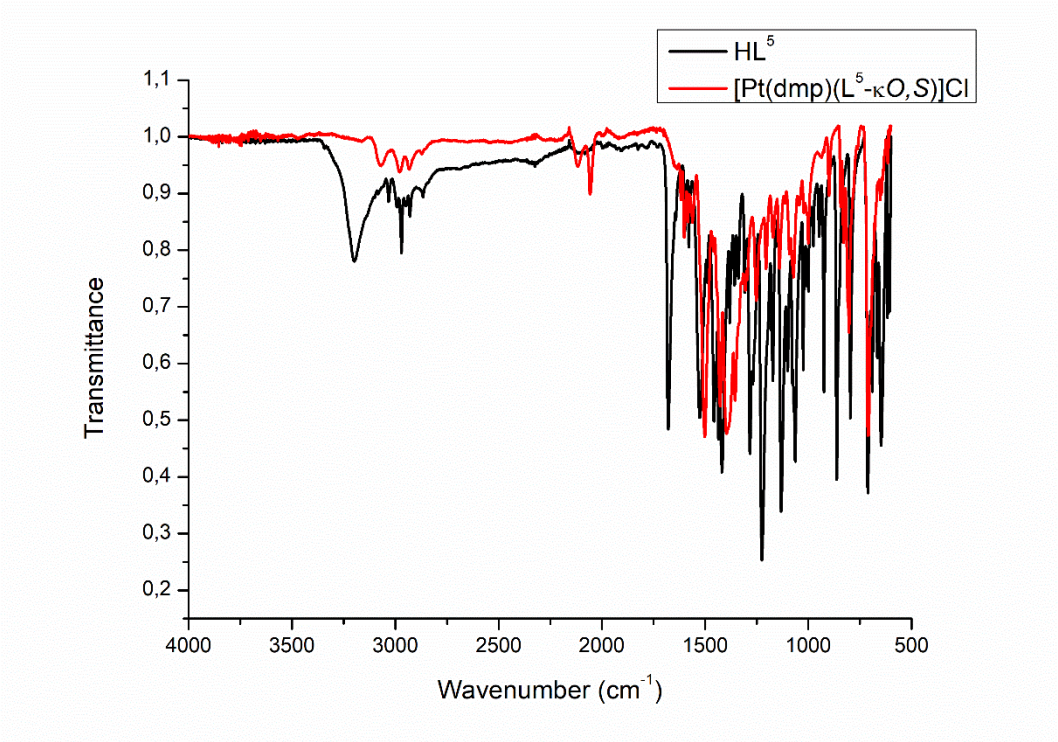


Figure A7: *Infra-red spectrum of HL^5 stacked alongside that of [Pt(dmp)(L^5-κO,S)]Cl complex.*

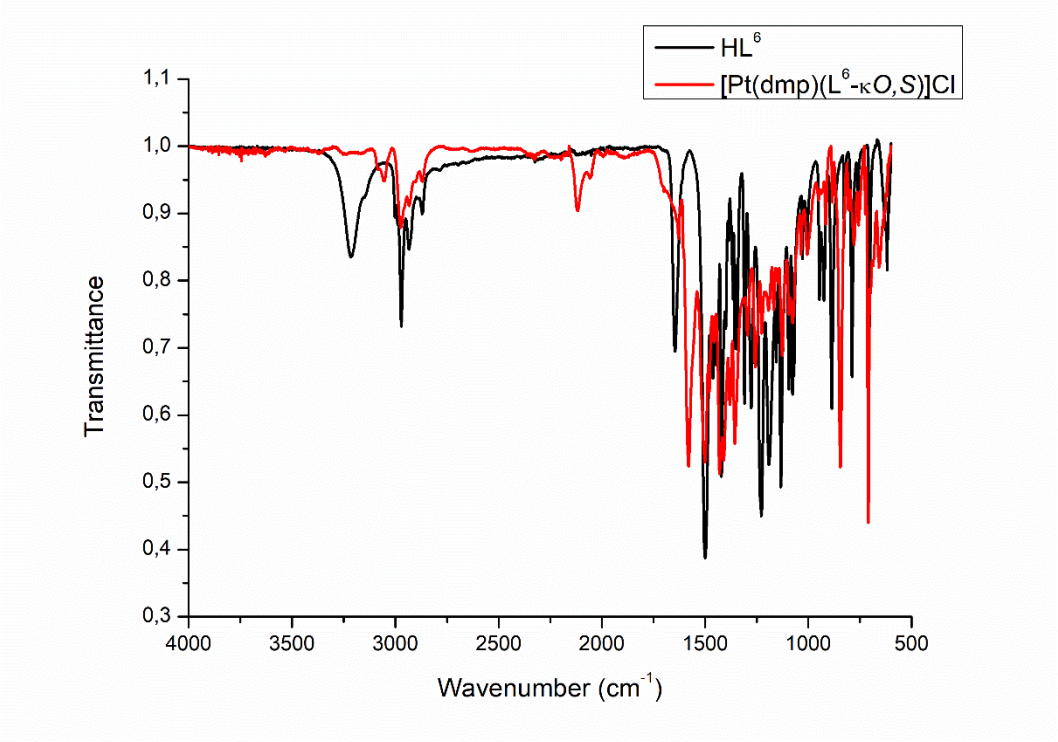


Figure A7: *Infra-red spectrum of HL^6 stacked alongside that of [Pt(dmp)(L^6-κO,S)]Cl complex.*

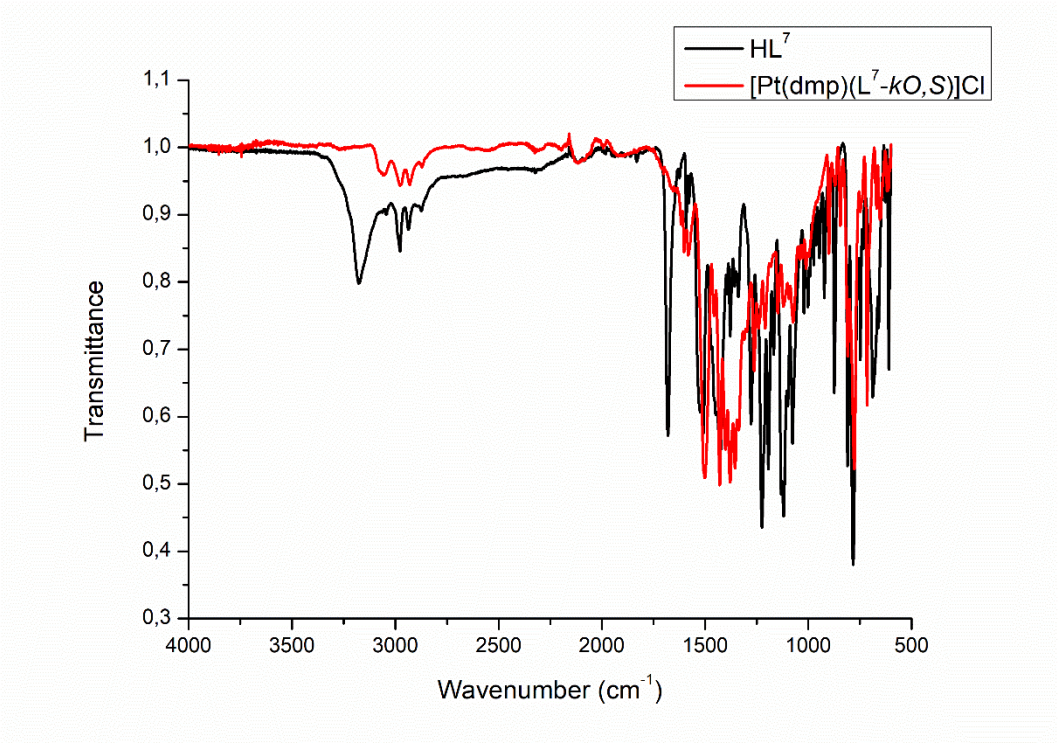


Figure A8: *Infra-red spectrum of HL^7 stacked alongside that of [Pt(dmp)(L^7-κO,S)]Cl complex.*

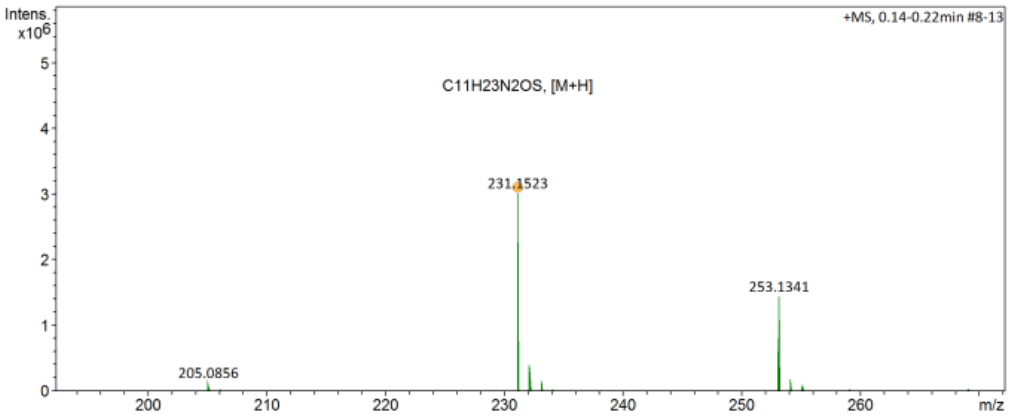


Figure A9*: High resolution mass spectrum of N,N-dibutyl-N'-acetyllthiourea (HL^2) prepared in HPLC grade methanol (m/z: calculated 230.15; observed 231.15 L+H).*

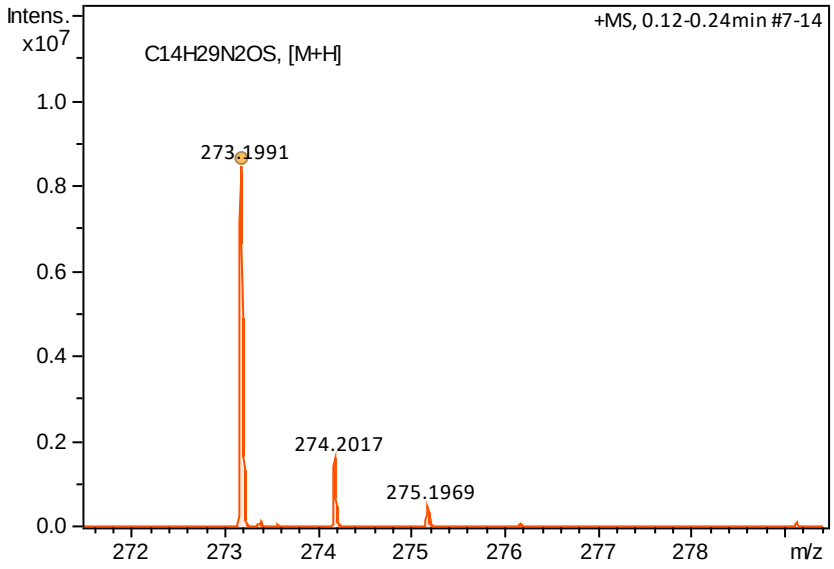


***Figure A10**: High resolution mass spectrum of N,N-dibutyl-N'-pivaloylthiourea (**HL^3**) prepared in HPLC grade methanol (m/z: calculated 272.19; observed 273.19).*

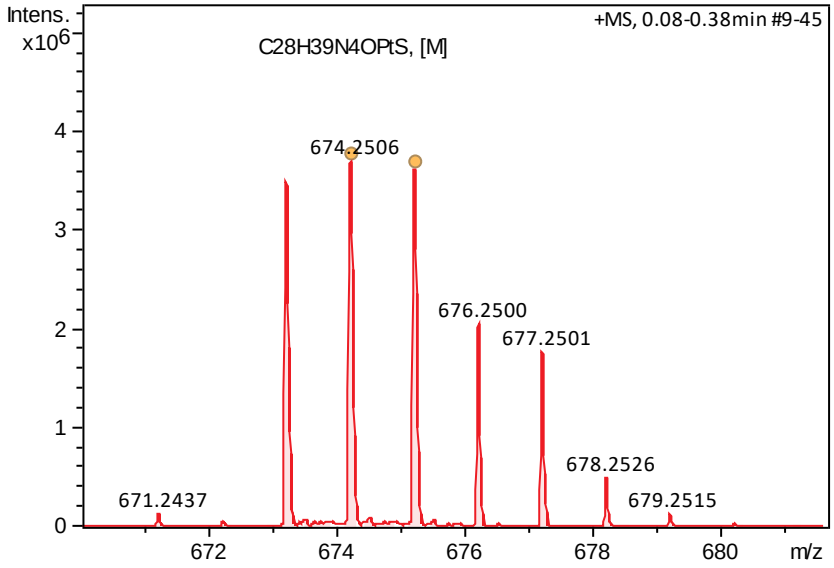


***Figure A11**: The high resolution mass spectrum of [Pt(dmp)(L^3-κO,S)]Cl prepared in HPLC grade methanol (m/z: calculated 674.25; observed 674.25).*

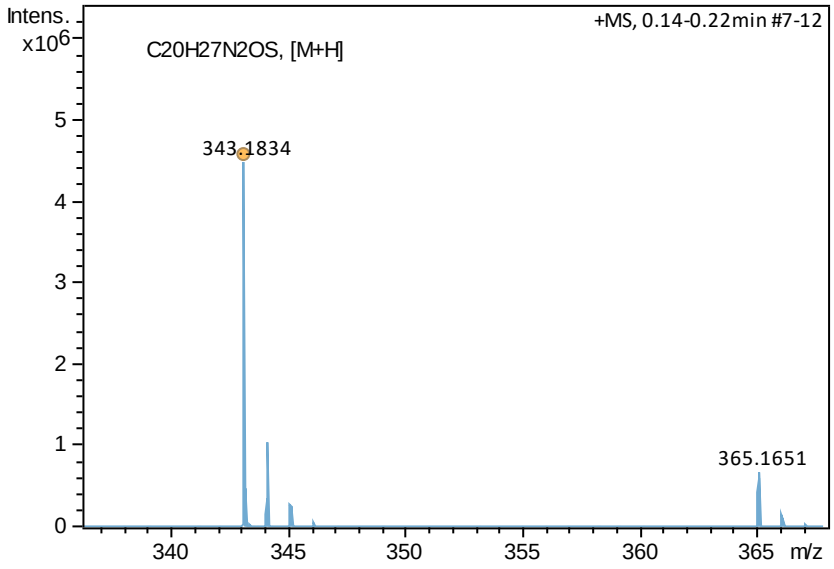


***Figure A12**: High resolution mass spectrum of N,N-dibutyl-N'-napthoylthiourea (**HL^4**) in prepared in HPLC grade methanol (m/z: calculated 342.18; observed 343.18).*

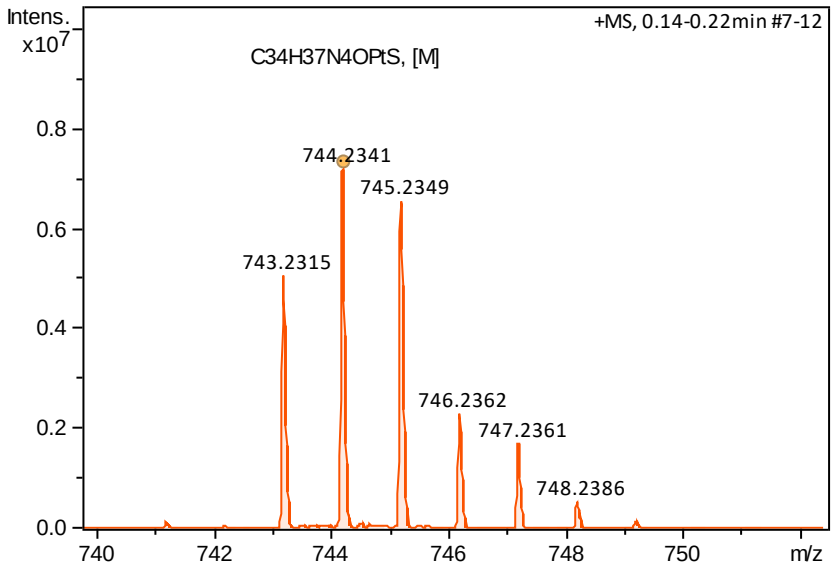


***Figure A13**: The high resolution mass spectrum of [Pt(dmp)(L^4-κO,S)]Cl prepared in HPLC grade methanol (m/z: calculated 744.23; observed 744.23).*

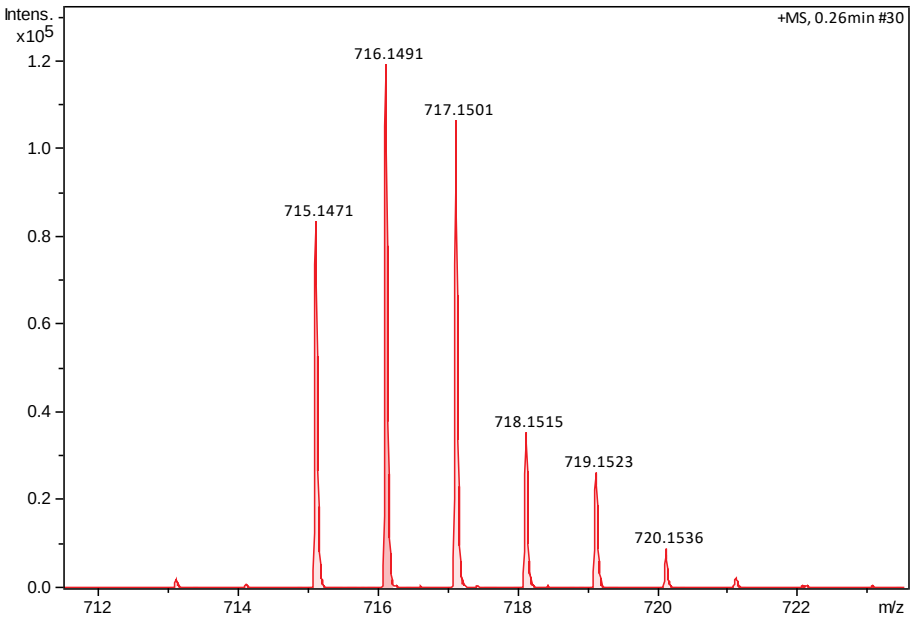


***Figure A14**: The high resolution mass spectrum of [Pt(phen)(L^4-κO,S)]Cl prepared in HPLC grade methanol (m/z: calculated 716.20; observed 716.15).*

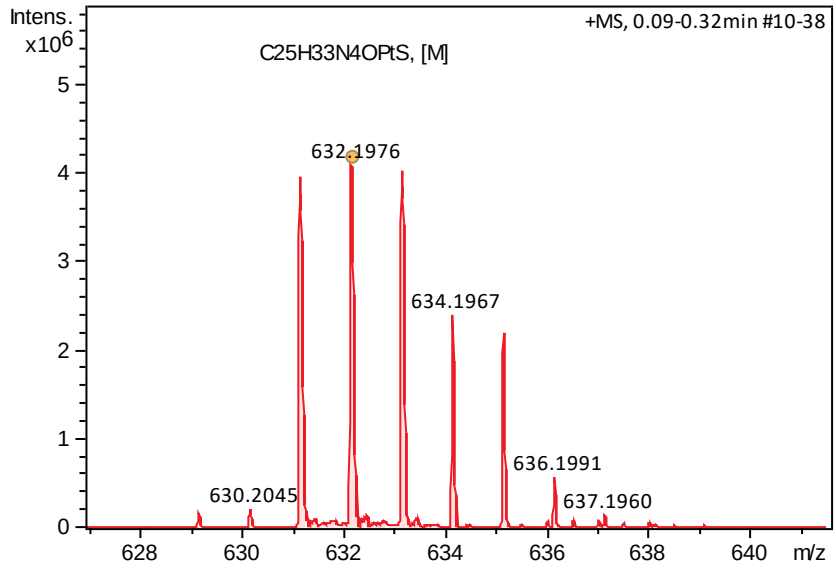


***Figure A15**: The high resolution mass spectrum of [Pt(dmp)(L^2-κO,S)]Cl prepared in HPLC grade methanol (m/z: calculated 632.20; observed 632.19).*

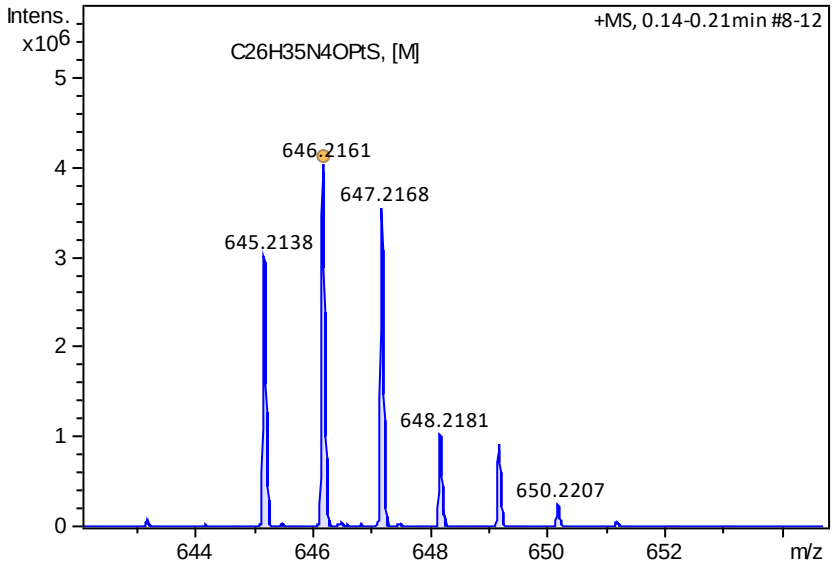


***Figure A16**: The high resolution mass spectrum of [Pt(phen)(L^3-κO,S)]Cl prepared in HPLC grade methanol (m/z: calculated 646.22; observed 646.22).*

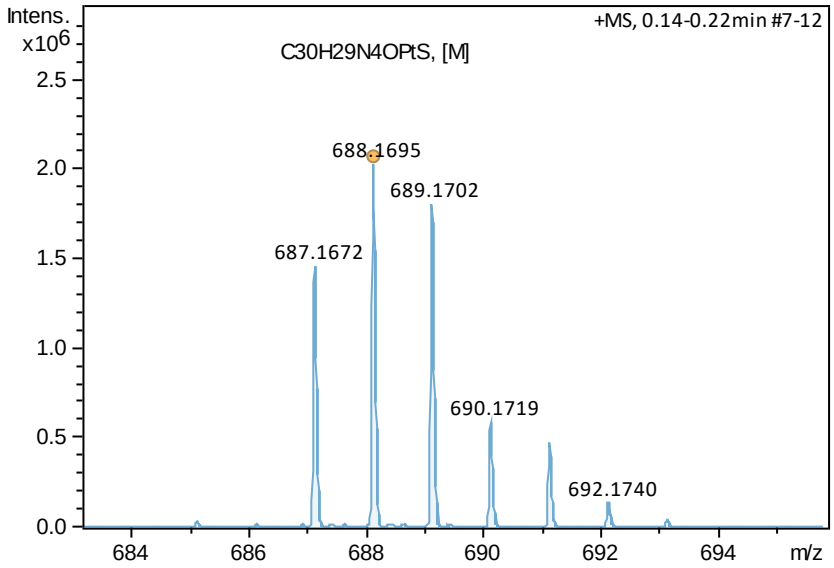


***Figure A17**: The high resolution mass spectrum of [Pt(dmp)(L^7-κO,S)]Cl prepared in HPLC grade methanol (m/z; calculated 688.17; observed 688.17).*

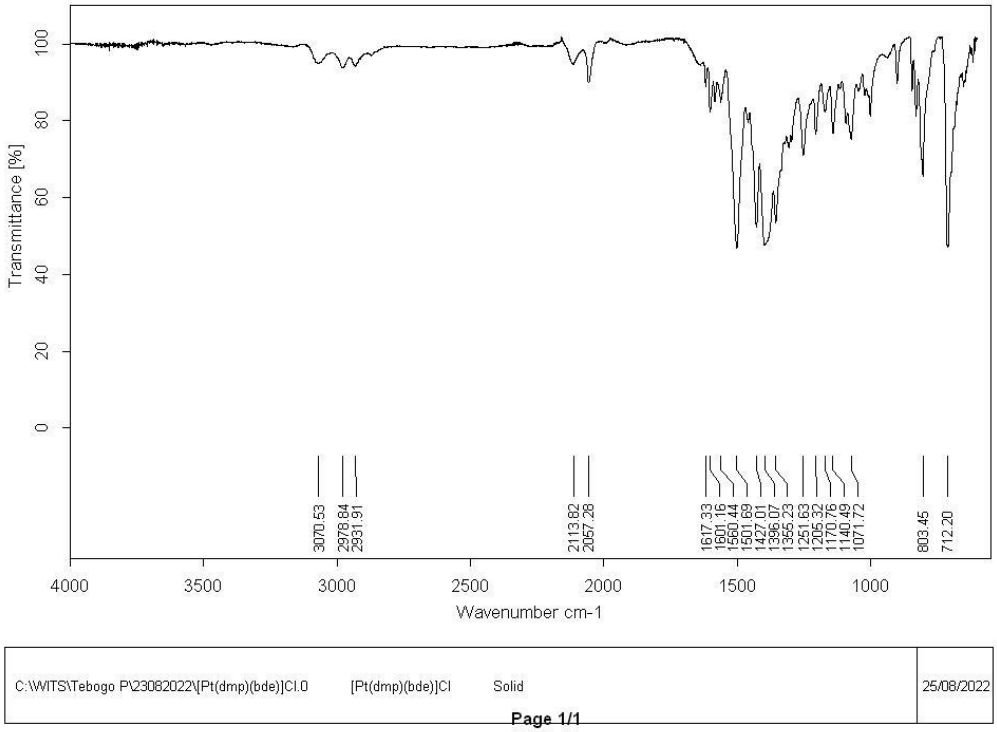


Figure A20: *Infra-red spectrum of [Pt(dmp)(L^5-κO,S)]Cl complex.*

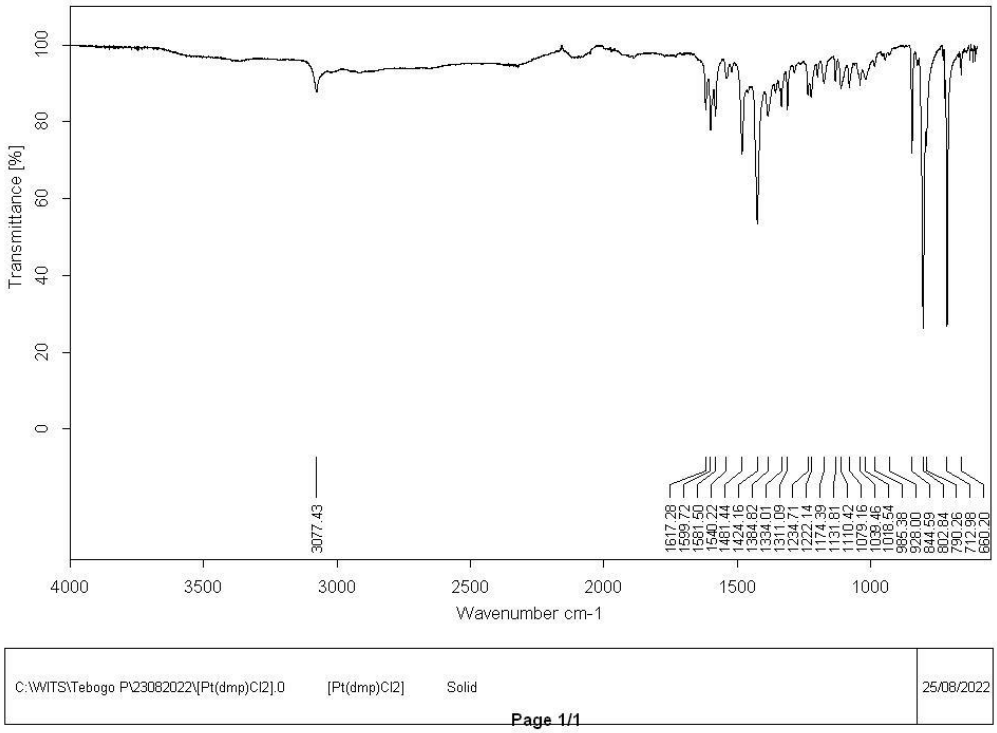


Figure A21: *Infra-red spectrum of $PtCl_2$(dmp).*

Appendix B: Chapter 3

I. Human ethics waiver certificate

UNIVERSITY OF THE WITWATERSRAND, JOHANNESBURG | HUMAN RESEARCH ETHICS COMMITTEE (MEDICAL

Human Research Ethics Committee (Medical)

Research Office Secretariat:
Faculty of Health Sciences, Phillip Tobias Building, 3rd Floor, Office 301/2/4, 29 Princess of Wales Terrace, Parktown, 2193
Tel +27 (0)11-717-1252 /1234/2656/2700
Private Bag 3, Wits 2050
Office email: HREC-Medical.ResearchOffice@wits.ac.za
Website: www.wits.ac.za/research/about-our-research/ethics-and-research-integrity/

Ref: W-CBP-180420-6 20/04/2018

TO WHOM IT MAY CONCERN:

Waiver: This certifies that the following research does not require clearance from the Human Research Ethics Committee (Medical)

Investigator: Miss Tebogo Peega (student no. 835353) et al

Supervisor: Dr Leonie Harmse

Department: Pharmacology

Project title: Synthesis, characterization and potential anti-cancer activity of novel platinum complexes

Reason: Laboratory analysis.
No human participants will be involved in the study.

Professor CB Penny
Chairperson: Human Research Ethics Committee (Medical)

UNIVERSITY OF THE WITWATERSRAND OFFICE OF THE DEPUTY VICE CHANCELLOR RESEARCH 20 APR 2018 RESEARCH OFFICE HREC (Medical) JOHANNESBURG

Copy – HREC (Medical) Secretariat: Zanele Ndlovu and Rhulani Mkansi.

II. Cytotoxicity effects of platinum complexes and free ligands at 5 µM

Table B1: *Percentage cell viability of H1975, A549 and HT-29 cells in response to 5 µM of [Pt(diimine)(L^n-κO,S)]Cl complexes and free diimine ligands after a 48 hour treatment.*

Platinum complexes	**Cell viability (%) ± SD at 5 µM**		
	H1975	**A549**	**HT-29**
[Pt(phen)(L^1-κ*O,S*)]Cl	20.6 ± 1,6	7.7 ± 3,2	4.3 ± 1,7
[Pt(phen)(L^2-κ*O,S*)]Cl	49.6 ± 3,8	22.9 ± 0,2	11.9 ± 2,3
[Pt(phen)(L^3-κ*O,S*)]Cl	18.0 ± 1,4	9.8 ± 0,3	6.5 ± 1,5
[Pt(dmp)(L^1-κ*O,S*)]Cl	5.5 ± 1,6	1.5 ± 0,2	1.8 ± 0,5
[Pt(dmp)(L^2-κ*O,S*)]Cl	9.2 ± 1,5	6.0 ± 1,1	1.5 ± 0,1
[Pt(dmp)(L^3-κ*O,S*)]Cl	1.4 ± 1,6	1.7 ± 0,4	1.1 ± 0,7
[Pt(dpq)(L^1-κ*O,S*)]Cl	43.4 ± 3,1	39.4 ± 5,4	61.0 ± 1,7
[Pt(dpq)(L^2-κ*O,S*)]Cl	34.6 ± 2,1	65.2 ± 5,3	51.5 ± 0,4
[Pt(dpq)(L^3-κ*O,S*)]Cl	21.1 ± 1,7	17.1 ± 3,1	20.9 ± 2,3
Cisplatin	76.9 ± 13,4	73.9 ± 11,9	94.0 ± 8,9
Diimine ligands			
phen	97.4 ± 9.50	80.9 ± 8.7	71.8 ± 20.7
dmp	63.6 ± 4.70	48.1 ± 3.9	38.7 ± 9.1
dpq	97.7 ± 5.50	83.4 ± 11.1	75.7 ± 8.6

Table B2: Percentage cell viability of H1975 cells treated with N,N-di(butyl)-N'-benzoylthiourea (HL^1), N,N-di(butyl)-N'-acetylthiourea (HL^2) and N,N-di(butyl)-N'-pivaloylthiourea (HL^3) at 50 µM for 48 hours. *A minimum of three independent repeats of the experiment were conducted (N=3). %cell viability ± SD.*

Acylthiourea ligand (HL^n)	**H1975**
HL^1	70.5 ± 3.7
HL^2	94.4 ± 3.3
HL^3	89.6 ± 0.85

III. Representative dose-response curves for determining IC_{50} values of platinum complexes and cisplatin

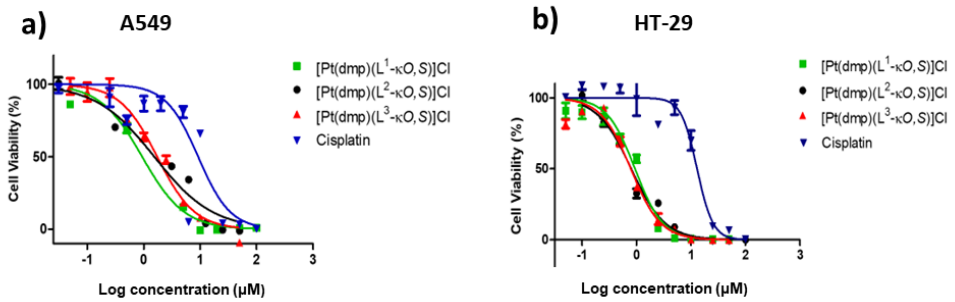


***Figure B1**: Representative dose-response curves of [Pt(dmp)(L^1-κO,S)]Cl, [Pt(dmp)(L^2-κO,S)]Cl, [Pt(dmp)(L^3-κO,S)]Cl and cisplatin against (a) A549 (b) HT-29 cells and following a 48 hour treatment*

IV. Evaluation of changes in cell morphology

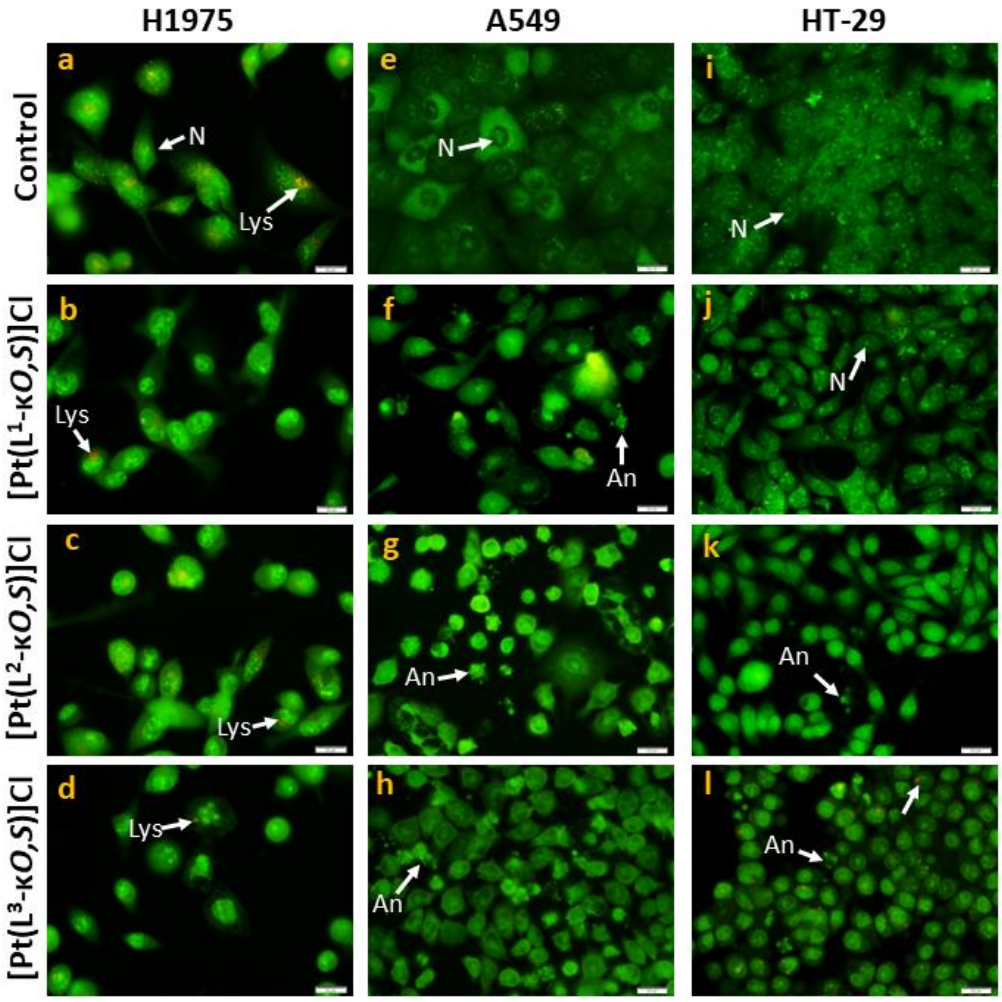


Figure B2: Photomicrographs showing acridine orange ----stained cancer cells. *H1975 and HT-29 cells were treated with 3 µM [Pt(dmp)(L^1-κO,S)]Cl, [Pt(dmp)(L^2-κO,S)]Cl , [Pt(dmp)(L^3-κO,S)]Cl and 15 µM cisplatin, A549 cells were treated with 5 µM [Pt(dmp)(L^1-κO,S)]Cl, [Pt(dmp)(L^2-κO,S)]Cl , [Pt(dmp)(L^3-κO,S)]Cl and 25 µM cisplatin for 18 hours. Images were captured using Olympus DP72 digital camera (Magnification 400X, Scale bar 20 µM). Legend: An: Apoptotic cell, Lys: Lysozomes, N: Nucleus*

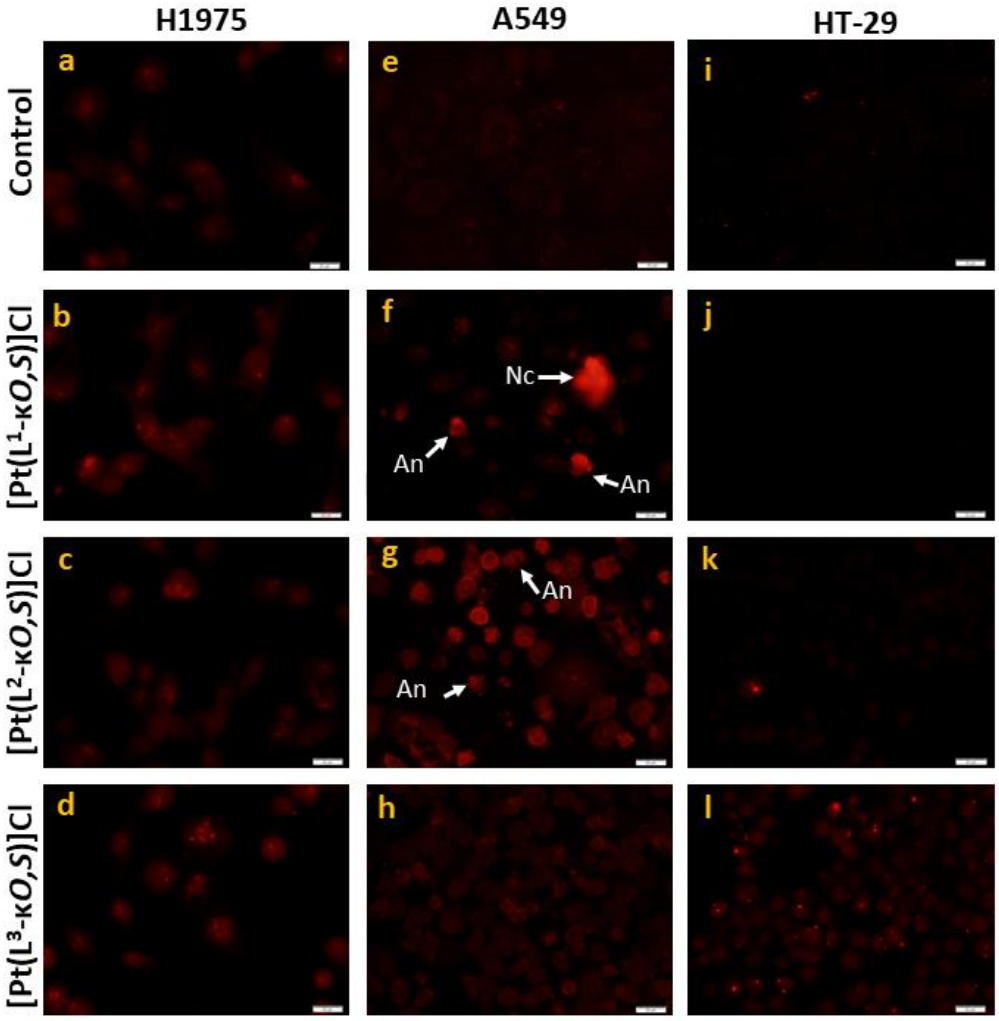


Figure B3: Propidium iodide stained cancer cells showing the absence of necrosis in H1975 and HT-29 cells and minimal necrosis in A549 cells. *H1975 and HT-29 cells were treated with 3 µM [Pt(dmp)(L^1-κO,S)]Cl, [Pt(dmp)(L^2-κO,S)]Cl , [Pt(dmp)(L^3-κO,S)]Cl and 15 µM cisplatin while A549 cells were treated with 5 µM [Pt(dmp)(L^1-κO,S)]Cl, [Pt(dmp)(L^2-κO,S)]Cl , [Pt(dmp)(L^3-κO,S)]Cl and 25 µM cisplatin for 18 hours. Images were captured using Olympus DP72 digital camera (Magnification 400X, Scale bar 20 µM). Legend: An: Apoptotic cell, Nc: Necrotic cell*

V. Annexin V-binding and Propidium iodide staining

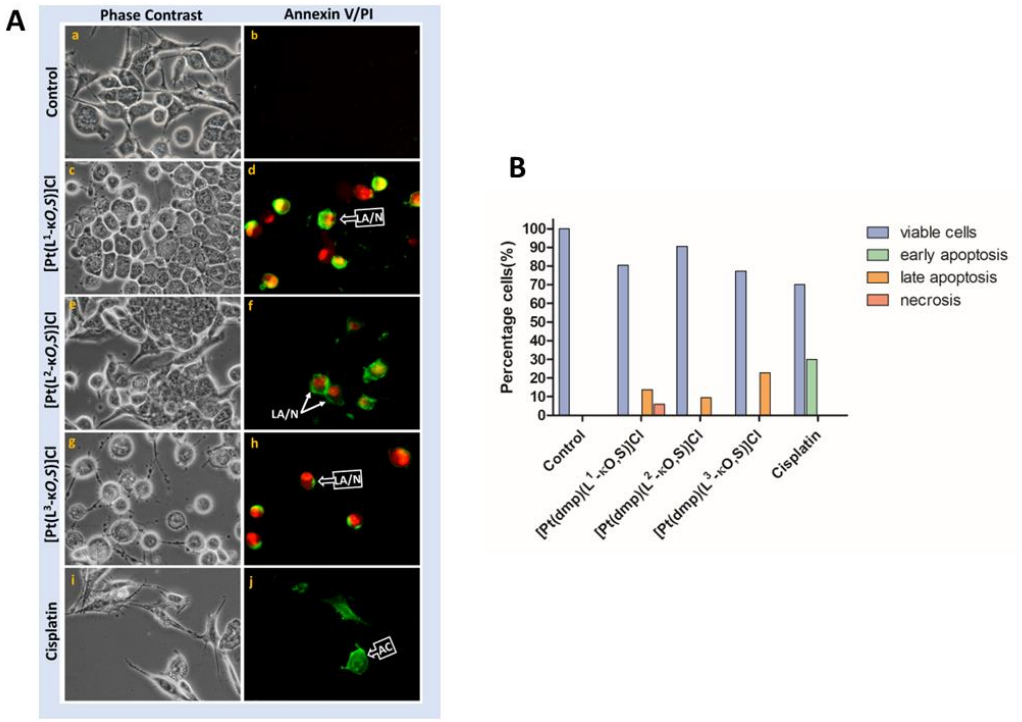


***Figure B4**: **Annexin V/PI staining in H1975 cells after exposure to [Pt(dmp)(L^n-κO,S)]Cl complexes and cisplatin for 18 hours.** H1975 cells were treated with 3 µM of [Pt(dmp)(L^1-κO,S)]Cl, [Pt(dmp)(L^2-κO,S)]Cl, [Pt(dmp)(L^3-κO,S)]Cl complexes and 20 µM cisplatin for 18 hours. A) Photomicrographs of H1975 cells (Magnification 400X; Scalebar: 20 µm). Annotation: LA/N= Late apoptosis/Necrotic cell, AC= Apoptotic cell, RC= round cell, V= Vacuole. B) Bar graphs showing the percentage of viable, early apoptotic, late apoptotic and necrotic cells.*

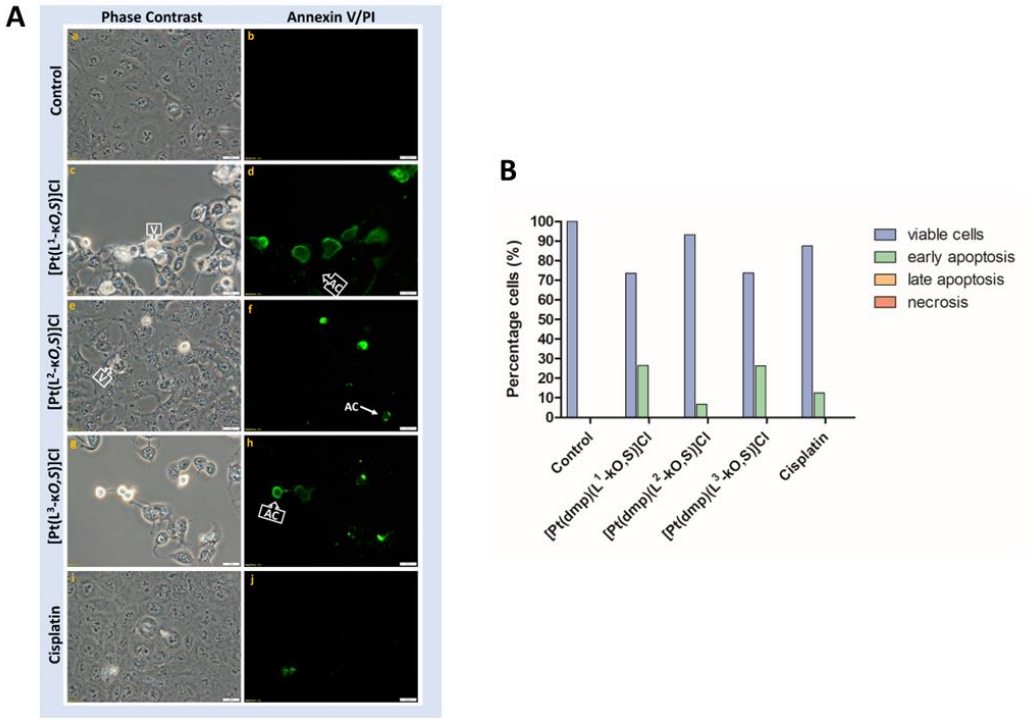


***Figure B5**: **Annexin V/PI staining in A549 cells after exposure to [Pt(dmp)(L^n-κO,S)]Cl complexes and cisplatin for 18 hours**. A549 cells were treated with 5 µM of [Pt(dmp)(L^1-κO,S)]Cl, [Pt(dmp)(L^2-κO,S)]Cl, [Pt(dmp)(L^3-κO,S)]Cl complexes and 25 µM cisplatin. A) Photomicrographs of H1975 cells are shown in panel a-j. (Magnification 400X; Scalebar: 20 µm). Annotation: AC= Apoptotic cell, V= Vacuole, RC= Round cell. B) Bar graphs showing the percentage of viable, early apoptotic, late apoptotic and necrotic cells.*

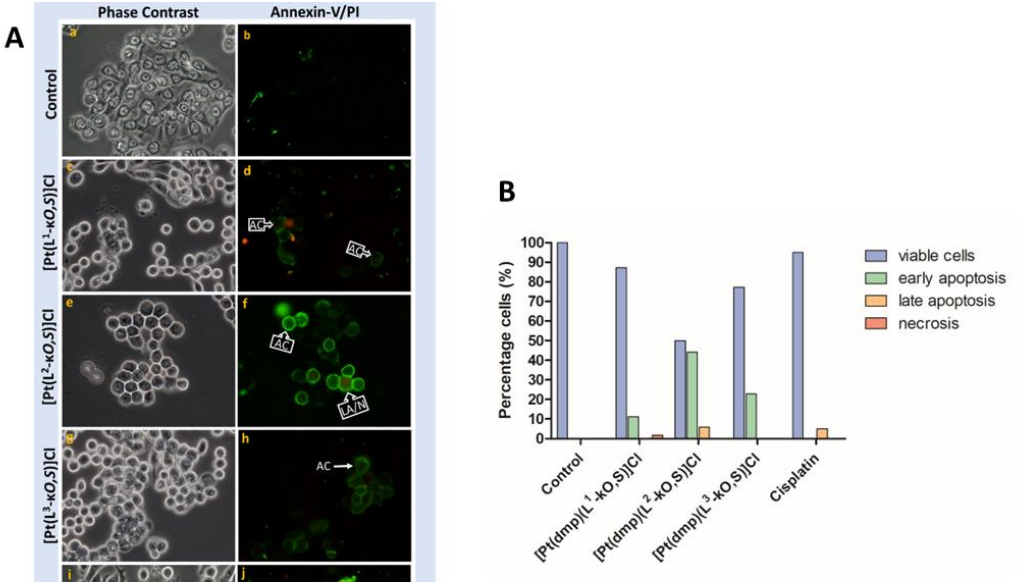


***Figure B6**: **Annexin V/PI staining in HT-29 cells after exposure to [Pt(dmp)(L^n-κO,S)]Cl complexes and cisplatin for 18 hours.** HT-29 cells were treated with 3 µM of [Pt(dmp)(L^1-κO,S)]Cl, [Pt(dmp)(L^2-κO,S)]Cl, [Pt(dmp)(L^3-κO,S)]Cl complexes and 15 µM cisplatin A) Photomicrographs of HT-29 cells are shown in panel a-j. (Magnification 400X; Scalebar: 20 µm). Annotation: LA/N= Late apoptosis/Necrotic cell, AC= Apoptotic cell. B) Bar graphs showing the percentage of viable, early apoptotic, late apoptotic and necrotic cells*

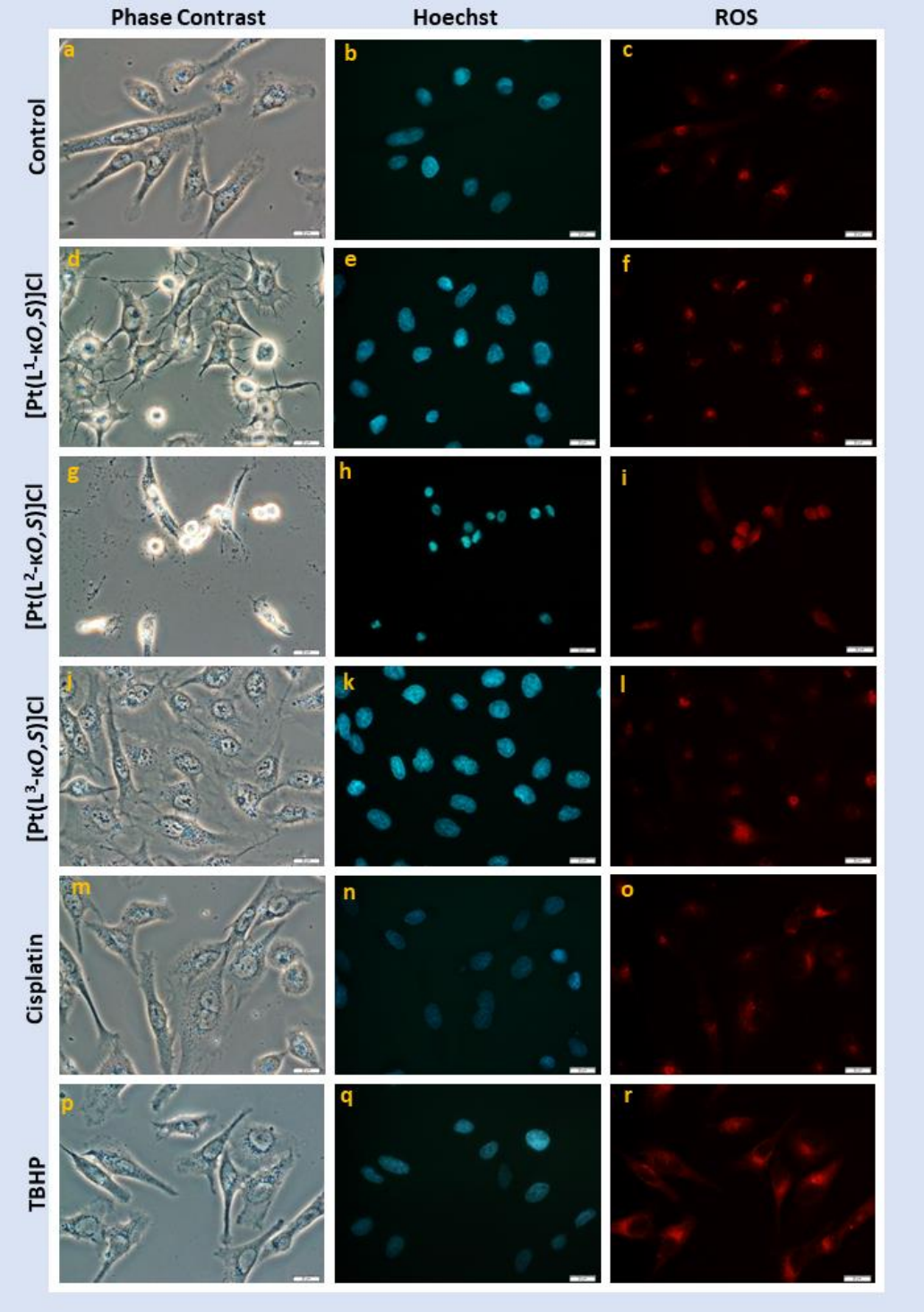


Figure B7: Effects of platinum complexes, cisplatin and TBHP on ROS generation in H1975*. Photomicrographs of H1975 cells showing increased ROS levels when treated with 3 µM of [Pt(dmp)(L^1-κO,S)]Cl, [Pt(dmp)(L^2-κO,S)]Cl, [Pt(dmp)(L^3-κO,S)]Cl complexes, 15 µM cisplatin and 20 µM tertiary-butylhydroperoxide. Cells were counterstained with Hoechst 33342 to observe the nucleus (Magnification 400X; Scalebar: 20 µm).*

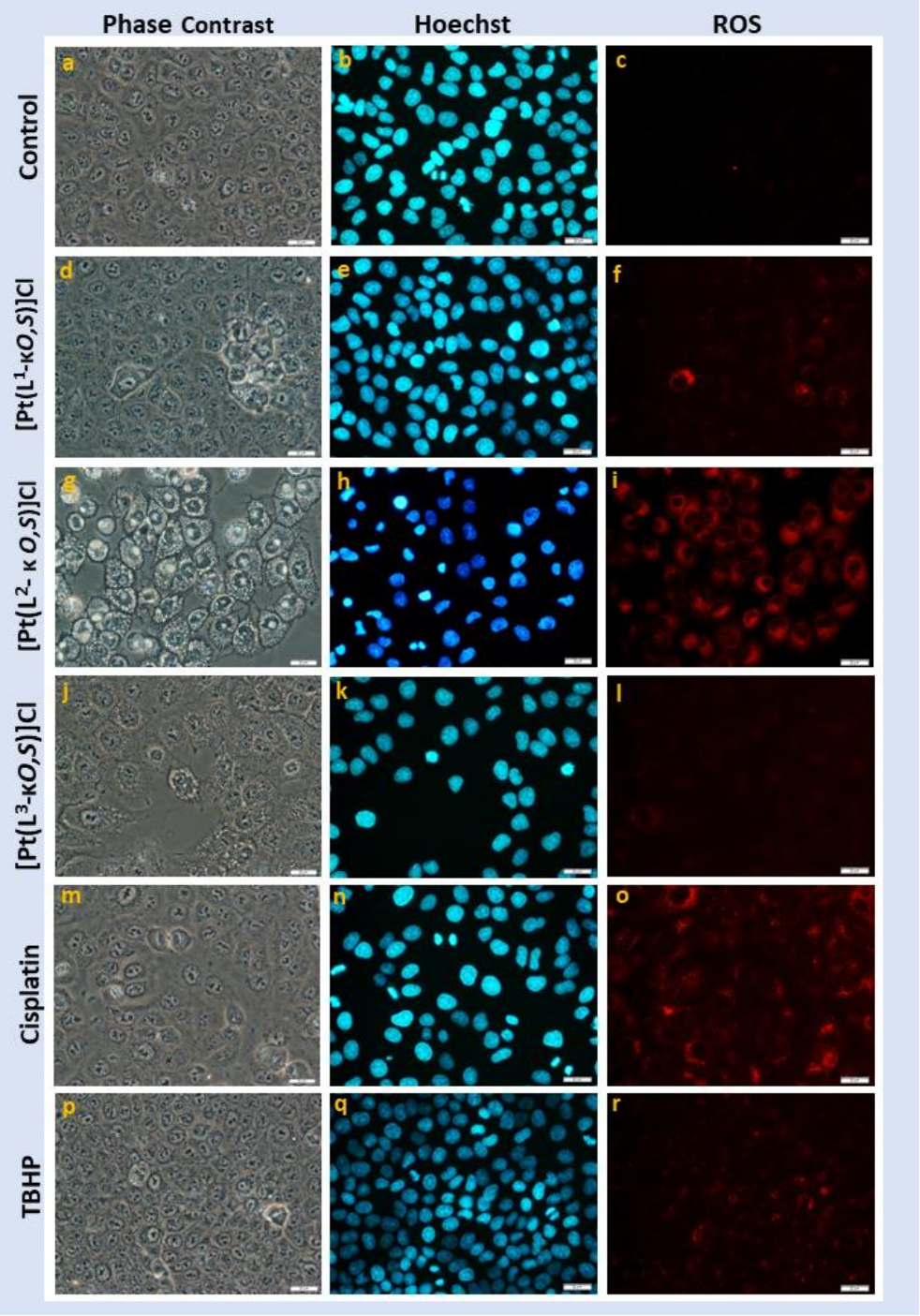


Figure B8: Effects of platinum complexes, cisplatin and TBHP on ROS generation in A549 cells. *Photomicrographs of A549 cells showing increased ROS levels when treated with 5 µM of [Pt(dmp)(L^1-κO,S)]Cl, [Pt(dmp)(L^2-κO,S)]Cl, [Pt(dmp)(L^3-κO,S)]Cl complexes, 25 µM cisplatin and 20 µM tertiary-butylhydroperoxide for 4 hours. Cells were counterstained with Hoechst 33342 to observe the nucleus. (Magnification 400X; Scalebar: 20 µm).*

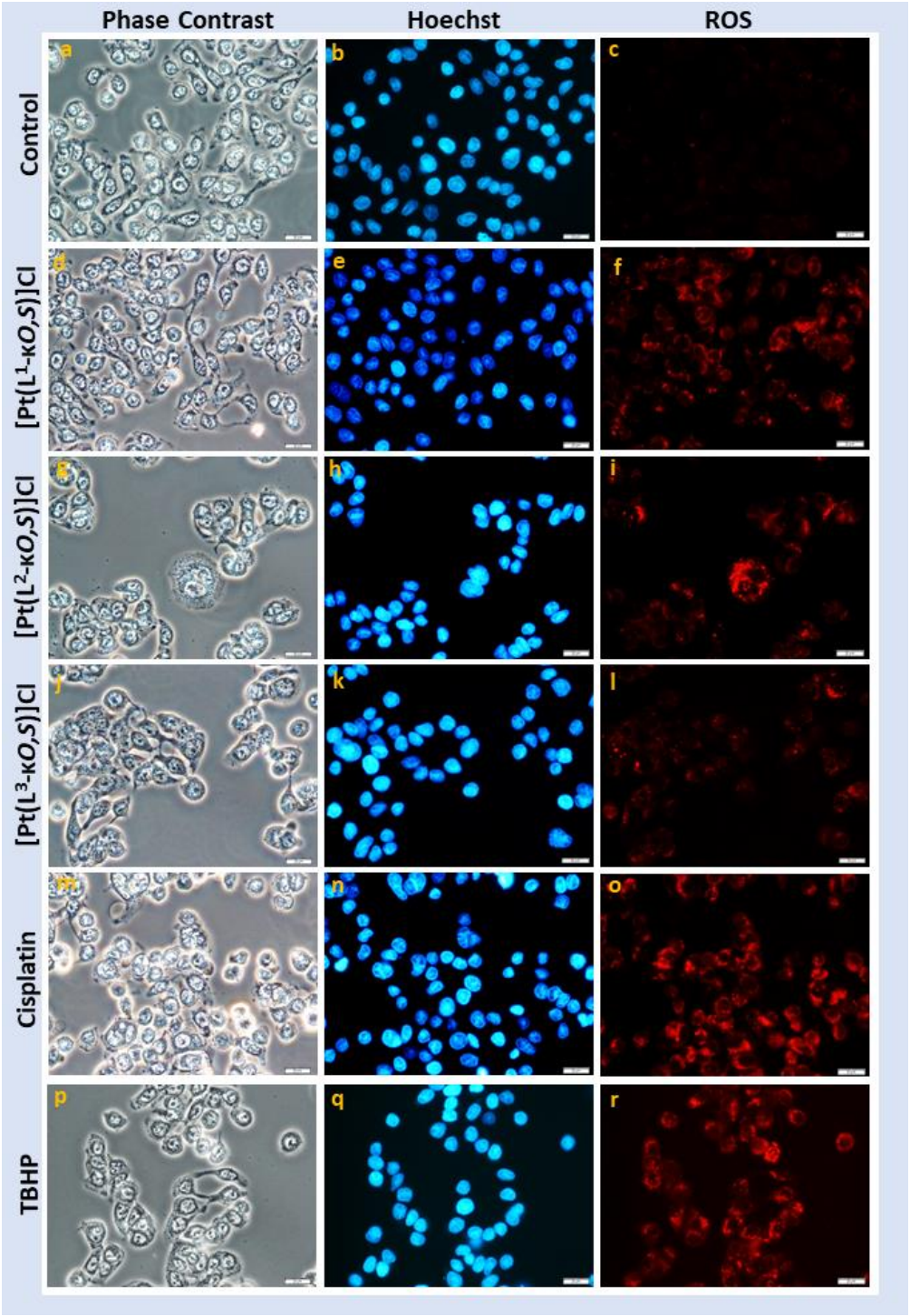


***Figure B9**: **Effects of platinum complexes, cisplatin and TBHP on ROS generation in HT-29 cells**. Photomicrographs of HT-29 cells showing elevated ROS levels after treatment with 5 µM of [Pt(dmp)(L^1-κO,S)]Cl, [Pt(dmp)(L^2-κO,S)]Cl, [Pt(dmp)(L^3-κO,S)]Cl complexes, 25 µM cisplatin and 20 µM tertiary-butylhydroperoxide for 4 hours. Cells were counterstained with HO to observe the nucleus. (Magnification 400X; Scalebar: 20 µm)*

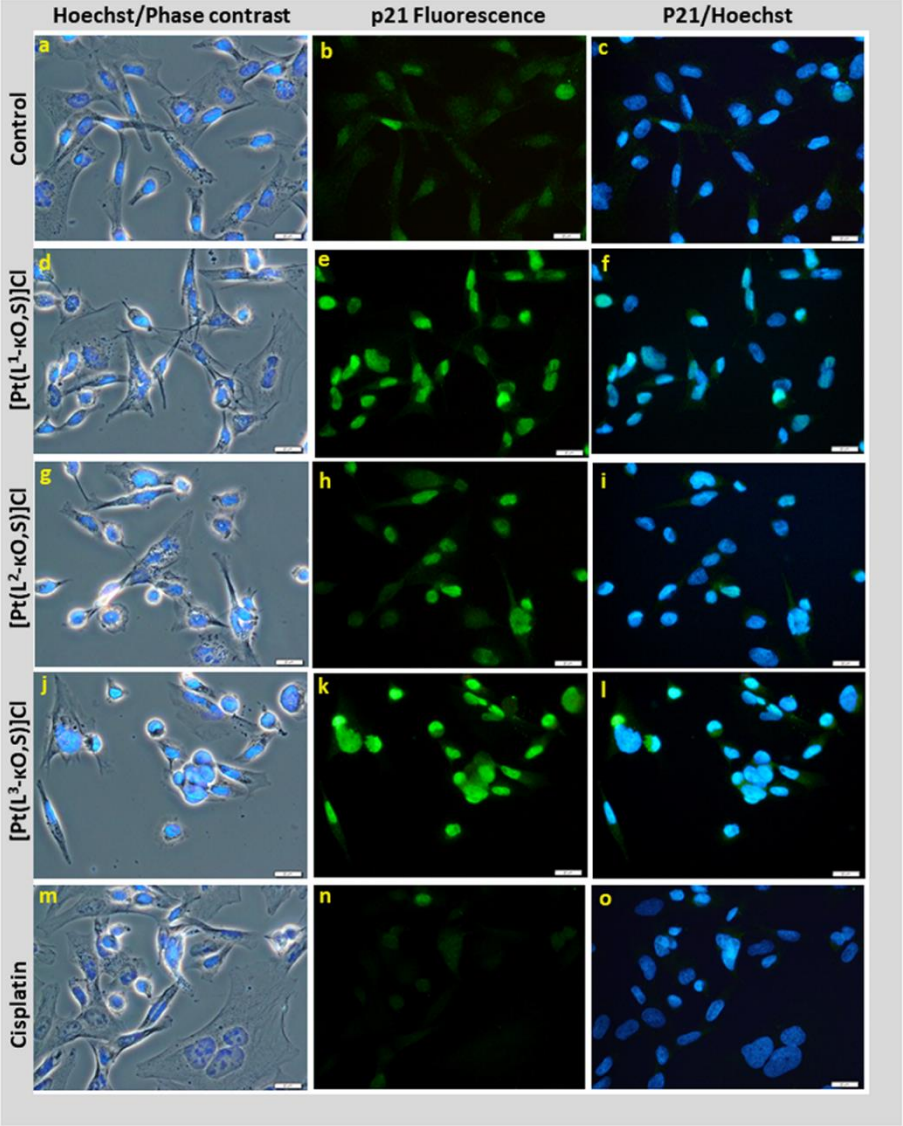


***Figure B10**: **Photomicrographs of H1975 lung cancer cells, showing the nuclear expression of p21.** Cells were treated with 3 µM of [Pt(dmp)(L^1-κO,S)]Cl, [Pt(dmp)(L^2-κO,S)]Cl, [Pt(dmp)(L^3-κO,S)]Cl complexes and 15 µM cisplatin for 18 hours. Cell nuclei were counterstained with HO and merged with p21. Panel a-b shows the untreated negative control cells. (Magnification 400X; Scalebar: 20 µm).*

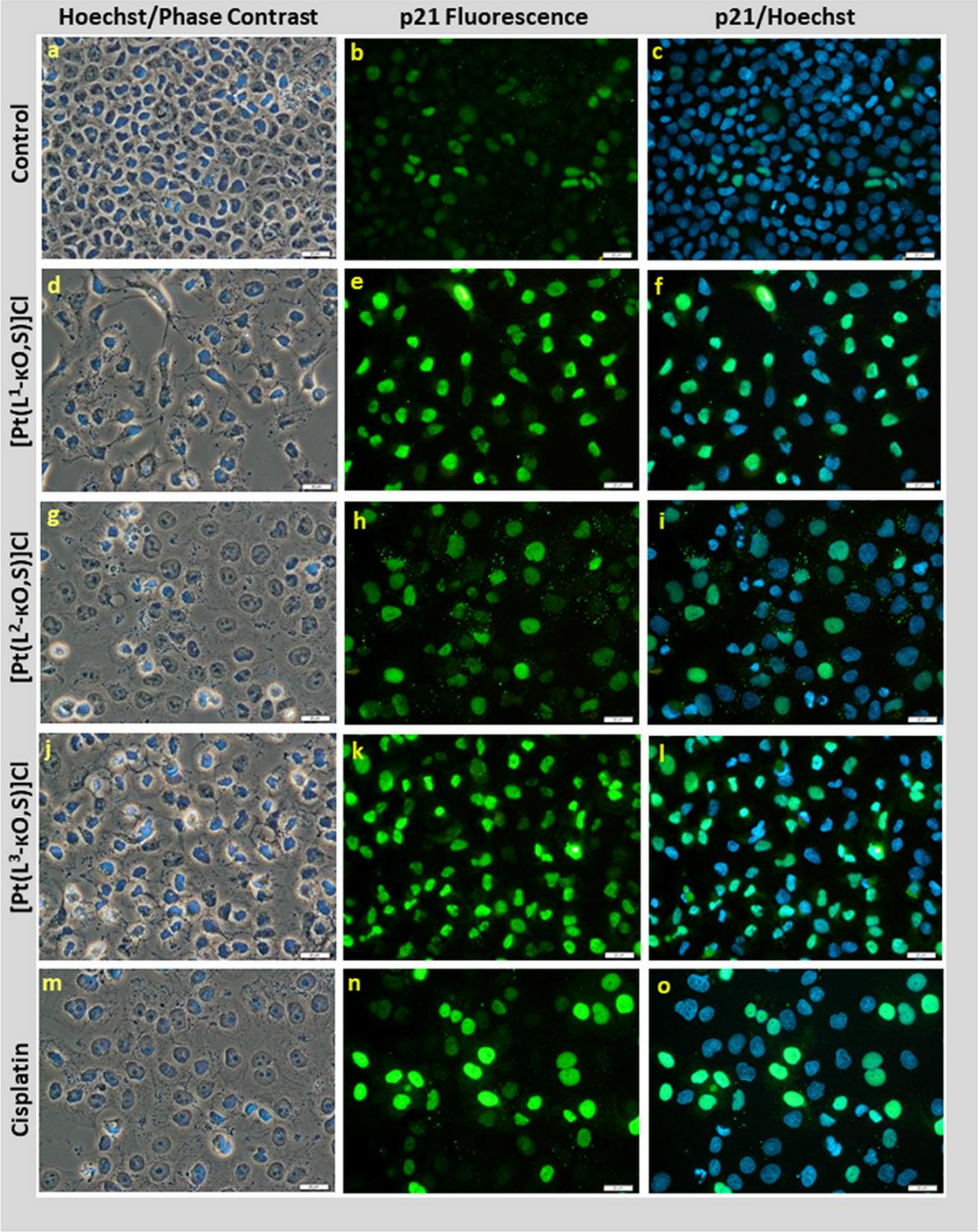


***Figure B11**: **Photomicrographs of A549 lung cancer cells, showing the nuclear expression of p21.** Cells were treated with 5 µM of [Pt(dmp)(L^1-κO,S)]Cl, [Pt(dmp)(L^2-κO,S)]Cl, [Pt(dmp)(L^3-κO,S)]Cl complexes and 25 µM cisplatin for 18 hours. Cell nuclei were counterstained with HO and merged with p21. Panel a-b shows the untreated negative control cells. (Magnification 400X; Scalebar: 20 µm).*

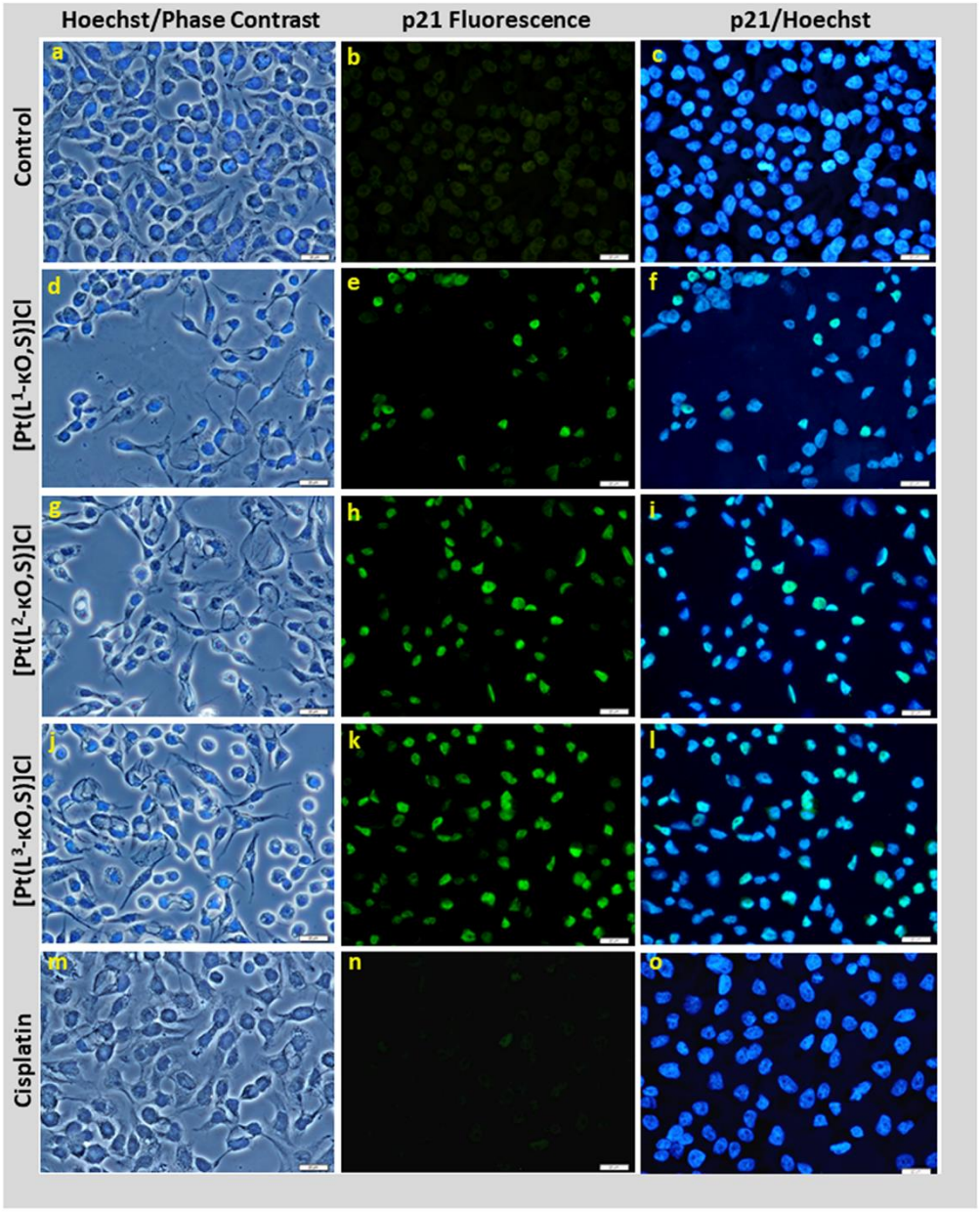


***Figure B12**: **Photomicrographs of HT-29 lung cancer cells, showing the nuclear expression of p21.** Cells were treated with 3 µM of [Pt(dmp)(L^1-κO,S)]Cl, [Pt(dmp)(L^2-κO,S)]Cl, [Pt(dmp)(L^3-κO,S)]Cl complexes and 15 µM cisplatin for 18 hours. Cell nuclei were counterstained with HO and merged with p21. Panel a-b shows the untreated negative control cells. (Magnification 400X; Scalebar: 20 µm).*

Appendix C: Chapter 5

1. Circular dichroism

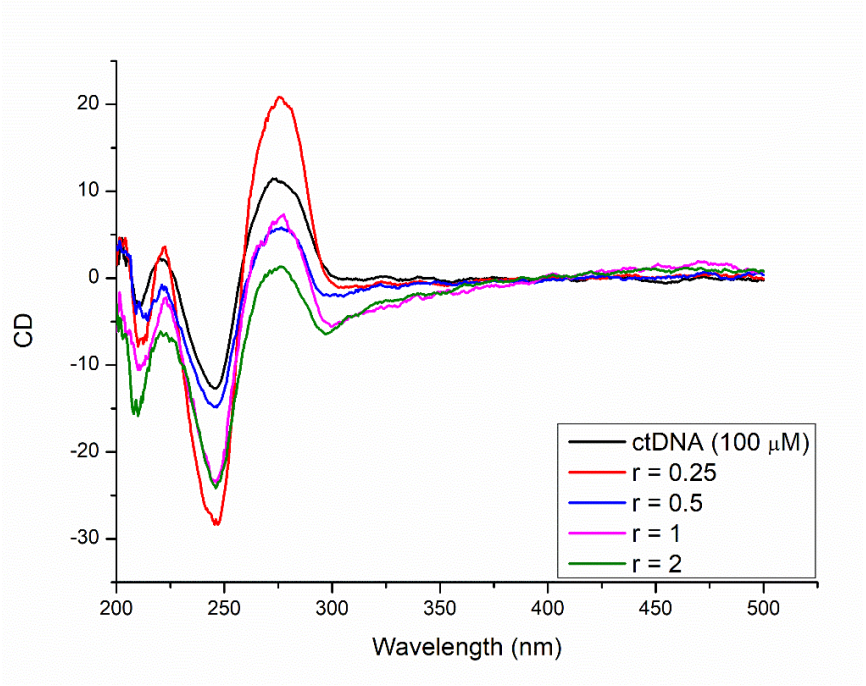


***Figure C1**: CD spectra [Pt(dmp)(L[1]-κO,S)]Cl at 25 μM, 50 μM, 100 μM in PBS (pH 7.4).*

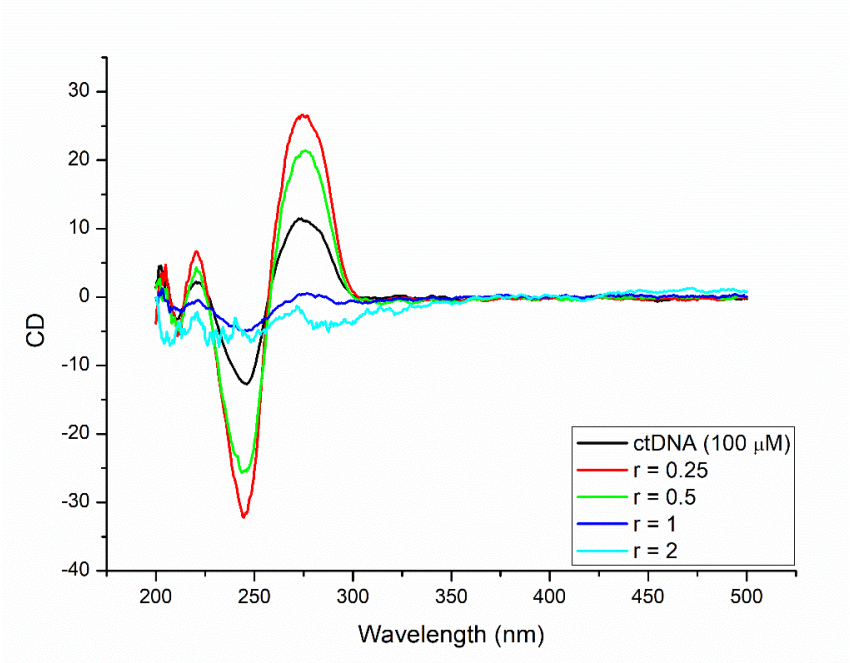


***Figure C2**: CD spectra [Pt(dmp)(L[3]-κO,S)]Cl at 25 μM, 50 μM, 100 μM in PBS (pH 7.4).*